UNIVERSIDADE DE LISBOA
INSTITUTO SUPERIOR TÉCNICO

Optimization of the seismic design of reinforced concrete bridges using evolutionary algorithms

Vítor Armando Teixeira Camacho

Supervisor: Doctor Mário Manuel Paisana dos Santos Lopes
Co-Supervisor: Doctor Carlos Alberto Ferreira de Sousa Oliveira

Thesis approved in public session to obtain the PhD Degree in Civil Engineering
Jury final classification: Pass with Distinction and Honour

2021

UNIVERSIDADE DE LISBOA
INSTITUTO SUPERIOR TÉCNICO

Optimization of the seismic design of reinforced concrete bridges using evolutionary algorithms

Vítor Armando Teixeira Camacho

Supervisor: Doctor Mário Manuel Paisana dos Santos Lopes

Co-Supervisor: Doctor Carlos Alberto Ferreira de Sousa Oliveira

Thesis approved in public session to obtain the PhD Degree in Civil Engineering

Jury final classification: Pass with Distinction and Honour

Jury

Chairperson: Doctor Eduardo Nuno Brito Santos Júlio, Instituto Superior Técnico, Universidade de Lisboa

Members of the Committee:

Doctor Nuno Cavaco Gomes Horta, Instituto Superior Técnico, Universidade de Lisboa

Doctor Luís Manuel Coelho Guerreiro, Instituto Superior Técnico, Universidade de Lisboa

Doctor José Miguel de Freitas Castro, Faculdade de Engenharia, Universidade do Porto

Doctor Mário Manuel Paisana dos Santos Lopes, Instituto Superior Técnico, Universidade de Lisboa

Doctor José Joaquim Costa Branco de Oliveira Pedro, Instituto Superior Técnico, Universidade de Lisboa

Doctor Luís Augusto Ferreira Rodrigues de Macedo, Instituto Superior de Engenharia do Porto, Instituto Politécnico do Porto

Funding Institutions

FCT - Fundação para a Ciência e Tecnologia

2021

Acknowledgments

To my family: Inês, my parents and my sister Sofia for their love, patience, support, and encouragement.
To my friends, particularly Ricardo Póvoa, for his insight and advice.
To my supervisors, for their help, support, guidance, and their constant availability to meet and discuss different issues and ideas.

I would also like to acknowledge the InfraRisk doctoral programme organization for their efforts and initiatives, which helped in the improvement of all of the doctoral candidates' works.
I also acknowledge CERIS/DECivil for all the support.
The work in this thesis was developed with funding (grant number PD/BD/127802/2016) from Fundação para a Ciência e Tecnologia (FCT).

This thesis is dedicated to my father, who always did everything he could to help me succeed.

Contents

Abstract

Structural design optimization for the seismic action is a complex process due to several different factors, from the non-convex and non-differentiable nature of the optimization problem to the existence of discrete variables as well as design code limits. For these reasons, the classic gradient-based optimization methods are not ideal to be used for structural optimization. In this work, meta-heuristic optimization techniques are employed, concretely evolutionary algorithms, which are used for the seismic design optimization of reinforced concrete bridges. Bridges with spans between 20m and 45m, total length up to 1000m, and piers under 30m in height were studied. A multi-objective optimization methodology is defined, which allows the optimization of bridges using more than one fitness function simultaneously. With this methodology, several works are developed with different goals, such as, revising behaviour factors used for reinforced concrete bridge design, definition of conceptual design strategies for bridges with different irregularity profiles and different total lengths, and also development of predictive seismic response and surrogate models based on machine learning techniques. The theme of spatial variability of the seismic action and its effect on long bridges was also developed. This effect, which is associated to loss of coherency of the seismic action between distant points, has significant impact in structures with long footprints. Long bridges are an example of such structures, and spatial variability of the seismic action applied to long reinforced concrete bridges is a theme about which there are not many published studies. The thesis overall presents a set of methodologies for analysis and optimization, which have the goal to provide mathematical formalism and automatize design processes which design engineers already perform in an informal way, based on their experience via trial and error. It is expected that these methodologies complement the design engineer's work. The thesis also presents a set of results and design strategies for bridges with different lengths and irregularity profiles. All the results are obtained by taking advantage of the ductility of reinforced concrete structures and abandoning some of the classical seismic design preconceptions from force-based design approaches.

Keywords: Nonlinear seismic analysis; Structural optimization; Evolutionary algorithms; Seismic design of RC bridges; Spatial variability of seismic actions.

Resumo

A otimização do dimensionamento de estruturas para a acção sísmica é um processo complexo devido a vários factores, desde a natureza não convexa, não diferenciável do problema de otimização, bem como a existência de variáveis discretas e limites impostos pelos códigos de dimensionamento. Por estas razões, os métodos clássicos de otimização com base em gradiente, não são ideais para utilizar no âmbito de otimização estrutural. Neste trabalho, são utilizadas técnicas meta heurísticas de otimização, concretamente algoritmos evolutivos, os quais são utilizados para a otimização do dimensionamento sísmico de pontes de betão armado. Pontes com vãos entre 20m e 45m, com comprimento total até 1000m, e com pilares com menos de 30m de altura foram estudadas. É definida uma metodologia de otimização multiobjectivo que permite a otimização de pontes com mais do que uma função de fitness em simultâneo. Com essa metodologia são desenvolvidos vários trabalhos com diferentes objectivos, tais como, revisão dos coeficientes de comportamento para pontes de betão armado, extração de regras de dimensionamento com base no histórico de pontes analisadas através do algoritmo de otimização, e aplicação a pontes com diferentes perfis de irregularidade de pilares e de comprimento total da ponte por forma a definir estratégias de dimensionamento com base em irregularidade e comprimento, e também o desenvolvimento de modelos preditivos de resposta sísmica com base em técnicas de *machine learning*. Também foi desenvolvido o tema da variabilidade espacial da acção sísmica e o seu efeito em pontes longas. Este efeito que está associado com a perda de coerência da acção sísmica entre pontos afastados, e tem maior impacto em estruturas que sejam extensas por natureza. As pontes longas são um exemplo disso, e a aplicação de variabilidade espacial da acção sísmica a pontes longas de betão armado é um tema sobre o qual não existem muitos estudos publicados. A tese globalmente apresenta um conjunto de metodologias de análise e de otimização, os quais têm por objectivo dotar de formalismo matemático e automatizar alguns processos que os engenheiros de projecto já fazem de forma menos formal com base na sua experiência e através de tentativa e erro. Espera-se que estas metodologias sejam, por isso, um complemento ao trabalho do engenheiro. A tese também apresenta um conjunto de resultados e estratégias de dimensionamento, para pontes de comprimentos e perfis de irregularidade de pilares diferentes. Todos estes resultados são obtidos tirando o máximo partido possível da ductilidade de estruturas de betão armado, ao considerar a acção sísmica como um misto de força aplicada e deslocamento imposto, abandonando algumas preconceções clássicas de dimensionamento com base em forças aplicadas.

Palavras-chave: Análises sísmicas não lineares; Otimização estrutural; Algoritmos evolutivos; Dimensionamento sísmico de pontes de betão armado; Variabilidade espacial da acção sísmica.

List of Symbols

Chapter 1:

RC – reinforced concrete

NSGA-II – non-dominated sorting genetic algorithm II

EC8 – Eurocode 8

RSI – relative stiffness index

SVSGM – spatially variable seismic ground motions

Chapter 2:

Δ_{max} – maximum displacement

q – q-factor defined by EC8 equivalent to seismic behaviour factor

R – reduction coefficient

F_{el} – elastic force

F_r – reduced force

Δ_y – yield displacement

μ – ductility factor

PBSD – performance-based seismic design

LCC – life-cycle cost methodologies

ϕ – cross-section curvature

M – bending moment

E – young modulus

G – shear modulus

I – cross-section moment of inertia

K – stiffness

Δ – displacement

H – pier height/length

V – shear force

Δ_u – ultimate displacement

RC – reinforced concrete

fsr – flexural steel reinforcement

EC8 – Eurocode 8

DOF – degree of freedom

σ – material stress

ε – material strain

ε_s – steel strain

ε_{su} – steel ultimate strain

f_{cm} – concrete mean compressive strength

E_{cm} – concrete mean young modulus

f_{ct} – maximum concrete tensile strength

f_{cu} – ultimate concrete compressive strength

f_c – maximum concrete compressive strength

f_{ck} – characteristic concrete strength

f_{ym} – steel mean strength

E_{ym} – steel mean young modulus

ϕ_y – cross-section yield curvature

$\phi_{y,EC8}$ – cross-section yield curvature estimated with EC8 formula

υ – Poisson ratio

A_a – half of the cross-section's longitudinal steel reinforcement

χ_y – cross-section yield curvature

χ_u – cross-section ultimate curvature

c_y – depth of the neutral axis at yield

c_u – depth of the neutral axis at failure of the cross-section

M_y – yield bending moment

M_u – ultimate bending moment

EI_{sec} – effective flexural stiffness at yield

LEA – linear elastic analysis

σ_{su} – steel ultimate stress

σ_{sy} – steel yield stress

v – reduced axial force

ε_c – concrete strain

ε_{cu} – ultimate concrete compressive strain

D – cross-section diameter

D-cover – cross-section diameter minus cover concrete

D_{core} – cross-section core diameter (equal to D-cover)

d_c – neutral axis depth

lsr – longitudinal steel reinforcement

λ – shear ratio

δ_s – displacement due to shear

δ_b – displacement due to bending

ϕ_i – ith normalised eigen vector

δ_{ij} – Kronecker delta

M – mass matrix

UL – uniform load

SM – single mode

MM – multi mode

β_i – modal participation factor

S_{di} – ith spectral displacement

υ – vector of imposed displacements

V_i – yield strength of the ith pier or isolator

K_{ei} – elastic stiffness of ith isolator

Δ_{ei} – yield displacement of ith isolator

N2 – N2 pushover method

MAC – modal assurance criteria

MSF – modal scale factor

K_d – deck stiffness

K_p – pier stiffness

ψ_i – ith normalised mode shape

RP – regularity parameter

RSI – relative stiffness index

THDP – transverse horizontal displacement profile

SPA – nonlinear static pushover analysis

NDA – nonlinear dynamic analysis

MCS – Monte Carlo simulation

FBD – force-based design

DBD – displacement-based design

DDBD – direct displacement-based design

SDOF – single degree-of-freedom

ACSM – adaptive capacity spectrum method

DAP – displacement-based adaptive pushover

a_g – design ground acceleration on rock

S – soil parameter

T_1 – fundamental period of vibration

T_B, T_C, T_D – seismic design spectrum reference periods according to EC8 and the Portuguese National Annex

Chapter 3:

RC – reinforced concrete

ε_{cu} - ultimate concrete compressive strain

MBD – multi body dynamics

f – objective functions

x – design variables

y – state variables

g - constraints

NSGA-II – non-dominated sorting genetic algorithm II

FEM – finite element method

EA – evolutionary algorithms

GA – genetic algorithms

Chapter 4:

RC – reinforced concrete

MOP – multi-objective optimization problem

NSGA-II – non-dominated sorting genetic algorithm II

MCS – Monte-Carlo simulation

NDA – nonlinear dynamic analysis

GA – genetic algorithm

MOEA – multi-objective evolutionary algorithms

MOEA/D – multi-objective evolutionary algorithm based on decomposition

MODdEA – multi-objective evolutionary algorithm that diversifies population by its density

ANN – artificial neural networks

RBO – reliability-based optimization

FLC – fuzzy logic controller

DE – differential evolution

BSA – backtracking search algorithm

FA – firefly algorithm

ICA – imperialista competitive algorithm

SGA – search group algorithm

FEM – finite element model

NCGA – neighbourhood cultivation genetic algorithm

HVAC - heating, ventilating and air conditioning

SOP – single-objective optimization problem

LCC – life-cycle cost

SVM – support vector machines

PSO – particle swarm optimization

SSI – soil-structure interaction

MCDM – multi-criteria decision-making method

SMA – shape memory alloy

equalDOF – equal degree-of-freedom

α, β – Newmark method parameters

EC8 – Eurocode 8

EC8 - 2 – Eurocode 8, part 2 (bridges)

MPICH2 – message passing interface implementation

CTS – constrained tournament selection

EAX – extended arithmetic crossover

DM – diversified mutation

δ_{shear} – shear displacement

δ_{flex} – flexural displacement

f_m – objective function m

x_d – decision variable d

g_i – constraint i

L_d – lower limit decision variable d

U_d – upper limit decision variable d

ε_{cu} - ultimate concrete compressive strain

ε_c - concrete compressive strain

f_{cm} - concrete mean compressive strength

E_{cm} – concrete mean young modulus

f_{ym} – steel mean strength

E_{ym} – steel mean young modulus

ε_{su} – ultimate steel strain

TYD-MOP – truly disconnected multi-objective problems

EAF – empirical attainment function

POF – Pareto-optimal front

POS – Pareto-optimal set

CoV – coefficient of variation

PBD – performance-based design

SV – steel volume

CV – concrete volume

stdev -standard deviation

Chapter 5:

MOO – multi-objective optimization

EC8 – Eurocode 8

EC8 - 2 – Eurocode 8, part 2 (bridges)

RC – reinforced concrete

q – q-factor (behaviour factor)

q_s – overstrength dependent component of q

q_μ – ductility dependent component of q

q_ξ – damping dependent component of q

NSGA-II – non-dominated sorting genetic algorithm II

r_i – local force reduction factor

M_{sd} – design bending moment

M_{rd} – design flexural resistance

EA – evolutionary algorithms

POS – Pareto-optimal set

MOEA – multi-objective evolutionary algorithms

PGA – peak-ground acceleration

SDOF – single degree-of-freedom

MOP – multi-objective problem

f_{ym} – steel mean strength

f_{um} – steel ultimate strength

E_{ym} – steel mean young modulus

ε_{sy} – steel yield strain

ε_{sh} – steel hardening strain

ε_{su} – steel ultimate strain

f_{cm} – concrete mean strength

E_{cm} – concrete mean young modulus

ε_{cu} – concrete ultimate compressive strain

D – ductile structure

LD – limited ductile structure

CoV – coefficient of variation

d_{yi} – ith pier yield displacement

R_u – ultimate displacement

Sd_t – target displacement

R_y – yield displacement

Sd_y – yield displacement of the bi-linearized model

F_{ym} – structure's yield strength using mean material properties

F_{um} – structure's ultimate strength using mean material properties

$F_{el,eff}$ – inertia force from the application of the N2 method using the structure's effective stiffness

m_q – slopes of the q vs q_{dy} graphs

PIrr – pier irregularity measure

Chapter 6:

THDP – transverse horizontal displacement profile

SPA – nonlinear static pushover analysis

RC – reinforced concrete

NDA – nonlinear dynamic analysis

RSI – relative stiffness index

ACSM – adaptive capacity spectrum method

RP – regularity parameter

fsr – flexural steel reinforcement

GA – genetic algorithms

K_{SS} – superstructure stiffness

K_{IS} – infrastructure stiffness

$E_{c,SS}$ – concrete superstructure young modulus

I_{SS} – superstructure moment of inertia

L_{SS} – superstructure length

$K_{eff,p}$ – pier effective stiffness

I_{yy} – moment of inertia

J – torsional constant

f_{cm} – concrete mean strength

E_{cm} – concrete mean young modulus

ε_{cu} – concrete ultimate compressive strain

f_{ym} – steel mean strength

E_{ym} – steel mean young modulus

ε_{su} – steel ultimate strain

NSGA-II – non-dominated sorting genetic algorithm II

TYD-MOP – truly disconnected multiobjective problems

MODdEA – multi-objective evolutionary algorithm that diversifies population by its density

MOP – multiobjective problems

ε_c – concrete compressive strain

d_T – superstructure transversal peak displacement

lnRSI – logarithm of the Relative Stiffness Index

K_{total} – total pier stiffness along the bridge

POS – Pareto-optimal set

SDOF – single degree-of-freedom

MOEA – multiobjective evolutionary algorithm

POF – Pareto-optimal front

ANN – artificial neural networks

v – normalized axial force

x – initial variable

μ – mean of variable x

s – standard deviation of variable x

z – standardized variable x

MLP – multi-layered perceptron

CART – classification and regression tree

ReLU – rectified linear unit

SMOTE – synthetic minority oversampling technique

NAxialF – normalized axial force

MAE – mean absolute error

MSE – mean square error

$Conn_i$ – ith pier-deck connection

MDOF – multi degree-of-freedom

FEM – finite element method

Chapter 7:

RC – reinforced concrete

SVSGM – spatially variable seismic ground motions

SMART-1 – strong motion array in Taiwan

GM – ground motion

FEM – finite element method

Ψ – incidence angle

ω – angular frequency

$\gamma(\omega)$ – coherency function

CPDF – conditional probability density function

HOP – Hao-Oliveira-Penzien model

α – coherency drop parameter (except the α in the Newmark method)

d – distance between points/stations

L_{ij} – lower triangular matrix obtained from the Cholesky decomposition of the coherency matrix

A_{im} – amplitudes of the generated signal

ϕ_{mk} – random phases of the generated signal

α, β – Newmark model parameters

S_0 – power spectral density

S_{ij} – smoothed cross spectrum between stations i and j

V_r – apparent wave propagation velocity in the bedrock

TH – time-history

PSD – power spectral density functions

LW – Luco and Wong model

f_{ym} – steel mean strength

f_{um} – steel ultimate strength

E_{ym} – steel mean young modulus

ε_{sy} – steel yield strain

ε_{sh} – steel hardening strain

ε_{su} – steel ultimate strain

f_{cm} – concrete mean strength

E_{cm} – concrete mean young modulus

ε_{cu} – concrete ultimate compressive strain

DD – average pier displacement demand

SV_{20}/SV_{30} – spatial variability with $\alpha=2x10^{-4}/3x10^{-4}$

SDOF – single degree-of-freedom

Index of Figures

Index of Tables

1 Introduction

In this thesis, the author presents novel optimization techniques and developed methodologies, which apply those techniques to the optimization of a certain type of common RC bridges. Even though all case-studies belong to a single bridge typology, many of the conclusions can be generalized to other typologies. Furthermore, the methodologies presented herein can be applied to any type of structure and/or action, thus not being exclusively applicable to RC bridges, nor being exclusive for the seismic action. These methodologies are applicable to any problem and are particularly advantageous when applied to problems with certain characteristics, which will be presented in later chapters.
The relevance/importance of this thesis' output can be divided into different categories: 1) Development of structural optimization methodologies which can be emulated and applied to other types of structures and problems; 2) Application of the optimization methodologies obtaining results for the calibration of Eurocode 8 (CEN 2005) behaviour factors and a ductility-irregularity function; 3) Application of the optimization methodologies to long irregular bridges with results allowing to extract design rules based on bridge irregularity classifications; and 4) Application of spatially variable seismic ground motions to long bridges, identifying how spatial variability influences the displacement demand of piers along regular and irregular bridges. The relevance of these four outputs is of different types, where 1)'s importance is associated to the methodology applied and less regarding the obtained results, 2) on the other hand, has more relevance in the obtained results. In the case of 3), its results are important but, most of all, the qualitative conclusions and subsequent design rules are relevant. Finally, 4) is important regarding the methodology for obtaining spatially variable ground motions and the results of their application to the bridge case-studies, defined herein. In addition to these points, this thesis shows how different factors influence the ductility of concrete elements and how the traditional design methods do not take full advantage of that ductility. Additionally, this thesis shows how machine learning techniques and parallel computation can be employed to improve the efficiency of works in structural engineering.

Optimization can have several meanings and it is usually associated to minimization problems, such as minimization of weight, or minimization of cost (which are in many cases equivalent). It is common to assume that the result of an optimization procedure is a solution that is better than every other solution, or some solution which is at the limit of a defined feasible region, i.e., the collection of solutions that do not violate any feasibility constraint such as design code limits. Due to this, optimization is frequently regarded with some scepticism since there is rarely such a thing as an optimal solution in real world problems. Also due to the notion that by reducing something in excess, the obtained result might be so close to the infeasible region that any slight change in design variables, site conditions or prior knowledge might result in the previously optimal solution becoming infeasible. In this thesis, it is shown that this is not always the case and the idea of optimization is not fixed to a given objective, and the results are only optimal regarding the optimization objectives that were chosen. In multi-objective optimization, where the output is composed by more than one solution, there is no single optimal solution but rather a set of non-dominated solutions that comprise several trade-offs between objectives. The same problem can also be modelled with more than one set of optimization objectives, which result in different optimal solutions, further reinforcing the idea of inexistence of global optimality. As mentioned above, the concept of optimization is frequently associated with minimization of cost or weight, but there can be several other optimization objectives, which cannot be optimized concurrently and that result in interesting solutions. Such objectives as maximization of performance/safety/resistance, which is frequently employed in this thesis, against cost minimization, or maximization of design standardization. Another notion surrounding optimization is that optimization results are case dependent, i.e., that the results of an optimization procedure are only applicable to the problem that was optimized. While this may be true to some extent, the collection and analysis of optimization results for different case-studies, and the results obtained within each search procedure can be used to find patterns and clusters in the data correlating good performance to specific variables, or to solutions with certain characteristics. This information gain can result in the definition of generalized design rules, or the definition of criteria for separating solutions into groups with similar behaviour. This falls into the realm of the concept of data mining, which is the extraction of knowledge from data sets, and can be obtained through the use of appropriate machine learning techniques, and large amounts of data. The former concerns the methodologies and techniques presented herein, while the latter concerns the maximization of computation capability which is made possible through parallel computing.

The reasons for having researched and employed these methodologies in this thesis were that the design of long bridges, particularly irregular bridges is usually a task based on some trial and error, past experience and force-based elastic design techniques, many of them based on incorrect notions about the ductility demand of RC elements. This thesis intends to provide, not only, new approaches and methodologies, but also a different mind-set regarding the design of irregular RC structures. These notions are obtained from the analysis of the results of tens of thousands of analysed bridge solutions from different case-studies concerning different bridge lengths, irregularity layouts, and other design variables, etc.

This thesis is thus multidisciplinary in the sense that it is not limited to structural engineering or earthquake engineering but tries to add value by stretching outwards to other disciplines, particularly in the realm of machine learning, to generate new approaches and attain new perspectives, in some cases, and confirm existing ideas, in other cases. The research for the development of this thesis gave origin to three already published papers (Camacho, Horta, et al. 2020) (Camacho, Lopes and Oliveira 2020) (Camacho, et al. 2021), and two other currently under review, as well as another paper presented at an international conference (Camacho, Horta and Lopes 2020).

The outline of this thesis is the following:

- The 1st (current) chapter is composed by introductory remarks and overview of the work with explanation of objectives and motivations in pursuing the chosen approaches.
- The 2nd chapter covers general concepts on ductility and seismic design of bridges, usual seismic design approaches and their fallacies regarding seismic behaviour, ductility, etc; a parametric study on the effect of different properties and variables on RC elements ductility;

new seismic design approaches and bibliographic research on the current state-of-the-art; domain of application of the study, with description of types of RC bridges in terms of dynamic behaviour; concept of long bridges and short bridges, regular bridges and irregular bridges, and corresponding irregularity profiles; the types of analysis that can be performed given the type of bridge, in terms of irregularity profile and length, that is, the effects of higher modes and methods of analysis that can capture those effects; finally, the choice of earthquake action and respective ground-motions to be used in subsequent chapters.

- The 3rd chapter introduces optimization in the mathematical sense, presenting both traditional gradient-based optimization methods and the employed meta-heuristic optimization methods.
- The 4th chapter builds on the methods presented in the 3rd chapter and applies them for bridge seismic optimization. In this chapter a framework for multi-objective optimization is introduced, and the link is made with the rest of the work, with the presentation of the application of evolutionary optimization techniques in the field of structural and earthquake engineering. This chapter then goes onto presenting the modified NSGA-II algorithm (Non-dominated Sorting Genetic Algorithm II), which is employed throughout the thesis, and its application to a case-study bridge. The entire chapter is based on the following paper (Camacho, Horta, et al. 2020).
- The 5th chapter applies the optimization methodology, presented in the previous chapter, to the optimization of the seismic design of bridges in the longitudinal direction. The results are used to calibrate/confirm the values prescribed by EC8 for the behaviour factors of ductile bridges. This, in addition to the definition of a pier irregularity measure, resulted in a new expression that returns an approximate value of the real behaviour factor. The entire chapter is based on the following paper (Camacho, Lopes and Oliveira 2020).
- The 6th chapter takes on the seismic analysis of bridges in the transverse direction and applies different approaches to both short and long, regular and irregular bridges. In this chapter, results from tens of thousands of dynamic analyses are processed and generalized behaviours are identified. Measures such as RSI (Relative Stiffness Index) and other stiffness related indices are employed to categorize bridges according to length and irregularity. From these results, design rules are proposed for different bridge categories. The entire chapter is based on two submitted papers currently undergoing peer review and a conference paper (Camacho, Horta and Lopes 2020).
- The 7th chapter investigates the influence of spatial variability in ground motions on the dynamic behaviour of long bridges, both regular and irregular. A methodology for obtaining SVSGMs (spatially variable seismic ground motions) that are compatible with the theoretical coherency models and with a given reference power spectrum is presented. A sensitivity analysis is performed over various parameters including wave propagation velocity and coherency loss, and the effects on regular and irregular bridges with various lengths are compared. At the end, many assertions are made on whether SVSGMs have negative impact on bridges, and in what way. The entire chapter is based on the following paper

(Camacho, et al. 2021). This chapter was added due to the lack of information in the literature on the impact of spatial variability on these types of structures. Spatial variability can impact the seismic design optimization results, especially for long bridges.

In the aforementioned chapters, the analyses are performed on a single bridge typology, concerning the deck's and piers' cross-section. There exist several variations of RC bridges in terms of pier cross-section, deck cross-section, span length, insertion in a curve, etc. There are also different ways to deal with seismic action, particularly through all sorts of dissipation devices. Regardless, the results and notions obtained in this thesis can be generalized to other bridge typologies. Concerning the fundamental period of vibration of the analysed bridges throughout the thesis (considering the elements effective stiffness), it varies essentially due to the variation of both diameter and flexural steel reinforcement, mostly between 0.4s and 1.5s. This range corresponds to the zones of the spectrum of constant acceleration (<0.6s) and constant velocity (>0.6s).

The seismic analyses did not take into consideration the vertical component of the seismic action, this was decided for the sake of simplification, since it would add more complexity to the seismic analyses without significant variation in the results due to the relatively small importance of the vertical component in these types of analyses for these types of structures. The vertical component is also not always available in sets of real ground motions, which is the case in this work.

2 General concepts of seismic design and ductility of reinforced concrete elements

2.1 Historical background, revision of concepts and myths of seismic design

Earthquakes are essentially imposed displacements on structures, even though historically they were (and still are) reduced to equivalent forces for design purposes.. Nowadays, it is amply known that a design that is based on giving the structure the ability to both deform and limit its imposed deformation, originates structures that are very well equipped to resist the seismic action.

It is clear that, for systems that remain with elastic behaviour, force-based design is perfectly adequate. However, regarding seismic actions, it is frequent that structures develop significant plastic behaviour, i.e., material nonlinearity. In these cases, design based on elastic analysis, without properly considering energy dissipation, force redistribution and a correct ductility assessment, originates inadequate and/or ineffective structures in resisting seismic actions.

The employment of traditional force-based design techniques based on equivalent inertia forces has historical background in earthquake engineering. It is naturally associated to the way civil engineers design structures for most types of actions, where the structure is designed with strength above the necessary to withstand the applied forces, otherwise collapse will occur. However, it has been recognized by some time now that, in terms of structural damage assessment, forces are less important than displacements when regarding seismic effects. In fact, structures are usually designed with ultimate strength which is lower than the "elastic" seismic forces, because it is recognized that a well-designed structure can withstand, in the plastic region, the displacements imposed by the seismic action without incurring in significant loss of load carrying capacity. This type of design implies damage but not collapse.

This part of the current chapter is mainly around the concept of ductility and its application to whole structures and not only at element or cross-section level, which is a fundamental, if not "the" fundamental, concept regarding this thesis.

2.1.1 Seismic force reduction coefficients and ductility

In Figure 2.1 there are three representations of the elastoplastic behaviour of a pier, representing three piers with the same mass and initial stiffness, but different ultimate strength. It is assumed that stiffness is independent of strength, according to the usual design practice of evaluating the stiffness as a function of the gross concrete sections. This is not true after cracking, however, for simplification purposes and to clearly convey the ideas in this chapter, this path will be followed for the time being. According to the equal-displacement theory, which still is largely accepted today, the displacements of a structure assuming it always remains in the elastic phase, are equal to the displacements in the plastic phase for the same seismic action (Priestley, Calvi and Kowalsky 2008). Taking this into consideration, the three aforementioned piers are subjected to the same maximum displacement Δ_{max}, when subjected to the same seismic action. This way, the concept of force reduction coefficient becomes clear in Figure 2.1 and is henceforth introduced in the discussion. This concept is fundamental for the seismic analysis and is usually referred to as the q-factor (according to the European terminology embodied in EC8), although the q-factor is more complex and is composed by a few other factors in addition to the ductility reduction factor, but this will be explained in-depth later on. For the pier with a fully elastic response, the value of F_{el} is reached at the Δ_{max} displacement. The other two piers (P2 and P3) are designed to have reduced strength, F_{R2} and F_{R3}, respectively, which are related to the elastic force F_{el} through the reduction coefficients:

$$F_{\mathrm{R2}} = \frac{F_{el}}{R_2} \ \ e \ \ F_{\mathrm{R3}} = \frac{F_{el}}{R_3} \tag{2.1}$$

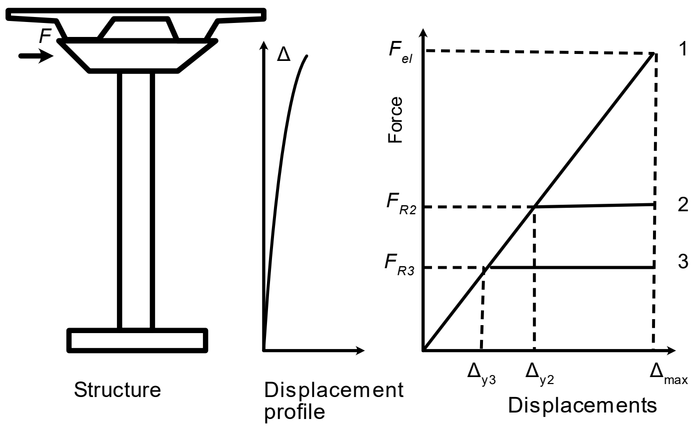

Figure 2.1 Three cases of piers with different force-reduction coefficients. The graph on the right-hand side shows the force in each pier against the displacement at the top of the pier. Adapted from (Priestley, Calvi, et al., Displacement-Based Seismic Design of Structures 2008).

Ductility can refer to available ductility or ductility demand. The first one concerns the capacity of a given structure or element to deform plastically before reaching a certain limit. The second is the ratio between the displacement (or other kinematic variable as rotation, curvature or strain) imposed by the seismic action to the structure or element and the respective yield value. The ductility factor is calculated as such for P2 and P3:

$$\mu_2 = \frac{\Delta_{max}}{\Delta_{y2}} = \frac{F_{el}}{F_{R2}} = R_2 \ \ and \ \ \mu_3 = \frac{\Delta_{max}}{\Delta_{y3}} = \frac{F_{el}}{F_{R3}} = R_3 \tag{2.2}$$

Therefore, the strength reduction coefficient (R) takes on the same value as the ductility factor (μ) if we assume the equal-displacement theory. With this in mind, it is clear that for inelastic systems, force has little preponderance on design, and the capacity to deform and sustain displacements becomes the most important factor for design. In elastic systems, using displacement or force as a design basis is equivalent. However, inelastic systems it is more logic to design based on displacements, since displacements are a much better indicator of damage and performance than forces.

2.1.2 Historical background

Seismic design performed by reducing the seismic action to equivalent forces has, as previously mentioned, an historical base. According to (Priestley, Calvi and Kowalsky 2008) the origins of modern seismic design is traced back to the 20s and 30s of the 20th century. After a series of earthquakes that originated many structural collapses in Japan, in the USA and in New Zealand, in an age where there was very little seismic design being done, it was concluded that the structures that were designed to withstand horizontal action due to wind loads had presented better seismic performance. From that point on, the seismic action began to be defined as an equivalent horizontal force equal to a percentage of the structure's weight, regardless of its period of vibration.

In later decades, around the 50s and 60s, research on seismic action and better comprehension of its nature allowed to associate the structure's period of vibration with the respective seismic inertia force. At the same time, dynamic time-history analysis began to be performed, which allowed to verify that many structures had resisted earthquakes that would have induced inertia forces, calculated assuming elastic behaviour, clearly above the ones the structure could resist. From these observations the concept of ductility is used in order to explain the "anomaly" of the non-collapse of these structures with "insufficient" strength. Subsequent formulations relating ductility and force-reduction coefficients are defined with the goal of providing a better predictor of the seismic inertia forces imposed on a structure during an earthquake.

In the 1970s and 1980s, ductility became the largest focus of earthquake engineering research, with experimental testing to attain the ductility of different structural elements and different materials under cyclic loading. The constitutive relationships of materials were first defined. This marked the first deviation from the seismic force-based paradigm. The seismic force began to be estimated with force reduction coefficients that reflected the expected available ductility of the structural system. Even so as today, design was done with the goal of attaining the design seismic forces, while available ductility and ductility demand were only verified after design.

It is only in the 1990s that research focuses more on the structures' ability to withstand displacements. The concept of performance-based seismic design (PBSD) is introduced, and it has been developed since then. In the last few decades, concepts such as displacement-based design, stiffness-based design, and others, have been introduced, and a larger emphasis on the stochastic nature of the seismic action and the uncertainty of the materials' properties has been given. Life-cycle cost methodologies (LCC) and risk-based frameworks are currently in the forefront of research. Large-scale computational analysis capabilities have allowed to begin applying methodologies based on machine learning techniques to extract more knowledge from large datasets of analysed structures. The present thesis is an example of the application of such methodologies to the seismic design of reinforced concrete bridges.

2.1.3 Current force-based design methodology

The current design methodology (force-based) has been improved throughout the decades and new design methodologies have been introduced in the last decades, as previously mentioned. Regardless, most design codes still promote force-based design, which many times originate inadequate seismic design solutions. In fact, force-based seismic design is still, nowadays, performed based on a series of myths and fallacies (M. N. Priestley 2003). The generic design procedure for a structure with a single degree-of-freedom is presented in the following:

1) The structure's geometry is pre-designed according to good practice notions, pre-design heuristics and/or past experience. The idea is that the final design has the same geometry or, at least, a similar geometry to the pre-designed one.
2) The stiffness of the cross-sections and elements are determined. How the stiffness is estimated varies from code to code, and within codes. The stiffness of an element can be assumed as the full uncracked stiffness, a percentage of this stiffness, a cracked stiffness, or an effective stiffness. A common effective stiffness that is used concerns the stiffness measured at yield.
3) In this step, the modal analysis of the structure is done, obtaining the vibration modes and respective frequencies. A rule of thumb defines 95% cumulative mass associated to the modes as the threshold to define relevant modes.
4) The design spectrum is determined. Here the main issue is the definition of the behaviour factor (q-factor), which is analogous to the strength reduction coefficient. This coefficient depends on several factors, but it is essentially associated to ductility. The q-factor affects the elastic spectrum to obtain the design spectrum. The codes usually define a maximum behaviour factor, which is usually somewhat conservative. This is verifiable via nonlinear analysis.
5) The inertia forces are calculated and distributed between the elements according to the stiffness of the elements. The steel flexural reinforcement is determined so that the strength of each element is higher than the internal forces in the element generated by the inertia forces. The confinement of the cross-sections is also determined in order that available curvature ductility exceed the corresponding curvature ductility demand.
6) Following is the analysis of imposed displacements. Here, displacements are deemed admissible by either comparing them to maximum drift values, or by comparing them to maximum displacements estimated from the cross-section's confinement. If the displacements are inside these limits, the design process is concluded. In case they are not, the stiffness of the elements is modified after which we go back to step 3.
7) The principles of Capacity Design are applied, where it is guaranteed that plastic hinges only appear in expected pre-determined sections in each element. This is fundamental for multi-degree of freedom systems.

2.1.4 Fallacies associated to traditional earthquake design

1) Interdependency between strength and stiffness

Most expressions to obtain the element's flexural stiffness are independent from the amount of flexural reinforcement, and consequently, independent from the elements' flexural strength. The expression that relates stiffness and strength is:

$$EI = \frac{M}{\phi} \tag{2.3}$$

Where ϕ represents the cross-section's curvature and M represents the respective bending moment. The assumption of initial stiffness independent from the amount of reinforcement, that is, constant for the same cross-section geometry, implies that the yield curvature is directly proportional to the cross-section's resisting bending moment, as seen on the left-hand side of Figure 2.2. In the detailed analysis, which will be presented in subsequent sections, it will be shown that, in fact, the yield curvature is essentially independent from the resisting bending moment and depends mainly on section geometry and axial force influence. What effectively varies with the yield bending moment is the cross-section stiffness, which is schematically shown in Figure 2.2.

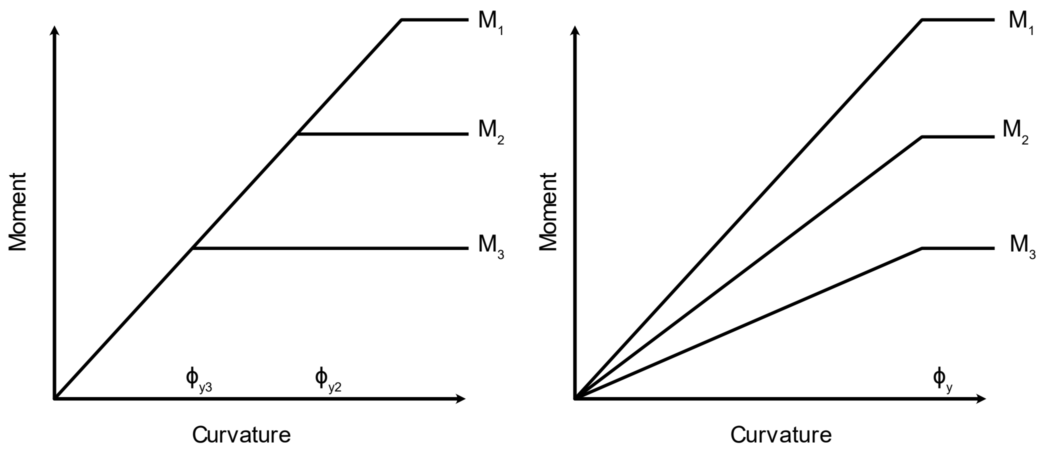

Figure 2.2 Different models for moment-curvature relationships. The model on the left-hand side is based on the assumption that cross-section stiffness is independent of cross-section strength, and the model on the right-hand side assumes that the yield curvature is independent from cross-section strength. Adapted from (Priestley, Calvi, et al., Displacement-Based Seismic Design of Structures 2008).

2) Validity of the equal displacement theory

The concept of ductility has been introduced in the beginning of Chapter 2, alongside the equal-displacement theory. However, this theory has some limitations. First, and according to (Priestley, Calvi and Kowalsky 2008), the equal-displacement theory is not exact regarding attained displacements. That is, the elastic displacements are different from the nonlinear displacements for both long and short period structures, due to the large variation of nonlinear displacements for different levels of ductility demand, since the ductility demand affects energy dissipation, which in turn affects the nonlinear displacements. Thus, it can be said that equal-displacement theory is applicable for medium period structures, while for long period structures it tends to overestimate displacements, and underestimate displacements for short period structures.

3) Irregular structures

Traditionally, the longitudinal seismic design of a structure such as the one in Figure 2.3, would be performed by assessing the elastic flexural stiffness of each vertical element (inversely proportional to the cube of each element's length), the sum of which corresponds to the structure's stiffness which is used to calculate the structure's period and subsequently, the inertia forces from the design spectrum. In the end, these inertia forces would be distributed between the vertical elements (piers) proportionally to their elastic stiffness.

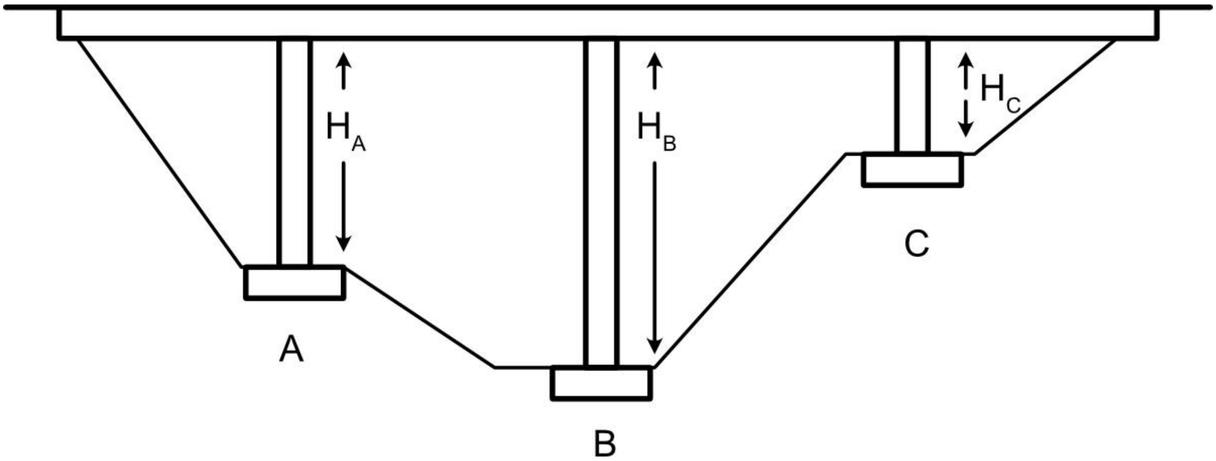

Figure 2.3 Bridge example with unequal piers. Adapted from (Priestley, Calvi, et al., Displacement-Based Seismic Design of Structures 2008).

The result from such a design procedure, is that the strength is concentrated essentially in the shortest pier, while the same cross-section size is kept for every pier. The piers, other than the shortest one, become essentially secondary elements in terms of strength and stiffness.

By using this design method that makes use of the elastic properties, the distribution of the horizontal inertia forces among piers is done by giving each pier the strength that corresponds to the intersection of its force-displacement graph with the vertical line that corresponds to the yield displacement of pier C in Figure 2.3. At this stage, the issue regarding the yield curvature has been corrected, having been set as equal for all piers. Since the yield displacements of the longest pier is much higher than that of the shortest pier, and the length of the plastic behaviour is similar, this results in a clear sub-usage of the ductile capacity of the longest piers, and an overload of the shortest pier as seen in Figure 2.4. In the following, the drawbacks from this situation will be discussed.

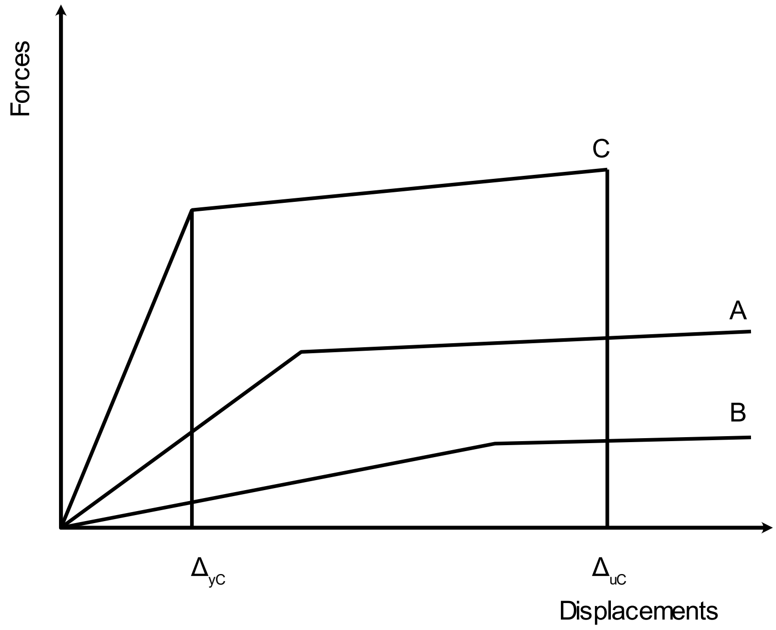

Figure 2.4 Force-displacement graphs of the piers from the bridge in Figure 2.3. Adapted from (Priestley, Calvi, et al., Displacement-Based Seismic Design of Structures 2008).

Assuming the connection between the pier and the superstructure as fixed, distribution of the inertia forces among the piers, resulting in V_A, V_B and V_C, is done proportionally to H_A^3, H_B^3 and H_C^3, since the lateral stiffness of the piers is given by,

$$K_i = \frac{3.EI}{H_i^3} \tag{2.4}$$

The consequence from this is that the base bending moments in each pier have values of,

$$M_i = V_i.H_i = \frac{3.EI}{H_i^3}.\Delta.H_i = \frac{3.EI}{H_i^2}.\Delta \tag{2.5}$$

That is, the bending moments are inversely proportional to the square of the piers' lengths. From here it follows that the shortest pier will have a much larger amount of flexural steel than the other two piers, as previously mentioned. This situation has three drawbacks:

- The first is that, by placing more flexural steel in the shortest pier, this pier's stiffness increases even more relatively to the other two piers, which makes this design strategy somewhat ineffective and inefficient. So, any subsequent design iteration in which the stiffness was updated, for instances considering the reinforced concrete cracked sections, would imply even larger strength to be placed in the shortest pier.
- Second, by having an element with a much larger flexural capacity, which in turns means a much larger shear demand than the others, the likelihood of having a fragile collapse due to shear increases. The structure might not be designed to resist only on the other two piers, since the strength of both piers is too small to be able to withstand the loss of the shortest pier, let alone the fact that shear failure may affect the vertical load bearing capacity.

- Third, the ability of the shortest pier to withstand displacements is reduced with such a significant increase of flexural steel, since this increases the ultimate curvature due to the increase in the depth of the compressed area of the critical cross-section. This can precipitate collapse of the pier due to excessive compressive strain in the concrete. This will be shown later on, in depth.

4) Relationship between strength, available ductility, and ductility demand.

It has been mentioned that it is becoming less uncommon for design engineers, after a pre-design based in Eurocode 8 prescriptions, to perform a verification via either inelastic pushover analysis or nonlinear dynamic analysis, in order to confirm the design in question, namely, to be sure about the employed behaviour factor for the seismic design. If, due to the results from the nonlinear analysis, the design engineer has to re-design the structure, he may eventually do that by increasing the strength of the structure, assuming that increases the ability of the structure to withstand the earthquake. However, it is known that in many cases, particularly in the case of bridges, this is not true. That is, the increase in strength does not imply the increase in earthquake resistance, in fact, it may be the opposite.

Regarding some of the usual assumptions in earthquake resistant design and considering that most of them originate from the fact that traditionally structural designers are used to model actions as applied forces, it is clear why there is the idea that the increase in strength correlates to an increase in structural safety. However, this is based on a few common misconceptions, both conveyed by Figure 2.5, which are:

- The stiffness of an element is independent from its cross-section’s strength.
- The equal-displacement theory is always applicable.

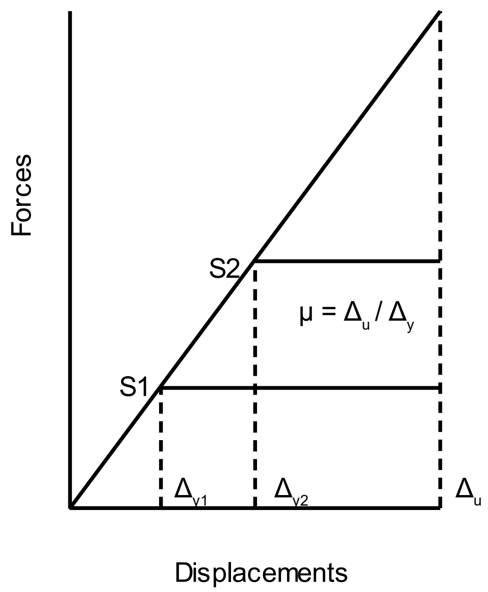

Figure 2.5 Incorrect relationship between force and displacement. Adapted from (Priestley, Calvi, et al., Displacement-Based Seismic Design of Structures 2008).

An 8-meter-high pier is given as an example, with flexural steel reinforcement ratio varying between 0.5% and 4.0%, taking as reference value 1.5%. The pier has a cross-section with a 1.8m diameter and a reduced axial force of 0.05, which is close to the expectable values for bridge piers. Figure 2.6, which is taken from (Priestley, Calvi and Kowalsky 2008), shows the effect of the variation of the flexural steel reinforcement, and consequently, the strength of the cross-section, on other characteristics such as available ductility.

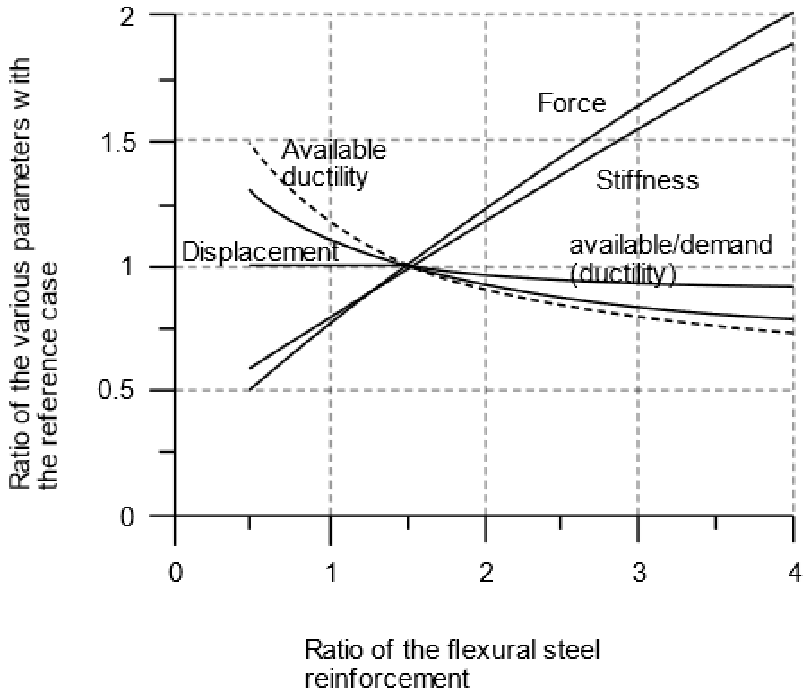

Figure 2.6 Values of displacement, available ductility, force, stiffness, and ductility demand for different values of flexural steel reinforcement ratio in percentages. The values are normalized by the reference case with 1.5% flexural steel reinforcement ratio. Adapted from (Priestley, Calvi, et al., Displacement-Based Seismic Design of Structures 2008).

An analysis of Figure 2.6 shows that force and stiffness are linearly correlated with the increase of flexural steel reinforcement. Regarding the available ductility, it is reduced with the increase in flexural steel reinforcement, which is later confirmed through the study of the influence of several RC cross-section properties on the values of yield curvature and ultimate curvature. With a flexural steel reinforcement (fsr) ratio of 0.5%, that ductile capacity is about 30% higher than that of the reference pier with an fsr of 1.5%. With an fsr of 4%, that same ductile capacity is 20% lower than the reference value. Consequently, the maximum allowed horizontal displacement follows the same trend as the ductile capacity, which corroborates the idea that the yield curvature is essentially independent from the fsr, since by keeping the yield curvature constant, the yield displacement also does not change and so it follows that if the available ductility is reduced, so must be the ultimate displacement of the pier. Thus, it becomes clear why the increase in strength of the cross-section is not necessarily a good solution when attempting to increase the seismic resistance of a structure. The reason is that, if the safety of a structure hinges on its ductility reserve, the increase in fsr precipitates some loss of that ductility. This can be verified in Figure 2.6, where there is an almost constant line that concerns the ratio between available ductility and ductility demand. This value is kept almost constant instead of reducing because besides the loss in ductility, the increase in fsr also precipitates a decrease of the imposed displacement of the earthquake, and so the ductility demand also decreases with the available ductility. Now, it was assumed that this pier belongs to a bridge whose period of vibration belongs to the interval of constant velocity of the earthquake spectrum, that is between 0.6 (for far-field events according to the Portuguese National Application Document to EC8, Part 1) and 2.0 sec. That way, the increase in stiffness due to the increase in fsr implies the decrease of the period of vibration, which in turn leads to an increase in the inertia forces but lower than the increase in stiffness, therefore it implies a decrease in the displacements the structure will have to withstand. This results in having an almost constant available ductility/ ductility demand ratio with only a slight decrease for larger values of fsr. From this, it can be concluded that there is no significant increase or decrease in the seismic resistance of the structure (measured by the seismic action the structure can withstand). In these conditions, with an increase of fsr, and so it follows that the fsr should not be increased with the explicit purpose of improving seismic performance, especially concerning critical piers and single DOF structures.

5) Necessity of development of seismic design methodologies

It is known that in the last few decades, seismic design has focused more on ductility and displacement demand. The design codes have been improved with the inclusion of rules concerning ductility, stiffness, and yield displacement estimation. These improvements have usually been made concerning displacements and ductility since the main shortcomings of design codes have usually concerned the assessment of both. Regardless, the main focus of most design codes remains associated to forces and strength, and the inclusion of ways to estimate ductility and effective stiffness plus the incorporation of nonlinear analysis as a posterior check fall into (Priestley, Calvi and Kowalsky 2008)'s definition of a "Force-Based/Displacement Checked methodology. However, these improvements alone are not sufficient to make an efficient and effective seismic design that addresses the real needs, economy of construction and seismic performance, if an adequate seismic assessment is not performed and an adequate design methodology is not employed, particularly concerning bridges.

2.2 Ductility of reinforced concrete (RC) elements subjected to imposed displacements

Ductility is an invaluable structural characteristic for the seismic performance of structures since without it most structures cannot withstand seismic actions because seismic actions often force structures to go into inelastic behaviour. Even for other actions, ductility is like a hidden reserve strength, as ductile structures have larger capacity to redistribute internal forces without collapse.

For many years, the traditional design assumption for the moment-curvature relationship has been that it is constant, regardless of the structure's strength, as the models are elastic. This incorrect perception is pointed out in (M. N. Priestley 2003) and (Priestley, Calvi, et al., Displacement-Based Seismic Design of Structures 2008) and implies that yield curvature depends on the section's strength, when in reality it doesn't. This has very important implications on ductility and earthquake resistance of RC structures, and is in the core of the methodology presented in this thesis. One of the implications is that more strength is not equivalent to more structural safety.

As mentioned previously, the objective of this thesis is to introduce a design optimization methodology that takes advantage of the ductility of structures to provide different design solutions for different bridge case-studies. For this, a correct assessment of what and how ductility is influenced by different characteristics and properties is essential. Ductility, at the cross-section level, is defined by the yield and the ultimate curvature. Both are assessed in this chapter, which is based on the work of (Brito 2011).

To assess the ductility of RC elements, in this section the analysis will be applied to a pier/column, fully restrained at the bottom and with a rotational restraint at the top, to which a displacement is imposed at the top, as shown in Figure 2.7. This column has a constant circular cross-section.

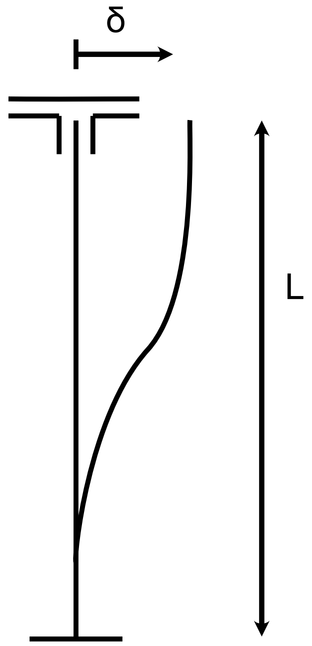

Figure 2.7 Column example with monolithic connection at both ends but subjected to imposed displacements at the top.

There is, of course, a relation between the imposed displacement at the top of the pier and the curvatures of the cross-sections at the pier's extremities. Thus, the curvatures can be thought of as externally imposed to the pier's cross-sections. Now, considering the column is not subjected to any axial force, it is possible to estimate the yield curvature of the cross-section by force equilibrium, assuming that the maximum strain in the fsr corresponds to the yield strain. By knowing the value of the curvature and the location of the neutral axis, the strain diagram of the cross-section is easily obtained, which then allows to calculate the stress in the materials in any point of the cross-section, as can be seen in Figure 2.8.

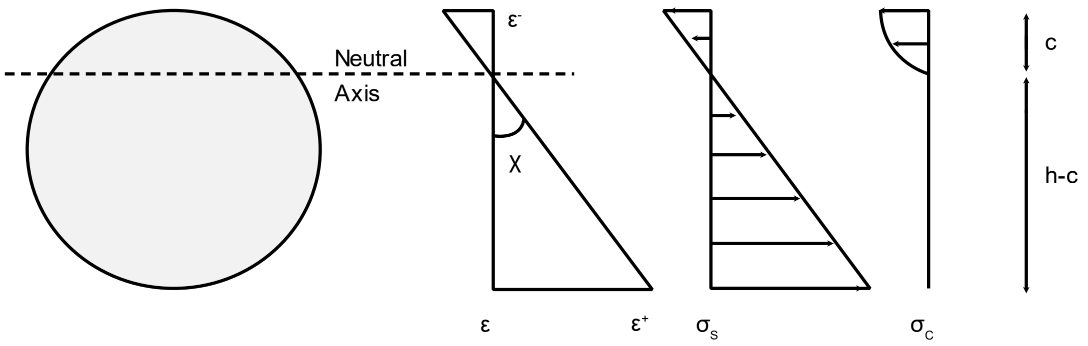

Figure 2.8 Position of the neutral axis at yield, and the stress and strain diagrams of the concrete cross-section.

The bending moment installed in the cross-section can be obtained through integration, from the following expression:

$$M = \int_{\Omega} \sigma\, y\, d\Omega \tag{2.6}$$

Through this approach, there are a few details that become apparent concerning the behaviour of RC elements subjected to imposed displacements:

- The position of the neutral axis almost does not vary with the variation of the cross-section's fsr, as long as the same distribution of the steel reinforcement is preserved in the cross-section. This can be confirmed by cross-section analysis.
- The material strain in the cross-section at yield depends essentially on the size of the cross-section in the bending plane, as long as the neutral axis' position does not vary significantly.
- From the two previous points, one can conclude that at yield there is no significant variation of the strain diagram when the fsr varies. As such, the stress diagram also does not vary.
- The previous points allow to conclude that the strain diagram and the yield curvature are independent from the fsr and independent from the yield bending moment. In fact, the yield bending moment is a property that depends on the amount of flexural steel reinforcement (fsr).

Considering all of these implications, one can be led to conclude that the current design process is based on applied forces and follows a logic that is an approximation, that at large deformations may be a gross approximation, because the design bending moment and fsr are dependent of each other, as moments depend on stiffness, which is a function of fsr, which depends on the bending moment.

In the traditional approach of seismic design:

- The design bending moment is an input for the analysis of the cross-section, obtained from the global structural analysis.
- The amount of fsr is then defined with the purpose of resisting that design bending moment.
- The curvatures and strain diagrams depend on the applied bending moment and the amount of fsr.

It is clear that this design logic is not compatible with interdependencies between fsr, stiffness, applied forces and ductility, and stems from the adaptation to seismic design of the design methodologies for other types of actions. If the design of a structure subjected to imposed displacements is done correctly and if the structure has enough ductility to sustain those displacements, then the structure does not even need resistance to inertia forces, as is the case with underground structures where the inertia forces are directly transferred to the surrounding soil by beams/slabs and peripheral walls.

In the case of above ground structures, there is need to resist inertia forces, and so the work performed in this thesis looks to balance ductility and strength, providing the best ways depending on the structure's characteristics. It will become clear that the amount of fsr in each pier can be somewhat arbitrary, as long as some conditions are respected. The same methodology also allows the design engineer to have some control over the structure, avoiding fsr distributions that either make the structure, or some columns, too stiff attracting too much horizontal forces, or too flexible to attract a relevant part of those horizontal forces, leading to damage in stiffer columns, or if it refers to all columns, lead to excessive horizontal displacements, causing excessive 2nd order effects.

The methodologies presented herein explore a few aspects of seismic design and dynamic behaviour of structures, which have to do with the ability of the structure to redistribute forces between elements with very different initial stiffness, the ability to respond differently to the same action due to different design approaches (different stiffness distributions). The effects on ductility and stiffness of a series of factors become apparent, as axial force, fsr, cross-section size, etc.

2.2.1 Analysis of a column subjected to imposed displacements

In this thesis, all of the case-studies have piers with circular cross-sections. The main reason is that circular cross-sections are ideal for bi-directional bending because circular cross-sections do not have principal directions of inertia due to radial symmetry. Regardless, there is little difference between the behaviour of circular and rectangular cross-sections in terms of ductility, and so all of the conclusions that are valid for circular cross-sections are also valid for rectangular cross-sections, except those where tensile reinforcement is concentrated in a single layer near the edge and with no web reinforcement, something that does not exist in real bridge columns. This is made clear in the work of (Brito 2011), and for that reason, in this section, a circular cross-section is used for the analyses, which concern the ability to accommodate displacements which are imposed through monotonic loading.

The distribution of flexural steel reinforcement (fsr) is radially uniform, and the cross-section is compact. Hollow cross-sections are not analysed, however, the qualitative differences between hollow and compact cross-sections are mentioned later on.

As mentioned, circular cross-sections are employed throughout this thesis and most of this section concerns circular cross-sections. However, for the first analysis two cross-sections, one circular (cross-section A) and one rectangular (cross-section B), are compared in terms of ductility. The objective is to show how steel distribution influences ductility, since the rectangular cross-section will only have fsr concentrated near the extreme fibres associated to a given bending direction. Of course, this fsr distribution is not common nor possible in most cases because the element has to have strength in both directions, but the example is, nonetheless, useful to have an idea of the effect that a shallow neutral axis has on ductility. This first analysis comparing cross-section A and B are taken from (Brito 2011). Concrete's constitutive relationship refers to confined concrete. In Figure 2.9, cross-sections A and B are presented, with their respective fsr distribution. The cover concrete was set at 6cm thick measured outward starting at the midpoint of the fsr. The strength of the cover concrete was discarded from the models. Figure 2.10 and Table 2.1 show the constitutive relationships for both concrete and steel, for this first example.

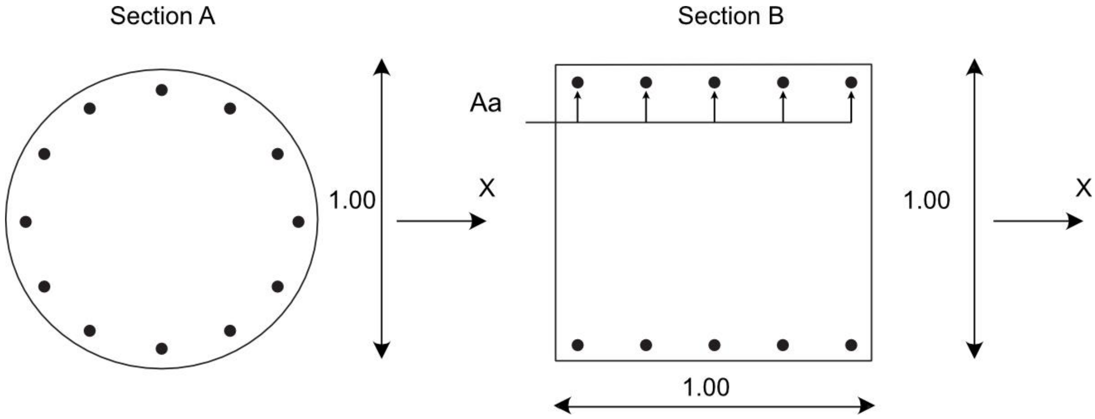

Figure 2.9 Cross-sections A (circular) and B (rectangular). In both, A_a corresponds to half of the flexural reinforcement area.

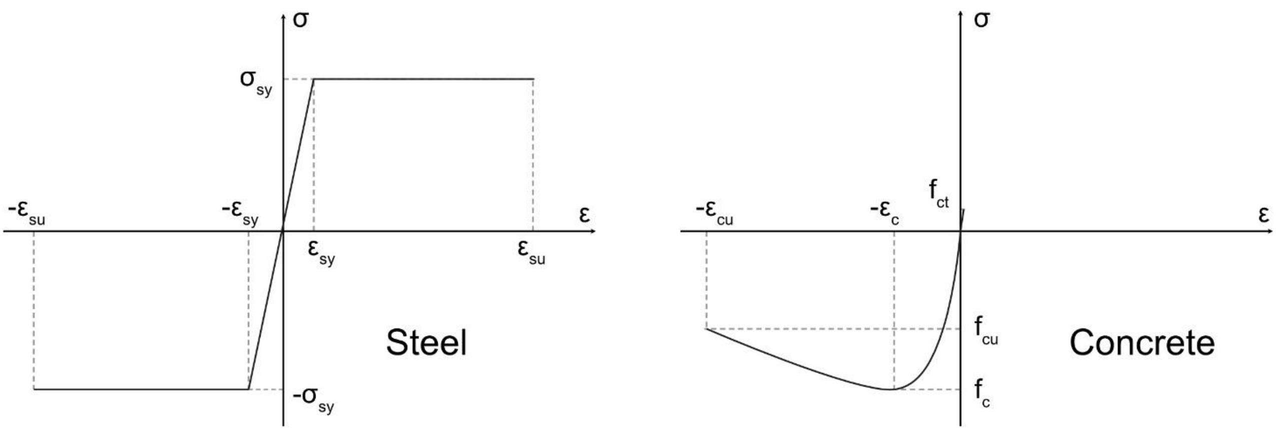

Figure 2.10 Steel and concrete constitutive relationships used in cross-sections A and B.

Table 2.1 Values for material properties used to build the constitutive relationships.

ε_{sy} (‰)	ε_{su} (‰)	σ_{sy} (MPa)
2.175	200	435

ε_{cy} (‰)	ε_{cu} (‰)	f_c (MPa)	f_{cu} (MPa)	f_{ct} (MPa)
2.0	15.0	35	25	0

For each type of cross-section, the author in (Brito 2011) performed the analysis for three different amounts of fsr, which are shown in Table 2.2, so that the effect that the amount of fsr has on the RC element's ductility becomes apparent. For both cross-sections, the distribution of the fsr is done according to the scheme in Figure 2.9, and the value of A_a in both Figure 2.9 and Table 2.2 corresponds to half of the total amount of fsr in both cross-sections A and B. The reason is to have a comparable amount of fsr in both cross-sections, since for cross-section B fsr is located near the edges in only one direction, while for cross-section A fsr is distributed radially.

Table 2.2 Amounts of flexural steel reinforcement used in both A and B cross-sections.

	Case 1	Case 2	Case 3
A_a (cm^2)	20	50	125
% fsr A	0,51	1,27	3,18
% fsr B	0,40	1,00	2,50

In Figure 2.11, the moment-curvature diagrams, for both cross-section cases and concerning all fsr quantities, are shown.

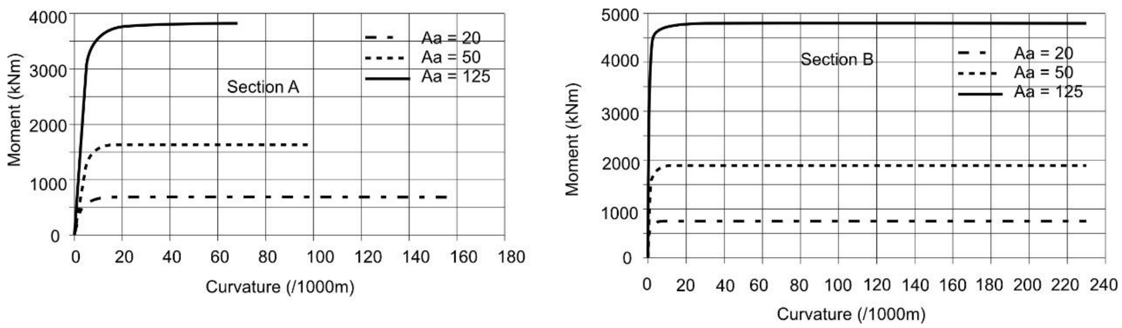

Figure 2.11 Moment-curvature diagrams of both cross-sections (A and B) reinforced with the reinforcement amounts given in Table 2.2.

It can be seen that the variation of the amount of fsr generates different results for both cross-sections. In the case of cross-section A, it is clear that the variation of the amount of fsr greatly influences the ultimate curvature. This effect stems from the increase of the depth of the neutral axis at rupture with the increase in the amount of fsr, due to that fsr being uniformly distributed around the cross-section. In the case of cross-section B, the fsr is concentrated near the extreme fibres of the cross-section, and as such, the compression force is almost entirely absorbed by the fsr which results in almost no variation of the ultimate neutral axis and, consequently, the ultimate curvature does not change, even though the strength of the cross-section varies proportionally. In the case of cross-section A, the increase in compression strength involves an increase in size of the cross-section's compressed zone, which affects the ultimate curvature since the increase of the neutral axis depth at rupture entails higher values of compressive strain in the concrete for the same value of curvature. It is concluded that, for cross-section A, the collapse criterium is excessive compressive strain in the confined concrete, due to a relatively larger compressed zone as the amount of fsr is increased, resulting in a decrease in the steel tensile strain. In fact, since the ultimate curvatures decrease with the increase in fsr, the conclusion is that the collapse is conditioned by the compressive concrete strain, at least in the two cases with more fsr. In cross-sections where the fsr distribution creates this tendency to increase the compressive zone with the increase in the amount of fsr, then such an increase is clearly a factor that reduces the cross-section deformation capacity. In Table 2.3, the results regarding the analysis of the moment-curvature diagrams are presented.

Table 2.3 Results for cross-sections A and B regarding bending moments, curvatures, depth of neutral axis, effective stiffness, etc.

Section A

Case	A_a (cm^2)	χ_y (‰/m)	χ_u (‰/m)	c_y (m)	c_u (m)	M_y (kNm)	M_u (kNm)	$\frac{EI_{sec}}{A_a}$ (MN)	$\frac{M_y}{A_a}$ (kN/m)	$\frac{M_u}{A_a}$ (kN/m)
1	20	3.104	160.535	0.179	0.093	472.24	685.89	76.07	236120	342945
2	50	3.391	97.238	0.239	0.154	1108.90	1615.89	65.40	221780	323178
3	125	3.772	67.577	0.303	0.221	2604.85	3751.29	55.25	208388	300103

Section B

Case	A_a (cm^2)	χ_y (‰/m)	χ_u (‰/m)	c_y (m)	c_u (m)	M_y (kNm)	M_u (kNm)	$\frac{EI_{sec}}{A_a}$ (MN)	$\frac{M_y}{A_a}$ (kN/m)	$\frac{M_u}{A_a}$ (kN/m)
1	20	2.870	229.029	0.122	0.008	716.28	765.36	124.78	358140	382680
2	50	3.105	229.335	0.179	0.009	1789.92	1914.05	115.29	357984	382810
3	125	3.444	229.641	0.248	0.009	4415.22	4785.02	102.56	353218	382802

The variables presented in the previous tables are the following:

χ_y – Yield curvature

χ_u – Ultimate curvature

c_y – depth of the yield neutral axis

c_u – depth of the ultimate neutral axis (related to the ultimate curvature)

M_y – yield bending moment

M_u – ultimate bending moment

EI_{sec} – effective stiffness at yield $\left(=\frac{M_y}{\chi_y}\right)$

In Table 2.3 it is clear that the neutral axis at yield and, consequently, the yield curvature doesn't undergo significant variations in both cases. In fact, a 525% variation in the amount of fsr originates a mere 21% variation in the depth of the yield neutral axis, while the yield bending moment varies proportionally with the fsr. Thus, it can be concluded that the yield curvature of the cross-section depends essentially on the steel's yield strain, cross-section's geometry and the distribution format of the fsr (and not its quantity). Figure 2.12 shows, more clearly, the effect of the variation of the fsr's amount on the value of the yield curvature. The two strain diagrams refer qualitatively to cases 1 and 3 from Table 2.2 and Table 2.3.

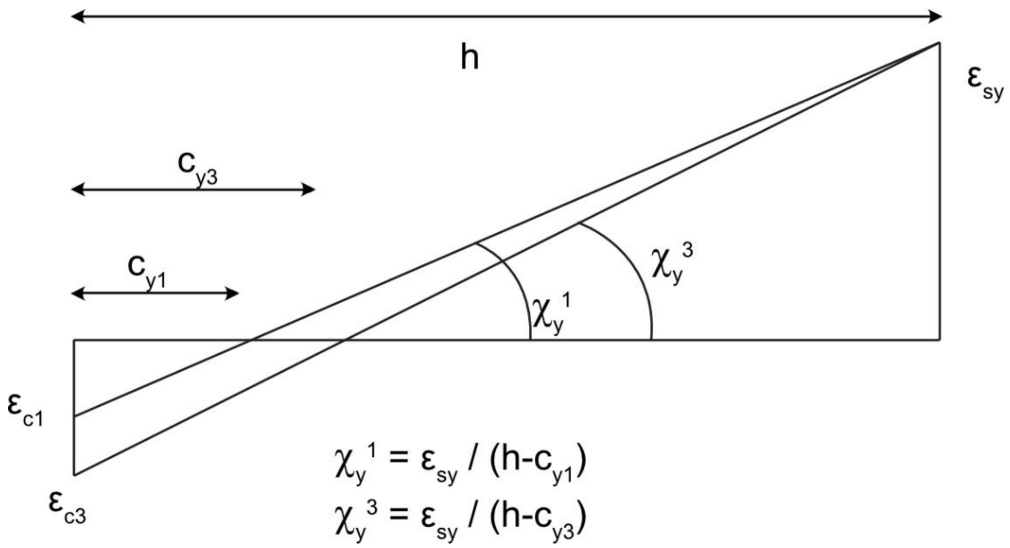

Figure 2.12 Strain diagrams for A_a cases 1 and 3 (Table 2.2 and Table 2.3)

Regarding Figure 2.13, it refers to the relationship between yield curvature and yield bending moment, and the subsequent link between yield stiffness and cross-section strength.

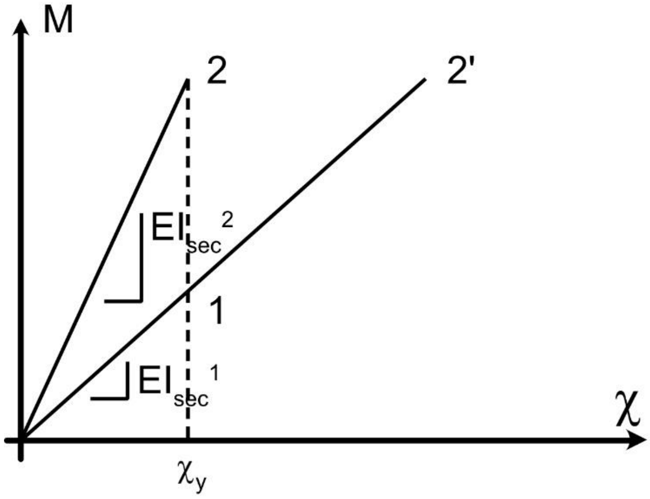

Figure 2.13 Relationship between yield curvature and yield bending moment and consequent link between yield stiffness and strength.

In Figure 2.13, point 1 represents yield for a given amount of fsr. By doubling the amount of fsr, the bending moment also doubles which, through a linear elastic analysis (LEA), takes us from point 1 to point 2', since $M = EI\chi$, and in a LEA EI is constant. What happens in reality is different, the strength of the cross-section increases in the same proportion as in the LEA case, however, the yield curvature does not change, which takes us to point 2. So, the key issue here is that the assumption that the cross-section's stiffness is independent from the amount of fsr, as it happens in LEA, is totally different from what happens in reality after initial cracking. The reason for this is that concrete cracking totally modifies the stiffness and position of the neutral axis and introduces the effect of the fsr in the cross-section's stiffness.

There is, nonetheless, a small variation of the yield neutral axis with the increase in fsr for both types of cross-sections. This slight variation has to do with the increase in the tension force at yield which has to be countered by an increase of the compressed zone/area. As a result, the tensioned zone is smaller, which leads to larger yield curvatures. Quantitatively, these values are different between both cross-section types because of their difference in shape and particularly in the distribution of fsr.

The rupture mode that is verified in cross-section A is due to excessive compressive strain in the concrete, for the two cases with more fsr. Conversely, for cross-section B, the rupture mode that takes place is by excessive tensile strain in the fsr. The concentration of the fsr close to the extreme fibres, in cross-section B, is what originates this difference in behaviour compared to cross-section A. The neutral axis depth at rupture in the case of cross-section B, which is always very shallow for every fsr amount ($c_u \approx 0$), has an impact on the ultimate curvature, resulting in a constant ultimate curvature value for any amount of fsr. This is in line with the ultimate curvature expression $\chi_u = \frac{\varepsilon_{su}}{h-c_u}$, from Figure 2.12, which for a constant c_u value (≈ 0) remains constant for a given cross-section. As for cross-section A, the variability in the ultimate curvature value results from a significant variability in the position neutral axis at rupture and subsequent variability in the value of c_u. In the case of cross-section A, the expression for the ultimate curvature, $\chi_u = \frac{\varepsilon_{cu}}{c_u}$, concerns the concrete compressive strain instead of the tensile steel strain. In real structures, it is more common to find this latter behaviour than the one seen for cross-section B. The simple fact that the seismic action can present itself in many directions, plus the need to design structures for other types of loads as well as code rules for the placement of fsr, means that it is usually not possible to have fsr distributions as in cross-section B, that is, only concentrated at the extreme fibres. As a result, ruptures from excessive tensile strain in the steel don't happen in practice for RC piers. The existence of axial compressive forces in the piers also increases the neutral axis depth and the tendency to rupture to take place on concrete and not on steel.

The most interesting result from this analysis might be perhaps what concerns the yield curvature due to the implications that this result has regarding the current seismic design methodology. As mentioned before, the yield curvature, $\chi_y = \frac{\varepsilon_{sy}}{h-c_y}$, has almost no variation with the variation of the amount of fsr, which results from the invariance of the location of the neutral axis at yield (c_y), for reasons already referred to. The implication of this is that it is not possible to avoid the yield of a cross-section by varying the amount of fsr when the action is imposed displacements. Therefore, a structure designed with a unitary behaviour factor, or as a Low Ductility structure according to EC8, will go into yield for the same imposed displacement as a High Ductility structure designed with a higher behaviour factor (assuming equal cross-section shape and size). The consideration of the results for cross-section A led to conclude that the increase in fsr, is not necessarily correlated with an increase in resistance for seismic actions, quite the contrary, due to the reduction of available ductility. The other conclusion is that an RC element can be designed with any amount of fsr as long as the group of RC elements has enough resistance to sustain the inertia forces.

Another factor that influences the capacity to accommodate displacements is the size of the plastic hinge/s that form/s in the RC element. This size has to do, among other things, with the constitutive relationship of the steel, particularly with the post-yield hardening and the ratio between σ_{su} and σ_{sy}.

A few ideas can be reinforced with this example. First, it becomes clear that the available ductility depends on the amount of fsr. As such, it is not possible to design a structure that will be subjected to imposed displacements, without before assuming an initial amount of fsr, necessary to evaluate the member stiffness, which in turn is necessary for global analysis. This results in a type of iterative design procedure in which the fsr in each cross-section is part of the input and not only part of the output. Another notion is that cross-sections with larger amounts of fsr are less ductile, and so it is not a very good idea to attempt to increase the resistance of an RC element to imposed displacements by increasing its strength through the inclusion of a larger amount of fsr, since that is not beneficial in terms of the element's global ductility.

In general terms, the procedures that can improve the ductility of an RC element, up to this point, are:

- Increasing the capacity of the RC cross-section to accommodate larger compressive strains (increase the ductility) by ways of adequate confinement.
- Decrease the depth of the cross-section's neutral axis, via concentrating the fsr close to the extreme fibres.
- Not increasing the depth of the neutral axis through the inclusion of more fsr, with the objective of resisting imposed displacements.

In the case of bridges, the second point can be difficult to manage, since piers have to have fsr for bending in both directions, not only due to the possibility of the seismic action in both directions, but also due to the existence of other loads and actions such as temperature, and creep and shrinkage in the concrete. As for the first point, it is the most fundamental point regarding the ductility of RC cross-sections, and will be mentioned throughout the thesis. In fact, ductility of RC cross-sections is only possible if the cross-sections are adequately confined. As for the third point, it is attained indirectly by ways of seismic design optimization and consequent improvement in the distribution of the fsr among piers.

However, it should be taken into account that the decrease in the amount of fsr is only possible to a certain point, which concerns the ability of the element to resist the permanent loads and the structure as a whole to resist the seismic inertia forces. As such, the definition of how much inertia force the element has to resist and the size of the cross-section are of big importance, since the cross-section's size is more influential to the element's ductility than the decrease in depth of its neutral axis.

In the following section, an analysis on the several factors that influence the ductility of a RC element are studied individually.

2.2.2 Factors that influence the ductility of an RC element

It has been said that the core of the approach that is suggested in this thesis is the ability of RC elements to sustain imposed displacements, in other words, the ductile capacity of RC elements. In the previous section, some characteristics have been presented that influence the ductility of RC elements. In the following section, other factors that influence ductility of RC elements are presented and studied.

The ductile capacity of RC elements depends, essentially, on the following factors:

- Shape and size of the cross-section

- Strength of the materials and ultimate strain of concrete
- Distribution of flexural steel reinforcement (fsr) and the ratio between the fsr under compression and the fsr under tension.
- Axial force
- Relation between the steel's ultimate stress and yield stress and post-yield stiffness
- Shear force
- Slope of the descending part of the concrete's constitutive relationship

It is easy to understand that the first four points can be studied through analysis of a cross-section. In the first point, concerning the cross-section's shape, has already been partially discussed, and will not be further pursued. The reason is that the two most common cross-sections for bridges have already been analysed and, in this thesis, only circular cross-sections are considered in the case-studies. This is representative of other cross-section shapes, as in real situations part of the flexural reinforcement is distributed between the extreme fibres of the flexural plane. However, regarding the cross-section's size, it will be shown that its variation, in the bending direction, affects the ductile capacity of an RC element significantly, even more so than the fsr.

The analysis of the other points will be done resorting to the presented column example, in Figure 2.7. The shear force effects and the effects concerning the slope in the concrete's constitutive relationship are approached qualitatively. Before initiating the analysis on the influence of the cross-section's size on its ductility, it is important to mention that the concrete compressive strain and its ultimate value define the cross-section's ability to deform, and the exceedance of said ultimate value constitutes the criterium for collapse, both in these analyses and throughout the rest of the thesis. Therefore, whichever the factor being studied, its impact on ductility has to do with that factor either affecting the concrete's ultimate compressive strain or affecting the depth of the critical cross-section's neutral axis.

Since ductility is the ratio between ultimate curvature and yield curvature, the following study on the impact of several factors on ductility is divided into two sections, the first concerning the impact on the yield curvature and the second on the ultimate curvature.

2.2.2.1 RC cross-section's yield curvature

The yield curvature of a RC cross-section depends mostly on the cross-section's shape and size, normalized axial force value and the steel reinforcement's yield strain. The steel reinforcement's yield strain depends on the quality of the steel. That will not be varied since A500 NR SD steel will be used in all test cases and case-studies, as it is the type of steel that is generalized in civil construction.

Mean values were adopted for all material properties, which are presented in the following table.

Table 2.4 Material properties used in the constitutive relationships of concrete and steel.

Concrete (C30/37)	
f_{cm} (MPa)	38
E_{cm} (GPa)	33
ε_c (unconfined) (‰)	3.5
Steel (A500NR)	
f_{ym} (MPa)	585
E_{ym} (GPa)	200
ε_{su} (‰)	94

Also, since the study is being performed always considering circular cross-sections in the piers, the size of the cross-section and the normalized axial force in each pier are the main factors that influence the yield curvature.

2.2.2.1.1 Cross-section's size

The larger the cross-section diameter is, the lower the corresponding yield curvature. The yield curvature, contrary to past beliefs in seismic engineering, is almost invariant for a given cross-section, if the variation of axial force is reduced. In fact, in EC8 - part 2 annex C (CEN 2005), which addresses the estimation of the effective stiffness of RC ductile members, there is an expression for the approximation of the yield curvature of RC circular sections. This expression only depends on two variables, yield strain of the steel (ε_{sy}) and section diameter (d):

$$\phi_y = 2.4.\varepsilon_{sy}/d \tag{2.7}$$

In Table 2.5, the influence of the diameter of the RC circular cross-section on the yield curvature is shown. Two values of the yield curvature are shown for each diameter: ϕ_y, is the curvature value at the stage in which the steel's yield strain of 2.925‰ is reached in the steel reinforcement; $\phi_{y,EC8}$, corresponds to the curvature given by equation (2.7) is reached. In the same table, the ratio between the variation of ϕ_y and the variation of the diameter value, is presented.

Table 2.5 Influence of the diameter of the RC circular cross-section on the yield curvature.

D (m)	**1.2**	**1.6**	**2**	**2.4**
D-cover (D_{core}) (m)	**1.14**	**1.54**	**1.94**	**2.34**
% long. Steel reinf.	1.50%	1.50%	1.50%	1.50%
v (norm. Axial F.)	0.15	0.15	0.15	0.15
ε_{sy} /1000	2.925	2.925	2.925	2.925
$\phi_{y,EC8}$	6.16	4.56	3.62	3.00
ϕ_y	4.66	3.46	2.76	2.29
variation ϕ_y		-26%	-41%	-51%
variation D_{core}		35%	70%	105%
Rate (var Φ_y/ var D_{core})		73.7%	58.3%	48.3%

In Table 2.6 and Table 2.7, the closest points relating to Φ_y and $\Phi_{y,EC8}$ were taken from the results of a non-linear analysis. These tables show the values of the coefficient, which in equation (2.7) is equal to 2.4. They also show bending moment, compressive concrete strain, tensile strain in the steel, yield curvature, neutral axis depth (d_c), etc.

Table 2.6 Results relative to yield curvature calculated with cross-section analysis.

D_{core} (m)	Coef eq. 1	ε_c ‰	ε_y ‰	ϕ_y	d_c (m)	d_c/D_{core}
1.14	1.84	-2.42	2.98	**4.73**	0.511	0.448
1.34	1.83	-2.41	2.95	**4.00**	0.602	0.450
1.54	1.82	-2.40	2.93	**3.46**	0.694	0.451
1.74	1.87	-2.45	3.01	**3.14**	0.782	0.449
1.94	1.86	-2.45	2.98	**2.80**	0.874	0.451
2.14	1.85	-2.45	2.97	**2.53**	0.968	0.452
2.34	1.86	-2.47	2.99	**2.33**	1.059	0.453

Table 2.7 Results relative to yield curvature calculated with the equation (2.7) found in EC8 - part 2.

D_{core} (m)	ε_c ‰	ε_y ‰	$\phi_{y,EC8}$	d_c (m)	d_c/D_{core}
1.14	-2.9	4.1	**6.17**	0.471	0.413
1.34	-2.9	4.2	**5.35**	0.551	0.411
1.54	-2.9	4.1	**4.58**	0.637	0.413
1.74	-2.9	4.2	**4.08**	0.720	0.414
1.94	-2.9	4.1	**3.63**	0.807	0.416
2.14	-3.0	4.2	**3.37**	0.885	0.414
2.34	-2.9	4.0	**2.94**	0.986	0.421

In Figure 2.14, both yield points are presented on the capacity curves of the 7 cross-sections with varying diameter.

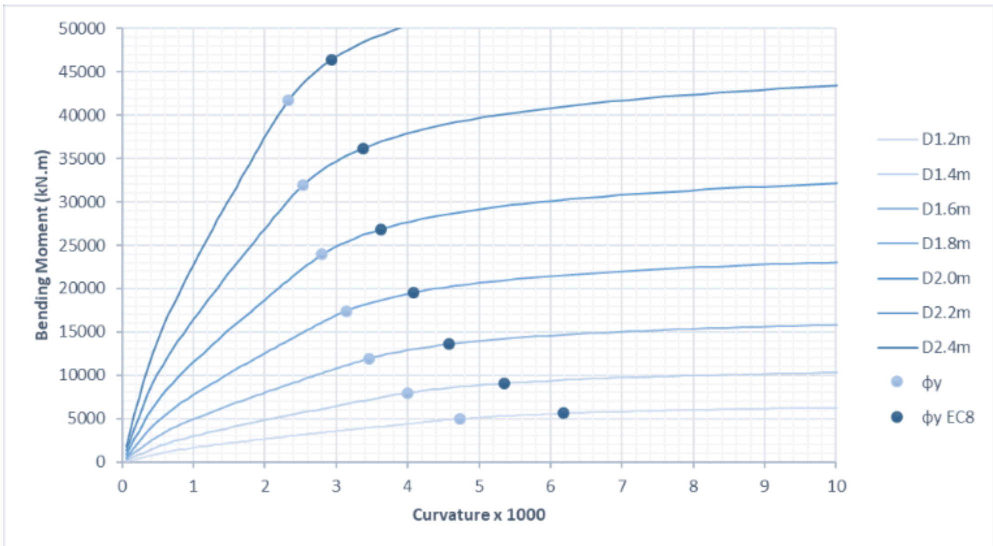

Figure 2.14 Locations of the yield curvatures, ϕ_y and $\phi_{y,EC8}$, on the capacity curves of cross-sections with different diameters.

The value of the coefficient, in the second column of Table 2.6, corresponds to the coefficient value for equation (2.7), which originally takes the value of 2.4, in order to obtain the curvature value in column 5 of Table 2.6. The values are all very similar and again the fluctuation in results is due to the step discretization, which makes it difficult to select the point where the exact strain value of 2.925‰ is obtained. Nonetheless, the values obtained are almost constant but lower than the value of 2.4 in equation (2.7). In Figure 2.15, both yield points are presented in graphs that show the variation of the cross-section stiffness (M_y/χ_y) with the curvature values (χ_y), for two section diameters. It is clear that the two points seem to represent the start of yield, ϕ_y, and the end of yield, $\phi_{y,EC8}$, since both define, roughly, the start and end of the plot segment with largest stiffness variation.

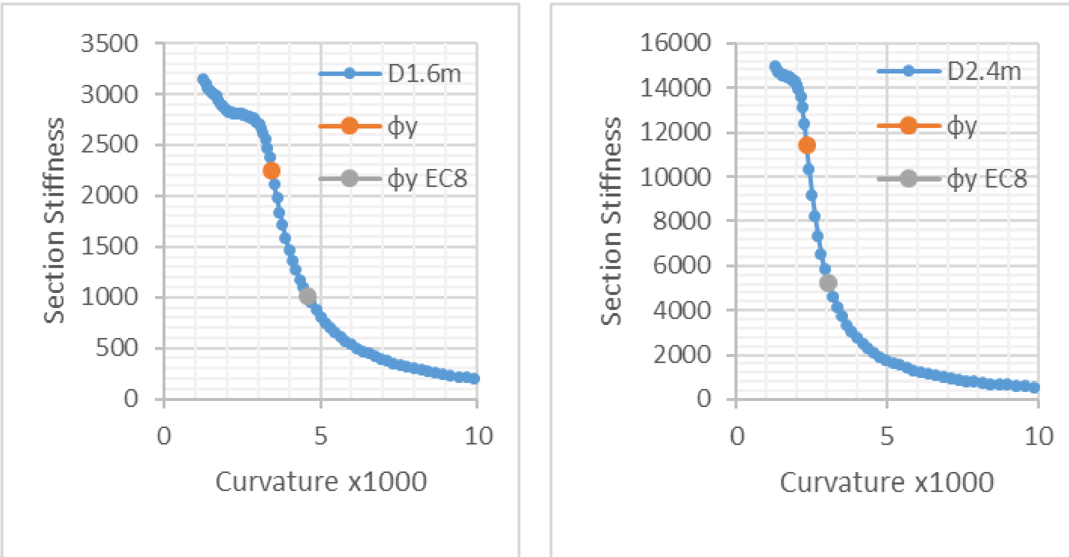

a) b)

Figure 2.15 Variation of the cross-section stiffness against curvature values. a) Cross-section diameter equals 1.6m; b) Cross-section diameter equals 2.4m.

2.2.2.1.2 Axial force in the element

An increase in the normalized axial force has a negative effect on ductility due to, among other effects, an increase of the depth of the neutral axis, as the yield curvature increases as the normalized axial force increases. However, this effect is not as noticeable as the effect of the cross-section's size, for the usual normalized axial force values present in bridge piers, i.e., under 0.3. We can see this in Table 2.8, where the yield curvature variation is shown in a cross-section where the only changing variable is the normalized axial force, which ranges from 0.05 to 0.3.

Table 2.8 Yield curvature variation in a cross-section with fixed diameter and varying normalized axial force.

D (m)	1.6	1.6	1.6	1.6
D_{core} (m)	1.54	1.54	1.54	1.54
% lsr	1.50%	1.50%	1.50%	1.50%
v (axial F.)	**0.05**	**0.1**	**0.2**	**0.3**
ε_{sy} ‰	2.925	2.925	2.925	2.925
$\phi_{y,EC8}$ ‰	4.558	4.558	4.558	4.558
ϕ_y ‰	3.02	3.24	3.64	4.05
var ϕ_y		7%	20%	34%
var v		100%	300%	500%
Rate (var ϕy/var v)		7.1%	6.8%	6.8%

In Figure 2.16, both yield points are shown on the capacity curves, one for each value of the normalized axial force. In a) the cross-sections have 1.6m diameter and in b) they have 2.4m diameter. Since equation (2.7) does not contemplate axial force, the value for $\phi_{y,EC8}$ does not vary between cases with the same diameter. In Figure 2.17, ϕ_y is plotted against the normalized axial force, for diameters 1.6m and 2.4m. It is clear that the variation is the same. This can be added to equation (2.7), in order to contemplate axial force in the yield curvature estimation, resulting in equation (2.8).

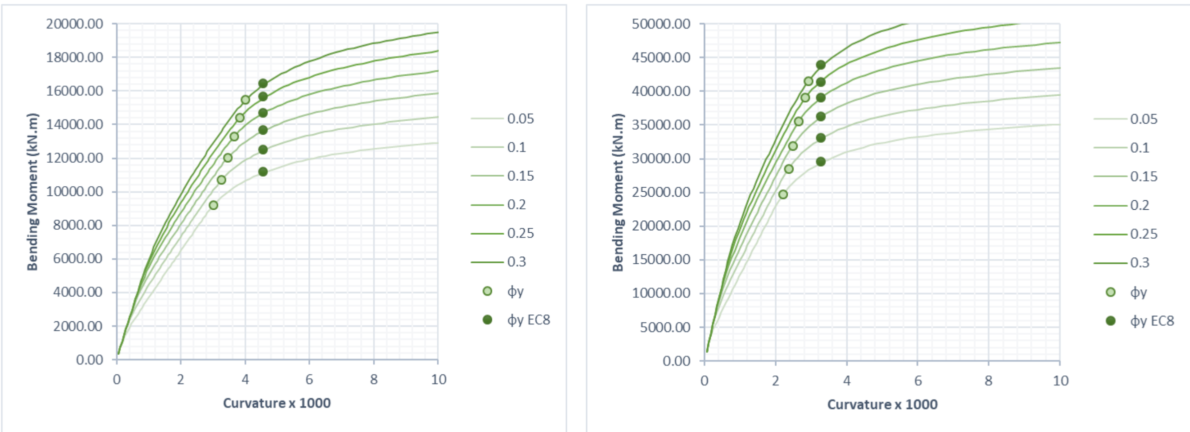

a) b)

Figure 2.16 Locations of the yield curvatures on capacity curves of sections with varying normalized axial force. a) Cross-section diameter equals 1.6m; b) Cross-section diameter equals 2.4m.

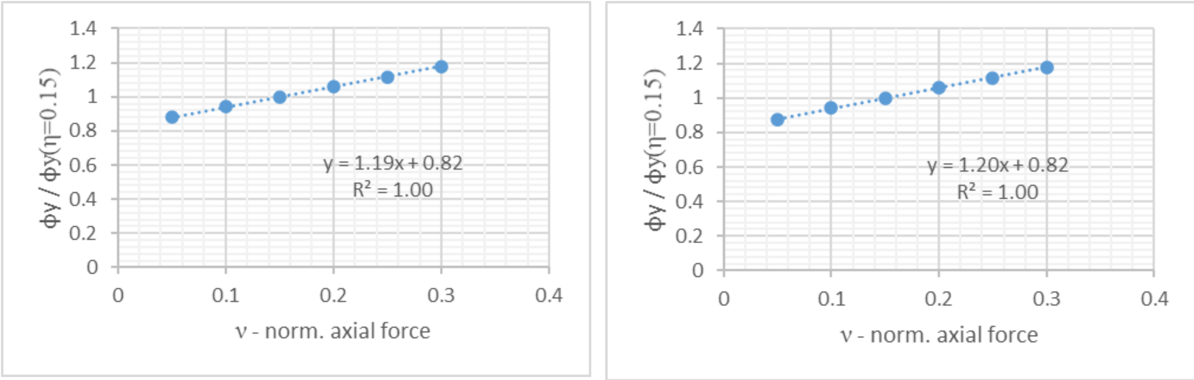

a) b)

Figure 2.17 Variation of the yield curvatures against normalized axial force. a) Cross-section diameter equals 1.6m; b) Cross-section diameter equals 2.4m.

$$\phi_y = (1.2\nu + 0.82) \cdot 2.4 \cdot \varepsilon_{sy}/d \quad (2.8)$$

Where *v* is the normalized axial force.

2.2.2.1.3 Ratio of steel flexural reinforcement in the RC cross-sections at the plastic hinge locations

The ratio of the longitudinal steel reinforcement has a very big influence on the cracked stiffness of the cross-section and almost no effect over the cross-section's yield curvature. In the next analyses, the ratio of the longitudinal steel reinforcement is the variable, while all other values are kept constant. In Table 2.9, the main results are shown. One can see that in this case the rate of variability ranges from 1.49% to 0.98%, which clearly shows that the longitudinal steel ratio has a very small effect on the yield curvature of the cross-section. In Figure 2.18 both yield points are plotted on each capacity curve for the different cases.

Table 2.9 Yield curvature variation in a cross-section with fixed diameter and varying percentage of longitudinal steel reinforcement (%lsr).

D	1.6	1.6	1.6	1.6	1.6
D_{core} (m)	1.54	1.54	1.54	1.54	1.54
% lsr	**0.60%**	**1.00%**	**2.00%**	**3.00%**	**3.50%**
v (axial F.)	0.15	0.15	0.15	0.15	0.15
ε_{sy} ‰	2.925	2.925	2.925	2.925	2.925
$\phi_{y,EC8}$ ‰	4.56	4.56	4.56	4.56	4.56
ϕ_y ‰	3.37	3.40	3.47	3.51	3.53
var ϕ_y		1.00%	2.88%	4.19%	4.72%
var %lsr		67%	233%	400%	483%
Rate(varϕ_y/ var%lsr)		1.49%	1.23%	1.05%	0.98%

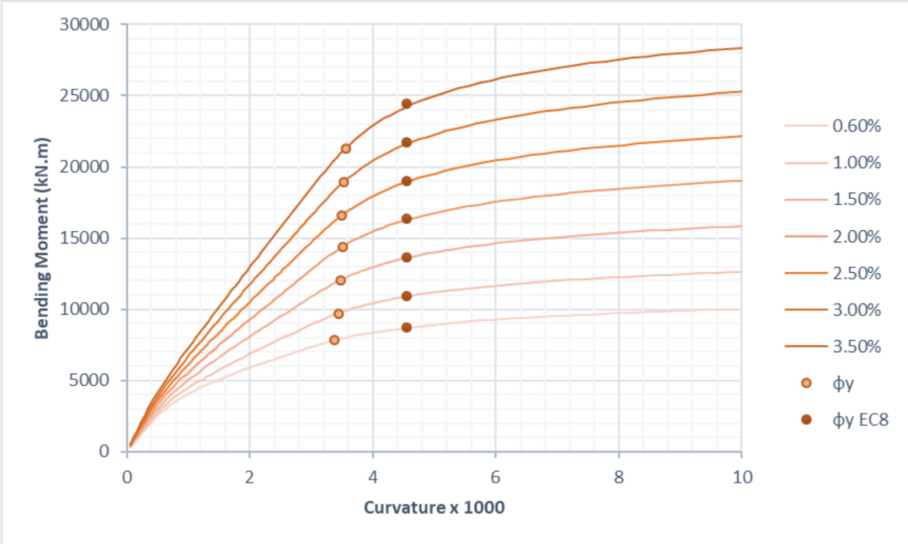

Figure 2.18 Locations of the yield curvatures on capacity curves of sections with varying percentage of longitudinal steel reinforcement.

2.2.2.2 RC cross-section's ultimate curvature

2.2.2.2.1 Cross-section's size

Besides influencing its yield curvature, the RC cross-section's size also influences its ultimate curvature. Comparing cross-sections with increasing diameters, and constant values of normalized axial force and longitudinal steel reinforcement ratio, as the cross-section's diameter increases the depth of the neutral axis increases proportionally, which results in smaller curvature values for the same compressive concrete strain value obtained at the most compressed fibre. In Table 2.10, the variables are presented, with the results for ultimate curvature and an analysis on the rate of variation of the ultimate curvature with the cross-section's diameter.

Table 2.10 Variation of ultimate curvature of a circular RC cross-section with varying of the cross-section's diameter.

D (m)	1.2	1.4	1.6	1.8	2	2.2	2.4
D-cover (m)	**1.14**	**1.34**	**1.54**	**1.74**	**1.94**	**2.14**	**2.34**
% long. Steel reinf.	1.50%	1.50%	1.50%	1.50%	1.50%	1.50%	1.50%
v (norm. Axial F.)	0.15	0.15	0.15	0.15	0.15	0.15	0.15
ε_{cu}	-0.02	-0.02	-0.02	-0.02	-0.02	-0.02	-0.02
ϕ_u /1000	72.46	63.06	55.69	49.66	44.80	40.93	37.67
variation ϕ_u		-13%	-23%	-31%	-38%	-44%	-48%
variation D-cover		18%	35%	53%	70%	88%	105%
Rate (var ϕ_u/var D-cover)		73.9%	66.0%	59.8%	54.4%	49.6%	45.6%

The rate shows similar values to the rate in Table 2.5, which is related to the impact on the yield curvature.

In Table 2.11, the ultimate curvature for each cross-section diameter is presented along with the ratio between ultimate curvature and both yield curvatures.

Table 2.11 Ratio between ultimate curvature and yield curvature for varying values of cross-section diameter.

D-cover (m)	ϕ_y /1000	$\phi_{y,EC8}$ /1000	ϕ_u /1000	ϕ_u/ϕ_y	$\phi_u/\phi_{y,EC8}$
1.14	4.73	6.17	72.46	15.32	11.74
1.34	4.00	5.35	63.06	15.78	11.79
1.54	3.46	4.58	55.69	16.09	12.15
1.74	3.14	4.08	49.66	15.82	12.16
1.94	2.80	3.63	44.80	15.99	12.35
2.14	2.53	3.37	40.93	16.17	12.14
2.34	2.33	2.94	37.67	16.16	12.83

Figure 2.19 is the same graph as Figure 2.14 but “zoomed out” to show the entire capacity curves, and to get a better idea of the variation of the cross-section’s ultimate curvature due to varying the diameter. It is clear that the cross-section’s diameter has a large influence on the ultimate curvature in addition to the large influence on the yield curvature.

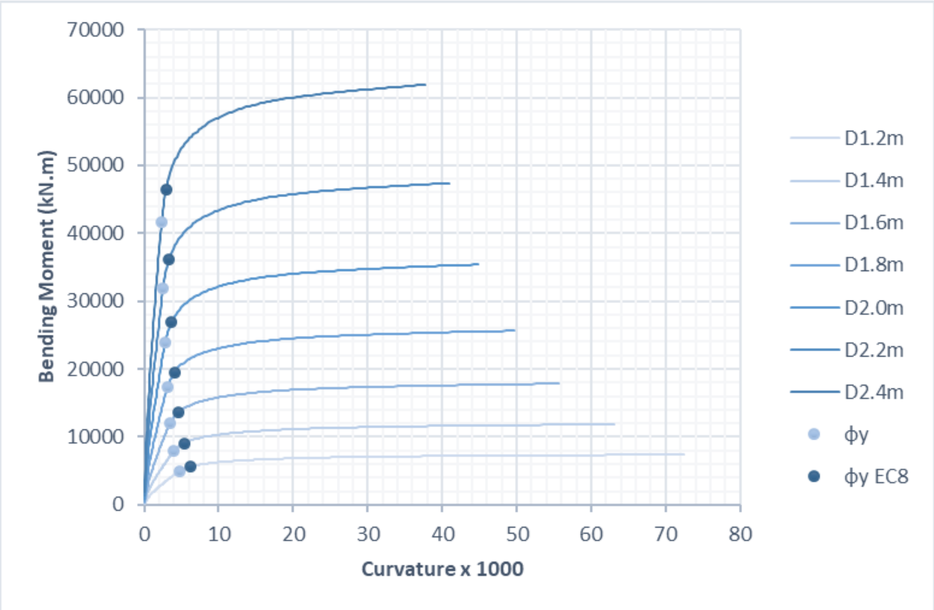

Figure 2.19 Capacity curves from Figure 2.14 with ultimate curvatures visible.

2.2.2.2.2 Axial force

Axial force has a negative influence on ductility mainly due to the negative influence on the ultimate curvature of an RC cross-section. This effect is due to the increase in the depth of the neutral axis, because of the increase in the size of the compressive zone necessary to increase the resultant of compressive stresses due to the applied axial force. This increase in the depth of the neutral axis means that for the same values of curvature there is an increase in the maximum compressive strain at the compressed fibres that are furthest away from the neutral axis. In RC cross-sections, subjected to bending and without significant shear effects, the concrete's ultimate compressive strain is the main collapse criterium, and is almost always more determinant than the ultimate strain of the flexural steel reinforcement, since these strain values are almost 10%, while the concrete's ultimate compressive strain, even when well confined, seldom reaches 2%. In Table 2.12, the results for ultimate curvature and an analysis on the rate of variation of the ultimate curvature with the normalized axial force are presented, for a section with D=1.6m and 1.5% longitudinal steel reinforcement.

Table 2.12 Ultimate curvature variation in a cross-section with fixed diameter and varying normalized axial force.

D (m)	1.6	1.6	1.6	1.6	1.6	1.6
D-cover (m)	1.54	1.54	1.54	1.54	1.54	1.54
% long. Steel reinf.	1.50%	1.50%	1.50%	1.50%	1.50%	1.50%
ν **(norm. Axial F.)**	**0.05**	**0.1**	**0.15**	**0.2**	**0.25**	**0.3**
ε_{cu}	-0.02	-0.02	-0.02	-0.02	-0.02	-0.02
ϕ_u /1000	69.14	61.22	54.33	49.36	44.72	41.49
variation ϕ_u		-11%	-21%	-29%	-35%	-40%
variation v		100%	200%	300%	400%	500%
Rate (var ϕ_u/var v)		-11.5%	-10.7%	-9.5%	-8.8%	-8.0%

In Table 2.13, the ultimate curvature for each normalized axial force value is presented along with the ratio between ultimate curvature and both yield curvatures.

Table 2.13 Ratio between ultimate curvature and yield curvature for varying values of normalized axial force.

ν **(norm. Axial F.)**	ϕ_y /1000	$\phi_{y,EC8}$ /1000	ϕ_u /1000	ϕ_u/ϕ_y	$\phi_u/\phi_{y,EC8}$
0.05	3.03	4.67	69.14	22.83	14.79
0.1	3.27	4.65	61.22	18.71	13.16
0.15	3.47	4.62	54.33	15.64	11.76
0.2	3.66	4.58	49.36	13.50	10.79
0.25	3.84	4.67	44.72	11.65	9.58
0.3	4.02	4.63	41.49	10.33	8.95

Figure 2.20 shows a set of graphs composed by capacity curves where the axial force is varied. It is very clear the compressive axial force's negative effects on the ultimate curvature of the circular RC cross-section.

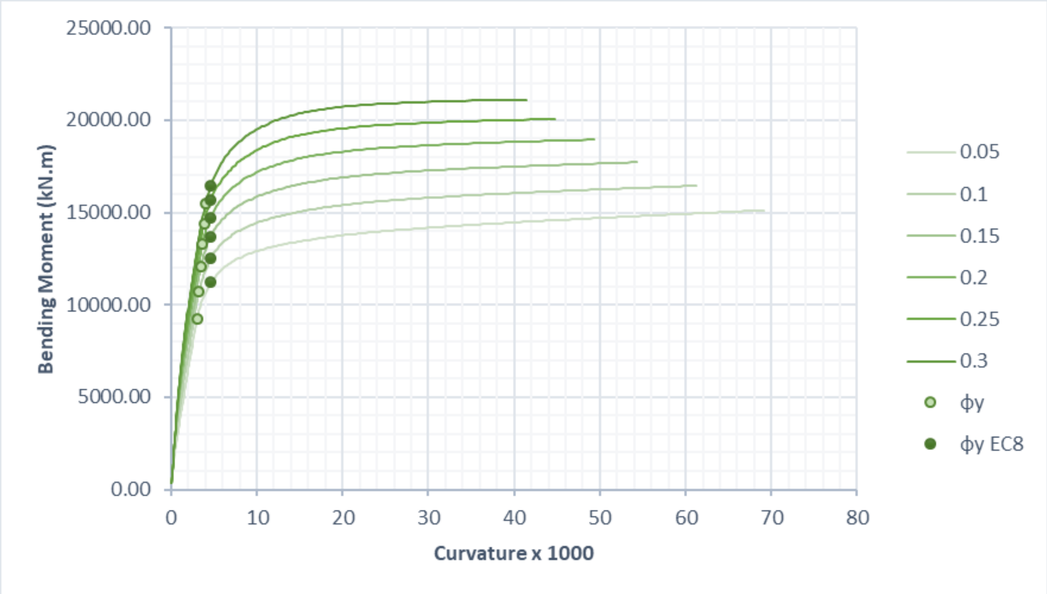

Figure 2.20 Capacity curves from Figure 2.16a) with ultimate curvatures visible.

2.2.2.2.3 Ratio of steel flexural reinforcement in the RC cross-sections at the plastic hinge locations

The amount of steel flexural reinforcement in RC cross-sections has a significant effect on ductility. This does not happen due to influence on the yield curvature, which has been shown that it has very little effect, but because of the effect on the ultimate curvature. In Table 2.14, analysis results for ultimate curvature and an analysis on the rate of variation of the ultimate curvature with the percentage of longitudinal steel reinforcement are presented.

Table 2.14 Ultimate curvature variation in a cross-section with fixed diameter and varying percentage of longitudinal steel reinforcement.

D (m)	1.6	1.6	1.6	1.6	1.6	1.6	1.6
D-cover (m)	1.54	1.54	1.54	1.54	1.54	1.54	1.54
% long. Steel reinf.	**0.60%**	**1.00%**	**1.50%**	**2.00%**	**2.50%**	**3.00%**	**3.50%**
v (norm. Axial F.)	0.15	0.15	0.15	0.15	0.15	0.15	0.15
ε_{cu}	-0.02	-0.02	-0.02	-0.02	-0.02	-0.02	-0.02
ϕ_u /1000	64.64	59.46	54.33	51.20	48.74	46.65	45.12
variation ϕ_u		-8.01%	-15.95%	-20.79%	-24.60%	-27.83%	-30.20%
variation %lsr		67%	150%	233%	317%	400%	483%
Rate (var ϕ_u/var %lsr)		-12.02%	-10.63%	-8.91%	-7.77%	-6.96%	-6.25%

In Table 2.15, the ultimate curvature, for each case of longitudinal steel reinforcement percentage is presented along with the ratio between ultimate curvature and both yield curvatures.

Table 2.15 Ratio between ultimate curvature and yield curvature for varying values of longitudinal steel reinforcement.

% long. Steel reinf.	ϕ_y /1000	$\phi_{y,EC8}$ /1000	ϕ_u /1000	ϕ_u/ϕ_y	$\phi_u/\phi_{y,EC8}$
0.60%	3.38	4.56	64.64	19.10	13.91
1.00%	3.44	4.56	59.46	17.30	12.86
1.50%	3.47	4.56	54.33	15.64	11.76
2.00%	3.51	4.56	51.20	14.60	11.04
2.50%	3.50	4.56	48.74	13.91	10.59
3.00%	3.52	4.56	46.65	13.24	10.11
3.50%	3.56	4.56	45.12	12.69	9.68

In Figure 2.21, the graphs show capacity curves of cross-sections where only the amount of flexural steel reinforcement is varied.

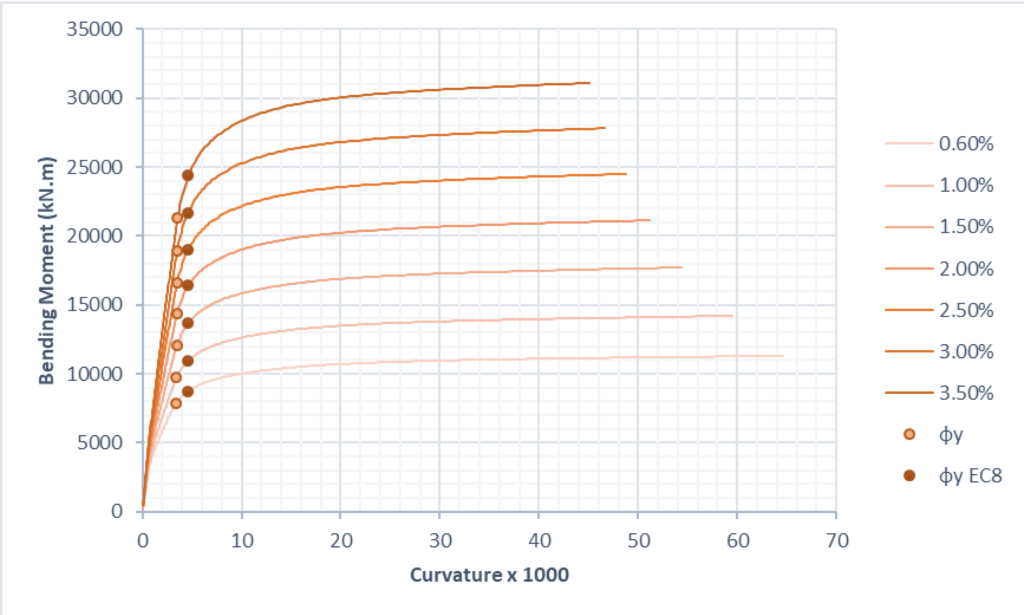

Figure 2.21 Capacity curves from Figure 2.18 with ultimate curvatures visible.

The reason why the ultimate curvature is reduced with the increase of the flexural steel reinforcement is because, analogous to what happens with the increase in compressive axial force, the plastic neutral axis depth is increased.

The compressed area of the RC cross-section is smaller than the tensioned area, since concrete has very low tensile resistance. By increasing the amount of flexural steel reinforcement homogeneously along the cross-section's perimeter, more steel will be placed in the tensioned area of the cross-section, which means that the compressed area must increase due to internal force equilibrium, resulting in an increase in depth of the neutral axis from cracking to rupture, and a subsequent reduction of the ultimate curvature.

2.2.2.2.4 Strength of concrete and steel

Starting with the effect of concrete quality, for most concretes used in construction the ultimate strain is ε_{cu} = 0.0035 for all types of concrete, but for very high strength concretes (f_{ck} > 50Mpa) there is a reduction in ε_{cu} (CEN 2005). Therefore, the analyses presented in this thesis are restricted to the most common used concretes. In this framework it can be stated that the concrete strength has no influence on the ability of the RC element to withstand compressive strains.

With a stronger concrete there is a reduction of the depth of the neutral axis, which results in an increase in ductility. The reason is that stronger concrete needs less area to have the same resulting compression force. On the other hand, this conclusion cannot be extrapolated for confined concrete, since with the increase in concrete strength, there is a reduction in ultimate concrete strain. This happens because with a stronger concrete the confinement is less effective.

Regarding the steel, the use of stronger steel allows to increase the strength of structural elements, thus allowing to have more slender elements. However, the use of high resistance steel, also increases the tensile force of the fsr, which for internal force equilibrium in the cross-section implies an increase in depth of the neutral axis, which results in a loss in ductility. This point shows that it is not good practice to use high strength steel with low strength concrete, while the opposite (strong concrete and weak steel) is not necessarily bad. However, to have slender elements with good capacity to resist the inertia forces it is important to use steel with good strength. In this case, there should be an equilibrium, and there isn't a criterion or an expression to obtain the ideal formulation. A good starting point is not using strong steel with weak concrete and vice-versa, pursuing a middle ground solution. As already referred to, in the analyses presented in this thesis only steel A500 is considered.

In Figure 2.22, the complexity of the impact of concrete and steel strength on ductility is described with a flow chart.

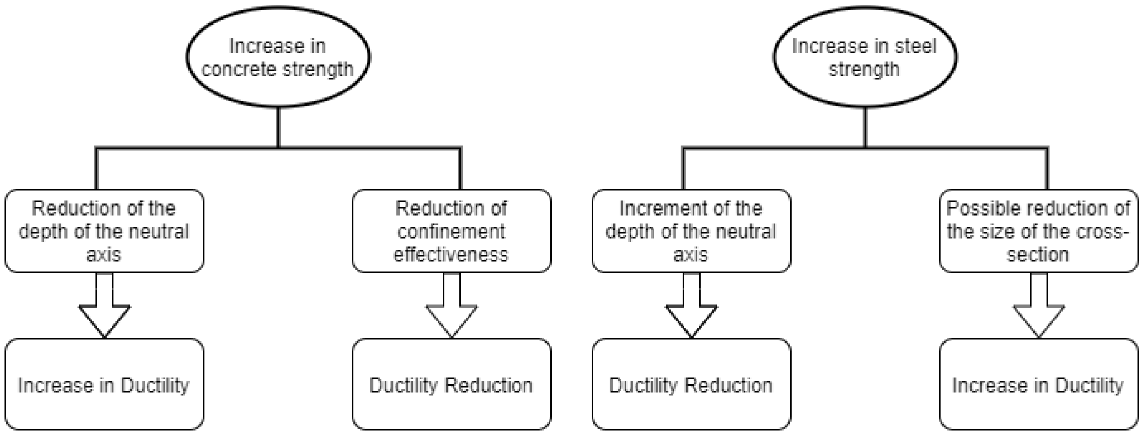

Figure 2.22 Flowchart explaining the effects on ductility of increasing the strength of concrete and steel

2.2.2.2.5 Shear force

As a general rule, RC elements in bridges, namely piers, have large length to cross-section height ratios, L/h, which avoid the influence of shear effects in ductility and deformation. There are, however, some (few) situations where the design leads to having bulky piers, owing this essentially to topographic impositions and bridge typology. In such cases, shear can have an important influence on the ductility of those elements and, consequently, on the bridge's ductility.

The influence of shear force can be measured through the shear ratio $\lambda = \frac{M}{Vh}$, in which h is the cross-section's height in the direction of the shear, and M and V refer to the critical section, usually at bottom and top of the pier. For elements that are not very slender, in the deformation plane, the λ parameter has a low value due to large shear forces. Such cases have the following effects:

- Reduction of the length of the plastic hinge which reduces its ability to accommodate deformations and to dissipate energy.
- Reduction of the area inside hysteretic loops due to pinching effects, further reducing the energy dissipation capacity.
- The tendency to originate ruptures by shear at smaller curvatures than the ultimate curvature. As such, a high amount of shear force can reduce the local ductility of structural elements. In RC elements with compact cross-section, adequate amount of transversal steel reinforcement, and moderate to low axial force, it is unlikely to occur rupture by shear for λ > 3.

For circular sections, as the ones employed in the thesis, there is the following relation:
For υ = 0.2 and fixed/monolithic connections:

$$\frac{\delta s}{\delta b} = \frac{\frac{FL}{GA_s}}{\frac{FL^3}{3EI}} = \frac{1.8}{4}\frac{D^2}{L^2}\ , where\ D = h,\quad \frac{\delta s}{\delta b} = \frac{0.45}{\left(\frac{L}{h}\right)^2} \tag{2.9}$$

For a length 3 times the height of the cross-section, that in piers with fixed connection on top and compact cross-section leads to λ = 3, the value of the shear displacement is 5% of the displacement due to bending.

As such, in well-conceived bridge structures, where λ > 3 for all piers, shear has little influence in the structure's behaviour, and disregarding the shear deformation means that only a slight underestimation of the available deformation capacity is being inserted in the model. Since nonlinear flexural deformation mechanism for plastic hinges is the most ductile mechanism for RC elements, every effort should be made to avoid going into plastic behaviour due to other forces and mechanisms. To that end, the principles of Capacity Design should be a main concern for structural design.

2.2.2.2.6 Slope of the descending portion of the concrete's constitutive relationship.

The constitutive relationship for confined concrete often includes a descending branch after maximum stress is attained, related to larger compressive strains. This descending branch is due to the degradation of the concrete at large strains, which has obvious influence on the RC element's ductility since this degradation induces an increase in the depth of the neutral axis, which, as already discussed, reduces the ultimate curvature of the cross-section. The absolute value of the slope of this descending branch can be reduced through the increase in confinement. Therefore, confinement improves ductility, not only due to the increase of the ultimate concrete strain, but also due to the slower decrease in concrete strength in the descending branch of the constitutive relationship.

2.3 Bridge characterization by length, irregularity, and types of deck cross-section. Indexes for irregularity and length.

It has been realized after past earthquakes that the direction of bridge movement and the nature of the damage to bridges is highly dependent on the bridge's geometry and irregularity. The irregularity issue has been substantially addressed in regard to buildings, however, concerning bridge design, this issue is still in development (Akbari and Maalek 2018). In a general sense, bridge irregularity has two sources: a) plan irregularity and b) pier length irregularity. In this thesis, only the latter is considered. The observations made during past earthquakes have been sufficient to indicate that even bridges with severe irregularities, due to geometrical characteristics and general configuration, may survive the design earthquake, provided that special care is exercised in the design process. Therefore, geometry is one of the most important parameters in the process of bridge design. The author of (Smith 2005) investigated the real response of the bridges that had been damaged in Northridge due to severe plan irregularities. He concluded that careful considerations are needed in the case of plan irregularity resulting from skew, taper and/or curvature.

An important cause for irregularity, and the one studied in this thesis, results from different stiffness of supporting vertical elements, such as piers, along the length of the bridge. Regarding this type of irregularity, some works have been done, especially concerning a specific class of multi-span reinforced concrete bridges with regular and irregular configurations and different degrees of irregularity. This type of bridge, and these studies have resulted in the development of many key concepts in the seismic analysis and design of bridges over the last two decades (Kappos, Saiidi, et al. 2012) (Kohrangi, Bento and Lopes 2015). The bridges analysed in this thesis are also multi-span reinforced concrete bridges and are similar in terms of typology as these bridges, however the methodologies and goals of this thesis are significantly different than that of the work that has been developed so far.

In effect, regarding the composition, goals and general theme of the past studies concerning this bridge typology (multi-span RC bridges), most of the literature can be divided into the analysis of three main categories: (a) the effect of higher modes and its reflection on the adequacy of different analysis methods for irregular bridges, (b) the development of the displacement-based design methodology for irregular bridges, and (c) investigating the seismic behaviour of irregular bridges that have seismic isolation or energy dissipation devices.

The work proposed and performed in this thesis does not fit into any of the three aforementioned categories. In fact, the goal of the thesis is to present techniques to aid and improve the design of irregular bridges, and the themes studied in each of the three categories are mentioned only qualitatively. Regarding (a), in this thesis the decision went essentially towards the use of nonlinear dynamic analysis (NDAs), and only in the longitudinal direction were nonlinear pushover analyses (NPAs) used. NDAs are the types of analysis that provide more reliable results with the drawback of requiring a larger amount of time. However, once the time issues are overcome, there is no reason to use another type of analysis method. Nonetheless, the findings of past works on the adequacy of different techniques concerning different irregularities are mentioned. As for (b), in fact displacement-based design has seen significant evolution in the past two decades, however its nature and the unfamiliarity of design engineers to the precepts of displacement-based design still makes it unpopular for use in industry. Furthermore, the methods are not without drawbacks, especially for long irregular bridges. In the case of (c), there have been many studies and real-world applications of seismic isolation and energy dissipation devices to bridges, however it is not easy to perform studies about the influence of such devices due to the unwillingness of most companies that develop these products in sharing the technical specifications and prices of their products which hinders the ability of performing cost-benefit analysis. Regardless, the study of how irregularities influence dynamic behaviour and how to design piers considering the dynamic behaviour is useful for the design with energy dissipation devices. Such devices are thus only mentioned qualitatively in this thesis.

Central to this thesis is the definition of whether a bridge is short or long, regular or irregular. Regarding irregularity, there are many definitions, and it can be associated to either dynamic behaviour, mechanical properties, such as position of the centre of stiffness in relation to the centre of mass, or merely a visual assertion based on the existence of piers with different lengths and their position along the bridge. The length can also influence whether a bridge is regular or irregular depending on the regularity definition being used, for example, if the regularity definition concerns the dynamic behaviour then length is a factor. In addition to the definition of regularity, the definition of whether a bridge is long or short is one of the central issues studied in this thesis, because as will become clear, the definition of a bridge as long or short is important to the design of the piers. There are several indexes that can be used to define either regularity or bridge length category (short/long) and some of them will be applied in this thesis, with one in particular being central to the work. In the following sections, the definition of regular and irregular bridges is further explored, and the regularity indexes are presented. After that, a linear elastic seismic analysis is performed on a set of bridges with varying characteristics, and two indexes are used to interpret the results, RP (Regularity Parameter) and RSI (Relative Stiffness Index). Section 2.3 closes with two sections, one concerning the actual categorization of bridges according to irregularity and length, which will be used throughout the thesis. The last section refers to the admissibility of different seismic analysis methods regarding bridge length and type of irregularity.

2.3.1 Definition of regular and irregular bridges

Various definitions for regularity of bridges have been proposed and as previously mentioned they follow different criteria, however they are all based on a similar concept, which is to differentiate bridges which have a THDP similar to a parabolic shape, or in other words, essentially dependent on a first vibration mode, from others in which the dynamic behaviour is reasonably influenced by upper modes. In the following a few definitions from the literature are mentioned, however it should be said that the definition in this thesis follows more of a visual definition of regularity mixed with some criteria from these following definitions.

1) A bridge is considered regular, according to (Akbari and Maalek 2010), (Fischinger 2003), (Isakovic and Fischinger 2000) and (Isakovic, Fischinger and Kante 2003), if its responses from different analysis methods do not show significant differences. Hence, irregular bridges comprise all those whose response shows significant differences between different analysis methods. This is in line with the inadequacy of simplified methods to be applied for the analysis of irregular bridges, due to not being able to capture their behaviour. In Section 2.3.4, the eligibility of different methods for bridges with certain types of irregularity is analysed.
2) A bridge is considered regular if its dynamic behaviour is not affected by the contribution of higher modes consisting of components acting in the same direction, (Akbari and Maalek 2010), (Fischinger and Isakovic 1999), (Isakovic and Fischinger 2005), (Isakovic and Fischinger 2006), (Isakovic, Fischinger and Kante 2003), (Isakovic, Lazaro and Fischinger 2008) and (Maalek, Akbari and Maheri 2009). Conversely, for irregular bridges the effect of higher modes on the response is usually considerable. This is very much related with the previous point, since simplified methods of analysis are only based on the first vibration mode, and that is the reason why such methods are not eligible to be applied to irregular bridges. However, this definition is somewhat flawed since very long bridges with pier regularity can show significant influence of higher modes on its dynamic behaviour.
3) A bridge is considered regular if the centre of mass of the structure coincides with its centre of stiffness. In these cases, the translational modes of vibration dominate the seismic response in the transverse direction and the rotational ones (rotations about a vertical axis) are not excited, thus not participating in the seismic response. By contrast, an irregular bridge's dynamic behaviour is composed by both translational and rotational modes of vibration, (Alvarez Botero 2004) and (Restrepo 2006). However, this definition of irregularity is not valid for bridges with symmetric irregularities regarding the centre of mass, and so it is a definition that is not general by any means. Furthermore, short bridges with asymmetric irregularities that have a dynamic behaviour similar to a first vibration mode due to the high stiffness of the deck relatively to the stiffness of the piers, would count as irregular even though its dynamic behaviour would be defined as regular according to the two previous points.

4) A bridge is considered regular if its modal shapes (taken from the elastic modal analysis) do not show significant differences from the corresponding modal shapes of the associated bridge without the piers' resistance in the transverse direction. This definition is related to one of the most well-known regularity indexes, which is presented in the next section and is also employed in this thesis, the Regularity Parameter (RP).

Most of the modern codes for the seismic design of bridges allow the use of a wide range of methods for the seismic analysis of bridges, from very simple elastic to very sophisticated inelastic methods. The simpler methods include uniform load (UL), single mode (SM) and multi-mode (MM) analysis while the sophisticated methods include various types of nonlinear static pushover analysis (SPA) methods as well as nonlinear dynamic analysis (NDA) using time-histories. The discussion concerning the types of seismic analysis that can be employed depending on the type of irregularity, takes place in a further section.

Concerning the issue of regularity, Eurocode 8, Part 2 (CEN 2005) uses "moment demand to moment capacity" ratios to somewhat guarantee simultaneous failure of piers of different heights on irregular bridges. This criterium is commented on in the chapter that concerns the study of the behaviour factors for RC bridges.

In the next section, different regularity indexes are presented among which are the two which are employed in this thesis.

2.3.2 Indexes for irregularity and length

In (Akbari and Maalek 2018) a comprehensive description of the state-of-the-art of regularity parameters is made and the following is based on that work. There are various regularity indexes that have been proposed by different authors, and most of them refer to techniques that perform operations on the eigen-vectors of the bridge's vibration modes, usually comparing the predominant modes of the bridges with and without piers. For example, the regularity parameter (RP) proposed by (Calvi, Elnashai and Pavese 1994) compares the dominant mode of vibration of a deck without the piers, with the dominant modes of the whole bridge (with the piers). The proposed index, RP, is computed as follows:

1.
$$RP = \sqrt{\frac{\sum_{i=1}^{n}(\phi_i^A M \phi_i^B)^2}{n}} \tag{2.10}$$

Where ϕ_i^A and ϕ_i^B are, respectively, the ith normalised eigen-vector corresponding to the entire bridge (referred to as the model A) and the normalised eigen-vector corresponding to the deck without piers (model B). M and n are, respectively, the mass matrix of the deck and the number of modes. The presented expression ranges from 0 to 1, where the value of 0 happens with an irregularity profile that causes the bridge's real modes to be completely different of the modes of the same bridge without piers (same deck in this case), and 1 where there is total correspondence between the bridge's modes with and without piers. A bridge is therefore deemed as regular if the RP value is close to 1. The modes that should enter the expression are the modes that combined account for more than 95% of the bridge's mass.

In the continuation of this study, a new index was proposed (Calvi and Pavese 1997) by subtracting the norm of the products of the off-diagonal terms to increase the sensitivity of the above index as follows:

2.
$$RP_1 = 1 - \frac{\sum_{i=1}^{n}\sum_{j=1}^{n}\left[\left(1-\delta_{ij}\right)\left|\phi_i^A M \phi_i^B\right|\right]}{n} \tag{2.11}$$

Where δ_{ij} is the Kronecker delta, which is equal to 1 if i=j and 0 otherwise.

An improvement of this index would be to consider the higher modes' effects and the expected frequency content of the input excitation. Therefore, further attempts have been made, starting from the assumption of knowing a desired displacement shape of the bridge. This is the case when a displacement-based approach is used, and a target deformed shape has been defined. The following equation has been proposed (Calvi and Pavese 1997):

3.
$$RP_2 = 1 - \frac{\sqrt{\sum_{i=1}^{n}(y_i - z_i)^2}}{\sqrt{\sum_{i=1}^{n}(y_i)^2} + \sqrt{\sum_{i=1}^{n}(z_i)^2}} \tag{2.12}$$

Where $y_i = \frac{\phi_i^T M \upsilon}{\phi_i^T M \phi_i}$ so that $\upsilon = y_1\phi_1 + y_2\phi_2 + y_3\phi_3 + \cdots$ and $z_i = \beta_i S_{di}$, where β_i , S_{di} and ϕ_i are, respectively, the ith modal participation factor, the ith spectral displacement and the ith eigen-vector of the whole bridge. Also, υ is the vector of the imposed displacements. In this index, the regularity has been quantified on the basis of the difference between a vector containing the product of modal mass and spectral amplification and a vector containing the coefficients producing the target deformed shape, when applied to the modes. For linear elastic responses, the index will assume a value close to 1 for regular bridges and would tend to 0 for irregular bridges.

However, when considering nonlinear behaviour, the previous index might not work correctly, because the index does not consider the strengths of the piers, and for irregular bridges some piers might penetrate significantly into nonlinear behaviour while others do not. To solve this issue, another index is proposed including a measure of the difference between the yield strength of the piers and the associated force that would be reached. The following expression was proposed in (Calvi and Pavese 1997):

4.
$$RP_3 = 1 - \frac{1}{2}\left[\frac{\sqrt{\sum_{i=1}^{n}(y_i - z_i)^2}}{\sqrt{\sum_{i=1}^{n}(y_i)^2} + \sqrt{\sum_{i=1}^{n}(z_i)^2}} + \frac{\sqrt{\sum_{i=1}^{m}(V_i - k_{ei}\Delta_{ei})}}{\sqrt{\sum_{i=1}^{m} V_i^2}}\right] \tag{2.13}$$

Where to the previous expression an additional part was added with V_i, k_{ei} and Δ_{ei} being, respectively, the yield strength of the ith pier or the isolator (if present), the elastic stiffness of the ith isolator and the yield displacement of the ith isolator.

Another type of regularity index (the previous four were of the same type) compares the seismic responses of a reference bridge in the transverse direction calculated according to different simplified elastic or inelastic analysis methods. The work (Isakovic and Fischinger 2000) presents two such regularity indexes which are calculated as the relative difference between the areas bounded by the displacement lines of the first and second iteration of the SM or the inelastic N2 (nonlinear static pushover analysis) methods. The difference in the response obtained is defined as the relative difference of areas bounded by the envelopes of the relative displacement lines. There are variations or extensions on the concept, for example, in (Akbari and Maalek 2010) the concept was extended to compare the areas defined by the displacement profile of two bridges, one representing a predefined regular bridge and the second being the bridge under investigation, both under the same seismic action. Another extension of the concept compares the displacement profiles between different analysis methods. The three types are presented respectively as 5, 6 and 7.

5.

$$Index^{SM}(elastic) = \frac{|A_1^{SM} - A_2^{SM}|}{|A_2^{SM}|} \tag{2.14}$$

$$Index^{N2}(inelastic) = \frac{|A_1^{N2} - A_2^{N2}|}{|A_2^{N2}|}$$

6.

$$I_1 = Index^{UL}(A,B) = \frac{|A_1^{UL} - B_1^{UL}|}{|B_1^{UL}|} \tag{2.15}$$

$$I_2 = Index^{SM}(A,B) = \frac{|A_1^{SM} - B_1^{SM}|}{|B_1^{SM}|}$$

7.

$$I_3 = Index^{UL-SM} = \frac{|A_1^{UL} - A_1^{SM}|}{|A_1^{UL}|} \tag{2.16}$$

$$I_4 = Index^{SM-MM} = \frac{|A_1^{SM} - A_1^{MM}|}{|A_1^{SM}|}$$

In the above expressions, A and B are, respectively, the areas bounded by the displacement profile associated with the bridge being analysed and the predefined regular bridge.

In (Maalek, Akbari and Maheri 2009) the authors investigated the applicability of the modal assurance criteria (MAC) and the modal scale factor (MSF), which are well recognised for modal correlation of structural responses, for irregular bridges. The formulas for the indexes based on both methods are (8), for MAC, and (9) for MSF:

8.

$$MAC(A,B,n) = \sqrt{\frac{\sum_{i=1}^{n}\left(\left|\phi_i^{A^T}\phi_i^B\right|^2 / \left(\phi_i^{A^T}\phi_i^A\right)\left(\phi_i^{B^T}\phi_i^B\right)\right)^2}{n}} \tag{2.17}$$

9.

$$MSF(A,B,n) = \sqrt{\frac{\sum_{i=1}^{n}\left(\phi_i^{A^T}\phi_i^B / \phi_i^{A^T}\phi_i^A\right)^2}{n}} \tag{2.18}$$

Finally, and very different from the previous indexes, there is the relative stiffness index (RSI), proposed by (Priestley, Seible and Calvi 1996) that measures the ratio between the stiffness of the deck (K_d) and the stiffness of the piers (K_p) of a bridge. The way this relates to irregularity is that the lower the stiffness of the deck regarding that of the piers, the more susceptible the bridge is to irregularity. The RSI has a very simple expression given by:

10. $$RSI = \frac{K_d}{\sum K_p} \tag{2.19}$$

This RSI index is used in the next section, applied to a large set of bridges that are subjected to elastic MM (multi-mode) analysis, alongside the RP index (1). Both expressions are explored more in depth in the next section and particularly the RSI, due to its ease of computation and the usefulness of its results, is employed throughout the entire thesis.

2.3.3 Identifying bridge length categories based on the influence of its piers to the deck's transverse horizontal displacement profile.

In this section the goal is to identify different case studies of concrete bridges that represent well different irregularities and length categories, which the design engineer can be faced with. Regarding the analysis in the transverse direction, the bridges can be divided into three main categories: short bridges, long regular bridges and long irregular bridges, according to their dynamic behaviour. The main difficulty with the definition of these categories is to define a few aspects: first, what is a short bridge and what is a long bridge, and by extension how easily are these two categories differentiated; second, how many different types of irregularities can we find in long bridges, how can these irregularities influence dynamic behaviour, and how can they be addressed in the framework of optimization.

To answer the first question, a short bridge is a bridge where the piers have very little or no influence on the transverse horizontal displacement profile of the deck, whereas a long bridge is defined as the opposite. In a short bridge, the deck has a relatively high stiffness (inertia around a vertical axis) in comparison to the piers in relation to horizontal transversal displacements and, for that reason, it is the deck that controls the movement of the bridge. A third group, the very short bridges could be defined: these would be the group in which the deck would control not only the horizontal displacement profile but also the amplitude of the profile. This means in practical terms that in this group of bridges the columns are only necessary to resist vertical loads while undergoing the horizontal displacements on top induced by the deck. In a long bridge, the deck is relatively slender and has relative low stiffness as compared to the piers, and so the piers control the horizontal transversal displacements of the deck, with the exception of the zones in the vicinity of the abutments, assuming that transversal displacements are restricted at these locations. In this thesis only short and long bridges are studied.

A bridge can be short/long in an absolute manner or in a relative manner. An absolute short bridge is a bridge that is short regardless of the stiffness that the piers, with a given fixed geometry, present. This means that if a bridge is categorized as being short using the full elastic stiffness of the piers, i.e., without appointing to the pier's stiffness reduction due to cracking or yielding, then the bridge is short. By extension, a bridge is absolutely "long" if its behaviour is categorized by "long" when the piers are assigned a stiffness equivalent to the secant stiffness of the piers at their maximum/ultimate horizontal displacement.

A bridge can also be relatively short and relatively long. In this case, the bridge's behaviour is of a long bridge when the piers have full elastic stiffness, and as the piers loose stiffness due to cracking and yielding the bridge's behaviour becomes closer to one of a short bridge where the deck has control over the transverse horizontal displacements.

Another way to identify a bridge's length category is by the percentage of inertia force that are distributed to the abutments. In a short bridge, most of the horizontal transversal inertia force is transferred to the abutments, while in a longer bridge a smaller percentage is. This is so, due to the relevance of the piers' stiffness in the horizontal dynamic behaviour in both cases. The difficulty in this situation is defining what percentage of inertia force transferred to the abutments defines the upper boundary of a long bridge, or the lower boundary of a short bridge.

As mentioned previously, two of the regularity indexes presented in the former section are used to characterise the irregularity of bridges. The two parameters are, as mentioned earlier, the RP (regularity parameter) and the RSI (relative stiffness index).

The regularity parameter (RP), as the name entails, measures the bridge's regularity by correlating the configuration of the vibration modes of the bridge with and without piers. Going further from the equation in the previous section:

$$RP = \sqrt{\frac{\sum_{j=1}^{n}\left(\left(\phi_j^T/\sqrt{\phi_j^T[M]\phi_j}\right)\cdot[M]\cdot\left(\psi_j^T/\sqrt{\psi_j^T[M]\psi_j}\right)\right)^2}{n}} \tag{2.20}$$

In which ψ and ϕ represent, respectively, the normalised mode shapes associated to the horizontal transverse displacement of the deck with and without piers, M is the mass matrix, and n is the number of modes such that the cumulative mass participation factor is above 90%.

As for the RSI this parameter compares the stiffness of the deck to the total stiffness of the piers, where the larger the value the stiffer is the deck in relation to the piers. Again, picking up from the expression in the previous section:

$$RSI = \frac{Ks}{\sum Kp} = \frac{384\cdot E_S\cdot I_S}{5L_S^3}\Big/\sum\frac{12\cdot E_P\cdot I_P}{H_P^3} \tag{2.21}$$

In which the values are for fixed deck connections (which allow rotations but not displacements) at the abutments (384/5), and piers with monolithic connections at both ends (12). E, I, H, and L are respectively, the young modulus, the inertia of the cross-section, the height of the pier and total length of the superstructure.

To be able to correlate these parameters with actual dynamic behaviour of bridges, a Monte Carlo Simulation (MCS) was performed to 1000 concrete bridges. In a first instance, only regular bridges were used, i.e., bridges where all the piers had the same geometry (length and cross-section). In the course of the MCS' 1000 simulations, several parameters were varied: length of largest span, length of end spans, number of piers, length of piers, and width of the deck. For each bridge simulation, the RSI parameter was calculated, and a multi-modal (MM) elastic analysis was performed with a Eurocode 8 (CEN 2005) response spectrum load case, with T_B=0.1s, T_C=0.6s and T_D=2s. For each analysis, the inertia forces in both abutments were obtained, as was the total inertia force, as well as the frequency and mass factor for the first vibration mode.

In the MCS, several independent variables were considered as inputs of the model. As most of the variables are imposed by external constraints like local topography where the bridge will be inserted, and width of the roadway, the variables were defined as uniform distributions between two limit values. The chosen limit values are those associated with reinforced concrete slab-girder bridges which are the focus of this analysis. In Table 2.16, the variables are described.

Table 2.16 Variables for MCS 1.

Var ID	Variables	Type	Distribution	Lower limit	Upper limit
X_1	Max span length	Independent	Uniform	25	35
X_2	End span length	Independent	Uniform	0.6*X_1	0.8*X_1
X_3	Number Piers	Independent	Uniform	2	12
X_4	Total Length	Dependent		-	-
X_5	Deck depth	Dependent		X_1/20	X_1/20
X_6	Deck width	Independent	Uniform	10	25
X_7	Pier Length	Independent	Uniform	5	25

In Figure 2.23, the RSI values are plotted with the percentage of inertia force transferred to the abutments. In Figure 2.24, the RSI values are plotted with the first transversal mode period.

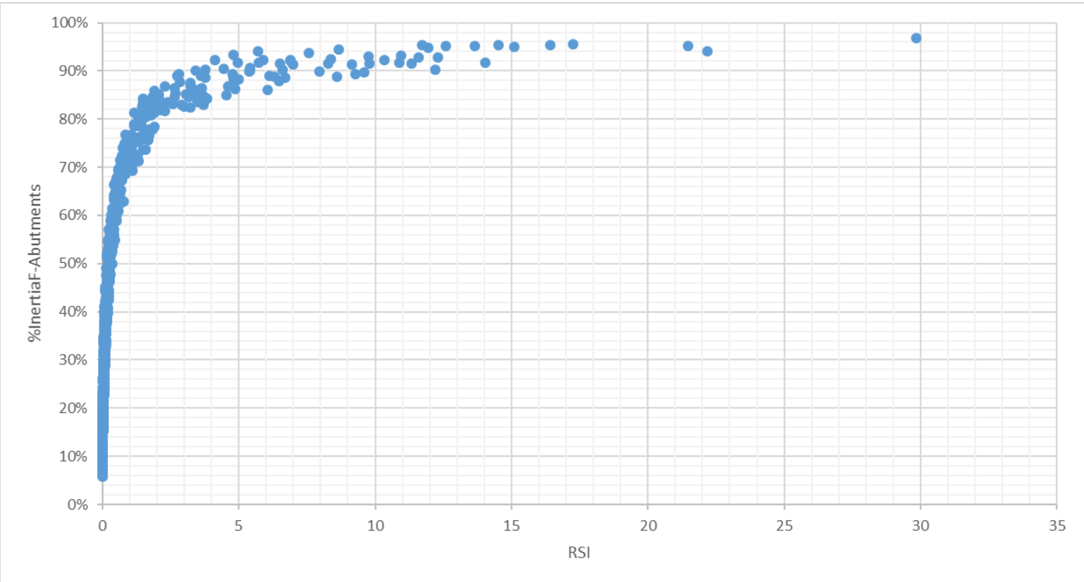

Figure 2.23 RSI and percentage of inertia force transmitted to abutments for MCS 1.

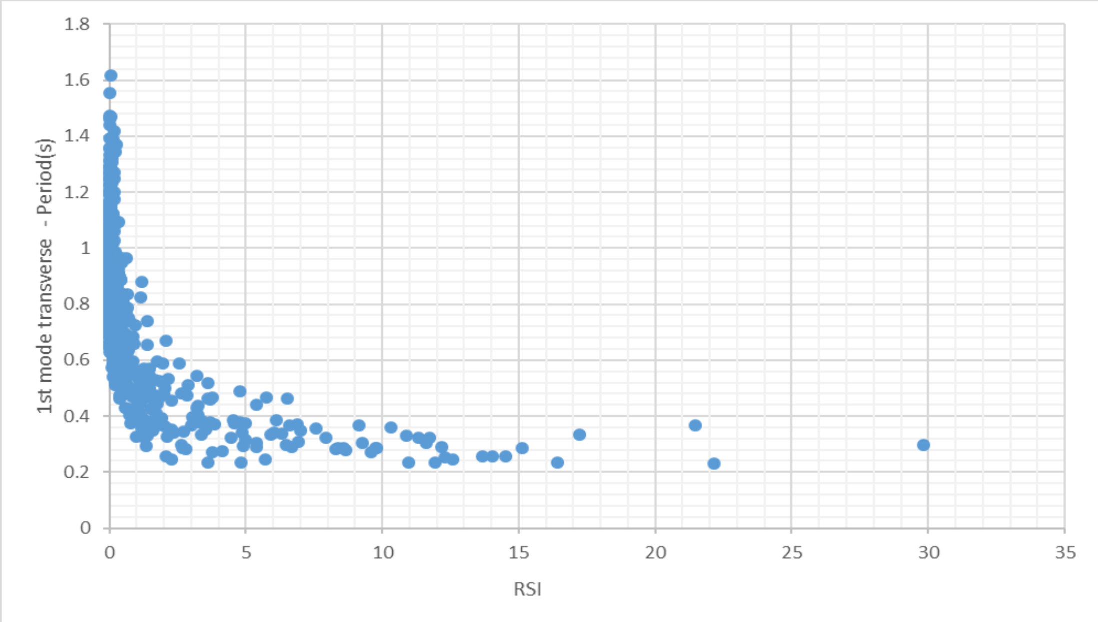

Figure 2.24 RSI and first mode transverse Period(s)

It is shown that there is a very clear correlation between the RSI and the percentage of inertia force transferred to the abutments. This shows that RSI is in fact a good indicator for relative stiffness between the deck and the piers, and it can be used as a predictor of the amount of inertia force that will be transferred to the abutments. However, this first analysis does not allow any conclusions on how to differentiate a “short” bridge from a “long” bridge. To achieve that to some extent, more analyses must be done.

A second MCS was performed, this time considering irregular pier geometry, and simulated results for 200 bridges. In this case, the RP was also calculated alongside the RSI. Each simulated bridge has two different pier geometries, defined as long pier and short pier, which are distributed along the bridge following three possible irregularity layouts:

- Irregularity layout 1 – Short piers at both ends and long piers in the middle.
- Irregularity layout 2 – Short piers starting on the left end and long piers starting at the right end.
- Irregularity layout 3 – Long piers at both ends and short piers in the middle.

In Table 2.17, the variables for MCS 2 are described. In Figure 2.25 the values of RSI are plotted against the values of the percentage of inertia force transferred to the abutments, and in Figure 2.26, the value of RSI is plotted against the values of RP.

Table 2.17 Variables of MCS 2. Short pier ratio represents the number of short piers divided by the total number of piers.

Var ID	Variables	Type	Distribution	Lower limit	Upper limit
X_1	Max span length	Independent	Uniform	25	35
X_2	End span length	Independent	Uniform	$0.6*X_1$	$0.8*X_1$
X_3	Number Piers	Independent	Uniform	5	20
X_4	Total Length	Dependent		-	-
X_5	Deck depth	Dependent		$X_1/20$	$X_1/20$
X_6	Deck width	Independent	Uniform	10	25
X_7	Short Pier Length	Independent	Uniform	5	10
X_8	Long Pier Length	Independent	Uniform	11	30
X_9	Short pier ratio	Independent	Uniform	0.1	0.5
X_{10}	Irregularity layout	Independent	Uniform	1	3

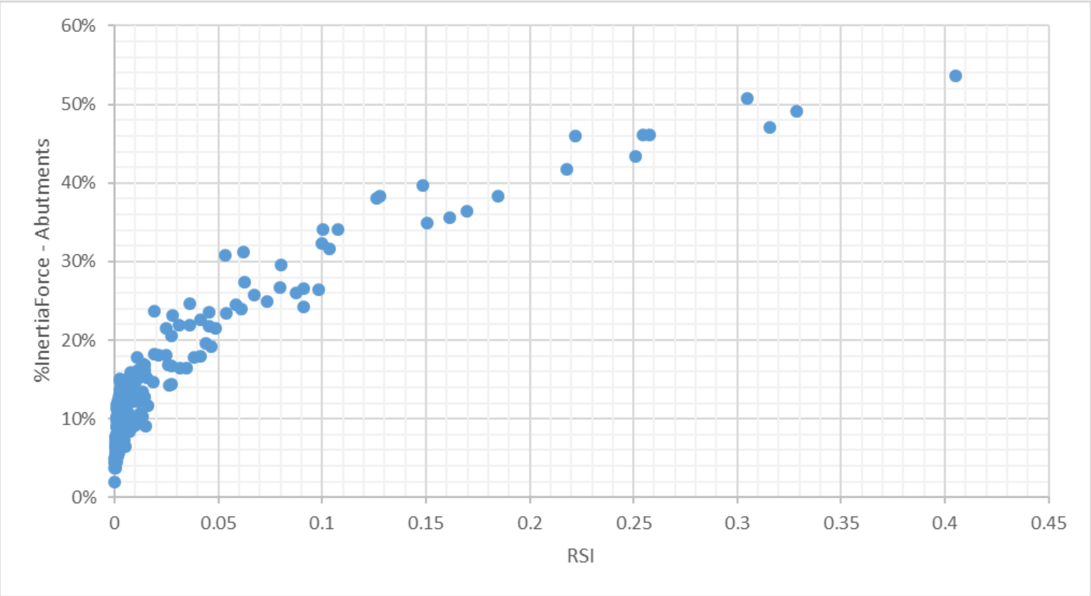

Figure 2.25 RSI and percentage of inertia force transmitted to abutments for MCS 2.

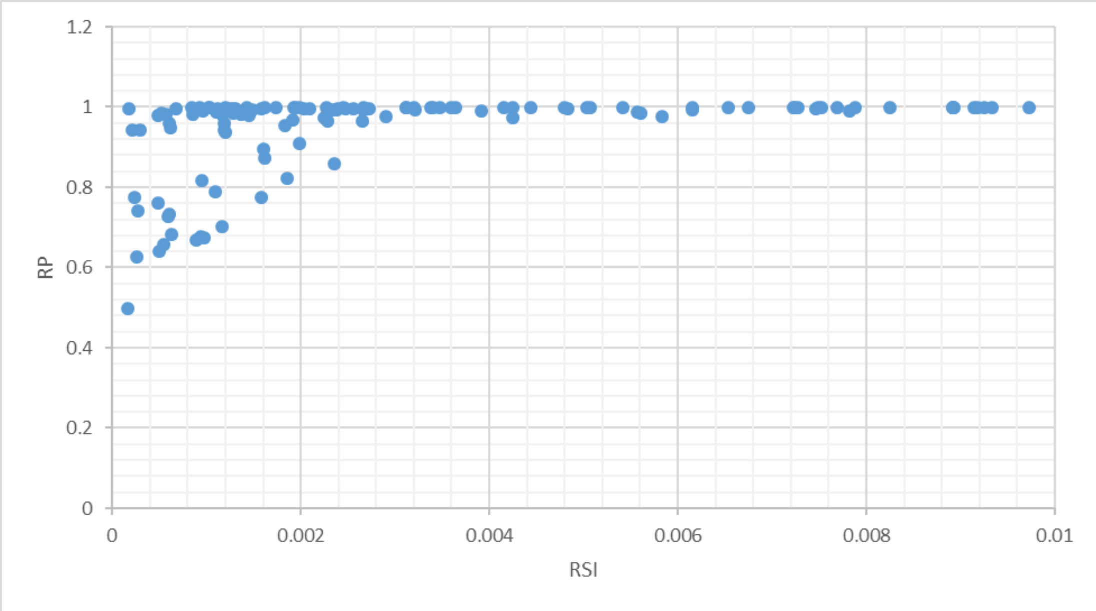

Figure 2.26 RSI and RP values

An example of the horizontal transverse displacement profile of the bridges with lower RP than 0.86 is shown in Figure 2.27.

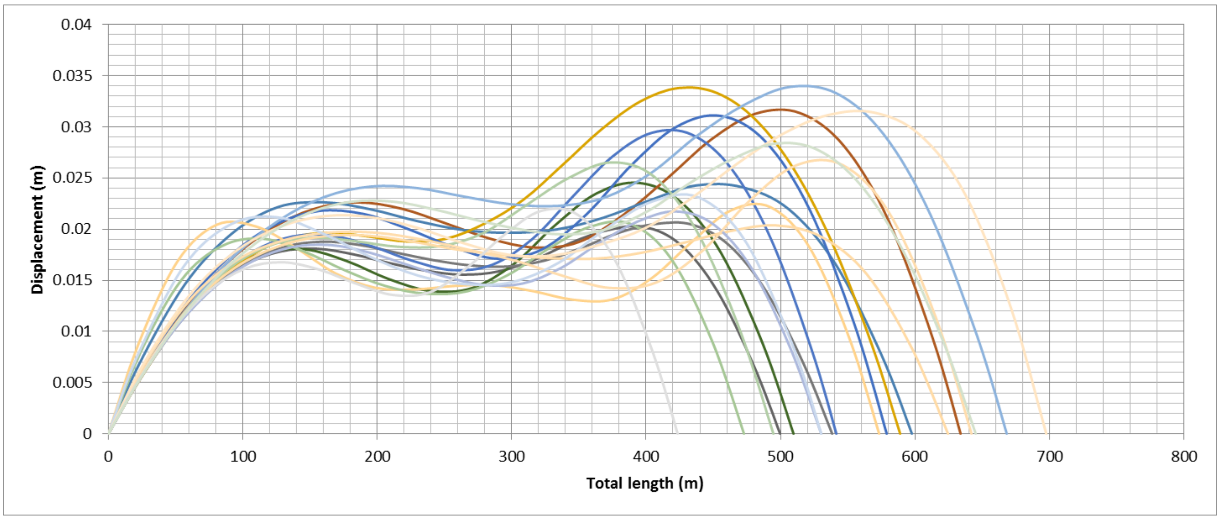

Figure 2.27 transverse horizontal displacement profile of the deck for bridges with RP value under 0.86

All the bridges shown in Figure 2.27, which present RP values under 0.86, clearly show “long” bridge behaviour, due to pier irregularity. It is also clear from Figure 2.26 that RP values lower than 0.86 only appear for RSI values lower than 0.0024. This shows that RSI may be a good indicator to use to define if a bridge might be prone to show “long” bridge behaviour. For this set of bridges, it is also observed that the maximum percentage of inertia force transferred to the abutments is of 15%.

Furthermore, only irregularity layouts 2 and 3 are represented in this set. Irregularity layout 1 does not have a large impact on the RP value. That, however, does not mean that bridges with irregularity layout 1 do not present “long” bridge behaviour. In fact, in Figure 2.28 a subset of bridges with irregularity layout 1 and RSI values under 0.0025 are presented, and it is possible to see that most of them present "long" bridge behaviour. However, neither of them present RP value lower than 0.98. On the other hand, and once again the maximum percentage of inertia force transmitted to the abutments, for that bridge subset, is again of 15%. This shows why, for many authors, bridges with irregularity layout 1 are considered to be regular, and only 2 and 3 are deemed irregular.

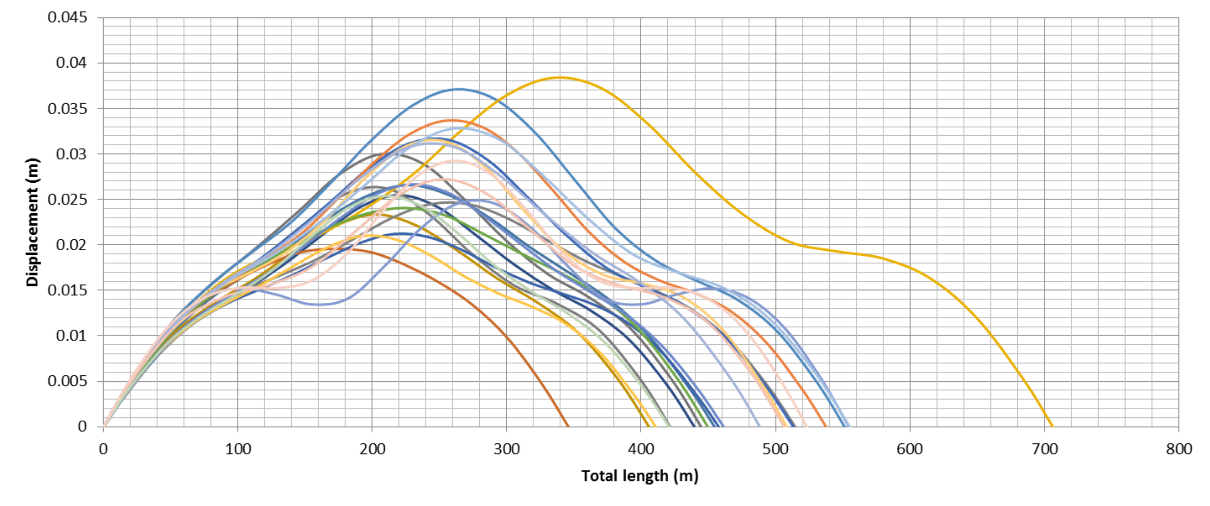

Figure 2.28 Subset of bridges with irregularity layout 1 and RSI values under 0.0025

Concluding it appears some types of irregularities have a large influence on the RP values, while others do not, however that does not mean that the bridge will not present a "long" bridge behaviour. In terms of the values of RSI and of the inertia force transmitted to the abutments, one can safely argue that a long bridge will usually present an RSI under 0.0025/0.003 and will not probably transfer more than 15% of the inertia force to the abutments. However, it must be said that the results presented here can vary significantly due to essentially three factors:

1. With nonlinear behaviour there is cracking and significant loss of stiffness in shorter piers, which means that the value of RSI changes during the seismic action. For that reason, the choice of stiffness of the piers has to be done carefully.
2. The use of another type of analysis, besides the inclusion of nonlinearity, that better captures the dynamic behaviour of the bridge and influence of higher modes can also significantly change the results.
3. The influence of the torsion of the deck (rotation about the longitudinal axis), which essentially has to do with the type of deck cross-section and also the number of piers at each pier position, influence the bridge's dynamics. This will be addressed later on and for the most part of the thesis the analysis is done for deck cross-sections where the torsional effects are prevented or restricted by the columns.

2.3.4 Categorization of the bridges, differences between categories. Choice of design variables.

This work focuses on reinforced concrete, RC, bridges. The main focus is on viaducts and bridges with span between 25 and 45 meters. These span-lengths are very common with viaducts and bridges with prestressed RC beam decks and constant height prestressed RC box girders.
Bridges with these span lengths can have total length ranging from under 100 meters to several hundred meters. The deck width can also vary quite a lot, depending on whether it is an urban viaduct in a large city with several lanes or just a two-lane bridge. This means that these bridges can present a large variety of dynamic behaviour due to the different geometry both in terms of length and deck width, which influence the stiffness of the deck to transversal horizontal displacements. In addition, the piers of the bridge or viaduct have an equally important effect on the dynamic behaviour of the bridge both in terms of individual stiffness and in terms of regularity in height along the bridge.

In the preceding section, several bridge examples were simulated and analysed subjected to an earthquake action in the transverse direction. The results obtained allowed to make some differentiation between bridges regarding length and regularity. The analyses were multi-modal elastic and thus are only useful to get an idea of the elastic behaviour of the bridge. Even though higher modes are applied, the loss of stiffness of the piers after cracking and yielding, which are not contemplated, can modify these modes, especially for longer more irregular bridges.

The results helped, however, to decide on how to subdivide the bridges into sub-groups with similar properties, which will be analysed in depth, and to better define these sub-groups in their main characteristics. It is assumed there are no expansion joints in each bridge. If there are intermediate expansion joints between abutments, this would be considered to be equivalent to have not one but more than one bridge.

1- Short Bridges:
   - Stiff deck, where the piers behave almost like double-fixed elements having little influence on the movement of the deck. In principle, the piers only must be designed to withstand displacements imposed by the deck and sustain the weight of the deck, only influencing the dynamic response of the bridge in cases where they must resist the earthquake in the longitudinal direction. However, even in this direction, usually the abutments restrict the longitudinal displacements to small values. So, as long as damage of expansion joints is tolerated under strong seismic actions, if columns are able to sustain the vertical loads and the maximum horizontal displacements compatible with deck deformations and dimensions of expansion joints, collapse of the bridge due to the columns is prevented.
   - It will be necessary to learn over which values of RSI bridges start having this behaviour.

2- Long Regular Bridges:

- In this case the deck has little influence on the dynamic behaviour. This type of bridge behaviour is associated to “bathtub” shape valleys or glacier valleys. A bridge built in a valley as such has very little variation of pier height along the length of the deck. This can also happen in urban settings.
- In very long bridges the piers may have to have fixed and/or sliding (sliding connections allow relative longitudinal displacements between deck and piers) connections to the deck, especially piers further away from the decks centre of stiffness due to temperature, creep, and shrinkage strains, which can influence the design of the piers for the earthquake in the longitudinal direction.

3- Long Irregular Bridges:

- There are three types of pier irregularities which affect the dynamic behaviour of the bridge differently in the transverse direction:
    i. Irregularity layout 1 - Short piers near the ends and long piers near the middle – This case is the most common and the least irregular type of bridge, being many times characterized as regular. In this case as seen in the results from the MCS in the last section, the RP parameter is high due to this type of irregularities since the predominant mode shape is still the first mode.
    ii. Irregularity layout 2 - Short piers on one side and long piers on the other side – In these cases asymmetric mode shapes gain bigger weight and the first mode loses importance. This can occur not only due to valley morphology but also due to soil effects.
    iii. Irregularity layout 3 - Short piers near the middle and long piers near the ends – In these cases the bridge has low RP value, opposed to Irregularity layout I (1). bridges. Here the second and third mode are usually more important than the first. There are even situations where the bridge behaves like two separate bridges divided by the short piers.

In Table 2.18 the irregularity types and possible normalization formats are presented.

Table 2.18 Bridge irregularity types and normalization formats

Category	Explanatory figure	Normalization format
1		One cross-section (all piers have the same cross-section), and one type of pier-deck connection (all monolithic or all fixed)
2		One cross-section (all piers have the same cross-section), and one, two or three type of pier-deck connections dependent on temperature, creep, and shrinkage effects (middle piers monolithic or fixed, external piers fixed or with sliding connections).
3i	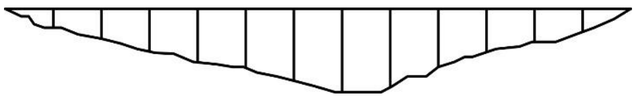	One or two cross-sections and one or more than one type of pier-deck connections depending on pier length differences and temperature, creep, and shrinkage effects (short piers with fixed or sliding connections, long piers monolithic).
3ii	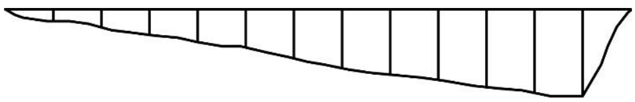	Two or more cross-sections (especially concerning different longitudinal steel reinforcement between short and long piers), and one, two or more types of pier-deck connections due to length differences and temperature, creep, and shrinkage effects (short piers fixed and/or with sliding connections, long piers monolithic).
3iii	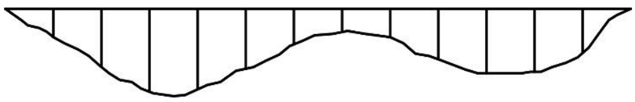	

We can also define intermediate categories to place bridges which fall in between two categories, however this and the separation between categories are two of the challenges.

This work has the objective of producing an optimization framework for the design of concrete bridges, and so it is important to define what can be the design variables for a given bridge. The piers and the foundations are usually the scope of earthquake engineering bridge design. The foundations depend on the pier design and in the framework of the analysis they can be considered secondary as their flexibility produce an effect equivalent to a reduction on pier stiffness, and so the piers are the focus of design. For the matter of simplification, the piers in all study cases will have circular cross-sections, however it will be shown that the same principles can be extrapolated for other cross-sections. It is also important to know what influences the strength and ductility of the piers, which is the subject of the previous

Section 2.2. Nonetheless, the main design variables are pier diameter (circular cross-section), longitudinal steel reinforcement, and transverse steel reinforcement for concrete confinement. In addition to these design variables, there are a few others that are importance but are sometimes imposed or defined attending to other criteria and not specifically for earthquake resistance, which are concrete and steel grade and type of connection between pier and deck. The shape of the piers' cross-section is also a possible design option. In several cases one can adopt either variable cross-section piers along height or thin blades of concrete that only have stiffness in the transverse direction, however in the scope of this work, the shape of the piers will be fixed to circular full section. In the previous section it has been shown that the conclusions may be valid for most of the other shapes of pier cross-sections, particularly rectangular cross-sections, and other compact sections.

2.4 Type of analysis: dynamic vs. pushover

In earthquake engineering, there is always a trade-off between efficiency of the method employed and result accuracy. In that sense, the question is usually whether to employ some form of nonlinear static pushover analysis (SPA) or resort to nonlinear dynamic analyses (NDA). In terms of bridges seismic behaviour in the transverse direction, the choice is not only between SPA and NDA, but also which SPA methods can be employed and why. For both issues, it all depends on regularity of the bridge and stiffness of the deck, or in other terms, whether other vibration modes, other than the first mode, are important.

Several works have been done on this issue and there have been SPA methods created to be employed specifically for bridge analysis, such as the Adaptive Capacity Spectrum Method (ACSM) by (Casarotti and Pinho 2007), which uses the DAP (Displacement-based Adaptive Pushover) algorithm by (Antoniou and Pinho 2004). The work (Kappos, Saiidi, et al. 2012) presents a chapter on the reliability of inelastic analysis methods. There, a table is presented on the recommended methods for the analysis of each type of bridge in the transverse direction (Table 2.19).

Table 2.19 Recommended method according to bridge type in Kappos et al (2012)

Type of bridge	Single-mode methods	Multi-mode methods		Nonlinear response history analysis
		Non-adaptive	Adaptive	
Response is governed predominantly by one mode, which does not considerably change: Short bridges on moderate to stiff soil, fixed at the abutments, and not supported by very short columns.	X			
The influence of higher modes is limited, and their shape does not considerably change when the seismic intensity is increased: Short bridges fixed at the abutments, supported by short side and long central columns.	X	X		
Considerable influence of higher modes, that do not significantly change the shape: Long bridges without very short central columns		X	X	
Considerable influence of one or a few numbers of modes, which significantly change the shape: Short bridges with roller supports at the abutments			X	
Considerable influence of higher modes, which significantly change their shape when the seismic intensity is changed: Short or long bridges supported by very short central and higher side columns.				X

Naturally, the methods to the right-hand side of the table are also suitable, in terms of reliability of results, when the methods to the left of them are suitable, however they may not be recommended due to being more time consuming.

In the present work, all the types of bridges in Table 2.18 are to be studied, and thus there are a couple of reasons why it has been decided to use only NDAs in the transverse direction:

- To maintain some type of consistency since only NDAs are suitable for all the types of bridges and to be able to compare results between bridge types it is deemed important not to vary the analysis method.
- The quality of the results after combining both directions, transverse and longitudinal, obtained from the SPA methods are at best debatable, and so to obtain reliable bi-directional results, the NDAs are much more suitable, if natural pairs of earthquake signals are used.

2.5 Force-based versus displacement-based seismic design

2.5.1 Force-based design

The force-based origins in earthquake engineering, as well as the force-based paradigm itself has already been presented in this thesis. Regarding irregular bridges, it is perhaps in the 1990s where the influence of irregularity on the expected ductility demand and the seismic behaviour of RC bridges is studied (Calvi, Elnashai and Pavese 1994) (Calvi and Pavese 1997). The approach in Eurocode 8 – Part 2 (CEN 2005) for bridge design (and buildings as well) is based on a single behaviour factor (q) or response modification factor (R). In this method, known as force-based design (FBD), the linear elastic response of a bridge structure is reduced by this factor for design purposes to consider the nonlinear response and the energy dissipation capacity of the bridge. This approach assumes that the bridge responds regularly with predictable or uniform ductility demand distribution throughout the different bridge piers.

In FBD, once the pier cross-section has been selected, a structural model is constructed. The design procedure usually entails the discretization of the deck mass as lumped masses at the top of the piers with a portion of the pier's mass added. The main parameters used in the analysis are the mass and elastic stiffness of the piers, eventually reduced.

The drawbacks with FBD is that performance is not easy to quantify due to the fact that forces are not good indicators of damage, and behaviour factors, which are meant to imply damage levels are highly variable, as will be referred to in Chapter 5. Many of the procedures used in bridge design are basically force-based and may be considered as reasonable design approaches that will lead to safe structures, but they do not attend to performance criteria at the initial design procedure, albeit checking displacements afterwards (force-based/displacement-checked) (Calvi, Casarotti and Pinho 2006). As mentioned before, even though the force-based design has its drawbacks, the design paradigm to which engineers are used to, makes it difficult to change towards displacement-based design, which also has its own drawbacks. What can be done is to adopt techniques and guidelines that, in a force-based framework facilitate the design by allowing to deal with nonlinearity and irregularity effectively, thus decreasing the number of iterations needed when performance-based design is done in a force-based framework.

There have been many works, in recent times, that have addressed the design of irregular bridges in a FBD framework. A good review on these works is present in this work (Akbari and Maalek 2018).

2.5.2 Displacement-based design

In essence displacement-based design (DBD) was developed by Priestley, Calvi and Kowalsky (Priestley, Calvi and Kowalsky 2008) with the objective allowing to perform a direct displacement-based design of a structure with a predetermined displacement level when subjected to an earthquake consistent with the design level. In direct displacement-based design (DDBD), design forces are obtained from the inelastic response of the system for a desired level of performance (Calvi, Casarotti and Pinho 2006) (Priestley, Calvi, et al. 2008) (Calvi, Priestley and Kowalsky 2013) (Kowalsky, Priestley and MacRae 1995) (M. J. Kowalsky 2002).

The DDBD procedure for MDOF bridge structures can be summarised in the following basic steps (Priestley, Calvi, et al. 2008) (Calvi, Priestley and Kowalsky 2013):

1. Determination of the design displacement shape.
2. Characterisation and evaluation of the equivalent SDOF system.
3. Application of the DBD approach to the SDOF system.
4. Determination of the pier's required strengths and ductility and design of reinforcement accordingly.

The authors in (Calvi, Casarotti and Pinho 2006) perform a comparative study between pushover design methods and FBD and DBD procedures, with the pros and cons of each strategy, as well as possible lines of development.

DDBD has advantages in terms of the way it deals with displacements, but it has a few drawbacks as well, particularly for very irregular bridges where the initially defined displacement shape has crucial influence on the result, as in these bridges higher order modes influence the THDP of the bridge. There have been several works on the development of DBD for both bridges and buildings and a good overview of this is given in (Akbari and Maalek 2018).

2.6 Bridge type singularities. Possible normalization formats for each bridge type. Factors that influence design decisions.

The design of bridges is constrained by several variables such as geometry (length, pier height, number of piers, span lengths, insertion in curve or straight alignment, etc.), soil characteristics, valley shape, location of the piers, etc... These variables or characteristics influence the type of bridge, materials and the eligible construction methods.

The design of the bridge and thus the choice of normalization formats that make sense for a given bridge is therefore dependent on a series of initial characteristics. A bridge beyond a certain length will have deck deformations due to temperature, as well as creep and shrinkage in the concrete, which have influence on the choice of the type of connections between superstructure and piers, and also the type of abutments. The soil characteristics influences the design of the abutments and the type of foundations. All these issues are closely related to the stiffness of the infrastructure and the ability to withstand the inertia forces and displacements conveyed by an earthquake action.

It is thus important to define for each type of bridge length, soil type and valley shape, the normalization formats that make sense for the design of the bridge.

In this section, a series of normalization formats will be commented on according to their eligibility to be used for the design of bridges with different initial characteristics in terms of bridge length, soil type and valley shape. The objective is to match/associate possible normalized pier design formats (normalization formats) to bridges according to their length and type of irregularity.

In the case of short bridges, the design procedure is relatively easy, since the temperature, creep, and shrinkage do not cause relevant effects, and the effects of seismic action are irrelevant or can easily be accounted for in the design of the abutments.

For long bridges, the design procedure is more complex. The characteristics of valley shape and soil type have relevant effects, and the temperature, creep, and shrinkage effects on the superstructure is significant and demands attention. In addition, the seismic action has relevant effects in the transversal direction, and the earthquake analysis in the transversal direction is much more complex than in the longitudinal direction.

2.6.1 Effects of temperature, creep and shrinkage

It is known that temperature, as well as concrete creep and shrinkage produce cumulative strains that can originate significant effects, particularly for long bridges. Usually, these effects are bundled up as an effective temperature action to which the deck is subjected thus being used to define pier-deck connections, placement of expansion joints, etc.

These effects are mentioned qualitatively in this section when defining possible normalization profiles for the bridges with different irregularity layouts. However, there is an issue associated to the way that these effects are usually regarded, which stems from the force-based thought paradigm in structural engineering.

When these effects are imposed on a deck, they develop stress and strains that propagate along the bridge from the stiffness centre. Considering a uniform temperature, these strains translate into imposed displacements at the top of the piers, which become larger the further away the pier is located from the stiffness centre of the bridge. The imposed displacements develop into stress and strain in the piers and can lead to important damage to the piers. When thinking of the issue in a force-based paradigm, the engineer is led to think that the cracking of the concrete in the piers results in a loss of stiffness and subsequent redistribution of stress to other piers, and so the stress that some piers are subjected in an elastic regime may be acceptable because that stress will be redistributed once those piers crack. As a result, the damage is reduced because the engineer is trained to think of damage as a function of stress instead of strain. This idea is incorrect.

There is in fact a loss of stiffness and a consequent stress reduction in the pier. However, damage is related to strain and not stress, as previously referred to, and strain is related to curvature (when the pier is subjected to bending) which is related to the displacement imposed at the top of the pier. The displacement in such a situation doesn’t decrease with the reduction of stiffness of the pier under analysis because the imposed displacement is only dependent on the temperature load and the position of the centre of stiffness, as the deck longitudinal displacements depends on the axial stiffness of the deck, which is usually far superior to the piers flexural stiffness. The centre of stiffness, with the cracking of the more distant elements relative to it might actually shift further away from the cracked elements, as illustrated in Figure 2.29, because the elements closer to the centre of stiffness, which are subjected to smaller imposed displacements and, eventually, less strain, did not lose as much stiffness. This leads to an increase in the imposed displacements of the already cracked piers, thus increasing the strain and subsequent damage. Even if that effect (shift of the stiffness centre) is not significant, the initial strain is not reduced even if there is stress "redistribution" with the loss of stiffness. For that reason, it is important to not think of actions due to imposed displacements on the basis of a force-based paradigm.

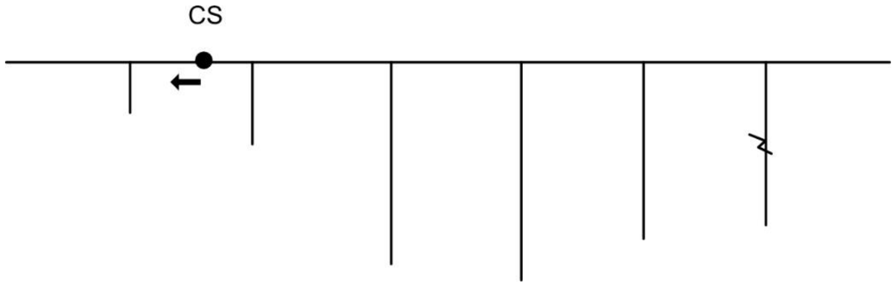

Figure 2.29 Centre of Stiffness of the deck and cracking of the pier due to deck-imposed displacements.

2.6.2 Long Bridges

In the past sections, four possible valley shapes were presented associated to long bridges. Three of them were related to irregular bridges, and one to regular bridges. These four valley shapes are qualitative examples of the type of valleys that are most common, and each one of them presents the design engineer with different challenges to solve. In this section, it is discussed what kind of normalization formats can be applied to design a long bridge inserted into each one of the four valleys, and at the same time how do other factors, such as temperature induced strain, influence the normalization formats.

Once again, by normalization format, one refers to a series of design decisions related to the infrastructure of the bridge (piers and foundations), so that all elements are normalized by being placed in one or more groups, inside which all elements present the same geometry, properties, and connections to the superstructure (deck). This normalization format is then used to assist in the optimization of the bridge design.

In Table 2.18, the valley shapes are presented, and shape 2, 3i, 3ii and 3iii all refer to long bridges. Concerning long bridges, two things are assumed. One, that the temperature strain effects on the superstructure can be significant for pier design. Two, that the effect of the seismic action in the transversal direction is relevant and important.

The nature of the abutments is a very important "variable in the equation". This will define if the seismic action in the longitudinal direction is important for pier design, and also which piers may be affected by the superstructure's temperature related deformations, and thus what connections can they have with the superstructure.

In terms of dynamic behaviour, the abutments can either be defined as having fixed or sliding connections for longitudinal actions. An abutment can also be both if, for instance, it has visco-elastic dampers, allowing for displacements due to temperature strains but not dynamic displacements due to earthquakes. The possibility of designing an abutment able to withstand the inertia forces of an entire bridge due to an earthquake depends on the type of soil and the surface slope at the location of the abutment. A weak soil and a steep valley slope may not allow for a fixed abutment. Also, a very long bridge cannot be fixed in its entirety to one abutment, in those cases if there is a fixed abutment than it could be necessary to “break-up” the bridge in several pieces through the use of expansion joints or use both abutments (as fixed). In this case, special devices to allow slow longitudinal movements due to temperature variations would be necessary in one or both abutments. Without going into possible use of expansion joints, if the valley slopes and the soil allow for fixed abutments there are a few possible normalization formats that may be possible to apply.

2.6.2.1 Long Bridge type 2

This bridge valley shape is characterized by being “bath-tub” shaped. This results in having piers with more or less the same length all along the bridge, as illustrated in Figure 2.30.

Figure 2.30 Long bridge 2 diagram

This case is one of the more trivial cases inside the long bridge family. Here all the piers have similar lengths, and this will result in a very typical transverse horizontal deck displacement profile of the bridge, when subjected to earthquake action, following a curve compatible with the first transverse vibration mode of the deck. For the infrastructure design, one of the main concerns in this case is the temperature induced strains in the deck and subsequent imposed longitudinal displacements on the top of the piers. This last issue depends, as it always does, on the nature of the abutments, and whether one of them is fixed, or both have sliding connections.

2.6.2.2 Solution 1 – One abutment fixed

By fixing one abutment, (in the longitudinal direction, in the transverse direction abutments are always considered fixed) the centre of rigidity of the deck is located on the fixed abutment. The temperature induced imposed displacements on the top of the piers are larger at the opposite side of the fixed abutment. This situation forces the design engineer to place sliding and/or fixed connections at the top of the piers furthest away from the fixed abutment. With a fixed abutment in the longitudinal direction, the earthquake action in the longitudinal direction is absorbed by the fixed abutment, and so only the earthquake action in the transversal direction will affect the piers. The earthquake action in the transversal direction will create a transversal horizontal displacement profile of the deck with larger displacements in the middle, compatible with the expected fundamental vibration mode of the deck in the transversal direction. Hence, the piers that are subjected to more ductility demand are the piers located at the middle of the bridge. The normalization format for this bridge solution can be as follows (Figure 2.31):

- Sliding connections, longitudinally, for the piers located furthest away from the fixed abutment. Fixed connections for the piers located in the middle and monolithic connections for the piers closer to the fixed abutment.
- Fixed connections for all piers in the transverse direction.
- Two groups of piers according to cross-section design: first group are the piers located at the middle. Second group are the piers located on both sides of the bridge. This differentiation is related to ductility demand.

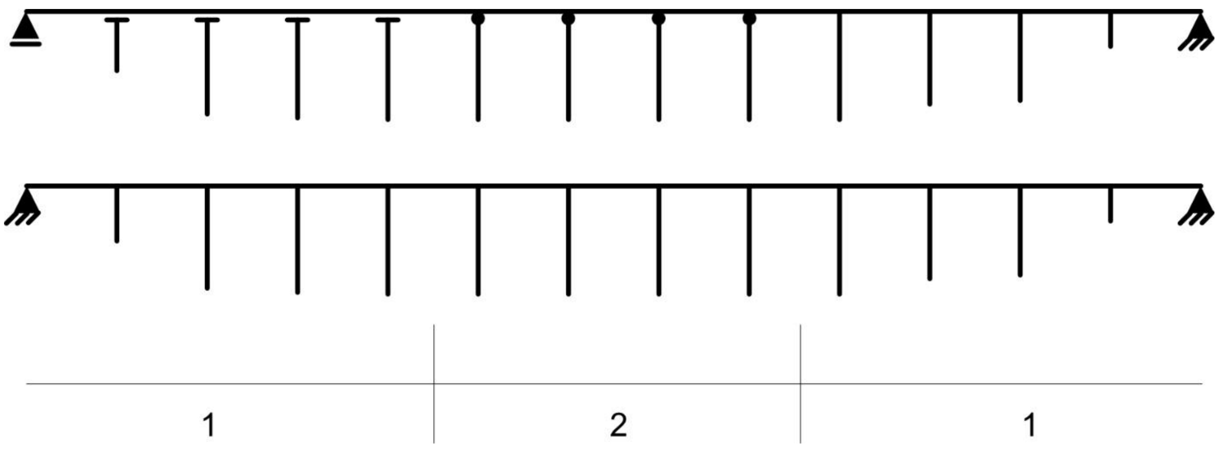

Figure 2.31 Solution 1 diagram for both directions, longitudinal direction (top), transversal direction (bottom) with pier groups according to cross-section

2.6.2.3 Solution 2 – Both abutments with sliding connections

If both abutments have sliding connections, the result is having the centre of rigidity located very close to the centre of gravity of the deck, since the piers are all the same length, they will all have roughly the same stiffness. So, in this case, the piers closer to both abutments undergo the large temperature induced displacements if they are connected to the deck in the longitudinal direction. In addition, the piers will have to withstand the longitudinal earthquake action as well as the transversal one. Since all the piers are similar, in the longitudinal direction the imposed displacements are the same for every pier and in the transversal direction the displacement profile of the deck will have a parabolic shape with maximum located at the centre. Therefore, the earthquake action, taking into account the effects in both directions, will demand more ductility from the piers located near the centre of the bridge.

In summary, on the one hand the temperature effects affect more the piers closer to the abutments, on the other hand, the earthquake action demands more ductility from the piers located closer to the centre of the deck. This would imply that the piers closer to the abutments have fixed connections longitudinally to the superstructure, however, this could result in increasing the demand of the central piers when subjected to the earthquake in the longitudinal direction. A possible solution is that all piers have fixed connections in the longitudinal direction. In the transversal direction, the larger ductility demand is required for the piers closer to the centre.

The normalization format, for this case, can be as follows (Figure 2.32):

- Longitudinally, fixed connections for all piers
- Transversally, either monolithic connections for all piers, or fixed only at the central piers. Either way, two groups of piers according to cross-section: piers on both ends in one group and piers at the centre in another group.

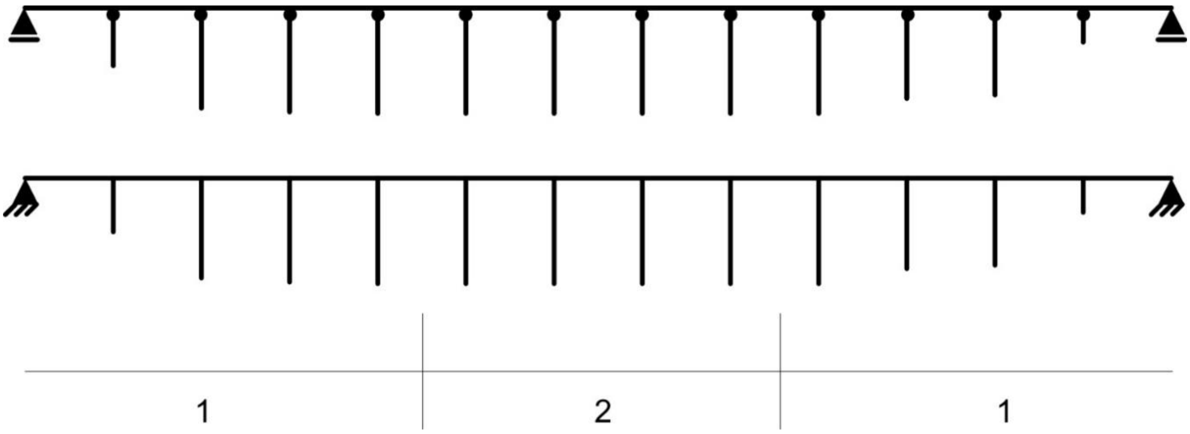

Figure 2.32 Solution 2 diagram with description in both directions, longitudinal direction (top) and transversal direction (bottom)

2.6.2.4 Long Bridge type 3i

This long bridge type (Figure 2.33) is characterized by being inserted into what can be defined as a typical “v” shaped valley. This valley shape is very common, and this bridge type is very similar to long bridge 2 in terms of dynamic behaviour. Put in other words, it is formally an irregular bridge regarding the infrastructure, however in terms of dynamic behaviour and the transversal horizontal displacement profile of the deck, it is a regular bridge, because the movement will be mostly defined by the fundamental transversal vibration mode of the deck.

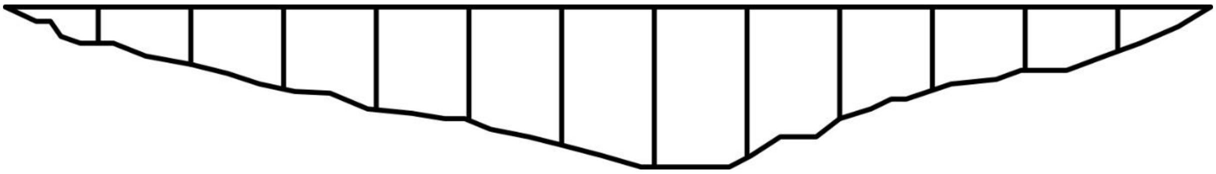

Figure 2.33 Example of valley shape of long bridge type 3i.

2.6.2.5 Solution 1 – fixed abutment on one side

The bridge in this case is characterized by having a sort of symmetry inherent to the type of valley. The fixed connection at only one of the abutments does not respect that symmetry, since there are short piers at both ends, and as a result, some piers can undergo too large longitudinal displacements due to temperature effects. Nonetheless, fixing one of the abutments results in an advantage, as it eliminates the concern of the earthquake in the longitudinal direction for the design of the piers.

By fixing one abutment in this case, there will be short piers subjected to relatively large temperature induced displacements, since the fixation of the abutment results in moving the location of the centre of rigidity to that abutment, and so the piers on the other side become subjected to the said temperature related displacements. This results in the need to place sliding and/or fixed connections between those piers and the deck, for the longitudinal direction.

For the earthquake action in the transversal direction the displacement profile of the deck is similar to the fundamental vibration mode of the deck, with larger displacements near the centre of the bridge. In this case the largest displacements are imposed on the taller piers, and for that reason, the ductility demand in all piers has a tendency to be similar, which is very beneficial for the pier design. The normalization format can be the following (Figure 2.34):

- Longitudinally, piers furthest away from the fixed abutment with sliding connections to superstructure and then progressively with fixed connections and monolithic connections closest to the fixed abutment.
- All piers with fixed connections have restrained rotations at the top in the transversal direction.
- All piers with the same cross-section

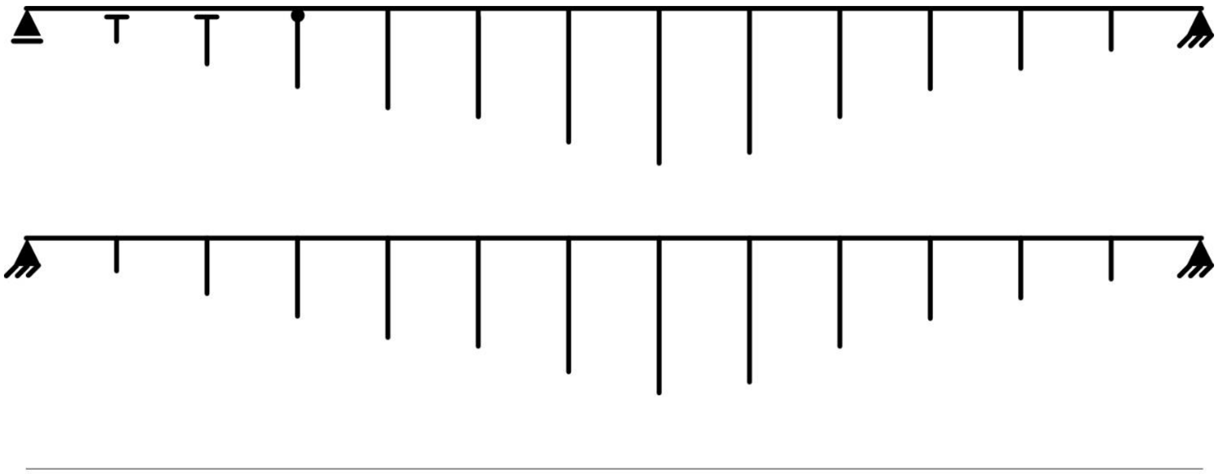

1

Figure 2.34 Solution 1 for long bridge type 3i in the longitudinal direction (top) and transversal direction (bottom).

2.6.2.6 Solution 2 – both abutments with sliding connections

With both abutments having sliding connections, the bridge centre of rigidity is located roughly in the centre of the deck. And so, temperature related imposed displacements at the top of the piers will have important effects on the piers closer to both abutments, which besides being the shortest piers are also the ones subjected to larger temperature related displacements. It would make sense to place sliding connections in the outer piers and fixed and finally monolithic connections as we go inward towards the middle. This is also useful when resisting the longitudinal earthquake since the short piers at both ends are the ones subjected to the largest ductility demands, as are the ones with the highest ratio between seismic displacement and length. It is discussable, however, when the piers have to resist the longitudinal earthquake, if it is a good option to “remove” all the shortest piers from the longitudinal earthquake resistance by providing them with sliding connections to the superstructure. This may result in keeping only very flexible elements to sustain the bridge longitudinally, which in turn can result in having very large displacements.

As for the transversal direction, the situation is the same as in solution 1, where the largest imposed displacements due to earthquake action are applied to the tallest piers. The normalization format can be the following (Figure 2.35):

- Longitudinally, outer piers with sliding connections to superstructure and then progressively with fixed connections and monolithic connections as we go inwards towards the middle.
- All piers monolithic transversally.
- All piers with the same cross-section.

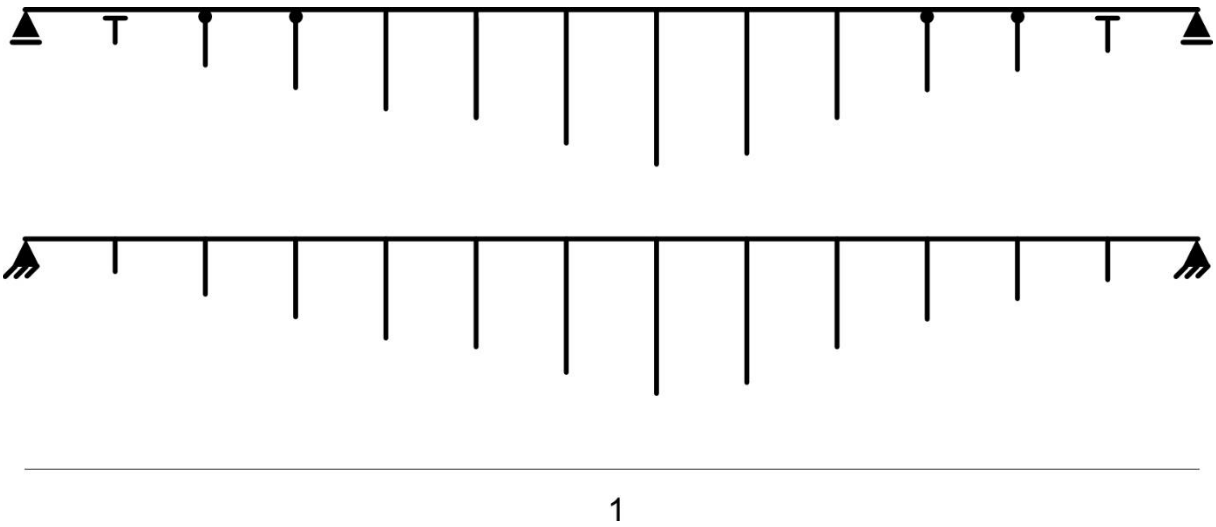

Figure 2.35 Solution 1 for long bridge type 3i in the longitudinal direction (top) and transversal direction (bottom).

2.6.2.7 Long Bridge type 3ii

Long bridge 3ii’s valley shape is characterized by starting with a shallow depth on one extremity, progressively increasing and reaching a maximum depth near the opposite extremity, after which there is a steep slope leading to the abutment, as illustrated in Figure 2.36 below.

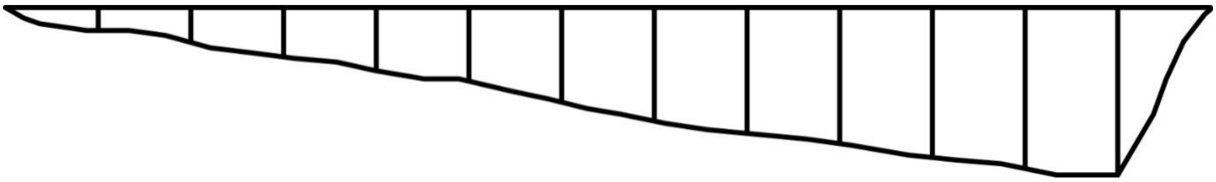

Figure 2.36 Valley shape for long bridge 3ii (ref. Table 3)

2.6.2.8 Solution 1 – Left-hand side abutment fixed

The abutment on the left-hand side has fixed connection and the abutment on the right-hand side has sliding connection. In this case, illustrated in Figure 2.37, the centre of rigidity is located on the left-hand side abutment, which means that the temperature-imposed displacements on the superstructure will increase towards the right-hand side abutment, meaning that the closer a pier is to the right-hand side abutment the larger these displacements are at its top. In this case, the shorter piers have less imposed displacement due to temperature than the longer piers. So, a normalization format that is compatible with these conditions would be:

- All piers with monolithic connections with the superstructure
- The ten piers divided into two groups according to cross-section, the group of shorter piers with one cross section, the group of longer piers with another cross-section

Since in this case, the longitudinal earthquake action is absorbed by the fixed abutment, the piers only have to resist the earthquake action in the transversal direction. The stiffness of the piers along the deck, were they to have the same cross-section, would suggest that the transversal horizontal displacement profile of the deck would induce larger displacements to the piers located at the centre-right position of the deck. The piers that would be critical would be the ones that are located closer to the centre, that would have larger ductility demand, and have less available displacement ductility than the longer ones to their right-hand side (probably the 4th 5th and 6th counting from the left-hand side abutment in this case).

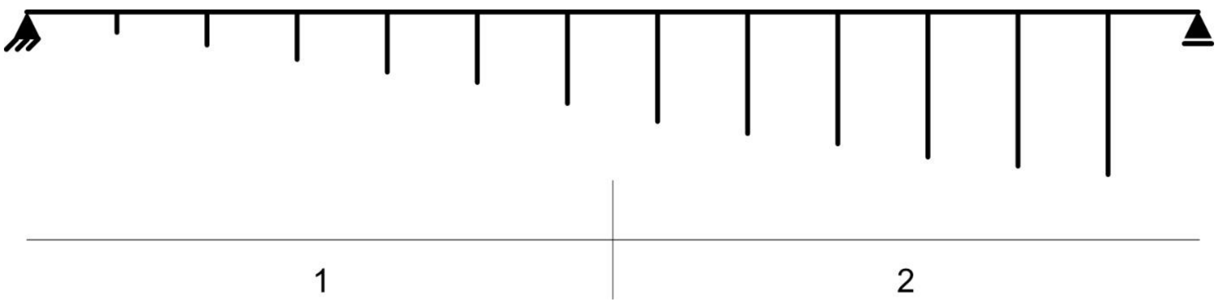

Figure 2.37 Solution 1 diagram for long bridge 3ii.

2.6.2.9 Solution 2 – Both abutments with sliding connections

In this case, the centre of rigidity will be located left of centre of the bridge due to the larger stiffness of the piers on the left-hand side. In this situation, the shorter piers located next to the abutment on the left-hand side may be subjected to large imposed displacements due to temperature, and so it may not be feasible to have monolithic connections in the case of those piers. And so, at least in the longitudinal direction the shorter piers may have to have fixed connections with the superstructure.

In addition, the earthquake action in the longitudinal direction is resisted by the piers, as the abutments in this case have sliding connections longitudinally. This means the ductility demand on the piers is increased. The earthquake in the longitudinal direction inserts the same imposed displacement at the top of all piers. This means that the shortest piers next to the left-hand side abutment can now be critical as well in terms of ductility demand versus available ductility

To summarize the normalization format for solution 2 (Figure 2.38):

- Fixed connections in both directions for the three/four leftmost piers.
- The ten piers divided into two groups according to cross-sections, shorter fixed piers in one group, and the other piers in the other group.

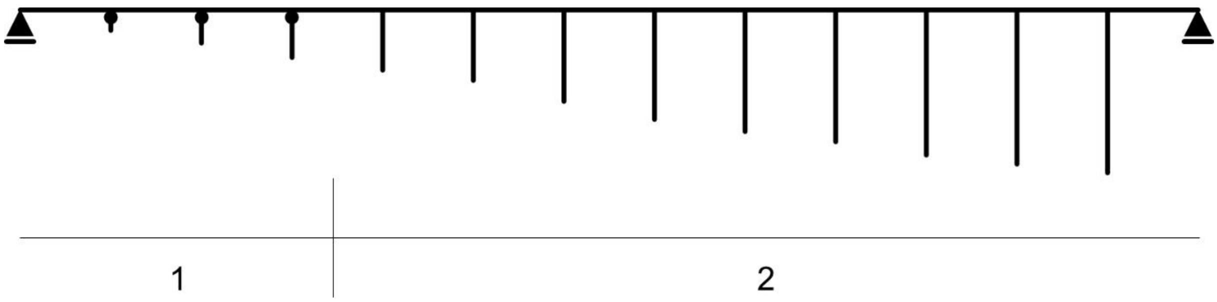

Figure 2.38 Solution 2 diagram

2.6.2.10 Solution 3 – Right-hand side abutment fixed

This solution is the most unfavourable for the piers in terms of imposed displacements due to temperature strains in the superstructure since the centre of rigidity is located on the right-hand side abutment. As a result, the largest temperature related imposed displacements affect the shortest piers on the left-hand side. In this case, it may be necessary to have sliding connections longitudinally for the three/four leftmost piers, fixed connections longitudinally for the middle piers and only monolithic connections for the tallest rightmost piers.

As for connections in the transverse direction, the longitudinal earthquake is resisted by the fixed abutment which means all piers can have monolithic connections as in solution 1.

To summarize the normalization format for solution 3 (Figure 2.39):

- Connections to the superstructure (longitudinal direction): Shortest piers – sliding connections, middle piers – fixed connections, tallest piers – monolithic.
- Connections to the superstructure (transversal direction): all piers have restrained rotations at the top.
- The ten piers divided into two groups of five according to cross-section, the group of shorter piers with one cross-section, the group of longer piers with another cross-section

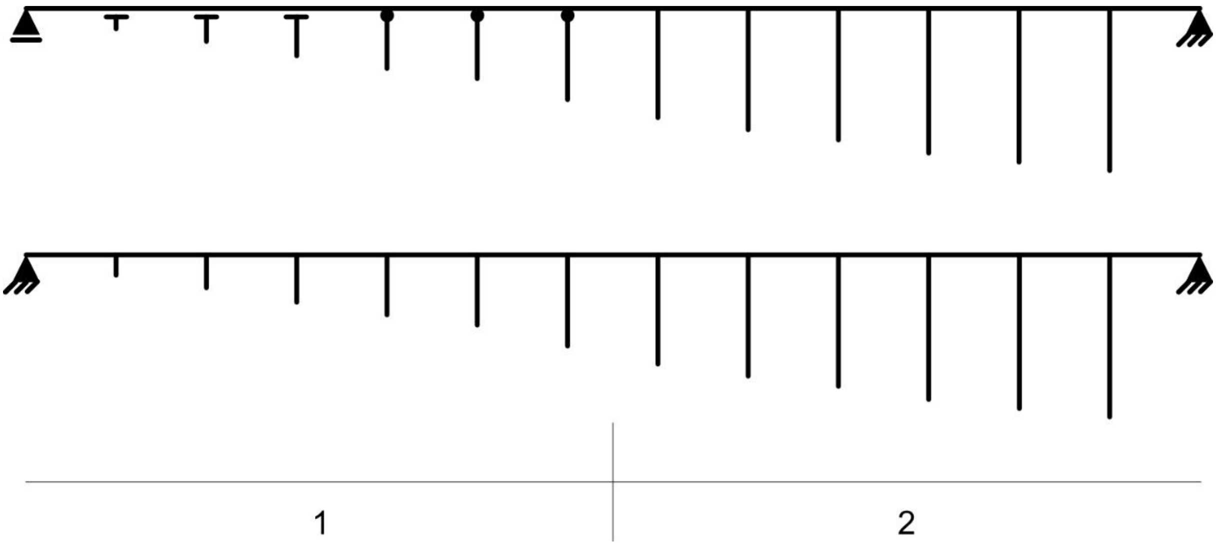

Figure 2.39 Solution 3. Longitudinal direction (top), Transversal direction (bottom).

2.6.2.11 Long bridge type 3iii

This is the fourth type of long bridge, according to pier (ir)regularity (Figure 2.40). This is perhaps the case to which results of seismic analysis in the transverse direction are more different from what is most common. Due to the nature of the irregularities, characterized by short piers at the middle of the bridge, which completely alter the usual dynamic behaviour of bridges, almost eliminating the relevance of the vibration mode that is usually the fundamental mode in the transverse direction, in which the entire deck moves to the same side, and giving larger relevance to other modes. The result is that, for these bridges, the use of any pushover analysis, from the trivial N2 method up to the complex and more time-consuming adaptive capacity spectrum method (ACSM) using the DAP algorithm, is discouraged. In fact, this type of bridge practically demands that any nonlinear analysis being done resorts to non-linear time-step dynamic analysis.

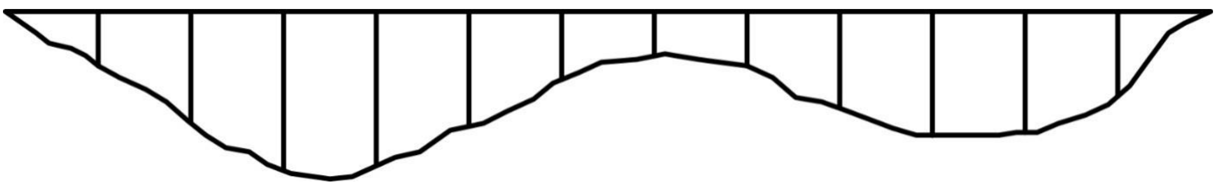

Figure 2.40 Valley shape for long bridge type 3iii

2.6.2.12 Solution 1 – One fixed abutment, sliding connections for central piers

In this case it is clear that the short central piers may undergo large longitudinal displacements due to temperature, in addition to the piers adjacent to the abutment with sliding connections. The solution is done with the placement of sliding and/or fixed connections at the middle piers and piers adjacent to the abutment with sliding connections. In this case there are no forces or displacements transferred to the columns due to the longitudinal earthquake action because the fixed abutment absorbs the earthquake inertia forces. The difficulty of the situation is, as was said before, in the dynamic behaviour in the transversal direction. For this, there can be a series of solutions that will be presented.

For this solution 1 (Figure 2.41), the most trivial way to solve the problem is to place sliding connections in the middle piers in the transversal direction as well. This solves the issue of having large horizontal forces on those piers and "restores" the usual fundamental vibration mode of the deck in the transverse direction. This solution may have a problem, since removing the short central piers from the earthquake resisting system in the transverse direction can result in overloading the adjacent piers.

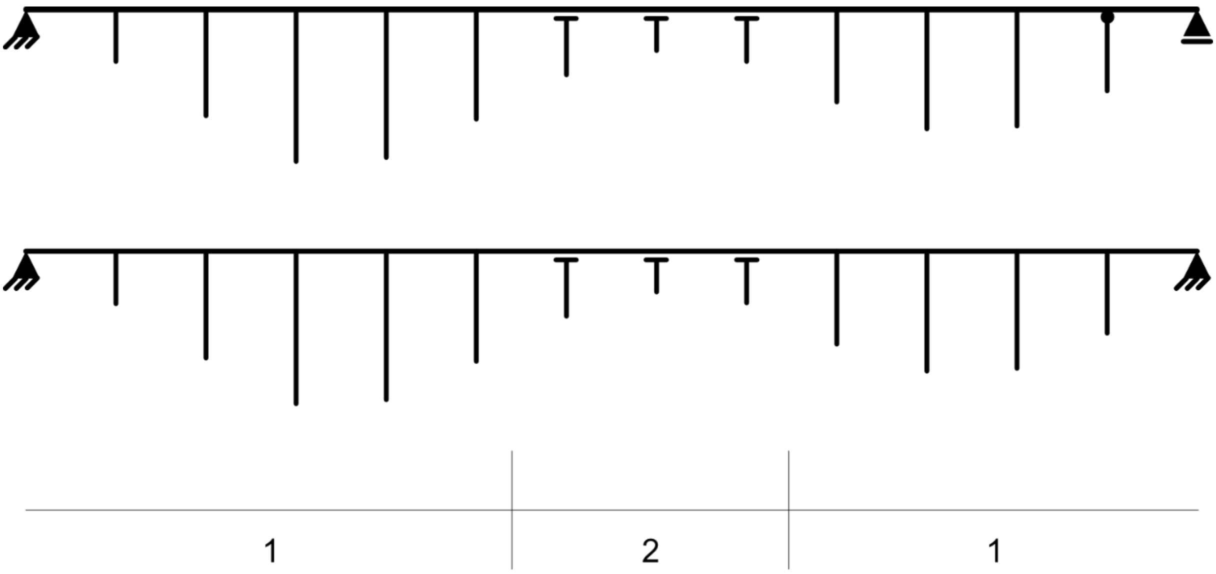

Figure 2.41 Solution 1. Longitudinal direction (top), Transversal direction (bottom).

2.6.2.13 Solution 2 – One fixed abutment, very stiff pier at the centre

In this case, the longitudinal solution is identical to the latter case, the difference is in the transversal direction, the shorter middle piers are monolithic (Figure 2.42), and if the stiffness of these piers is high enough, the bridge is forced to pivot around them, making the anti-symmetric mode shape and the second symmetric mode shape more predominant, figuratively dividing the bridge in two, and eliminating the ductility demand on the central piers.

The drawback of this solution is that a stiffer pier effectively means it will have little available ductility, and so this is only a good solution provided the ductility demand is even lower than the available ductility.

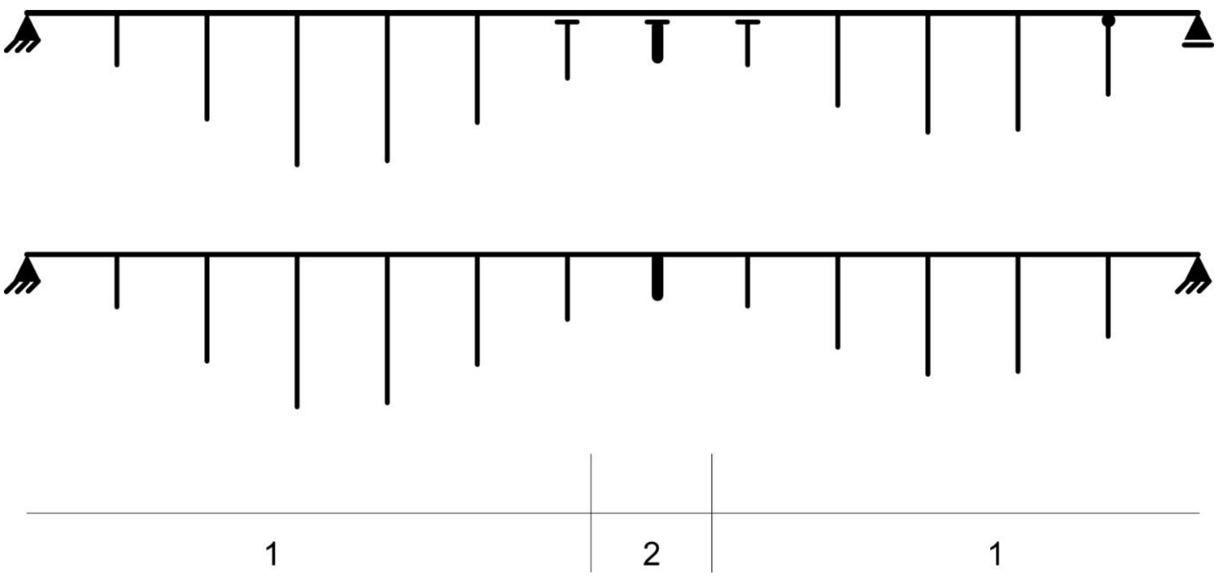

Figure 2.42 Solution 2. Longitudinal direction (top), Transversal direction (bottom).

2.6.2.14 Solution 3 – Both abutments with sliding connections, flexible central piers in the longitudinal direction

If both abutments have sliding connections, the central piers do not undergo relevant longitudinal displacements due to temperature, only the piers at both ends do. However, the earthquake action in the longitudinal direction is now relevant for pier design. The solution can be to divide the piers into two groups according to cross-section, being one group composed by the central piers, and another group composed by all the other piers. The central piers could have smaller cross-sections to be flexible in the longitudinal direction and have larger ductility, in an attempt to try to eliminate the stiffness differential between the longest and shortest piers of the bridge (Figure 2.43). In a way, it is conceptually the opposite from solution 2.

This solution has advantages and an important drawback if the central piers are also flexible in the transverse direction: the dynamic behaviour is more "standard" with a first mode with all the deck moving to the same side in the first mode in the transversal direction but due to a small cross-section those piers may have larger normalised axial forces, and that is the main factor leading to loss of ductility in a cross-section (besides bad detailing, of course). If the central piers are stiff in the transverse direction, this allows to use larger cross-sections avoiding large normalised axial forces in those piers but has the drawback of a less standard dynamic behaviour, as the first mode in the transverse direction may have a configuration with half of the deck moving to one side and the rest to the other, similar to a full sine between abutments.

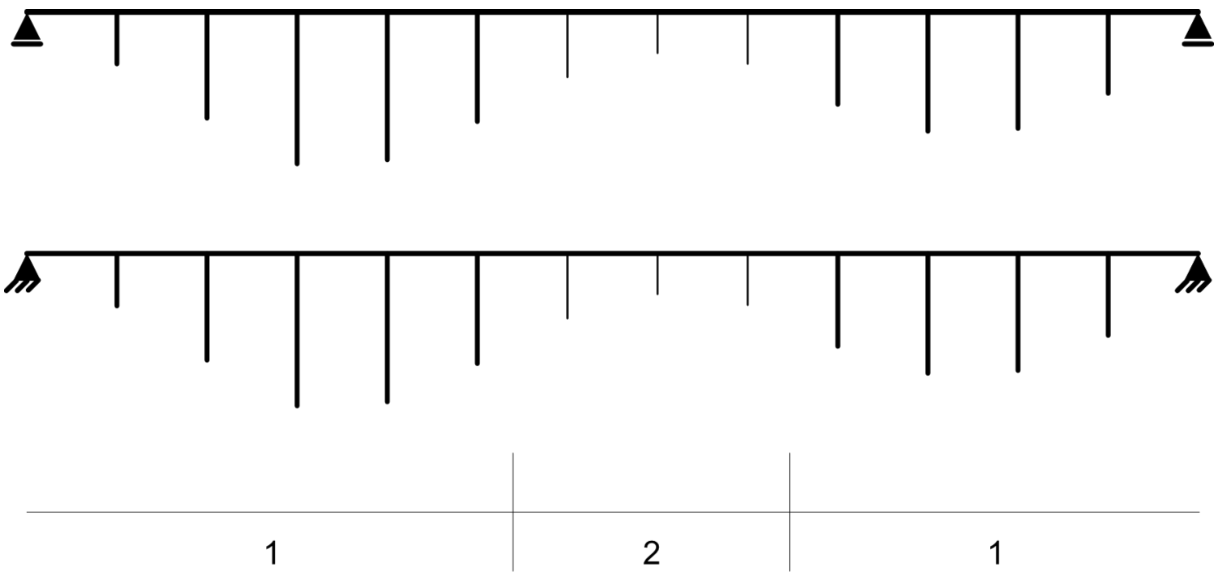

Figure 2.43 Solution 3. Longitudinal direction (top), Transversal direction (bottom).

2.6.2.15 Solution 4 – Two fixed abutments, bridge divided in half

Another solution might be to fix both abutments, thus eliminating the need to design the piers for the longitudinal earthquake action. The temperature related strains, in this case, have to be dealt with by i) using devices that are flexible for low speed of deformation, as it is the case of uniform variations of temperature, and fixed for actions in which displacements between extremities of the device change very quickly, as it is the case of the seismic action, or ii) by having one or two expansion joints at the middle of the bridge, over the central column. This would split the bridge in two also for the transverse direction. This case is the one where the bridge can be less pleasing aesthetically due to the large abutments and central column.

This solution can be defined, in a nutshell, as being a solution that transforms a type 3iii bridge into two type 3i bridges (Figure 2.44).

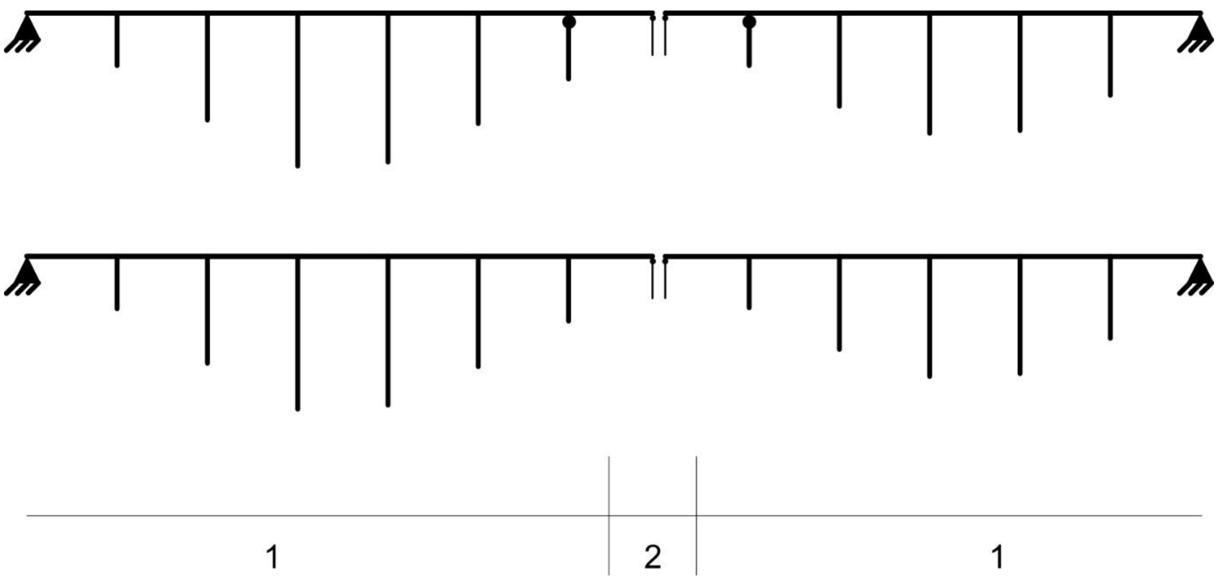

Figure 2.44 Solution 4. Longitudinal direction (top), Transversal direction (bottom).

2.6.2.16 Solution overview

For each bridge type the solutions presented attempt to normalize the bridge infrastructure design, while taking into account the main criteria that usually affect the design process, as is temperature, earthquake action and soil characteristics in a qualitative approach.

To further test which may be the best solution and why, a case study is to be created and tested with the different solutions, optimizing each solution in terms of pier cross-section design.

2.6.3 Foundation solutions for bridges due to soil characteristics

The soil characteristics will have influence on the foundations of the piers and abutments. In the case of the abutments, the soil will influence whether the abutment can be fixed in the longitudinal direction (good quality soil), as well as the type of foundations (piles or footing). As for the piers, it influences whether there can be direct foundations, footings, or indirect foundations, piles. The question of having footings or piles under the piers has more influence on the pier design than what would be expected. In fact, since one of the goals of optimization is normalization, there is a slight nuance when the piers have piles instead of footings. The footings are designed based on axial force and bending moment transmitted by the pier, and the soil's admissible stress. And so, if the bridge's piers have footings underneath, the normalization of the piers' cross-section also means the normalization of all the footings, provided the soil does not change too much between piers.

However, in the case of piles as foundation type, their design does not depend on the duo axial force and bending moment, but rather on axial force and shear force at the bottom of the columns. For this reason and for the case of irregular bridges, another kind of normalization can end up being more interesting. That is to design piers to have similar values of shear force at the bottom, in order to normalize pile design. This situation is not so ideal as is having piers with footings, where the normalization of the piers lead to the normalization of the footings, since the normalization of the piles leads to different pier cross-sections for each pier if their length is different.

2.7 Types of deck cross-section and its influence on bridge dynamics

This work is applicable to viaducts, mainly because the advantages of normalization are more noticeable for long bridges with relatively short spans, which are typical of urban viaducts. Urban viaducts also tend to be heavy, due to having more lanes, and have relatively short piers compared to bridges that have to span over deep valleys outside of the urban setting. Regardless of being a bridge or a viaduct, there are a few different deck types and pier connections that can be found in bridges or viaducts with around 20 to 45-meter span lengths. The importance of this is that these different arrangements of deck and pier connections influence the dynamic behaviour of the bridge, especially in the transversal direction.

The following are types of these deck and pier modules, so to speak:

1) Box girder, one pier
2) Reinforced slab bridge, two piers
3) Reinforced slab bridge, one pier with pier cap

The different deck cross-sections, represented in Figure 2.45, result in different dynamic behaviour, especially due to the effect of the torsional stiffness of the deck and respective boundary conditions in the displacements in the transversal direction. The existence of two piers provides high rotational stiffness around the longitudinal axis of the deck due to the binary formed by both piers. On the other hand, a girder on top of one pier can rotate around its longitudinal axis, and so the bridge has less stiffness to a transversal movement than the same bridge with two piers.

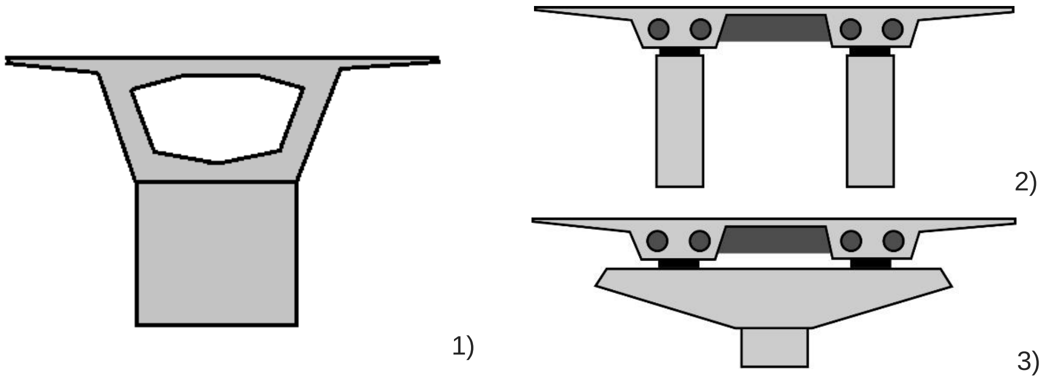

Figure 2.45 Types of deck cross-section according to different dynamic behaviour. From left to right and top to bottom 1), 2) and 3), respectively, from the list above.

As an alternative to cross-sections 2 and 3, beams with height larger than the width can be used in the deck cross section. This can lead to more economic solutions in cases in which there are no minimum height restrictions.

For case 1) the deck has a large torsional stiffness and the rotation of the deck and the top of the pier have total compatibility. There can be rotation of the deck but due to the deck's large torsional stiffness, the piers have little effect on the rotation of the deck around the longitudinal axis, and so the rotation at the top of the pier is influenced essentially by the deck's torsional stiffness. This influence decreases for the central zones of the deck, as they are further away from the abutments where the torsional rotations of the deck are restricted.

For case 2) even though the deck has little torsional stiffness, the two piers form a torque that does not allow rotation of the deck, and so, in this case there is no influence of torsion as in 1). However, unlike case 1), there cannot be any rotation of the deck (unless between piers). In this case, incompatibility of rotations between the deck and the top of the piers can exist, depending on the connections. In that case there would be rotation of the top of the piers without rotation of the deck, only distortion of the deck cross-section, concentrated on flexural deformation of the slab in the transversal direction (rotations about longitudinal axis) in the zone between beams.

For case 3) the deck has little torsional stiffness and it is prone to undergo torsional rotations. In this case, as in 1) there is total compatibility of rotations between the deck and the top of the piers. Unlike 1), however, the piers control the rotation of the deck due to the lack of torsional stiffness of the deck.

The three cases have, therefore, different dynamic behaviour, and in case 1) and 3) the torsional stiffness of the deck influences that dynamic behaviour, and in 2) it does not because there is no deck rotation. In this thesis, the case-studies are essentially case 2), albeit some behaviour comparisons between 2) and 1) and 3) in Chapter 6. Also, in Chapter 4, the case-study is a case 3) bridge, but otherwise case 2) is the focus of the thesis.

2.8 Choice of time-history signals, criteria, and scaling. Mean and variance of spectra.

To apply NDAs and obtain good results, it is critical to have adequate earthquake signals. The big difficulties that arise at this point is obtaining natural signal pairs that roughly match the seismic code elastic response spectrum of the region, or at least match the Tc period, i.e., the period at which the spectrum branch at constant acceleration ends, and constant velocity starts. After this, the set can be further filtered by eliminating the signals whose spectral accelerations are too different from the code's elastic spectrum at important frequencies.

Eurocode 8 dictates that a minimum of three signals are to be used if the maximum result among all signals is to be adopted, and a minimum of seven signals to adopt the mean result.

In addition, part 1 of Eurocode 8 (EC8 - 1) establishes the following criteria for the selection and scaling of ground motion records in the context of seismic assessments of structures: (i) the mean of the zero period spectral response acceleration values calculated from the individual time histories should not be smaller than the value of $a_g S$ for the site under study, being a_g the design ground acceleration on rock and S the soil parameter; (ii) and, in the range of periods between 0.2 T_1 and 2.0 T_1, where T_1 is the fundamental period of the structure in the direction where the record will be applied, no value of the mean 5% damping elastic spectrum, calculated from all time histories, should be less than 90% of the corresponding value of the 5% damping elastic response spectrum.

The code elastic response spectrum chosen to be the reference response spectrum for the scaling of the chosen ground-motion signals was the type 1 far-field earthquake, zone 2, soil C spectrum from the Portuguese national annex (IPQ 2010) which is associated to $a_g S$ =T_B=0.1s, T_C=0.6s, T_D=2s. The choice of using the far-field earthquake is due to it being usually more detrimental to bridges than the near-field earthquake. This is due to the larger Tc value of the far-field earthquake spectrum.

In a preliminary sorting, according to overall spectrum shape and Tc value, 16 natural ground-motion pairs were chosen. Of these 16, two subsets (4 and 9 pairs) were formed. These subsets comprise the signals whose spectrum varies less, at the most relevant frequencies, compared to the reference spectrum. The sorting and scaling were done resorting to the software SeismoSpect (SeismoSoft 2016), by SeismoSoft. The individual spectra of the 16 pairs and the mean spectrum are presented in Figure 2.46.

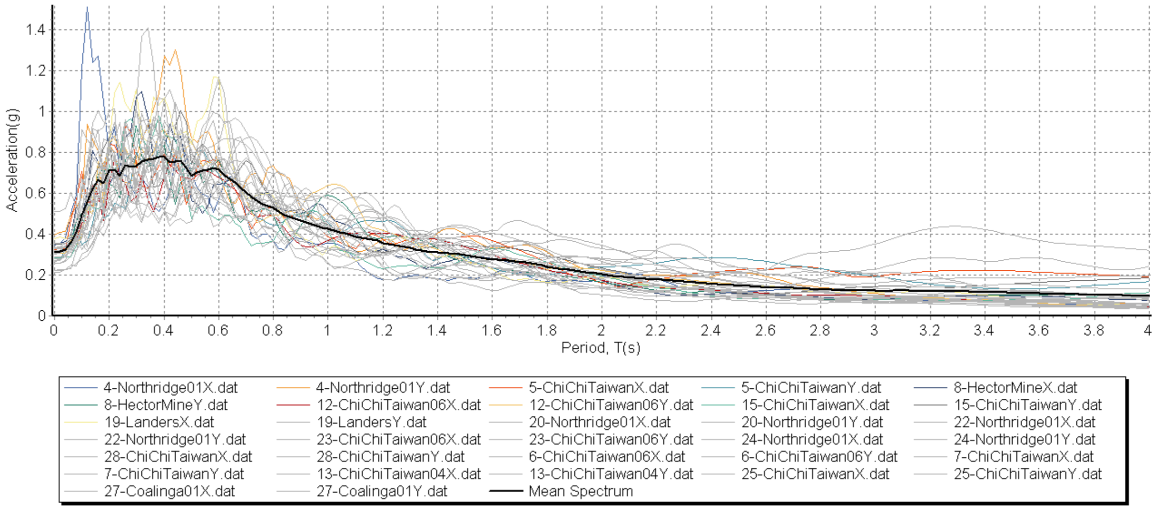

Figure 2.46 Spectra of the 16 pairs of natural signals and their mean.

In Figures Figure 2.47a to Figure 2.47c, the mean spectra for the set of 16 pairs and the two subsets of 9 and 4 pairs, respectively, are presented. The set of 4 pairs is comprised by the signals whose spectrum is closest to the reference Eurocode spectrum. Subsequently the set of 9 pairs is comprised by the set of 4 pairs plus 5 additional pairs that are a good match but not as good as the first 4 pairs. The set of 16 pairs is the initial set.

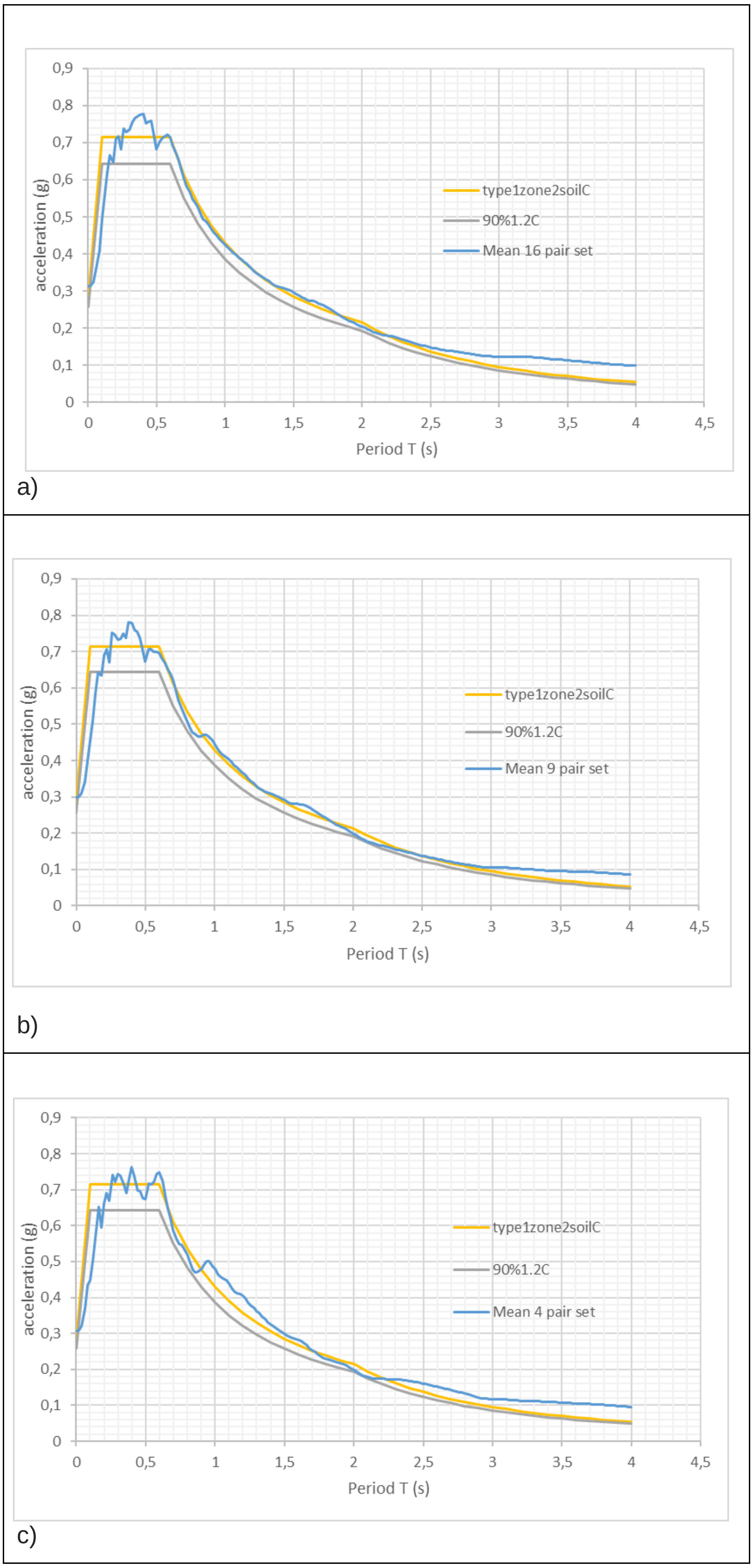

Figure 2.47 Reference spectrum and mean spectrum for each set of signal pairs. a) 16 pairs; b) 9 pairs; c) 4 pairs

For all three sets, particularly both subsets (4 and 9), the EC8 criteria are satisfied: the zero-period acceleration is larger in the mean spectrum than in the reference spectrum, and in the meaningful range of frequencies for bridges the mean spectrum is never beneath the 90% reference spectrum.

In Figure 2.48, the mean of each of the three sets (16, 9 and 4) are compared. Attending to the difference in the number of signals used for each mean result, one expects more variance in the mean values with less pairs in the set. However, since the set with least pairs is also the one which comprises the spectra more similar to the reference spectrum, the end result is that there isn´t much difference between the three mean spectra.

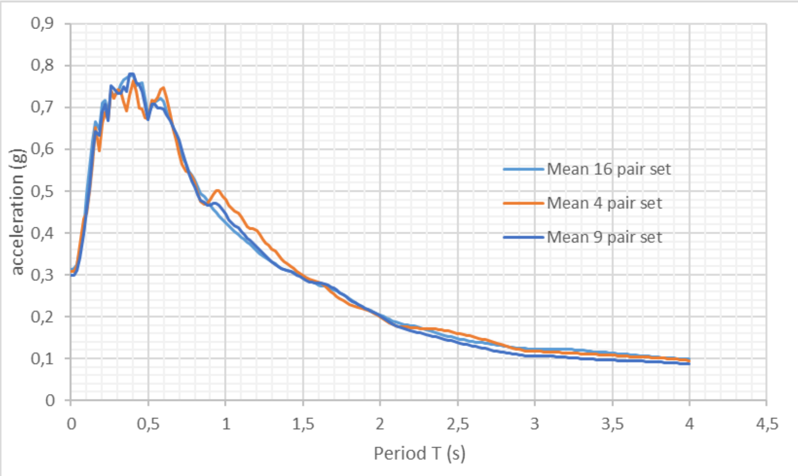

Figure 2.48 Comparison between the mean spectra of all three sets

In Figure 2.49 we have the spectra for the set of 4 pairs and 9 pairs plus and minus the standard deviation. There isn't a significant difference between the spectra of both subsets. For this reason, many of the analysis inside the iterative procedures loop, which will be addressed later, will be done resorting only to the 4-pair subset, and only at the end, for result confirmation will the 9-pair subset be used. It will be shown, in fact, that there is no big difference between the mean results of each subset.

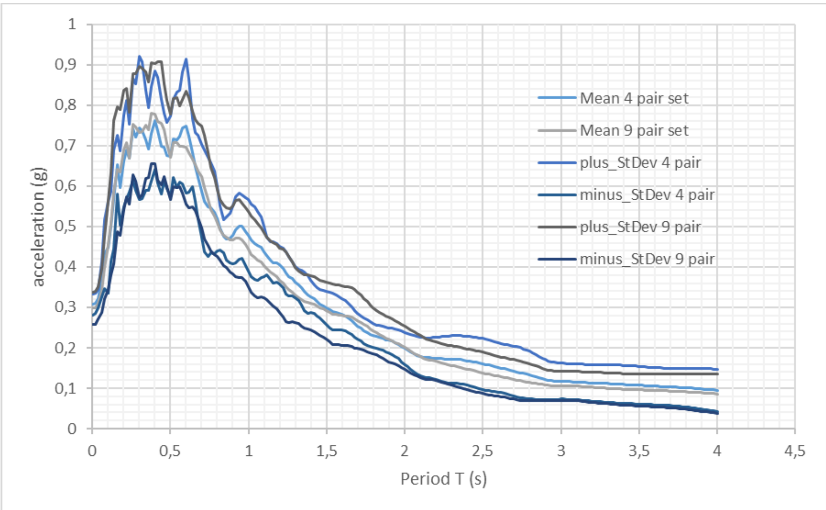

Figure 2.49 Mean plus and minus standard deviation for the sets of 4 and 9 pairs.

2.8.1 Mean response versus maximum response among all signals in set

When choosing to apply NDAs, a question arises on how to maintain reliability using the least number of signals possible. And the directives by Eurocode 8 state the minimum of 3 signals to use the maximum response among all signals or minimum of 7 to use the mean response. This is not a simple choice since there is a rather large difference between using the mean response and using the maximum response. Even following the criteria of Eurocode 8, one must be very careful in choosing the signals for use of the maximum response, because slightly different signals can stimulate a very different response in the structures, due to differences in the frequency content and peak sequences. For that reason, to use the maximum response, extra care must go into the choice of signals. In fact, using the mean response criteria allows having higher standard deviation between spectra of the signals in the set without jeopardizing the overall results. However, in the case of using the maximum response, it is enough for one of the spectra to have a peak at an important frequency value to influence the analysis, originating a result too dependent on that single signal. On the other hand, the maximum response is less time consuming than the mean response.

These issues must be weighed to decide on how to perform the NDAs because once again, deciding between reliability or accuracy and efficiency is not a trivial decision. The number of accelerograms used in this work is referred case by case in the next chapters.

3 Seismic structural optimization

3.1 Seismic optimization: Optimization and Normalization.

The proposed task is to develop a framework for bridge seismic design optimization. Optimization can be, however, a somewhat vague concept. What will be optimized? What are the constraints of the optimization? Optimization to a full extent in terms of amount of materials used, can deliver a design which is not practical to build, for having too many different elements with different cross-section, and thus would not be optimal for the construction phase. Normalization, on the other hand, means simplifying the project towards efficiency, as with prefabrication. Therefore, optimization should also mean normalization to some extent, but that is not enough. A structure might be normalized, but not optimal. And regarding bridge design, a normalization format employed for one bridge might not be applicable for another bridge.

The normalization format will depend on macro characteristics of the bridge, i.e., what kind of bridge it is and what category it belongs to (short or long, regular or irregular). The optimization will have to do with the variables chosen for optimization. In this thesis these will be the material quantities, constrained by the chosen normalization format and by design limits.

3.1.1 Normalization

When designing a RC bridge for seismic action there are several design variables to consider. The main ones are probably pier cross-section shape and size, amount of steel reinforcement in the piers, both longitudinal and transverse, and the piers' connections to the superstructure. In a bridge, it is common to vary, from pier to pier, the amount of steel reinforcement and the connection to the superstructure, depending on length and pier regularity along the bridge. The size and specially the shape of the pier is not common to vary in the same bridge.

If the piers have all the same length, in principle there is no reason why the steel reinforcement should be different from pier to pier. Also, if the bridge is not beyond a certain length, where temperature strain becomes important, then there is also no reason for having piers with different connections to the superstructure. This is the most simple and intuitive case of normalization. Other types of RC bridges, especially irregular long bridges, will need different normalization formats and part of the work will be testing and choosing between them.

3.1.2 Optimization

After the normalization format is defined, the design variables can be optimized. The optimization process is constrained not only by the normalization format, but also by design rules and by design criteria to resist the earthquake action. The two latter constraints delimit what is called the feasibility region of the optimization search, i.e., a solution is feasible if the design variables are inside possible values and the resulting bridge can resist the earthquake action.

The ability to resist the earthquake action can be defined in different ways, and it depends on what are the failure criteria of the structure. In the case of bridge piers, and in the framework of the current thesis this has been defined as the compression strain in the concrete being larger than the ultimate strain of confined concrete ε_{cu}. This is due to the fact that failure of concrete cover does not hinder the resistance of the structure and only leads to repair needs.

The optimization search has the objective of rendering the solution/solutions inside these constraints that minimize the amount of materials used.

3.2 Structural optimization

Structural optimization is the subject of making an assemblage of materials resist loads in the best way. However, to make any sense out of that objective we need to specify the term “best” (Christensen and Klarbring 2009). The first such specification that comes to mind may be to make the structure as light as possible, i.e., to minimize weight. Another idea of “best” could be to make the structure as stiff as possible, and yet another could be to make it as insensitive to buckling or instability as possible. Clearly such maximizations or minimizations cannot be performed without any constraints. For instance, if there is no limitation on the amount of material that can be used, the structure can be made stiff without limit and we have an optimization problem without a well-defined solution or set of solutions. Quantities that are usually constrained in structural optimization problems are stresses, displacements and/or geometry. Note that most quantities that one can think of as constraints could also be used as measures of “best”, i.e., as objective functions. Thus, one can put down a number of measures on structural performance – weight, stiffness, critical load, stress, displacement and geometry – and a structural optimization problem is formulated by picking one or more of these as objective functions that should be maximized or minimized and using some of the other measures as constraints.

3.2.1 Design process

Of course, the criteria used as example above are purely mechanical, and there are other criteria that can be used as objectives or constraints that correspond to economical, functional or aesthetical considerations. Some of these are not so easy to define mathematically and are often taken into consideration in other steps of the design process. In (Christensen and Klarbring 2009) these steps are summarized as:

1) *Function:* What is the function of the product (structure)? Concerning a bridge, how long and broad should it be, how many driving lanes, what are the expected loads, etc.
2) *Conceptual design:* What type of construction method? What type of structural typology? What are the possible pier locations and pier length? In bridge engineering these are all dependent variables and a decision on the structural typology influences and is influenced by the construction method, which in turn, is influenced by span length and whether the bridge is inserted in a curve or not, and span length depends on where the piers can be located, etc.
3) *Optimization:* Within the chosen concept, and within the constraints of function, make the product as good as possible. For a bridge it would be natural to minimize cost: perhaps by using the least possible amount of material, and/or by normalizing design. But other objectives make sense, especially concerning earthquake resilience.
4) *Details:* This step is usually controlled by market, social or aesthetic factors.

The traditional, and still dominant, way of realizing step 3) is the iterative-intuitive one, which can be described as follows. (a) A specific design is suggested. (b) Requirements based on the function are investigated. (c) If they are not satisfied, say the stress is too large, a new design must be suggested, and even if such requirements are satisfied the design may not be optimal (the bridge may be overly heavy) so we still may want to suggest a new design. (d) The suggested new design is brought back to step (b). In this way an iterative process is formed where, on mainly intuitive grounds, a series of designs are created which hopefully converges to an acceptable final design.
For mechanical structures, step (b) of the iterative-intuitive realization of step 3, is today almost exclusively performed by means of computer-based methods like the Finite Element Method (FEM) or Multi Body Dynamics (MBD). These methods result in that every design iteration can be done with confidence, and they allow the design process to be more effective and efficient. However, this does not lead to a change in strategy.
The mathematical design optimization method is conceptually different from the iterative-intuitive one. In this method, an optimization problem is formulated mathematically, where requirements are formulated as constraints, and the concept "as good as possible" is given precise mathematical form. As a result, step 3) in the design process is given a much more methodical and automatic nature in the mathematical design optimization method than in the iterative-intuitive approach. The subset of the mathematical design optimization that deals with mechanical problems is termed structural optimization, and in the next section, the basic formulation of such problems is presented.

3.2.2 Mathematical formulation of structural optimization problems

A structural optimization problem is essentially composed of the following components:

- *Objective function(s)* (f): This function is used to classify different designs. For every design solution there is a corresponding value of the objective function f, which indicates the quality of that design solution. The optimization problem can be defined either as a minimization or a maximization problem, but the most common is to define the problem as a minimization problem. Usually f measures weight, displacement in a given direction and in a given node, effective stress or strain or even cost of production.

- *Design variables* (x): This is usually a vector that combines all the variables associated to the optimization problem, and it is this vector that is changed during the optimization process. The design variables usually correspond to material properties or geometry.
- *State variable* (y): For a given structural design, that is, for a given design $\bar{x}$, $\bar{y}$ is a vector that represents the response of the structure. For a mechanical structure this means force, displacement, stress and/or strain. This state variable is sometimes implicit in the formulations because it is a function of $\bar{x}$
- *Constraints* (g): The constraints relate to the vectors of $\bar{x}$, $\bar{y}$ and also the objective function f and correspond to limits, either physical, for example, due to buckling or maximum stress or strain, or limitations imposed by design codes, for example maximum allowed displacement at mid-span or maximum allowed percentage of flexural steel reinforcement.

A general structural optimization problem takes the following form:

$$(SO)\begin{cases} \quad minimize\ f(\bar{x},\bar{y}) \\ subjected\ to \begin{cases} g(f)\ \leq 0 \\ g(\bar{y})\ \leq 0 \\ g(\bar{x})\ \leq 0 \end{cases} \\ L_d \leq\ x_d \leq U_d,\ \ 1 \leq d \leq n \end{cases} \tag{3.1}$$

3.2.3 Types of structural optimization problems

In structural optimization, x usually represents some kind of geometric feature of the structure. Depending on the geometric feature, a structural optimization problem can be divided into three classes (Christensen and Klarbring 2009):

- *Sizing optimization:* This is when x is some type of structural thickness or a material quantity i.e., cross-sectional areas of truss members (Figure 3.1), or the thickness distribution of a sheet, or ratio of flexural steel reinforcement.
- *Shape optimization:* In this case x represents the form or contour of some part of the boundary of the structural domain. Think of a solid body, the state of which is described by a set of partial differential equations. The optimization consists in choosing the integration domain for the differential equations in an optimal way (Figure 3.2). Note that the connectivity of the structure is not changed by shape optimization: new boundaries are not formed.
- *Topology optimization:* This is the most general form of structural optimization. In a discrete case, such as for a truss (Figure 3.3), it is achieved by taking cross-sectional areas of truss members as design variables, and then allowing these variables to take the value of zero, i.e., bars are removed from the truss. In this way the connectivity of the nodes is variable so we may say that the topology of the truss changes. If instead of a discrete structure we think of a continuum-type structure, such as a two-dimensional sheet, then topology changes can be

achieved by letting the thickness of that sheet take the value of zero (Figure 3.4). Frequently, shape optimization is taken as a subclass of topology optimization, but since practical implementations are based on very different techniques, so the two types are treated separately here.

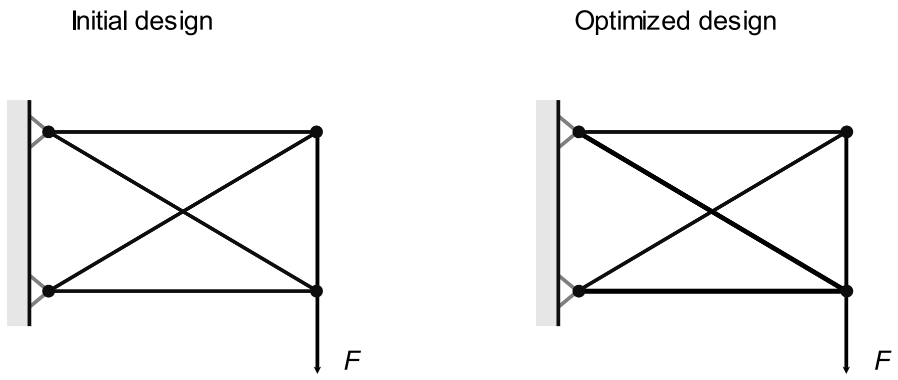

Figure 3.1 Sizing optimization applied to the cross-sections of a truss' elements (Christensen and Klarbring 2009).

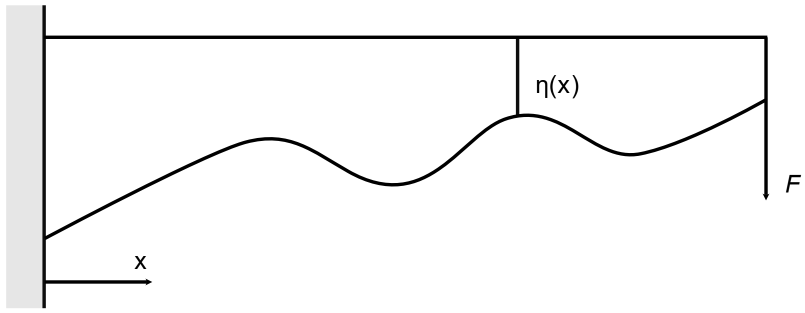

Figure 3.2 Shape optimization where the objective is to find the optimal shape $\eta(x)$ under force F (Christensen and Klarbring 2009).

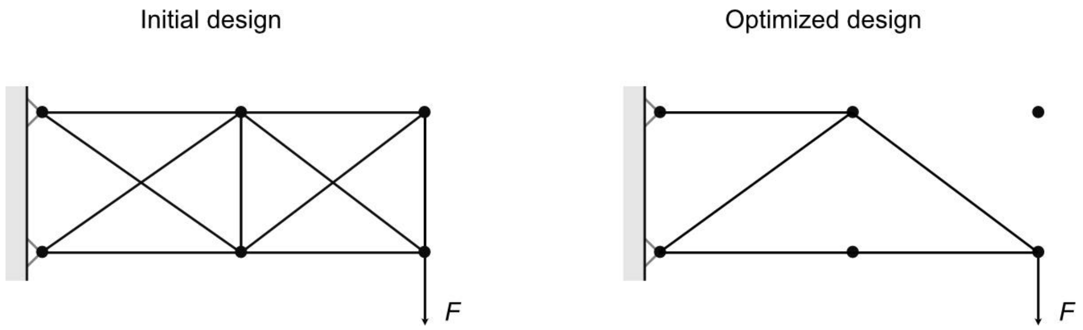

Figure 3.3 Topology optimization of a truss. Bars are removed by allowing cross-sectional areas to become equal to zero (Christensen and Klarbring 2009).

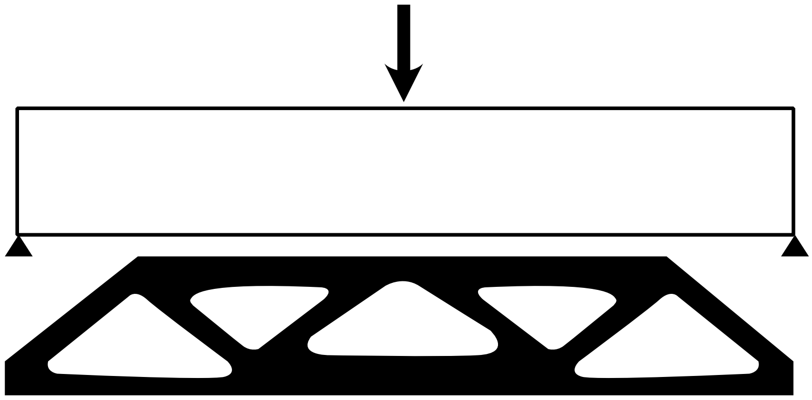

Figure 3.4 Topology optimization applied to a 2D continuum-type element (Christensen and Klarbring 2009).

3.3 Multi-objective optimization

The goal of optimization is to achieve a feasible solution which minimizes or maximizes one or more objectives. The need of finding an optimal solution in a problem comes mostly from the extreme purpose of either designing a solution for minimum possible cost of fabrication/construction-, or maximum possible reliability, or others. Therefore, optimization methods are of great importance in practice, particularly for engineering design, scientific experiments, and business decision-making (Deb 2001).
An optimization problem can be single-objective or multi-objective. When an optimization problem is modelled involving only one objective function, this is a single-objective optimization problem. The optimal set of a single-objective optimization problem has only one solution. Most optimization problems that we are used to deal with are single-objective optimization problems, usually solved through gradient-based methods. However, most problems in the real world have more than one objective function. A multi-objective optimization problem is a trade-off problem, where you have more than one conflicting objective, that is, the optimization of all objectives is not possible to obtain in one single solution. Traditionally, this problem is addressed by developing a weight vector composed by a weight for each objective, therefore transforming a multi-objective problem in a single-objective problem, also called preference-based multi-objective problems. This solution has a drawback, since one must define a priori a weight vector that defines the relative importance of each objective regarding all the others. By defining a weight vector, one is already making a design decision and thus eliminating several solution possibilities from being optimal, as will be shown later. Unfortunately, this must be done to solve solutions through the traditional gradient-based methods, since these methods cannot handle multiple solutions.

3.3.1 Multi-Objective Optimization Problems

The fundamental difference between single-objective and multi-objective problems, is that in multi-objective problems the optimal set has multiple solutions. This set is called the optimal Pareto set. A Pareto set is composed by solutions that are not dominated by any other solution in that same set. The short definition of domination is the following: a solution A dominates solution B, if A is not worse than B in any objective, and A is better than B in, at least, one objective.

To illustrate these differences an example is given. In a decision to buy a car, there are several cars available from which to choose, and the prices can range from under 10.000 euros to several hundred thousand euros. Given car A with a cost of 10.000 and car B with a cost of 150.000, if this decision were a single-objective optimization problem, with price as the only objective, then car A would be the optimal solution. If car A were the cheapest car available, everyone would buy car A and car A would be the only car on the streets. However, minimizing price is not the only objective if we add maximizing comfort as a second objective the solution changes. It is intuitive that minimizing price and maximizing comfort are usually conflicting objectives. The cheaper the car, the less comfortable and vice-versa. Let us say that car A has a comfort level of 40% and car B of 90%, and there is no car more comfortable than car B. For someone who is rich, and for whom price is not an issue, car B is the optimal choice. Cars A and B are the extreme solutions, they are solutions that maximize one of the objectives, however there are more possible choices in between these extremes that present a trade-off between price and comfort. In Figure 3.5, a set of solutions, containing solution A and B, are presented. It is clear that each of these solutions (A, 1, 2, 3 and B), in relation to any other solution in that set, is better in one objective and worse in the other. This is a Pareto set for this two-objective problem.

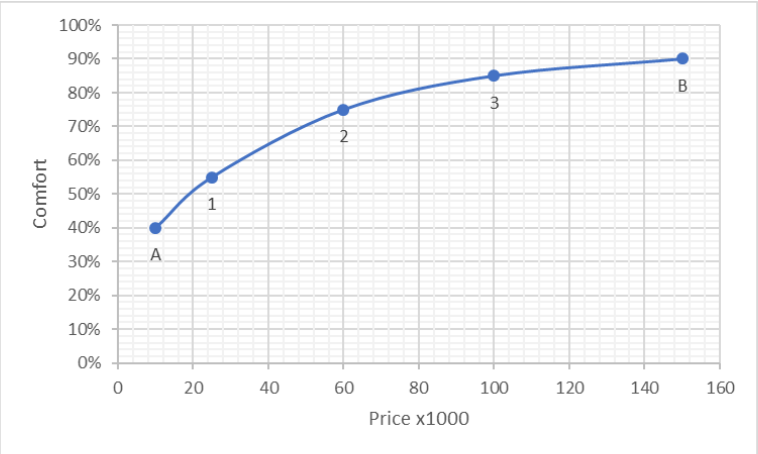

Figure 3.5 Price vs Comfort.

If there is no other feasible solution that dominates an element of this set, then this set is the optimal Pareto set, which is the desired output of a multi-objective optimization problem. Also, it is interesting to think that each solution in the optimal Pareto set corresponds to a different weight vector if one would have transformed this multi-objective problem into a single-objective problem.

3.3.2 Evolutionary Algorithms

As said before, the result of solving a multi-objective optimization problem is an optimal set with multiple solutions, also called optimal Pareto set. To solve a multi-objective optimization problem, one must resort to methods different than gradient-based methods. One family of methods capable of solving these problems are evolutionary algorithms (EA).

Evolutionary algorithms are a group of metaheuristic search algorithms. This means that they are not programmed to explicitly solve a mathematical problem, rather they search over a large feasible set of possibilities to find an approximate solution to the problem, without the need to test the whole set of feasible solutions. Evolutionary algorithms, as the name implies, are inspired and mimic nature’s evolutionary principles. It is Darwinism applied to optimization problems. One of the main characteristics of EAs is that in each iteration they use a population of solutions, instead of a single solution as in point-by-point methods. Since EAs use a population of solutions at each iteration, the output of an EA is also a population of solutions, which means that it is ideal for multi-objective optimization problems. In fact, if an optimization problem has only one optimal solution, then all the solutions in the EA population will converge to that optimal. On the other hand, if there is more than one solution, a well-designed EA will have many of the optimal solutions in its final population.

In this work, the NSGA-II (non-dominated sorting genetic algorithm) was implemented and partly modified to suit the problem in hand.

Genetic algorithms (GAs) are a type of EA. These are two concepts that commonly mean the same thing. GAs are search and optimization procedures that are motivated by the principles of natural genetics and natural selection. Some fundamental ideas of genetics are borrowed and used artificially to construct search algorithms that are robust and require minimal problem information. In Figure 3.6, we present a working procedure of a genetic algorithm, as shown in (Deb 2001).

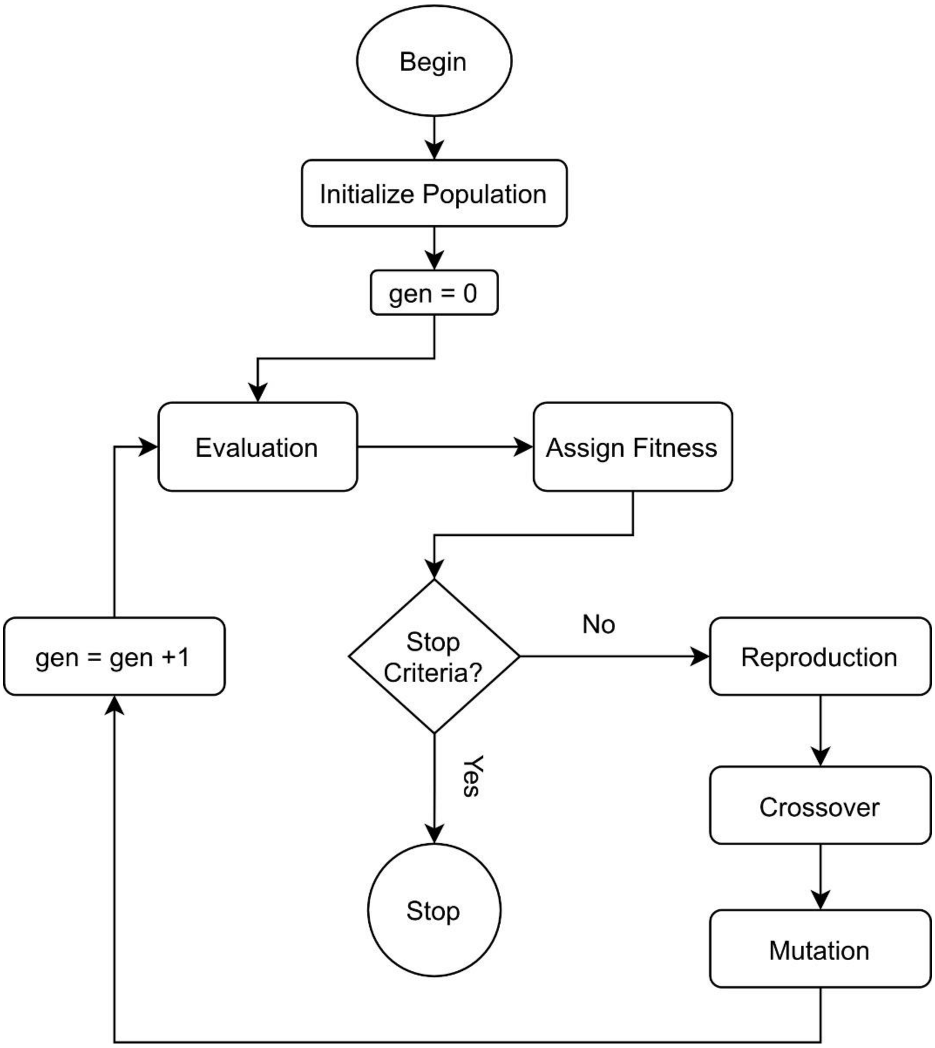

Figure 3.6 Working principle of a genetic algorithm in Kalyanmoy Deb (2001)

The procedure starts by generating an initial population of solutions, these solutions are evaluated for each objective function of the problem and a fitness vector is assigned to each solution. A fitness vector is nothing more than the evaluations of a solution by each objective function. A condition of convergence is checked and in case the problem has not converged then the solutions are selected for reproduction and are paired together (every solution is paired with another at random). Afterwards, an offspring population is generated through a crossover operator that mixes the genetic information of the parent population. Finally, some of the offspring are randomly chosen to undergo mutation of their genetic information. The offspring population is then evaluated, and a new population is generated according to the nature of the GA, whether it is an elitist GA or not. In the case of a non-elitist GA, the offspring population is the new population in the next iteration. In the case of an elitist GA, the offspring population is compared with the parent population and the least fit solutions of each population are removed, generating a new population composed by a mixture of parents and offspring. The procedure continues until a convergence criterion is met, usually this is a measure of convergence of the population's most fit solutions.

There are different families of GAs. Elitist and non-Elitist GAs according to the way that solutions pass from generation to generation; Real-parameter and binary-coded GAs according to the nature of the variables, continuous or discrete. There are also several different types of selection, crossover and mutation operators that must be well chosen to be applicable for the problem in hand. There are also different techniques to manage constraints.

4 Optimizing Earthquake Design of Reinforced Concrete Bridges based on Evolutionary Computation Techniques

This chapter presents a methodology for the earthquake design of reinforced concrete (RC) bridge infrastructures based on the application of multi-objective evolutionary techniques. The purpose of the methodology is to allow better decision making for the earthquake design of bridges by proposing optimized solutions which offer trade-offs between material quantities, performance/robustness and cost. For this, two multi-objective optimization problems (MOPs) were defined with two sets of objectives: the first objective-set optimizes the amount of material used in the piers; the second set of objectives comprises a cost function and a performance metric. The NSGA-II algorithm was adapted and applied with real coded variables and multiple nonlinear dynamic analysis performed in each fitness evaluation. The results of the runs show different Pareto fronts strongly associated with solution schema of pier-deck connections and steel distribution between piers. The results also allow to perceive the influence of ductility through the impact that certain variables in certain piers have on the performance of solutions. The importance of support conditions/connections between infrastructure and deck and of confinement of piers is clear. The results of the two MOPs show that sub-optimal solutions in terms of volume of materials used may be interesting in terms of reliability gain. In the end, the results of applying the methodology present solutions which offer trade-offs and information gain valuable for bridge design.

4.1 Introduction

Optimal earthquake design of structures is inherently complex, not only due to the complexity in calculating the non-linear response of structures subjected to dynamic actions, due to geometrical and material non-linearity, but also due to the earthquake action being a stochastic process with great uncertainties. This makes it impossible to derive an analytical formulation for the problem of non-linear seismic analysis, which means that any attempt in optimization cannot be performed by means of the traditional gradient-based solutions. Hence, the inclination towards population-based methods and other meta-heuristics, such as Genetic Algorithms, Simulated Annealing, Harmony Search etc. There have been several studies of structural optimization using population-based approaches, mainly associated to steel structures (Sarma and Adeli 2000) (Soh and Yang 1996) (Rao, et al. 1992). Much work has since been done related to earthquake engineering, but not much work can be found for optimization of reinforced concrete (RC) bridge infrastructure seismic design. The drawback for use in an earthquake engineering context is that the computational demand associated with population-based strategies is magnified with the need of using several earthquake records for the structural verification in a non-linear dynamic analysis (NDA) framework; and even more so if a performance-based design approach is used, where model uncertainty demands multiple tries, usually with Monte-Carlo simulations (MCS). In the context of bridges, this non-linear dynamic framework can be a necessity, since it has been shown

(Kappos, Saiidi, et al. 2012) that bridges, in particular long irregular bridges in terms of pier length, should not be analysed through simplified methods, including non-linear static procedures. This situation results from the fact that the response of the structure is usually associated to more modes than just the first fundamental vibration mode and, furthermore, the importance of the modes can change during the earthquake action as some elements suffer stiffness reduction and others don't.

The necessity of devising a framework for the optimization of such structures is real. It is also important to be able to extract knowledge that can be generalized, from the process of optimization. In fact, the timeframe for projects made in design firms is short, and so there is no time to perform an iterative process of several NDAs, which are computationally demanding on their own, and NDA analysis contemplates many runs in many iterations. Furthermore, NDA analysis requires specific software and knowledge of nonlinear dynamic analysis and each run in each iteration takes minutes or hours to complete (depending on the program used and model complexity), not seconds. Therefore, most firms carry out their design using in-house "heuristics" and "common sense" based on experience or in traditional beliefs, which in many cases may be flawed in terms of theoretical background (M. N. Priestley 2003).

In this chapter a methodology is proposed for the seismic design of RC bridge infrastructures, based on a two-phase approach application of evolutionary algorithms. In this two-phase approach, the optimization is performed for two objective-sets, in which the second phase is initiated with the first phase's final population. The first phase employs two of the main objectives for infrastructure design, trade-off between steel and concrete quantities, while the second phase searches the trade-off between cost and performance. The optimization variables are associated to bridge pier design: pier-deck connections, pier cross-section dimensions (diameter), flexural steel reinforcement and pier steel confinement. All variables, with the exception of pier-deck connections, go into the calculation of the objectives associated to material quantities and cost. The split in two objective-sets allows to reduce the computational demand associated with performing the optimization over three or four objectives, which is particularly important in a non-linear dynamic framework. The objective of the methodology is not only to obtain optimized solutions associated to each objective-set, but also to utilize the entire population generated during the search to extract meaningful information for design, associated to feasibility and earthquake performance. Variable schema strongly associated to feasibility are identified, particularly associated to non-quantifiable variables such as pier-deck connections. As for performance, variables are ranked according to their importance on the seismic performance of the structure by evaluating the evolution of their mean and variance values through progressive performance states.

The study's structural model of the piers is a full fibre model where geometric and material non-linearities are considered, from P-delta effects to non-linear constitutive relationships for the materials.

The NSGA-II (Deb, et al. 2002), mentioned in Section 3.3.2, was the adopted Genetic Algorithm (GA) since it is a reference algorithm being one of the most used Multi-Objective Evolutionary Algorithms (MOEAs), together with MOEA/D (Zhang and Li 2007) and MODdEA (Chow and Yuen 2012). It can well address most types of multi-objective problems (MOPs) with very good results even with complex MOPs. It was partially adjusted and modified for the problem addressed in this thesis of structural seismic optimization, particularly concerning the genetic operators.

There are many possible metaheuristics that can be employed for structural optimization, other than GAs in general and MOEAs in particular. In the following section many examples of diverse metaheuristic applications to structural engineering are presented. A review (Zavala, et al. 2013) of the field of multi-objective metaheuristics applied to problems focusing on the optimization of the topology, shape, and sizing of civil engineering structures shows the most relevant features of algorithms and their applications.

This Chapter 4 paper will continue with Section 4.2 on related work, where more applications of different techniques of meta-heuristic algorithms in the field of structural engineering are discussed, with special emphasis on evolutionary computation techniques. Subsequent Sections 4.3 and 4.4 introduce the dynamic behaviour of bridges and discuss the applied earthquake action, respectively. In Section 4.5, evolutionary computation techniques are introduced more in depth, and the MOPs are characterized with the definition of variables, objectives and constraints. Section 4.6 introduces the case study and presents the results, and finally, Section 4.6.3 holds the concluding remarks.

4.2 Related Work

In structural engineering several studies have been made in applying different machine learning algorithms with diverse objectives in mind. As it happens commonly, artificial neural networks (ANN) have been applied to some extent. For example, for predicting structural response or for making deterministic and probabilistic constraint checks, as in (Papadrakakis and Lagaros 2002). In this study a GA and ANN hybrid is used to perform a reliability-based optimization (RBO). In a first phase, Monte-Carlo simulations (MCS) are performed to train the ANN for structural response. In the second phase the trained ANN predicts the structural response of the GA's population, as the GA performs the optimization with a single-objective function associated to total weight.

The harmony search algorithm was created in 2001 (Geem, Kim and Loganathan 2001), and has been applied for structural optimization of steel structures (Geem and Lee 2004). In fact, steel structures and in particular steel trusses have been the subject of several GA applications as well, due to the large number of variables and the code restrictions, these structures were the subject of several early applications of heuristics. It was for steel trusses that many early studies with hybrid GAs were developed, especially Fuzzy-GAs (Sarma and Adeli 2000) (Soh and Yang 1996) (Rao, et al. 1992) that integrate an FLC (fuzzy logic controller) for the population generation, with the goal of steering the search strategy of the GA to a more expedite convergence.

More recent works have been done using different meta-heuristics applied to structural engineering. The work (Tugilimana, Coelho and Thrall 2019) presents an application of simulated annealing and gradient-based search which are applied to topology optimization, dynamic grouping and spatial orientation of trusses. The optimization problem is single-objective and minimizes total volume of the truss. The author of (Chikahiro, et al. 2019) employed a differential evolution (DE) algorithm to optimize the reinforcement layout for deployable emergency mobile bridges. In this DE three single-objective functions were employed: weight (W) minimization, load (P) maximization and a third objective function which minimizes W+1/P. Another example is (Pedro, et al. 2017) which employs and compares many heuristics: Backtracking Search Algorithm (BSA), Firefly Algorithm (FA), GA, Imperialist Competitive Algorithm (ICA) and Search Group Algorithm (SGA). The study performs a two-stage optimization with a single cost objective for the design of steel-concrete composite I-girder bridge superstructures. In the first stage the optimization is performed using an approximate analytical model to locate an optimum region which is the starting point of the next stage, where a finite element model (FEM) is employed.

Specifically concerning GAs, there are many examples of recent works which employ GAs in structural optimization. The authors in (Alam, Kanagarajan and Jana 2019) utilize a single-objective GA to perform optimal design of thin-walled open cross-section columns for maximum buckling load. In this study, the single objective maximizes the critical buckling load in a constrained problem where the total area of the cross-section is kept constant. Combined effects of torsional and flexural buckling are considered, and different geometries of cross-sections are generated in case-studies with varying column length. The authors in (Arellano, Tolentino and Gómez 2019) employ the NSGA-II algorithm for a multi-objective optimization, with three objective functions, of cable overlap length in multi-span cable-stayed bridges with criss-cross cables. The authors in (Ha, Vu and Truong 2018) also utilised a GA to optimize the design of stay cables of steel cable-stayed bridges, in this case minimizing the deck vertical and pylon horizontal deflections coupled in a single-objective.

In building engineering, GAs are also employed for several applications as in (Lee 2019), where the Neighbourhood Cultivation Genetic Algorithm (NCGA) is employed for the optimization of building geometry as passive design and an HVAC system as an active design, using a multi-objective approach with three objectives.

In the field of earthquake engineering, many papers have been published, where the application of GAs or other heuristics are central to the work.

In (Tsompanakis and Papadrakakis 2004), an RBO is performed on steel buildings. The optimization performed on a single-objective problem (SOP) with size variables, where the objective function is to minimize structural weight. A two-level RBO is performed where on a first step a deterministic optimization is done, followed by a stochastic optimization after having an initial convergence. The authors in (Fragiadakis and Papadrakakis 2008) used the same method as in (Tsompanakis and Papadrakakis 2004) but applied to RC buildings. Again, this author proposes a framework where a SOP with size variables is solved. As it happens frequently in earthquake-resistant design of buildings, global performance indicators are used, with special emphasis on inter-story drift ratio.

In (Liu, Burns and Wen 2003), a GA is employed in a method that optimizes structural earthquake-resistant design with Life-Cycle Cost (LCC) considerations. It is applied to buildings using nonlinear static (pushover) methods. The optimization problem is a MOP with two objectives: the first is the initial cost of the structure and the second is lifetime seismic damage repair costs.

In (Lagaros and Papadrakakis 2007), the NSGA-II algorithm is employed for robust seismic design optimization of steel structures. Here a multi-objective approach is done using two objectives associated with weight and displacements.

The authors in (Rojas, Foley and Pezeshk 2011) developed a method to optimize steel buildings in a PBD framework. In this instance, a two-objective problem is solved obtaining Pareto sets from which there is some information extracted to aid decision making, resorting to the values of the objective functions that bound the Pareto set. The optimization is a sizing optimization, which is usually the case in structural engineering works.

A few collections of works exist in (Lagaros and Tsompanakis 2007) and (Plevris, Mitropoulou and Lagaros 2012). In both collections, many works from several authors are presented, where the main theme is structural seismic design optimization. Different structures are analysed, and many heuristics employed such as tabu-search, ANN, support vector machines (SVMs), particle swarm optimization (PSO) etc.

More recent studies that employ meta-heuristics in earthquake engineering include (Mergos 2018). In this study a GA optimizes the steel reinforcement of RC frames in a displacement-based framework, using nonlinear pushover analysis. The procedure uses a single-objective function that minimizes cost. In (Martínez, Curadelli and Compagnoni 2014) a method was developed for optimal placement of nonlinear hysteretic dampers on planar structures under seismic excitation. The method optimizes a single-objective function composed by two objectives associated with maximum interstory drift and base shear force. In (Curadelli and Amani 2014), a two-objective SOP that optimizes an integrated design of a frame structure and a passive control system is presented. The optimization is done for several objective weights which are then presented in the form of a Pareto-front.

There are many studies that employ meta-heuristics in earthquake engineering and use ground-motions for the analysis. Some examples include (Esfandiari, et al. 2018). In this study, a single cost objective is minimized to optimize RC frames subjected to earthquake action. The earthquake action was simulated by real accelerograms and the dynamic analyses were performed using three ground-motions. In this study a particle swarm optimization algorithm was employed coupled with multi-criterion decision making. In (Bybordiani and Kazemzadeh Azad 2019), an exponential big bang-big crunch optimization algorithm is employed to perform optimization of steel frames under seismic loading considering dynamic soil-structure interaction (SSI) in order to quantify the effects of earthquake records on the optimum design. The optimization procedure minimizes a single-objective function related to the weight of the structure and also employs three real ground-motions for the analysis. In (Wang, et al. 2019), a multi-criteria decision-making method (MCDM) is applied to optimize shape memory alloy (SMA) cable restrainers for longitudinal seismic protection of isolated simply supported highway bridges, through the minimization of a single-objective composed by the weighted sum of relative displacements and base shear. In this case the dynamic analyses were performed with a set of five real accelerograms. In (Azizi, et al. 2019), a SOP with objective function based on peak interstory drift is minimized by an upgraded whale optimization algorithm employed for the optimization of a fuzzy controller applied to a seismically excited nonlinear steel building. For the analyses a set of four real accelerograms was employed, two near-field and two far-field.

Regarding the existing literature, the present work introduces a few approaches that are novel. Furthermore, the study of seismic design of RC bridge infrastructures has not been extensively studied in frameworks using meta-heuristics, as far as the author is aware. The following points intend to highlight the novel aspects of this study and also the aspects in which this study is different than most of the studies that employ GAs and other heuristics in structural optimization:

1) As mentioned, not many works regarding optimization and meta-heuristics focus on RC bridge infrastructure seismic design optimization. The works associated to bridge seismic optimization typically focus on dissipation devices or are associated to cable-stayed bridges.
2) Few works use the results to derive decision making information. The author also did not find any study that took advantage of the entire population generated in all runs to perform variable sensitivity analysis, in the extent that is performed in this study.
3) It is difficult to find works that employ a two-phase optimization procedure with change in optimization objectives. Only in an aforementioned work was a two-phase approach found (Pedro, et al. 2017), but here the two-phase approach is associated to a change of fitness evaluation method, and not a change in objective functions.
4) The majority of works employ SOPs or transform MOPs into SOPs by defining weights to the objectives. It is easy to find works that employ MOPs, but they are, nonetheless, less common than works that employ SOPs.
5) The majority of works that employ optimization meta-heuristics do not use fibre models and, in general, resort either to static nonlinear analysis or dynamic analysis with lumped plasticity. In addition, the analysis and design were performed in both directions (longitudinal and transverse) simultaneously.

4.3 Bridge seismic design – typology and analysis

The seismic design of RC bridges essentially comprises the design of the infrastructures of the bridge, namely piers, foundations, and abutments. Aspects like the length and cross-section of the bridge's superstructure (deck), position and number of the piers, are usually defined by other factors: topography, soil, construction method, the type of rail or roadway in which it is inserted (freeway or not, number of lanes, curve or straight alignment), cost, etc. Therefore, seismic design deals with geometry, size, amount of steel for piers and foundations and with the connection between the piers and the superstructure. In this work, the focus will be the design of piers and the connections to the superstructure.

4.3.1 Structural model and analysis definition

The structural modelling and analysis were performed with the OpenSEES software (McKenna and Fenves 1999).

4.3.1.1 Piers

The piers were modelled as force-based fibre elements and each pier divided into three of said elements, with smaller elements closer to the extremities, where plastic hinges are expected to form. Each element subdivided into 5 integration points. The cross-sections at each integration point are divided into several radial and tangential (spike and wheel) fibre elements. The fibres follow the constitutive relationship of Kent-Scott-Park (Scott, Park and Priestley 1982) for concrete and Menegotto-Pinto (Menegotto and Pinto 1973) for steel. The geometric non-linearities considered for the piers were P-delta effects.

4.3.1.2 Deck

The deck was modelled as an equivalent elastic beam, with distributed mass. The mass matrix defined was the consistent mass matrix. As for the connections between deck and superstructure, these were modelled with two equalDOF constraints linking an extra node between the pier node and the deck node. The equalDOFs then free the degrees-of-freedom associated with each type of connection, for each direction.

4.3.1.3 Seismic analysis

The seismic analysis was performed by time-step integration of the ground motions using Newmark's average acceleration method to compute the time history, with parameters of α and β equal to 0.5 and 0.25, respectively. The solution of the nonlinear residual equation was done with Newton-Raphson algorithm with line search to increase the effectiveness of the Newton-Raphson algorithm.

The time-step of the integration was 0.01s. The seismic analysis was performed simultaneously in the longitudinal and transversal direction.

Non-convergence issues were only associated with non-equilibrium of P-delta effects.

4.4 Strong-motion records

Several pairs of natural strong-motion records were selected to perform the NDAs. They were selected to match, as closely as possible, a specific EC8 response spectrum (CEN 2005), as shown in Section 2.8.

The 4-pair set in Figure 2.49 was chosen for the analysis. In the figure, one can compare the standard deviation of the spectrum with 4 and 9 strong motions. It is visible that the standard deviation is not very different in both cases, which suggest that results for a search procedure are suitable with 4 strong motions. There are many works that employ similar number of ground motions in the search procedure: (Azizi, et al. 2019), (Bybordiani and Kazemzadeh Azad 2019), (Esfandiari, et al. 2018) and (Wang, et al. 2019).

4.5 Evolutionary Algorithms

4.5.1 NSGA-II application and MOP definition

For this work, multiple objectives were defined for bridge optimization, and so the emphasis will be on MOEAs and MOPs. There are several MOEAs, which vary in terms of genetic operators and other nuances, such as ability to address specific types of MOPs. There are also several types of MOPs in terms of shape of Pareto set and front, disconnected MOPs, monotonic MOPs, etc. There is extensive literature about GAs (Deb 2001) (Goldberg 1989) that can be checked for more in-depth information about these algorithms and the various nuances.

The Non-Dominated Sorting Genetic Algorithm (NSGA-II) was chosen for being a reference MOEA, a very efficient and broadly applicable algorithm, and one of the most widely used GAs. The NSGA-II can obtain, for most MOPs, a well distributed approximation of the Pareto-optimal front, very close to the real Pareto-optimal front. A few modifications to the original algorithm were employed, particularly on the genetic operators. The genetic operators were adapted from the MODdEA algorithm (Chow and Yuen 2012).

As already mentioned, the goal is the optimization of RC bridge earthquake design of infrastructures. The design of the piers is made in terms of size variables such as diameter of the concrete sections and amount of flexural steel and confining steel. In addition to the size variables, there is another variable type that can be defined as a convergence variable, i.e. a variable that does not affect directly the quantitative optimization but affects the feasibility of solutions, which is the connection between the pier and the superstructure. The methodology was applied to an irregular bridge in terms of pier length. As already mentioned, fibre models were used for the piers and the structural analyses were performed with the OpenSEES (McKenna and Fenves 1999) extension of the Tcl/Tk language interpreter. The code was parallelized, and the runs were done with OpenSEESMP with multiple parallel processes, in order to have a significant speed-up of the GA runs.

Parallelization was performed on an AMD Threadripper 1950X 16-core processor, capable of running 32 simultaneous threads. The message passing interface used was MPICH2. The elapsed time for a one generation run, with the non-parallelized version was about 120 minutes and with the parallelized version, running 32 simultaneous processes, was 6 minutes, resulting in a speed-up factor of about 20. The processes that were parallelized were the individual NDA analysis of each solution. The speed-up factor of 20 is lower than the theoretical speed-up value of 32, which is the number of parallel processes. This loss in efficiency could be due to a bottleneck effect in the MPICH2, but the author is not sure. Some typical bottlenecks were checked for, such as disk writing speed and communication overhead between parallel processes, but these seemed not to be the issue. This was not pursued further since it is somewhat beyond the scope of the work.

Different objective/fitness functions were studied, and GA runs were performed with 2 objectives. Only local performance indicators were used, more specifically concrete compressive strain at the critical sections of each pier. Unfeasibility (collapse) was defined as the violation of the ultimate concrete strain at the critical sections of any pier at any point in time of the nonlinear dynamic analysis. Second-order effects are considered in the analysis and there are a few constraints associated to maximum and minimum steel ratio in the RC cross-sections according to EC8, maximum and minimum cross-section diameters, respecting design limits, avoiding members that would be considerably affected by shear and avoiding extremely slender elements.

4.5.1.1 Overview of modified NSGA-II application

The NSGA-II algorithm, as most GAs is composed by a selection, mutation and crossover operators. In this application of NSGA-II, the reproduction/selection operator used is the constrained tournament selection (CTS) method. The population size N of the GA runs was set to 128. The Extended Arithmetic Crossover (EAX) and the Diversified Mutation (DM) operators were adapted from the MODdEA algorithm (Chow and Yuen 2012), due to the property of being parameterless. In Figure 4.1, the flowchart of the MOEA applied to the problem of seismic structural design is shown.

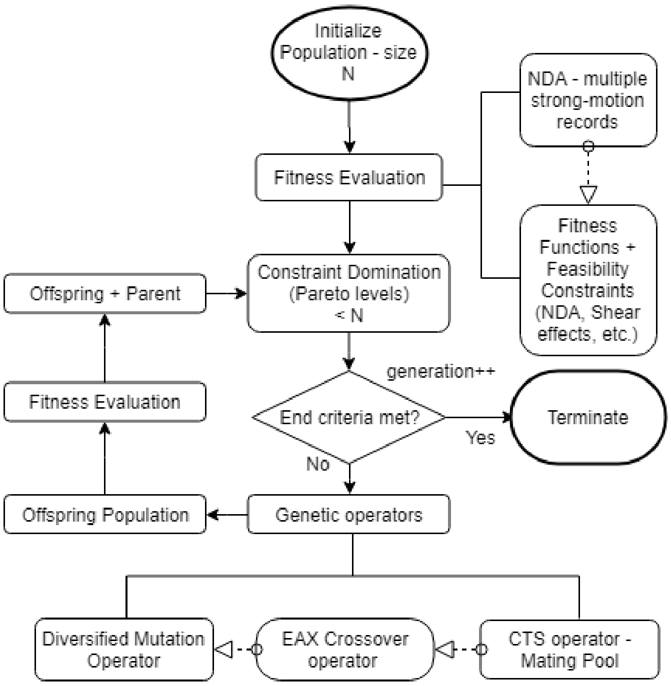

Figure 4.1 Flowchart of the applied MOEA

The working process of the algorithm is the following: 1) A random population, size N, is initialized; 2) The population is evaluated based on the objectives and constraints. The objectives are material quantities, steel and concrete, and the constraints are associated to structural resistance to earthquake, and code requirements. The earthquake resistance is evaluated resorting to non-linear analysis methods, either static or dynamic; 3) The population is ranked through a constraint domination procedure, which defines the various Pareto levels; 4) The genetic operators are applied, and the offspring population is obtained; 5) The offspring population is evaluated based on the objectives and constraints; 6) The offspring population is merged with the parent population; 7) The constraint domination procedure is applied to the merged population, comprised of the offspring and parent population, and new Pareto levels are defined. Dominated solutions ranked worse, after the threshold of N solutions is reached, are rejected, maintaining the population size constant at N solutions; 8) The end criteria, which are maximum number of generations and convergence criteria applied to the Pareto-optimal set, are checked. If they are not reached the cycle enters a new iteration, which starts back at step 4).

4.5.2 Pseudocodes of the optimization algorithm

Next the Pseudocodes of the "Main procedure" and of the "Procedure Fitness Functions" are shown:

Pseudocode of the Main procedure

Input: Population size **N**, Bridge Geometry **BG**, Earthquake **EQ,** Max number generations **MaxGen**

Begin

Initialize Current Population **P,** number generations **nG = 0,** num. stable gener. **nsG = 0**

For i = 1 **To** N **Do**

 # Each bridge solution P(i) is subjected to the earthquake action #

Feasibility **F(i)** = Procedure Evaluate **(P(i), EQ, BG)**

 # The result of the analysis defines feasibility #

(F(i), FFunc(i)) = Procedure Fitness Functions **(F(i), P(i), BG)**

 # Fitness functions are calculated, and constraints are checked #

 # If constraints don't check: F(i) = feasible **->** *F(i) = infeasible #*

End of For

 # The current population is divided into Pareto levels #

Pareto Levels $\mathbf{PL_N}$ = Procedure Constraint Domination **(FFunc, F, P)**

 # 1) A feasible solution is dominated by a feasible solution with better fitness. 2) An infeasible solution is dominated by an infeasible solution with better fitness. 3) A feasible solution always dominates an infeasible solution. #

While nG < MaxGen **And** nsG < 5 **Do**

Mating Pool **MP** = Procedure Constrained Tournament Selection **(PL, P, FFunc)**

 # Each solution is selected twice for tournament. A solution wins the tournament if its Pareto level is lower than the competition's. If the Pareto level of two competing solutions is the same, they are ranked based on a crowding distance metric measured in the objective space. #

Offspring **Os** = Procedure Extended Arithmetic Crossover EAX **(MP, P)**

Offspring Mutation **OsM** = Procedure Diversified Mutation DM **(Os)**

For i = 1 **To** N **Do**

Offspring Feasibility **OF(i)** = Procedure Evaluate **(OsM(i), ES, BG)**

(OF(i), OFFunc(i)) = Procedure Fitness Functions **(OF(i), OsM(i), BG)**

End of For

 # The current population and offspring population are joined and then divided into Pareto levels #

$\mathrm{FFunc} = \mathrm{FFunc} \cup \mathrm{OFFunc};\ \mathrm{F} = \mathrm{F} \cup \mathrm{OF};\ \mathrm{P} = \mathrm{P} \cup \mathrm{OsM}$

While $|\mathrm{PL_N}| \leq$ N **Do**

Pareto Levels $\mathbf{PL_N}$ = Procedure Constraint Domination **(FFunc, F, P)**

End of While

$P = P \cap \mathrm{PL_N}$

If $\mathrm{PL}_1^0 \neq \mathrm{PL}_1^{-1}$ **Then**

nsG = 0

Else nsG ++

End If

nG++

End of While

Pseudocode of "Procedure Fitness Functions"

Input: Feasibility **F(i),** Solution **P(i),** Bridge Geometry **BG**

Begin

Initialize Steel Area **SA** = 0, Concrete Area **CA** = 0

FlexSteelList = P(i).FlexSteel; D = P(i).SectDiameter;

$\mathrm{SectArea} = \pi D^2/4$

For j = 1 To Number of Piers **Do**

AS = FlexSteelList(j)

 # Objective Functions #

$\mathrm{SA} = \mathrm{SA} + \mathrm{AS} \cdot \mathrm{SectArea}$

$\mathrm{CA} = \mathrm{CA} + \mathrm{SectArea}$

 # Here the section diameter variable is the same for all piers. #

 # End of Objective Functions #

 # Constraints: shear effects. #

$$ShearEff(j) = \frac{\delta_{Shear}}{\delta_{Flex}} = \frac{\frac{FLPiers(j)}{GA_{Shear}}}{\frac{FLPiers(j)^3}{\alpha EI}} = \frac{\alpha(j)EI}{GA_{Shear} \cdot LPiers(j)^2}$$

 # Where α(j) is either 12 for monolithic piers or 3 for fixed piers.

If ShearEff(j) > 10% **Then**

Shear **is True**

End If

If (ShearEff) **is True Then**

SA = SAmax

CA = CAmax

F(i) = Infeasible

End If

End For

FFunc(i) = {SA, CA}

Return {F(i), FFunc(i)}

4.5.2.1 Variables

The optimization problem was modelled with real discrete variables. The number of variables in the model is equal to $3n + 1$, where *n* is the number of piers in the bridge. The three variables related to each pier are: 1) Longitudinal reinforcement steel; 2) Transversal reinforcement steel (for concrete core confinement); and 3) Type of connection of the pier to the superstructure. In addition to these variables associated to each pier, there is a global variable for all piers which is the cross-section diameter. It was decided that the diameter of the piers, for a matter of aesthetics and standardization of construction, should be a variable which would be kept equal for all piers, as it usually happens in bridge design. All variables are real discrete.

1) Longitudinal reinforcement steel – This variable is the percentage of longitudinal steel reinforcement in the cross-section ranging from the minimum according to EC8 - 2 (CEN 2005) of 0.6% and up to 3.50%. The discretization step is of 0.05%.
2) Transversal reinforcement steel – This variable is divided into tuple sets of confining steel rod diameters and confinement spacing. Four possible variations were defined from a minimum confinement of (10, 10) to a maximum confinement of (16, 10), where the first value is the diameter of the steel rods in mm, and the second value is the spacing between the confinement in cm.
3) Type of connection of the pier to the superstructure – this variable was defined having 4 possible values: 1) Monolithic connection; 2) Elastomeric bearings - Fixed-connection longitudinally and restrained rotation transversally; 3) sliding connection longitudinally and restrained rotation transversally; and 4) sliding connection in both directions. This variable does not translate into quantities of material; therefore, it does not directly influence the objective functions, which are focused on initial cost and material minimization. However, this variable is critical for obtaining feasible solutions.
4) Cross-section diameter – While the other variables are related to one pier, this variable is the same for all piers. The minimum diameter is 1.0 meter, and the maximum is 3.0 meters. These values are default, and the upper and lower limits can be changed for different case-studies.

Figure 4.2 shows the generic cross-section with the variables 1, 2 and 4 identified.

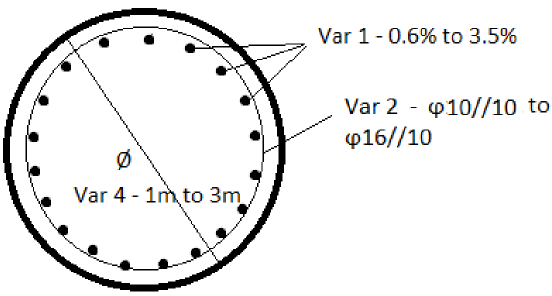

Figure 4.2 Circular pier cross-section and decision space variables.

In Figure 4.3 there is a representation of the cross-section of the deck with elastomeric bearings. The illustration's purpose is to show that in the transversal direction, there is no rotation between the deck and the pier, regardless of the connection between them, as long as there are two parallel supports per column. This is due to the torque transmitted by both points of support. Therefore, rotations between the deck and the column are only possible in the longitudinal direction.

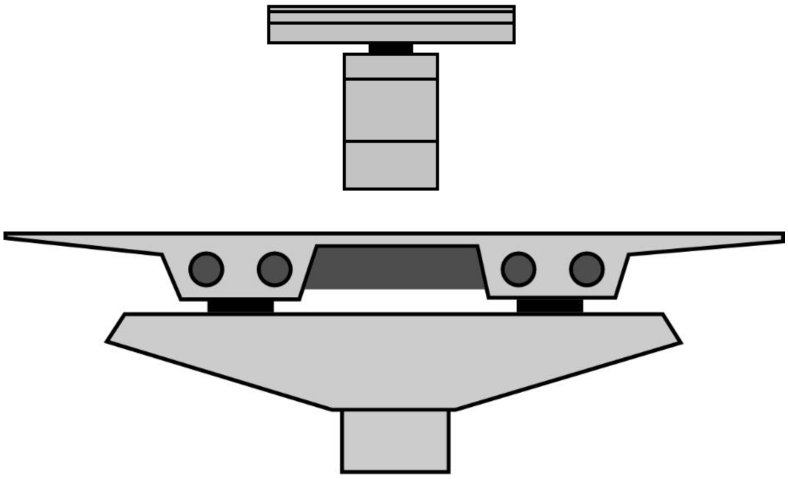

Figure 4.3 Longitudinal (top) and transversal (bottom) representation of deck with bearings. Longitudinal direction - fixed connection is possible. Transversal direction - the rotation at the top of the pier is always equal to the torsional rotation of the deck.

4.5.2.2 Objective Functions

Two sets of objective functions were defined to be used in separate runs. The first objective function set is composed by two objective functions: 1) concrete volume in the piers, and 2) steel volume in the piers. A second set of objectives was defined, also composed by two functions, and which are usually used in LCC analysis: initial cost and performance. The performance fitness function measures the difference between compressive strain demand and maximum admissible compressive strain, and the initial cost fitness function sums the price of steel and concrete in the piers by multiplying the volume of each by the respective price per volume.

The reason for the use of two sets of objectives instead of one set composed by four objectives are essentially two-fold: scalability and relative importance between the objectives.

In the scalability front, the fitness evaluations in earthquake design are very time-consuming and having more objectives means increasing the population considerably and/or running more generations. Furthermore, it is more difficult to have a good distribution along the Pareto front and there is also the issue with representation and interpretation of the results.

In terms of relative importance between objectives, it makes sense to give more relevance to objective-set 1. In reality, the main focus is steel and concrete amount and its trade-off. Also, since the last population of the first run is used as the initial population of the second run, it means that the second run is quicker because much of the search effort to find feasible solutions has been already performed.

4.5.2.3 Fitness Evaluations

The fitness evaluations are based on the seismic NDAs of the generated bridge solutions, which are done resorting to OpenSEES (McKenna and Fenves 1999). The seismic NDAs are performed with multiple strong motion records, the value of the results of all strong motions are averaged and then the structure is deemed as feasible or infeasible. During the search procedure, only 4 strong motion records are used. At the end, the full set of records is used to confirm the quality of the solutions in the obtained in the approximate Pareto-optimal set.

4.5.2.4 Constraints

The model has four constraints, three associated with the variables of the solutions and one associated to the fitness evaluations, i.e., the seismic analysis.

The three constraints associated to variables penalize the solutions for excessive slenderness, for having more than a defined threshold of sliding connections and for being vulnerable to shear effects. The latter one is checked by checking if the ratio between elastic shear displacement and elastic flexural displacement, assuming a force F assigned at the top of the pier and monolithic or fixed connection, with α equal to 12 or 3, respectively, is lower than 10%:

$$\frac{\delta_{Shear}}{\delta_{Flex}} = \frac{\frac{FL}{GA_{Shear}}}{\frac{FL^3}{\alpha EI}} \leq 10\%, \tag{4.1}$$

The fourth constraint, which is associated to the fitness evaluations, defines if a solution is feasible or infeasible. At the end of the seismic analysis the maximum compressive strains are checked at each fibre located in the critical sections of the plastic hinges that have formed, and it is checked whether the compressive strain is larger than the maximum compressive strain for confined concrete, allowed in that section. The maximum allowed compressive strain is calculated according to EC8 - 2 (CEN 2005) considering the steel reinforcement in the cross-section, especially the confining steel. It is assumed that shear failure is avoided by not allowing solutions with thick elements that would be prone to relevant shear effects, according to equation (4.1).

There are two types of penalizations due to constraint violation:

- The first type of penalization is associated to the design constraints, such as non-compliance of maximum slenderness, non-compliance of excessive shear effects due to short piers, non-compliance of excessive displacements of the bearings, etc. The violation of these constraints entails a penalization of the fitness functions f_m by increasing them to their maximum value (in a minimization problem), and by deeming them infeasible.
- The second type of penalization is associated to the failure in resisting the seismic action. In this case, if the solution fails, it is simply deemed infeasible, but no penalization of the fitness functions f_m is given. However, in comparison with feasible solutions, an infeasible solution is always dominated by the former even if the fitness values are better. These solutions are always

better than the ones who fail the design constraints (first penalization) since those, besides being infeasible, have their fitness values maximized (in a minimization problem).

In conclusion, there are two types of penalizations but only one pertains to the fitness functions. The penalization of the fitness functions is always the maximization of their values. This is to avoid more subjective decisions as defining different penalizations according to different constraints, or levels of violation of said constraints.

In case of non-convergence due to P-delta effects in any of the four ground-motions, the solution is deemed infeasible.

4.5.2.5 Summary of the Multi-Objective Problem

The mathematical formulation of the problem follows:

$$\begin{cases} \min\limits_{1 \le m \le 2} f_m(\bar{x}) \ (objective\ set\ 1) \\ \left(\min f_1(\bar{x}), \max f_2(\bar{x})\right) (objective\ set\ 2) \\ s.t.: \\ g_i(\bar{x}) \le 0, \ \ 1 \le i \le 3 \\ g_i(fe(\bar{x})) \ge 0, \ \ i = 4 \\ L_d \le x_d \le U_d, \ \ 1 \le d \le n \end{cases} \tag{4.2}$$

Where $\bar{x}$ is the decision variable vector with size n, and g_i represents the four constraints. Constraint 1 to 3 are associated to slenderness, shear effects and excessive sliding connections. These three constraints are functions of the decision variable vector, $\bar{x}$. Constraint 4 is a function of the fitness evaluation (seismic analysis) and relates to the structural collapse criterium (ε_{cu}-ε_c).

$$\begin{cases} if\ g_{1\le i\le 3}(\bar{x}) > 0 \Rightarrow \begin{cases} infeasibility = yes \\ f_{1\le m\le 2}(\bar{x}) = max\ f_{1\le m\le 2}(obj.set\ 1) \\ f_1(\bar{x}) = max\ f_1, f_2(\bar{x}) = min\ f_2\ (obj.set\ 2) \end{cases} \\ if\ g_{1\le i\le 3}(\bar{x}) \le 0 \wedge g_{i=4}(fe(\bar{x})) < 0 \Rightarrow infeasibility = yes \\ if\ g_{1\le i\le 3}(\bar{x}) \le 0 \wedge g_{i=4}(fe(\bar{x})) \ge 0 \Rightarrow infeasibility = no \end{cases} \tag{4.3}$$

Afterwards, in the constraint tournament selection and when defining constraint domination for solution ranking and defining Pareto levels, infeasible solutions are always dominated by feasible solutions. Between two feasible or two infeasible solutions, the fitness function values are compared and define the domination.

4.6 Application example and results

An irregular RC bridge has been chosen to illustrate the methodology and show the results and conclusions that are possible to draw from the application of the methodology. This work is proof of concept and the chosen example is thought to be adequate to illustrate the merits of the framework, since it is an irregular bridge with irregularity layout defined by piers increasing in height gradually from one abutment to the other making it a relatively complex bridge for seismic design. The author believes that the successful application to this example is enough to show that the framework can be applied to mostly any RC bridge, regardless of number of design variables or irregularity layout.

In Figure 4.4, a scheme of the bridge is presented. It is 280 m long and follows the irregularity layout mentioned above. The piers are, from left to right: 7, 9, 11, 13, 15, 17 and 19 meters long. The cross-section shape of the piers has been defined as circular. The cross-section of the superstructure is that of a standard RC beam/slab as seen in Figure 4.5.

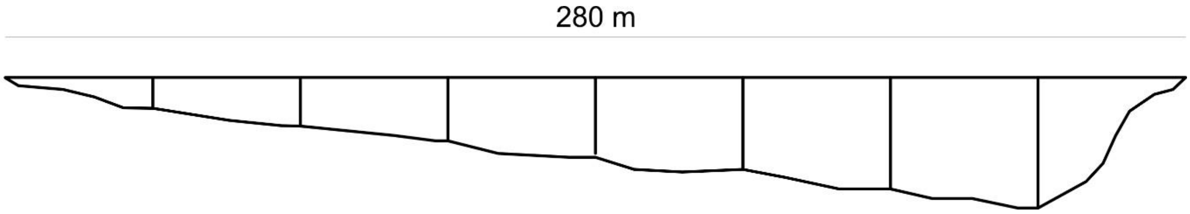

Figure 4.4 Longitudinal profile of the case study bridge.

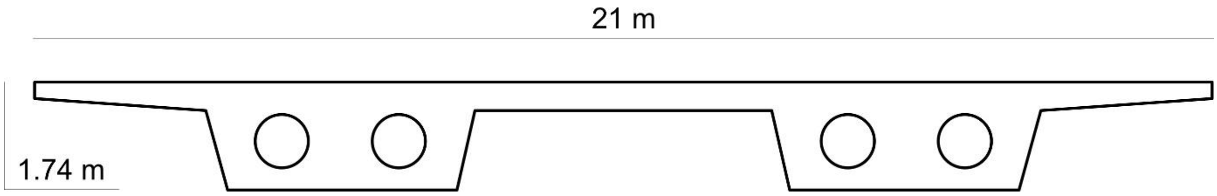

Figure 4.5 Cross-section of the case study's deck.

The design variables, as mentioned before, are only related to the piers. The foundations are not addressed in the analysis.

In Table 4.1, the values associated to the deck's cross-section are presented and in Table 4.2, the mean values associated to the material properties are presented. All values in both tables are deterministic.

Table 4.1 General properties of the superstructure.

Span length (m)	35
Cross-section area (m^2)	17.675
Moment of Inertia along vertical axis (m^4)	547.018
Moment of Inertia along horizontal axis (m^4)	5.272
Torsional constant (m^4)	10.932

Table 4.2 Material properties used in the model.

Concrete (C30/37)	
f_{cm} (MPa)	38
E_{cm} (GPa)	33
ε_c (unconfined) (‰)	3.5
Steel (A500NR)	
f_{ym} (MPa)	585
E_{ym} (GPa)	200
ε_{su} (‰)	94

In Table 4.3 and Table 4.4, the decision variables are presented. The decision variables are the variables which the optimization algorithm modifies in the search for the optimal solutions. The decision variables are directly or indirectly associated to the optimization goals.

Table 4.3 Variables that compose the decision space of the MOP.

	Pier 1 – 7m	Pier 2 – 9m	Pier 3 – 11m	Pier 4 – 13m	Pier 5 – 15m	Pier 6 – 17m	Pier 7 – 19m
Connection to deck	X_1	X_2	X_3	X_4	X_5	X_6	X_7
Longit. Reinf. steel	X_8	X_9	X_{10}	X_{11}	X_{12}	X_{13}	X_{14}
Section Diameter	X_{15}	X_{15}	X_{15}	X_{15}	X_{15}	X_{15}	X_{15}
Transv. Reinf. steel	X_{16}	X_{17}	X_{18}	X_{19}	X_{20}	X_{21}	X_{22}

Table 4.4 Variable intervals

	Lower Value	Upper Value	Discretization Step
X_1 to X_7	1	4	1
X_8 to X_{14}	0.6%	3.5%	0.05%
X_{15}	1.0 m	3.0 m	0.025 m
X_{16} to X_{22}	1	4	1

This case study was optimized for two different objective sets. Multiple runs were performed for each objective set.

4.6.1 Objective set 1: Steel volume + Concrete Volume

A total of 8 runs were performed for objective-set 1, the relative low number of runs has to do with two aspects, first, the long time it takes for one run to complete, and second, the fact that the final Pareto fronts are almost superimposed, and so little variability was found between the final results. In Figure 4.6, the 8 final Pareto fronts are presented. In Figure 4.7 the same results are presented but as concrete and steel cost. The result of run 1 is presented in Figure 4.8, in the objective space.

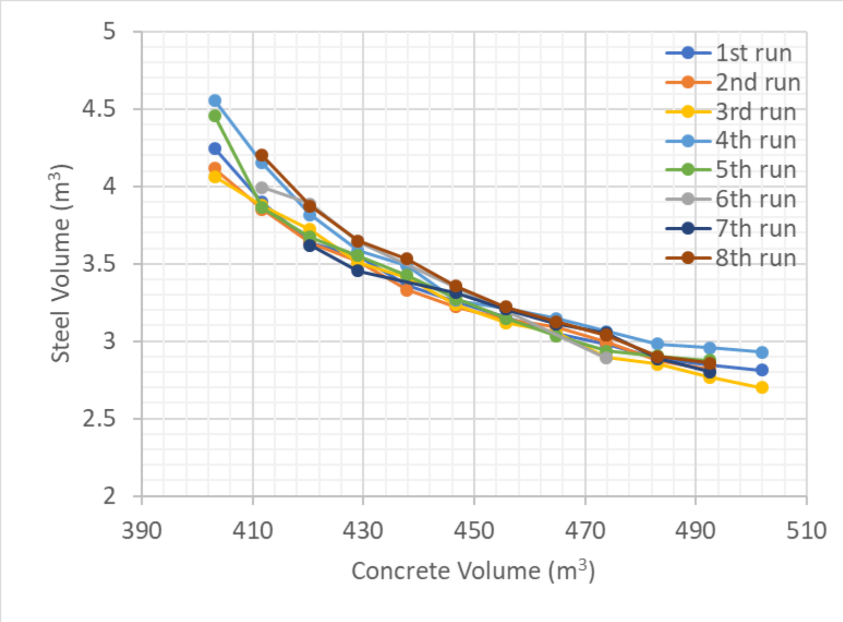

Figure 4.6 Final Pareto fronts obtained from the 8 runs with objective-set 1.

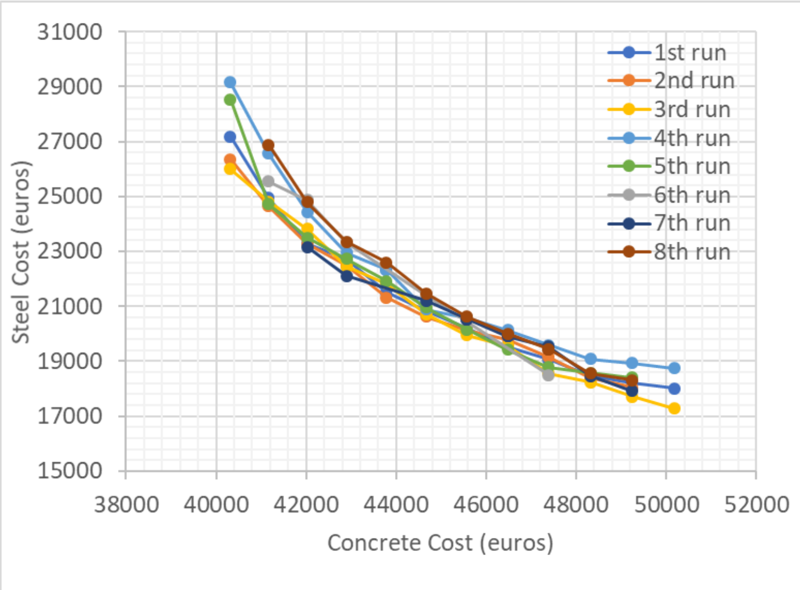

Figure 4.7 Final Pareto fronts obtained from the 8 runs with objective-set 1, presented as concrete and steel cost.

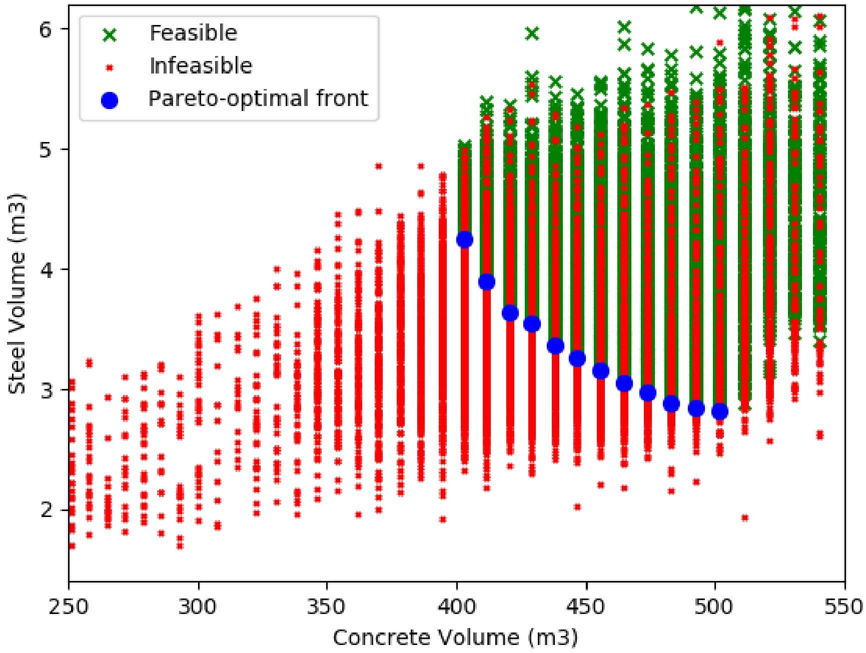

Figure 4.8 Results of GA run 1, in the objective space. The small red xs represent infeasible solutions, the green xs are feasible solutions and the blue circles compose the approximate Pareto-optimal front.

In Figure 4.9, the progression of the fitness values of both objective functions are presented, related to the 1st run. This gives an idea of the convergence of the algorithm applied to this problem.

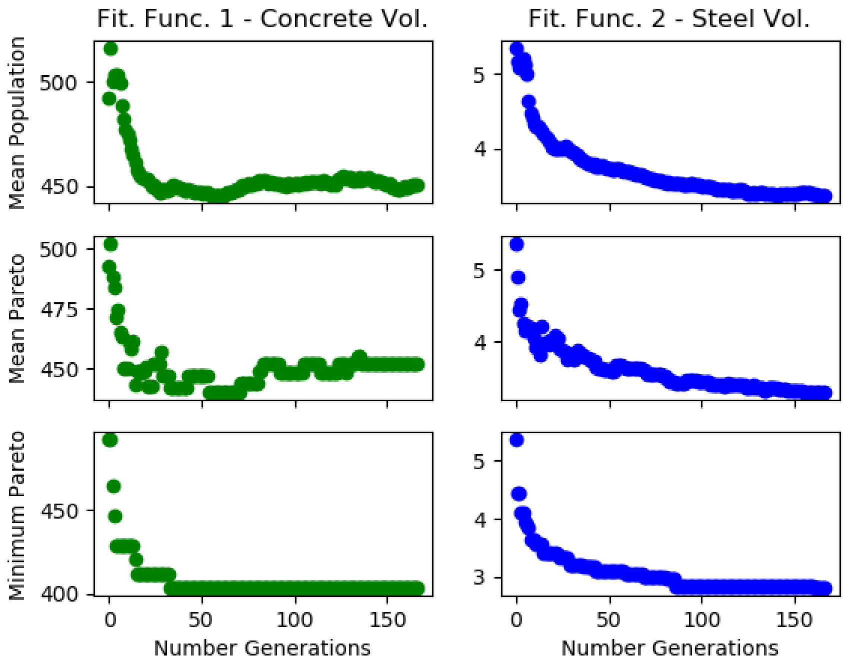

Figure 4.9 Results of the 1st run: mean fitness values in the population and mean and minimum fitness value in the Pareto front. The results are related to each of the fitness objectives and per generation.

To illustrate the degree of variability in the results, the mean and standard deviation of the approximate Pareto-optimal fronts (POFs) are calculated and presented in Table 4.5. Also, the area enclosed by the POFs' standard deviation is compared with the approximate explored feasible region in Figure 4.10.

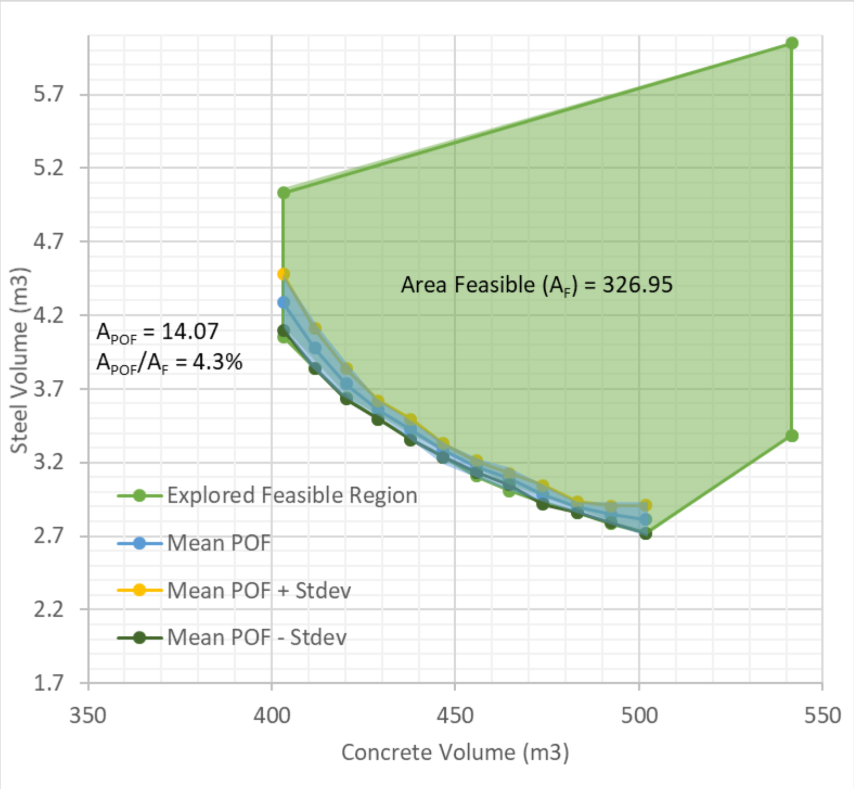

Figure 4.10 Comparison between the feasible region area and the envelope of the mean POF plus and minus the standard deviation.

Table 4.5 Mean, standard deviation and coefficient of variation of the POFs.

Mean POF			
CV	SV	stdev SV	CoV SV
403.1	4.29	0.19	4.4%
411.7	3.98	0.13	3.4%
420.3	3.73	0.10	2.8%
429.0	3.56	0.06	1.8%
437.8	3.42	0.07	2.0%
446.7	3.28	0.05	1.4%
455.7	3.17	0.04	1.2%
464.7	3.09	0.04	1.2%
473.9	2.98	0.06	2.1%
483.1	2.90	0.04	1.3%
492.5	2.85	0.06	2.0%
501.9	2.81	0.09	3.3%

The results show small variability between the results of the runs. The author considered that this aspect coupled with the knowledge that NSGA-II performs well even for non-convex and truly disconnected MOPs (TYD-MOPs) (Chow and Yuen 2012) was enough to be confident with good approximation to the real Pareto front. Nonetheless, there are several performance metrics in the literature and methodologies to evaluate the quality of solutions presented in the Pareto fronts (Fonseca and Fleming 1996) (Zitzler and Thiele 1998). One of the most used metrics is the Hypervolume metric (Beume, et al. 2009) and another one is the Empirical Attainment Function (EAF) (Fonseca, et al. 2011).
The following analysis of the trade-off solutions will be performed based on only one run.
Figure 4.8 shows that below the approximate Pareto-optimal front (POF), characterized by the blue dots, there are no feasible solutions, however above the POF, there continues to exist a large density of infeasible solutions. This has to do with essentially two factors:

- Inadequate set of connections between piers and superstructure, which largely influences the ductility demand of each pier.
- Whether the critical piers, in terms of ductility demand, are well confined. In addition, the critical piers, in terms of ductility demand, are different for different connection sets between piers and superstructure.

The approximate Pareto-optimal set (POS) is characterized by solutions with a pattern in the values that some variables assume, particularly the connections of the piers to the superstructure are the same throughout the entire set, while other variables such as steel reinforcement and pier diameter vary from solution to solution. However, even the steel reinforcement between the piers follows a given distribution pattern.
Besides the approximate Pareto-optimal front (POF), there are other sub-optimal Pareto fronts associated to different sets (schemata) of connections of the piers to the superstructure, and different steel distributions. As for the solutions in the POS, they all present the pier-deck connections present in Figure 4.11.

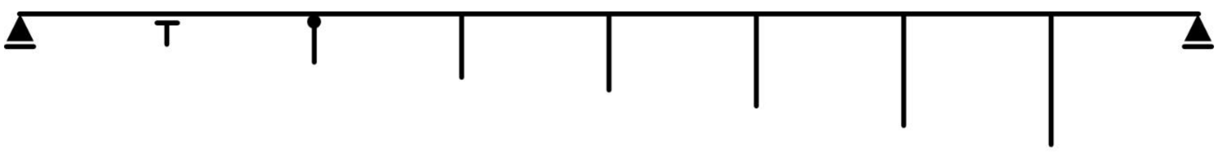

Figure 4.11 Representation of the pier-deck connections present in the POS solutions.

The gain of the runs with objective-set 1 is two-fold. First, a trade-off is obtained between the volumes of reinforcement steel and concrete employed in the design of the piers. Second, the algorithm finds the best combination of connections (Figure 4.11) and steel distribution.
In Figure 4.12 and Figure 4.13, one can see the trade-offs between the variables associated to the objectives of the solutions present in the POS.

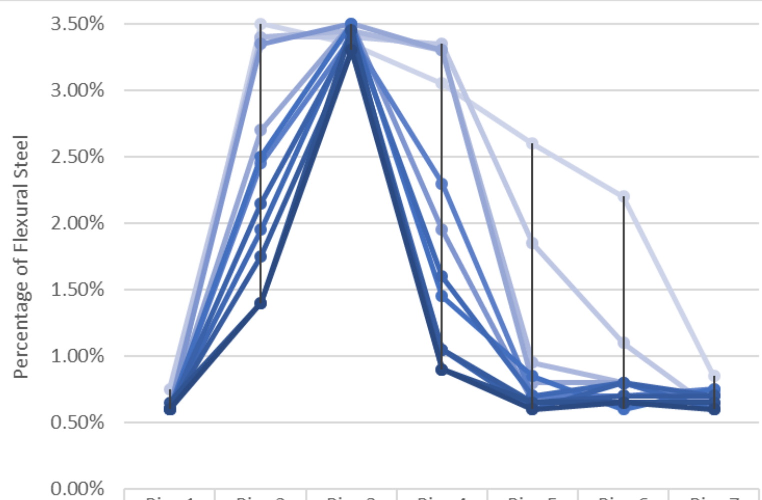

	Pier 1	Pier 2	Pier 3	Pier 4	Pier 5	Pier 6	Pier 7
2.375	0.60%	3.50%	3.35%	3.05%	2.60%	2.20%	0.85%
2.4	0.75%	3.40%	3.40%	3.35%	1.85%	1.10%	0.60%
2.425	0.60%	3.40%	3.45%	3.30%	0.95%	0.80%	0.60%
2.45	0.60%	2.70%	3.50%	3.30%	0.80%	0.80%	0.60%
2.475	0.60%	3.35%	3.50%	1.95%	0.65%	0.80%	0.65%
2.5	0.60%	2.45%	3.40%	2.30%	0.70%	0.70%	0.75%
2.525	0.60%	2.50%	3.50%	1.45%	0.85%	0.60%	0.75%
2.55	0.60%	1.95%	3.45%	1.60%	0.70%	0.80%	0.60%
2.575	0.60%	2.15%	3.40%	1.05%	0.60%	0.80%	0.70%
2.6	0.60%	1.75%	3.30%	1.05%	0.65%	0.70%	0.70%
2.625	0.65%	1.40%	3.45%	0.90%	0.65%	0.65%	0.65%
2.65	0.60%	1.40%	3.30%	0.90%	0.60%	0.65%	0.60%

Pier Position

Figure 4.12 Solutions in the POS showing trade-off between flexural steel at each pier per pier diameter, as well as the steel distribution. The series labels refer to pier diameter values.

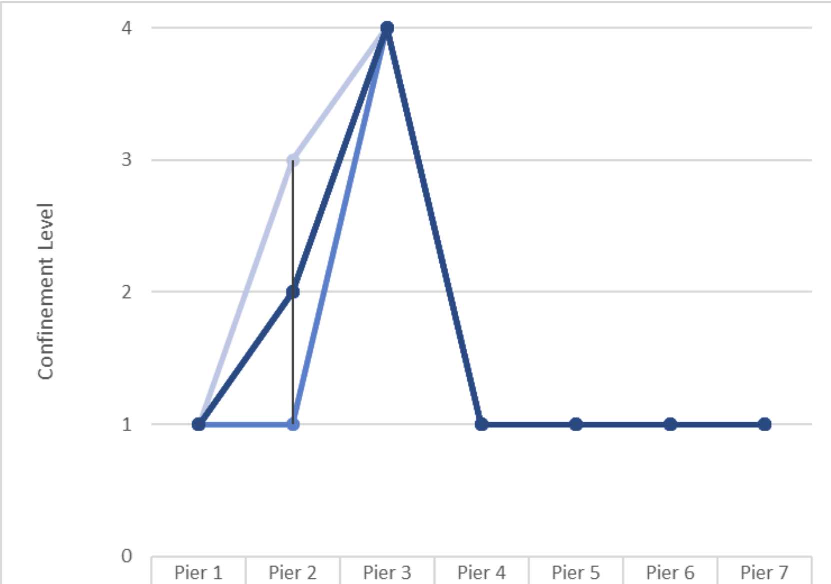

	Pier 1	Pier 2	Pier 3	Pier 4	Pier 5	Pier 6	Pier 7
2.375	1	2	4	1	1	1	1
2.4	1	3	4	1	1	1	1
2.425	1	2	4	1	1	1	1
2.45	1	2	4	1	1	1	1
2.475	1	1	4	1	1	1	1
2.5	1	1	4	1	1	1	1
2.525	1	2	4	1	1	1	1
2.55	1	2	4	1	1	1	1
2.575	1	2	4	1	1	1	1
2.6	1	2	4	1	1	1	1
2.625	1	2	4	1	1	1	1
2.65	1	2	4	1	1	1	1

Pier Position

Figure 4.13 Solutions in POS, showing the confinement level required at each pier, and the small variability in results. The series labels refer to pier diameter values.

The steel distribution shows an increasing necessity of steel as we decrease the pier diameter. As the critical pier, Pier 3, reaches the maximum steel allowed, the steel must be distributed to the other piers, to increase global resistance. As for the confinement level, it does not vary by much. The critical pier (Pier 3), which has the largest ductility demand, is the one with most of the confinement requirements, and since confinement only has a local effect, the variability is not so large as with flexural steel where the change in one pier can alter the global bridge behaviour. It is also clear that there are very well-defined patterns of steel distribution associated to the pier-deck connections that optimize the earthquake resistance.

The variable values associated to the connections have already been explained in 4.5.2.1. The values for the confinement are defined as 4 possible confinement configurations, where the value of 1 corresponds to minimum confinement of 10mm steel rebar spaced by 10cm, and the value of 8 is the maximum confinement of 16mm steel rebar spaced by 10 cm. The complete set of confinement solutions is {{10, 10} {12, 10} {16, 15} {16, 10}}.

4.6.2 Objectives set 2: Initial Cost + Performance

The initial population for this GA run, is set as the final population of the previous GA runs, performed with Objective set 1. This has a couple of advantages: the search effort, to reach the feasible region, is reduced and the optimal and sub-optimal solutions from the previous GA run are compared according to performance and price functions.

The cost of material was fixed at 0.82 euros/kg for A500NR steel, and 100 euros/m^3 for C30/37 concrete. The cost is only associated to the material in the piers. It is important to refer that the different pier-deck connections also have different costs, but these were not accounted for in the cost function.

The performance was defined as the minimum difference between maximum compressive concrete strain allowed (ε_{cu}) and compressive concrete strain recorded (ε_c) in any given section in the piers. Again, the compressive concrete strain is the only criteria for collapse since, elements prone to shear effects are avoided. To note in this instance the optimization problem is a minimization-maximization (Min-Max) problem, where cost is to be minimized and performance maximized, unlike with Objective-Set 1, which is a Min-Min problem. This results in a different position of the Pareto front in the cartesian graph of the objective space, as visible in Figure 4.14, than compared to the Pareto front from Objective-set 1.

Six GA runs were performed with objective-set 2 and in Figure 4.14 the POFs are presented. The results show, as with objective-set 1, a small variability in the results, with all POFs almost super-imposed.

In Figure 4.15, one of the runs is presented, with feasible and infeasible solutions visible. The green Xs represent feasible solutions, the red dots represent infeasible solutions, and the blue circles represent the POF.

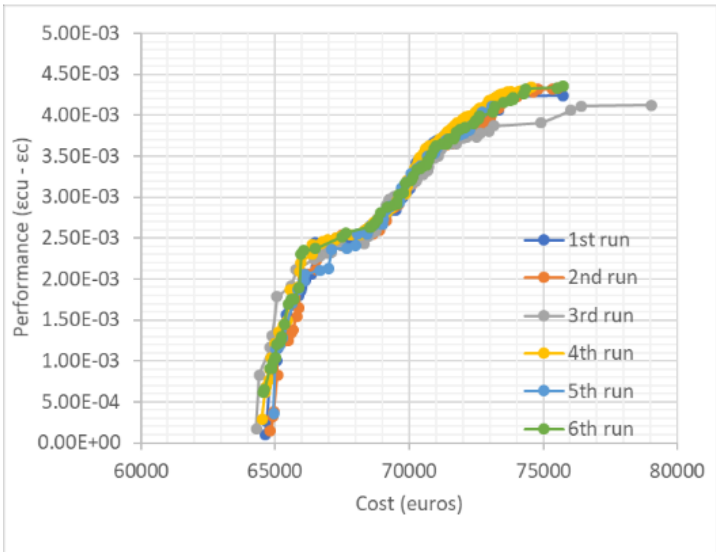

Figure 4.14 Final Pareto fronts obtained from the 6 runs with objective-set 2.

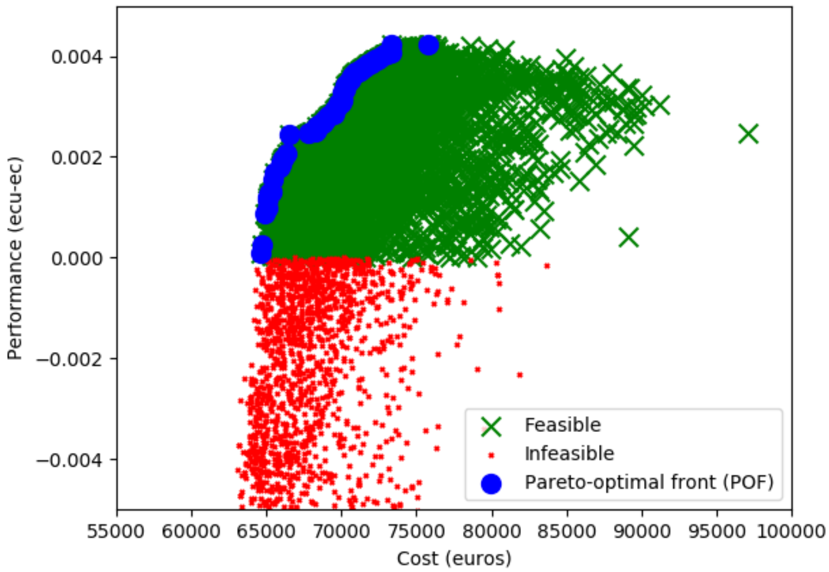

Figure 4.15 Result of run 1 with objective-set 2, where the red dots represent infeasible solutions, the green Xs represent feasible solutions and the blue circles represent the approximate Pareto-optimal front (POF).

The interest in these runs is to associate performance levels, associated to structural safety/reliability under seismic action, and to identify what variables have larger influence in the increase of safety, and what does increase in safety look like in the objective space of objective-set 1.

In Figure 4.16, the entire population history from the 6 GA runs with objective-set 2 is presented in the objective space of objective-set 1. In addition, colour coding divides the solutions in different performance levels. The performance levels are in Table 4.6.

Table 4.6 Definition of the performance levels

Perf. Lvls	1	2	3	4	5
ε_{cu} - ε_c	0.0-0.0015	0.0015-0.003	0.003-0.0035	0.0035-0.004	> 0.004

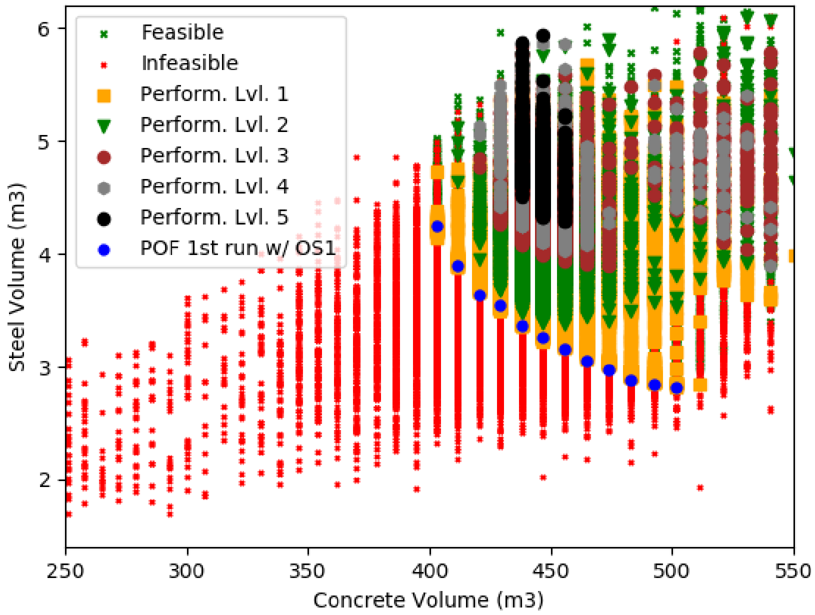

Figure 4.16 Solutions of all populations/generations analysed in all 6 runs with objective-set 2, represented in the objective space of objective-set 1.

The performance levels appear to be parallel to the Pareto front. All solutions continue to have the same pier-deck connections (Figure 4.11) that were obtained in the POS solutions with objective-set 1.

4.6.2.1 Solution selection

To illustrate a final decision, an example of a solution that could be chosen by a decision maker is one located close to the knee region of Figure 4.15 and is presented in Table 4.7. Knee regions of Pareto-fronts are interesting because they represent zones where a slight increase in one objective means a large degradation in another and are thus good regions to look for final solutions (Parreiras and Vasconcelos 2009).

Table 4.7 Selected solution's variables and objectives

	P1	**P2**	**P3**	**P4**	**P5**	**P6**	**P7**
P-D connect.	3	2	1	1	1	1	1
% Flex. steel	0.6	3.4	3.5	2.4	0.6	0.6	0.6
Confin. level	1	3	4	2	1	1	1
P Diam (m)	2.5						
Cost (Euro)	66500						
Perform. (ε_{cu}-ε_{c})	0.0024						

In Figure 4.17 and Figure 4.18, the solution is shown in the objective space of both objective sets.

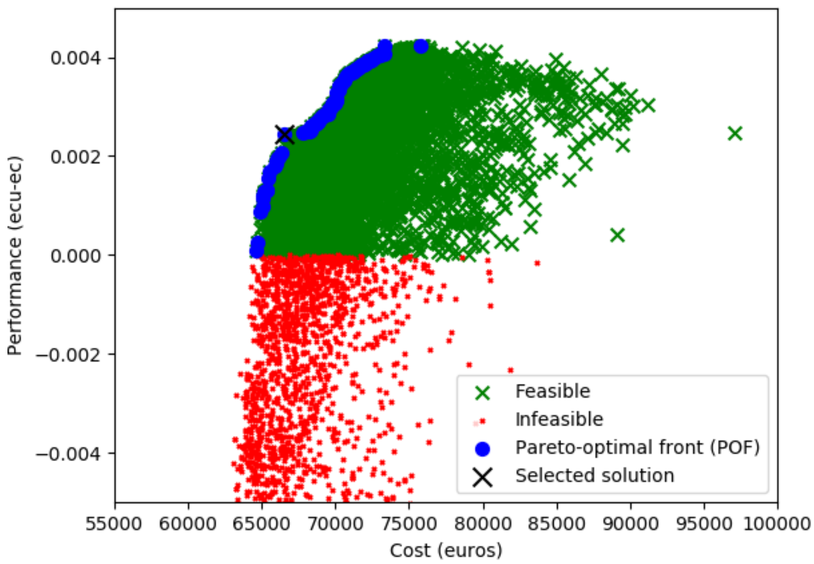

Figure 4.17 Selected solution in objective-set 2.

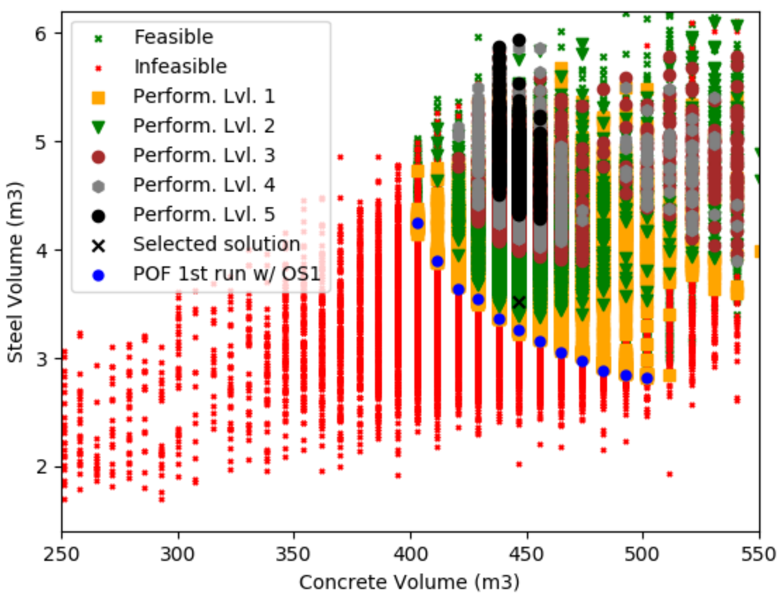

Figure 4.18 Selected solution in objective-set 1.

There are also many methodologies for decision making in multi-objective optimization (Parreiras and Vasconcelos 2009) (Zhang, Chen and Chong, Decision consolidation: criteria weight determination using multiple preference formats 2004), which can be applied in future works.

4.6.2.2 Variable importance

The main objective of the run with objective-set 2 is the identification of important variables that have large influence on structural safety/reliability. In a search procedure as is a GA, where variables are varied from solution to solution, by classifying solutions according to well defined performance levels, it is logical that the variables that have a decreasing CoV and monotonic behaviour of the mean value as the performance level increases, are likely to be important variables since that shows that they are correlated to an increase in the performance level.

In Figure 4.19 and Figure 4.20, the mean values and CoV of the flexural steel reinforcement variables in each performance level are presented. These results are obtained from the entire feasible population of the 6 GA runs, which is in total 47966 solutions.

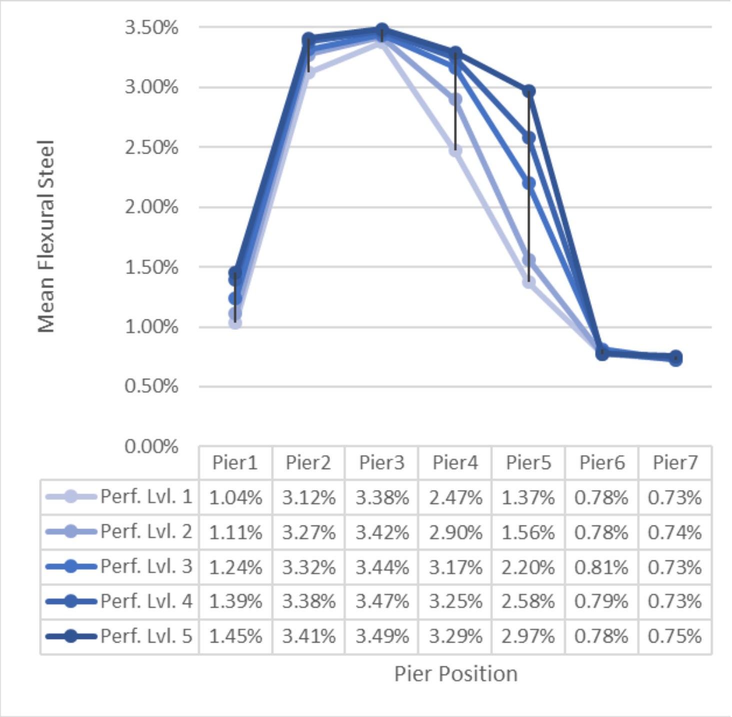

	Pier1	Pier2	Pier3	Pier4	Pier5	Pier6	Pier7
Perf. Lvl. 1	1.04%	3.12%	3.38%	2.47%	1.37%	0.78%	0.73%
Perf. Lvl. 2	1.11%	3.27%	3.42%	2.90%	1.56%	0.78%	0.74%
Perf. Lvl. 3	1.24%	3.32%	3.44%	3.17%	2.20%	0.81%	0.73%
Perf. Lvl. 4	1.39%	3.38%	3.47%	3.25%	2.58%	0.79%	0.73%
Perf. Lvl. 5	1.45%	3.41%	3.49%	3.29%	2.97%	0.78%	0.75%

Figure 4.19 Mean flexural steel reinforcement of all feasible solutions in each performance level, per pier.

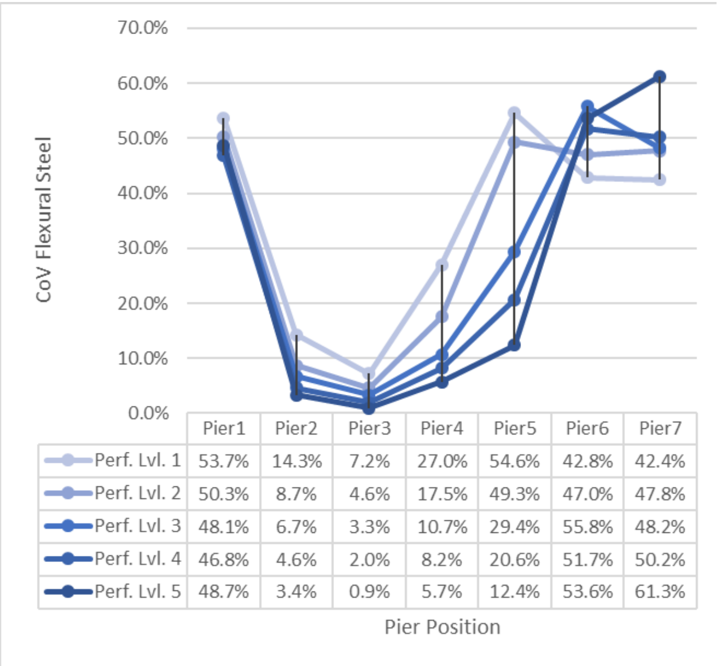

	Pier1	Pier2	Pier3	Pier4	Pier5	Pier6	Pier7
Perf. Lvl. 1	53.7%	14.3%	7.2%	27.0%	54.6%	42.8%	42.4%
Perf. Lvl. 2	50.3%	8.7%	4.6%	17.5%	49.3%	47.0%	47.8%
Perf. Lvl. 3	48.1%	6.7%	3.3%	10.7%	29.4%	55.8%	48.2%
Perf. Lvl. 4	46.8%	4.6%	2.0%	8.2%	20.6%	51.7%	50.2%
Perf. Lvl. 5	48.7%	3.4%	0.9%	5.7%	12.4%	53.6%	61.3%

Figure 4.20 Coefficient of variation of the flexural steel reinforcement variables in each performance level, per pier.

In Figure 4.21 and Figure 4.22, the mean values and CoV are presented for the confinement steel reinforcement.

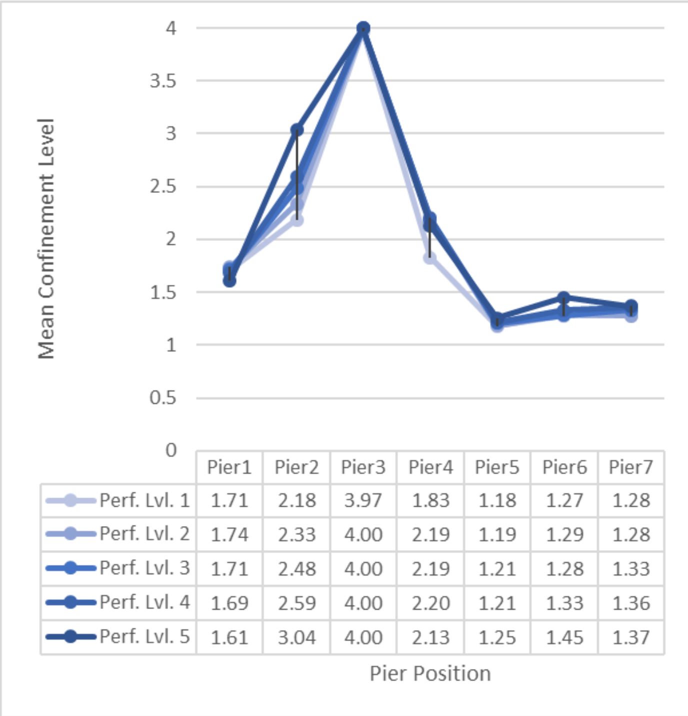

	Pier1	Pier2	Pier3	Pier4	Pier5	Pier6	Pier7
Perf. Lvl. 1	1.71	2.18	3.97	1.83	1.18	1.27	1.28
Perf. Lvl. 2	1.74	2.33	4.00	2.19	1.19	1.29	1.28
Perf. Lvl. 3	1.71	2.48	4.00	2.19	1.21	1.28	1.33
Perf. Lvl. 4	1.69	2.59	4.00	2.20	1.21	1.33	1.36
Perf. Lvl. 5	1.61	3.04	4.00	2.13	1.25	1.45	1.37

Figure 4.21 Mean confinement steel reinforcement of all feasible solutions in each performance level, per pier.

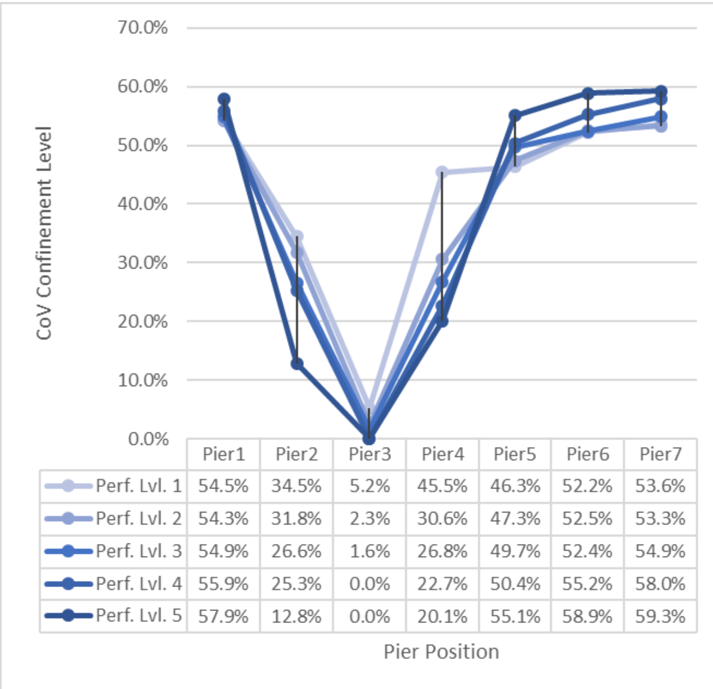

	Pier1	Pier2	Pier3	Pier4	Pier5	Pier6	Pier7
Perf. Lvl. 1	54.5%	34.5%	5.2%	45.5%	46.3%	52.2%	53.6%
Perf. Lvl. 2	54.3%	31.8%	2.3%	30.6%	47.3%	52.5%	53.3%
Perf. Lvl. 3	54.9%	26.6%	1.6%	26.8%	49.7%	52.4%	54.9%
Perf. Lvl. 4	55.9%	25.3%	0.0%	22.7%	50.4%	55.2%	58.0%
Perf. Lvl. 5	57.9%	12.8%	0.0%	20.1%	55.1%	58.9%	59.3%

Figure 4.22 Coefficient of variation of the confinement steel reinforcement variables in each performance level, per pier.

The results presented in Figure 4.19, Figure 4.20, Figure 4.21 and Figure 4.22, show which variables are most important and allow to perform a rank of importance of those variables on structural safety/reliability. This is shown by the monotonic increment of the mean value as the performance level also increases. In addition, the decrement of the CoV also shows that the variable is allowed less and less variation as the performance level increases which is also a measure of criticality. In that sense the flexural steel reinforcement can be ranked, from most important to least important:

1. Pier 3
2. Pier 2 and Pier 4
3. Pier 5

For flexural steel reinforcement piers 1, 6 and 7 are of little importance, since their CoV is always very large and also does not present a decreasing monotonic behaviour.

As for the confinement steel reinforcement, it can be ranked, from most important to least important:

1. Pier 3
2. Pier 2
3. Pier 4

In terms of confinement steel reinforcement piers 1, 5, 6 and 7 are of little importance for the same reasons explained in the case of the flexural steel reinforcement.

The results from the GA runs show that pier confinement and pier-deck connections, and not only flexural steel reinforcement and its distribution between the piers, are critical variables for the feasibility of solutions, which goes in line with the importance of ductility in seismic design. The critical piers are the ones that have shorter effective lengths, as expected. The increase in performance level by increasing the flexural steel reinforcement in non-critical piers shows the ability of redistribution of forces in ductile structures subjected to earthquakes.

As mentioned earlier, the cost function does not account for the cost of pier-deck connections. This can be an issue if the costs are very different between connections, and if there is significant variation in the pier-deck connections among feasible solutions. As mentioned previously, the POS solutions all have the same pier-deck connections and so the impact of that issue in these runs will be minimal. In other implementations the cost of the connections can be added to the cost function to reflect the impact of the price differences between connections in the overall cost of the solution.

4.6.3 Conclusions

The application of the GA for the optimization of RC bridge seismic design has allowed to find patterns in the feasible solutions that are associated to combinations of connections between infrastructure and superstructure, as well as critical piers in terms of ductility demand. The results show that to obtain a feasible solution, the connections and the confinement of critical piers is vital as expected, besides the amount of flexural reinforcement. The methodology can be applied to aid in the early stages of the design to define critical variables. The Pareto fronts for objective-set 1 show a clear trade-off between volume of steel and volume of concrete in the piers. For objective-set 2, we obtain a trade-off between initial cost and safety margin. This safety margin is an initial brush on LCCa and PBD, also giving an idea of the relevance of sub-optimal solutions obtained with objective-set 1 and allowing a better notion of the importance of certain variables.

Also, the analysis of the entire search population of a GA run and classification of the solutions according to attribute values can be very useful for extracting knowledge from large and complex data, both in quantity of instances and variables. The identification of critical variables/attributes can be important for the engineer and doing this for several bridge typologies can provide an important knowledge base for design.

To reiterate the main highlights of this study, concerning novel approaches and applications:

- A two-phase approach is defined, with change in objective-set, which allows to explore more objectives without a scale-up in population size and number of generations per run.
- The study optimizes bridge infrastructure seismic design in a multi-objective framework in which trade-off solutions between steel and concrete volume, and cost and performance are obtained.
- The optimization allows to perceive correlation between feasibility and certain variable arrangements (schema), namely associated to pier-deck connections.
- The entire search history of the GAs is used for sensitivity analysis of the decision variables, checking their relative importance in different pre-defined performance levels. This allows to define critical variables.
- The methodology can be applied in design firms for more complex irregular bridges which are difficult to design for seismic actions. Design firms can also use the methodology for identification of critical variables for different bridge layouts in order to extract design rules and guidelines.

In terms of drawbacks, one of the most noticeable is the time expensive nature of these analyses. As mentioned in 4.5.1, the fitness evaluations were parallelized between 32-threads, which allowed for a speed-up of a factor of 20, reducing the run-time for one generation from 120min to 6min. The total runtime varied from run to run, depending on the number of generations, but frequently was around 15 hours (150 generations). Without parallelization of processes it would be impractical. This is one of the main difficulties for applying this method in design firms, alongside the difficulty to implement the methodology with commercial software suites.

In order to reduce this time complexity, a solution can be to apply a single-objective version, with cost as the objective. This would reduce the necessary population size and the number of generations of a run. The drawback would be not having information gain from the objective trade-off. However, since time constraints are significant in design firms, this could prove advantageous.

Another possible approach to reduce the time complexity of the optimization procedure, especially in cases with very long bridges where the number of design variables can become very large, would be to bundle piers into pier groups according to pier height and location along the bridge. In this situation, piers belonging to the same pier group would have the same variable values, thus resulting in a significant variable reduction. The advantages would be in terms of standardization of design.

The techniques and methodologies presented in this chapter have several possible applications, not only limited to the optimization of a given bridge but also applied towards more general analyses, such as calibration of behaviour factors, as is presented in the next chapter.

5 Revision of behaviour factors

Seismic behaviour factors represent the ratio between the strength of a structure, assuming it always maintains an elastic behaviour, and the strength demand with plastic behaviour and consequent loss of stiffness, at the seismic target displacement. This value is closely related to ductility and to energy dissipation due to hysteretic behaviour. The use of behaviour factors allows to design structures with elastic models, without having to explicitly account for material non-linearity while taking advantage of ductility. However, the definition of these values is not easy, and is dependent on several factors. In bridges, these factors can be, among others, regularity of the bridge in terms of pier height, concrete and steel quality, size of elements and amount of steel reinforcement, pier confinement, etc. These factors influence ductility demand and available ductility in different ways and through Multi-Objective Optimization, MOO, the infrastructure solutions that maximize the use of the available ductility under a given earthquake action and for a given bridge superstructure, pier height scheme and ductility class according to Eurocode 8 – part 2, can be obtained. Those optimized solutions, which are obtained through the minimization of steel and concrete in the piers as concurrent objectives, are associated with the maximum behaviour factors that can be used in the design of a given bridge and can be compared with the values recommended by EC8 – part 2. Without loss of generality, the methodology is applied to a set of case-studies composed of RC bridges with four 30-meter spans and circular piers, analysed in the longitudinal direction and without accounting for abutment effects. With the results from the MOO, the behaviour factors associated to solutions with different ductility levels and pier irregularity schemes are calculated and equations are derived, relating the obtained behaviour factors with a pier irregularity measure and ductility level. The results also show the importance of the choice of stiffness used in the design process.

5.1 Introduction

The discussion on behaviour factors is not new and has been the matter of several works throughout the years and applied to different types of structures. Related to this discussion, over the last two decades, the understanding of seismic behaviour of structures and seismic analysis methods have evolved greatly. The works by Priestley have identified a variety of myths associated to seismic analysis and design (M. N. Priestley 2003) and underlined the importance of ductility in seismic resistance, among other aspects. As a result, new paradigms in earthquake engineering have surfaced such as the well-known displacement-based design (Priestley, Calvi, et al., Displacement-Based Seismic Design of Structures 2008) (Calvi, Priestley and Kowalsky, Displacement-Based Seismic Design of Bridges 2013), which takes ductility into account explicitly in the seismic design of structures. Even though displacement-based design may be more adequate to earthquake engineering than force-based design, the latter one is still widespread in engineering firms. In addition, designs obtained with linear elastic methods frequently end up not being checked with non-linear methods. Therefore, the discussion surrounding behaviour factors is still important and remains the subject of extensive studies.

A few examples of these studies are presented. An earlier example is the work (A. J. Kappos 1999), where ductility and overstrength were accounted for in the evaluation of behaviour factors of medium and low-rise concrete structures. In this work, the behaviour factor was presented as $q = q_s q_\mu q_\xi$, where q_s, q_u and q_ξ represent, respectively the overstrength-dependent component (both elastic and plastic), the ductility-dependent component and the damping-dependent component (only if additional dissipation elements are added). In more recent works, (Kappos, Paraskeva and Moschonas 2013) behaviour factors were analysed for concrete bridges in Europe, where a set of existing bridges with different characteristics were studied. Subsequently, the q_s and q_μ values were calculated for each case. More recently a study (Žižmond and Dolšek 2016) calculated the impact of several factors, that are implicit in design according to Eurocodes, in the values of q_s and q_μ. Factors such as mean material strength, capacity design, actual amount of reinforcement and minimum Eurocode requirements, were evaluated for three concrete structure sizes. The assumptions and requirements prescribed by the Eurocodes that are implicit in the behaviour factor values were taken into account in the present study (Fardis, et al. 2005) (Kolias, et al. 2012). In this study, the methodology for the evaluation of the behaviour factors uses novel techniques of meta-heuristic search algorithms.

The purpose of the study presented in this chapter is, resorting to non-linear methods and optimization algorithms, to obtain optimal earthquake designs of reinforced concrete bridges, and then check what the maximum behaviour factor would be if that bridge design had been obtained through linear elastic force-based methods. The study focuses on RC bridges with four 30-meter spans and circular piers, analysed in the longitudinal direction. The purpose is then to ascertain which variables related to bridge geometry, material quantities and constitutive relationships have more influence in the ductility and in the behaviour factors. Finally, for each case study, the minimum and maximum behaviour factor values are checked and equations that relate the behaviour factors with the ductility demand are derived. Thus, the optimization of design resorting to evolutionary algorithms, and using non-linear analysis methods for the evaluation of the solutions yields reliable results that minimize the difference between ductility demand and available ductility, while simultaneously maximizing available ductility. This means that the solutions that are obtained from that optimization, effectively maximize the usage of ductility and represent the solutions that correspond, for a given bridge, to the maximization of the behaviour factor, which can then be compared to the values defined in Eurocode 8 (CEN 2005) (CEN 2005). In addition, by performing several runs while varying parameters such as concrete quality, steel post yield stiffness, maximum allowed confinement, pier height irregularity, etc., one obtains a sensitivity analysis of the behaviour factor's value in respect to those parameters.

The structure of this chapter is the following: in 5.2 the behaviour factor is defined according to EC8. In Section 5.3, the objectives and methodology are presented. In Section 5.4, the definition of the case studies, its' variables and constraints, as well as the definition of the earthquake action and integration with the NSGA-II algorithm (Deb, Multi-Objective Optimization Using Evolutionary Algorithms 2001), are presented. Section 5.5 is where the results, discussion and derivation of expressions that associate the obtained behaviour factors with ductility and pier irregularity are shown.

5.2 Behaviour Factors and Ductility

5.2.1 Behaviour factors in EC8 – part 2

The behaviour factor reflects the structure's available ductility only if the ductility demand matches it. According to EC8 – part 2 (CEN 2005) the behaviour factor reflects the capability of ductile members to withstand, with acceptable damage but without failure, seismic actions in the post-elastic range. EC8 – part 2 also defines a list of available levels of ductility and respective behaviour factors and defines the requirements for a structural element to be considered a ductile member. The procedure for which the behaviour factors are to be applied is linear elastic analysis based on the design spectrum defined in EC8 – part 1 (CEN 2005).

In EC8 – part 2, the requirement for defining a member as ductile is the capability to develop flexural plastic hinges, which is deemed to be ensured when certain detailing rules and capacity design procedures are applied. The behaviour factor's values are also dependent on regularity and axial force in the members.

5.2.1.1 Regular and irregular seismic behaviour of ductile bridges

The regularity of the bridge can influence the value of the behaviour factors. The way to take that into account, according to EC8 - part 2, is through the calculation of a local force reduction factor, r_i, associated with member i, and relating to the maximum value of design moment at the intended plastic hinge location, $M_{Ed,i}$, and the design flexural resistance of the same section with its actual reinforcement under the concurrent action of the non-seismic action effects in the seismic design situation, $M_{Rd,i}$:

$$r_i = q \frac{M_{Ed,i}}{M_{Rd,i}} \tag{5.1}$$

It can be considered that the ratio $\frac{M_{Ed,i}}{M_{Rd,i}}$ is not a good measure of irregularity, as the yield curvature of a cross-section varies very little with M_{Rd} (M. N. Priestley 2003). Therefore, varying M_{Rd} does not delay or anticipate yielding of a cross-section, so it almost does not affect energy dissipation. An indicator of irregularity must be a measure of differences in the beginning of the plastification of columns plastic hinges, therefore should be a function of column yield displacements. This can eventually be expressed as a function of columns geometry (height and dimension in the flexural plane at the plastic hinge) and boundary conditions but is almost independent of M_{Rd} at the plastic hinges.

5.3 Objectives and Methodology

The prime objective of this study is to perform a review on behaviour factor values used for the design of RC bridges to resist earthquake actions, in the longitudinal direction, and compare against values prescribed by EC8. Another objective is to present the methodology of the study, which takes advantage of the results from multi-objective optimization to obtain optimized solutions in terms of the use of their ductility. Finally, and not less important, the presentation of expressions for calculating the behaviour factor according to pier irregularity and ductility class, or even independently of the ductility class. To carry out these objectives, a methodology was devised and is presented. The methodology can be summarized in the following steps:

1. Definition of the case-studies in which variables that have influence on ductility are varied, with emphasis on pier irregularity and confinement. These case-studies are composed of RC bridges with four 30-meter spans and three circular piers.

2. Optimization search with Evolutionary Algorithms (EA) (Goldberg 1989) for each case-study – A set of solutions are obtained that maximize the ratio between ductility demand and available ductility in the piers, while minimizing the amount of material in the piers and guaranteeing seismic resistance. The solutions obtained from this algorithm are not the result from a design method, they are the result from a metaheuristic search, and therefore are unbiased.

3. Calculating the behaviour factors of the optimized solutions of each case-study – The behaviour factors that would be necessary to design the optimized solutions obtained from step 2, if a traditional force-based design procedure were to be employed.

4. Comparison of the obtained behaviour factors with the behaviour factors prescribed in EC8 and finding expressions that correlate ductility and pier irregularity with the said behaviour factors.

Central to this methodology is the application of multi-objective evolutionary algorithms, particularly the same modified NSGA-II applied in the previous chapter.

5.4 Bridge Seismic Design – Longitudinal Direction

The optimization procedure obtains solutions which simultaneously maximize the ratio between ductility demand and available ductility without reaching the collapse criteria, while minimizing the amount of material used (total concrete and steel in the piers). This means that the solutions in the final Pareto-optimal set (POS) of each case-study correspond to the maximum behaviour factor values that can be used, for that bridge, since the ductility and the demand are both maximized. In non-optimized solutions, we may have more available ductility, but if that ductility is “unused by the structure” during the earthquake action, then it doesn't exist for matters of the response of the structure. With this methodology, it is possible to do a comprehensive comparison of maximum behaviour factors, varying multiple characteristics and variables associated to RC bridges, from material quality to relative pier length, etc.

5.4.1 Definition of case-study bridges: variables and earthquake action.

The bridges that will be analysed in this study are relatively short bridges with three piers and span lengths of 30 meters. These bridges will only be subjected to the earthquake action in the longitudinal direction. The cross-section shape of the piers is circular. The deck is simply supported on the columns, that is, there is compatibility of horizontal and vertical displacements between both, but the deck and columns are free to rotate relatively to each other. In the abutments the only deck displacements restricted are the vertical ones, the horizontal longitudinal displacements are free. Usually expansion joints are designed to ensure this. Possible restrictions to deck longitudinal displacements by the abutments were not considered.

There are two types of variables in the model. The first type is associated with the variables that are varied during the optimization process, that is, in the MOEA procedure. These variables are related to the design of the piers. The second type are variables that remain constant during the optimization process (MOEA) but are varied to make different case-studies. These variables are generally not associated to pier design but influence the results.

5.4.1.1 Optimization variables

1. Longitudinal reinforcement steel – This variable is the percentage of longitudinal steel reinforcement in the cross-section of each column (it can change between columns) ranging from the minimum according to EC8 - 2 of 0.6% and up to 3.50%. The discretization step is of 0.05%.
2. Cross-section diameter – While the other variables are related to one pier, this variable is the same for all piers. The minimum diameter is 1.0 meter and the maximum is 2.5 meter.

Figure 5.1 shows the generic cross-section with the variables 1 and 2 identified.

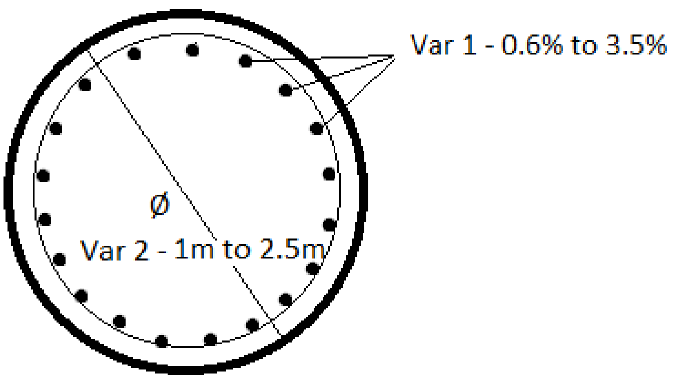

Figure 5.1 Circular pier cross-section and decision space variables.

5.4.1.2 *Case-study variables*

The second type of variables are, mostly, not directly associated to pier design and are not modified during the optimization process, as already mentioned. The purpose is to obtain the sensitivity of ductility and maximum behaviour factor values for several variables. The variables are the following:

- Concrete quality: B35, B45
- Pier irregularity (relative pier length ratio): 7-7-7, 7-9-11, 7-11-14, 7-14-21, 7-8-9, 5-5-5, 5-7-9, 5-9-11, 5-11-14, 5-6-7, 5-7-7 and 5-5-7 (where in each set the numbers represent the height of the 3 columns of the bridge
- Self-weight (weight of the deck): 3120-ton, 6240-ton
- Steel post-yield stiffness: 1000 MPa (0.5% Es), 2000 MPa (1.0% Es)

The various case-studies were defined through combinations of the values of these variables. Each one of the variables influences the ductility of the model in different ways. The purpose is to try to have a comprehensive study of the main factors that influence ductility of RC bridges.

5.4.1.3 *Earthquake action*

The seismic analysis method used in the execution of this work was non-linear static analyses with the N2 method (Fajfar 2000). The earthquake spectrum relative to earthquake type 1, zone 2, soil type C from Eurocode 8 – Part 1 and the Portuguese National Annex (IPQ 2010) was selected as the earthquake action for all case-studies, which corresponds to a PGA of 0.285g.
The N2 method was applied for the analyses of bridges in the longitudinal direction, which can be reduced to a single degree of freedom (SDOF) problem in a straight bridge. In these cases, the N2 method produces reliable results according to (Kappos, Saiidi, et al. 2012), since the influence of modes other than the fundamental vibration mode is negligible.

5.4.2 Finite element model definition

The structural models used for the simulation of the earthquake response of the solutions were defined and analysed with OpenSEES software (McKenna and Fenves 1999), particularly the variant OpenSEESMP which facilitates to run several models in parallel. The OpenSEES/OpenSEESMP software is a library extension of the Tcl/Tk language interpreter. This facilitates the integration of structural analysis with several pre- and post-processing programming procedures, which is fundamental for integrating structural design and analysis with optimization algorithms.
For the modelling of the bridges in OpenSEES, fibre elements were used for the piers, specifically force-based fibre elements. Each pier was divided into three elements, where the elements containing the expected plastic hinges had a larger density of integration points to better capture curvature variations. The deck was modelled as a linear elastic element.

5.4.2.1 Material properties

The mean values of the materials' mechanical properties were used. For the steel, the material used was A500NR, and B35 and B45 for the concrete. The values used to define the steel constitutive relationship were taken from (Pipa 1993) and are shown in Table 5.1. The values for the concrete are shown in Table 5.2.

Table 5.1 Mean values for the mechanical properties of the A500NR SD steel from Pipa.

Mean values	A500NR SD
f_{ym} (MPa) – yield stress	585
f_{um} (MPa) – ultimate stress	680
E_{ym} (GPa) – Young modulus	200
ε_{sy} (‰) – yield strain	2.93
ε_{sh} (‰) – strain at beginning of hardening	14
ε_{su} (‰) – ultimate strain	94

Table 5.2 Mean values for the mechanical properties of the B35 and B45 concrete.

Mean values	B35 (C30/37)	B45 (C40/50)
f_{cm} (MPa) – unconfined maximum stress	38	48
E_{cm} (GPa) – Young modulus	33	35
ε_{cu} (‰) – unconfined ultimate strain	3.5	3.5

5.4.2.2 Materials' constitutive relationships

The model used for the concrete fibres was a Mander concrete material object (Mander, Priestley and Park 1988). The stress and strain values used in the concrete model were calculated using the expressions in Annex E from Eurocode 8 – part 2 for confined concrete, and particularly for circular sections. For the steel reinforcement fibres, a uniaxial Giuffré-Menegotto-Pinto model with isotropic strain hardening was used. For both concrete and steel, the constitutive relationships were built using mean values of material properties, shown in Table 5.1 and Table 5.2.

5.5 Results and Discussion

5.5.1 Case-studies

The case-studies, to which the optimization procedure was applied, resulted of combinations of the case-study variables defined on 5.4.1.2. These so-called case-study variables remain constant throughout the optimization procedure, while the optimization variables constitute the variables that are changed during the optimization procedure. This way, the impact of the case-study variables on the ductility and behaviour factors become apparent since there are 29 case-studies covering many combinations of the defined case-study variable values. In Table 5.3, the case-studies with the respective combination of variables are presented.

Table 5.3 Case-studies and respective variables.

Case-study	Pier height (m)	Deck weight (ton)	Concrete	Ductility Class	Steel post-yield stiff. (MPa)
1_1	5_5_5	3120	B35	Ductile	1000
1_2	5_5_5	3120	B35	Limited Ductile	1000
1_3	5_5_5	**6240**	B35	Ductile	1000
2_1	7_7_7	3120	B35	Ductile	1000
2_2	7_7_7	3120	B35	Limited Ductile	1000
2_3	7_7_7	3120	B35	Ductile	**2000**
2_4	7_7_7	3120	**B45**	Ductile	1000
2_5	7_7_7	**6240**	B35	Ductile	1000
3_1	7_9_11	3120	B35	Ductile	1000
3_2	7_9_11	3120	B35	Limited Ductile	1000
4_1	7_11_14	3120	B35	Ductile	1000
4_2	7_11_14	3120	B35	Limited Ductile	1000
4_3	7_11_14	3120	B35	Ductile	**2000**
5_1	5_7_9	3120	B35	Ductile	1000
5_2	5_7_9	3120	B35	Limited Ductile	1000
6_1	5_9_11	3120	B35	Ductile	1000
6_2	5_9_11	3120	B35	Limited Ductile	1000
7_1	5_11_14	3120	B35	Ductile	1000
7_2	5_11_14	3120	B35	Limited Ductile	1000
8_1	7_8_9	3120	B35	Ductile	1000
8_2	7_8_9	3120	B35	Limited Ductile	1000
9_1	5_6_7	3120	B35	Ductile	1000
9_2	5_6_7	3120	B35	Limited Ductile	1000
10_1	5_5_7	3120	B35	Ductile	1000
10_2	5_5_7	3120	B35	Limited Ductile	1000
11_1	5_7_7	3120	B35	Ductile	1000
11_2	5_7_7	3120	B35	Limited Ductile	1000
12_1	7_14_21	3120	B35	Ductile	1000
12_2	7_14_21	3120	B35	Limited Ductile	1000

The procedure, for each case-study, is to run the MOEA modifying the optimization variables defined in 5.4.1.1, while keeping the variables in Table 5.3 fixed. The optimization variables are modified in the MOEA procedure with the goal of minimizing the MOP objectives. The MOP objectives are: 1) area of concrete in the piers; 2) area of steel in the piers. Additionally, for the solution to be feasible, the solution must be able to resist the earthquake action. The analysis is performed with non-linear static procedures. The main collapse criterion is excessive compressive strain in the concrete, at the plastic hinge sections, which means that it is assumed that capacity design provisions are enforced, thus preventing other failure modes.

The cross-section confinement placed in each solution is equal to the minimum confinement associated to each of the ductility classes defined by EC8 - part 2. To attain such pier confinement levels for each solution, the amount of transverse reinforcement needed for each pier's critical cross-section is calculated individually. The transverse reinforcement is thus dependent on the reduced axial force, flexural steel and cross-section size of each pier. This way, all piers of all bridge solutions are guaranteed to have the minimal confinement prescribed by EC8 for the respective ductility level (Ductile or Limited Ductile). In this sense, the confinement level is not an optimization variable, but can be considered, indirectly, a case-study variable since it is associated with the ductility class from Table 5.3.

5.5.2 Behaviour factors obtained from the optimization runs

The POSs (Pareto-optimal sets), which are obtained at the end of the optimization runs, represent the solutions that are optimal in regard to the objective functions (material quantities), and as a result maximize the use of their available ductility, hence maximizing their behaviour factor. For every solution in the POSs, the ultimate displacement (R_u) is thus almost equal to the target displacement (Sd_t), as it is visible in Figure 5.2. Furthermore, the POSs were obtained without resorting to any preconceived notions of design, other than capacity design provisions and code limits, and are the result of the process of an evolutionary algorithm, EA, with the N2 method being used to perform the seismic analysis. Hence the results have no bias associated to pre-conceptions of a seismic design method for RC structures, since they are merely the result of a search process with a meta-heuristic tool.

In Figure 5.2, an example of the N2 method applied to a bridge solution in POF 3-1 is shown. The bi-linearization used in the N2 method was done preserving the area under both curves (capacity curve and bi-linearized curve) equal, from the origin to Sd_t.

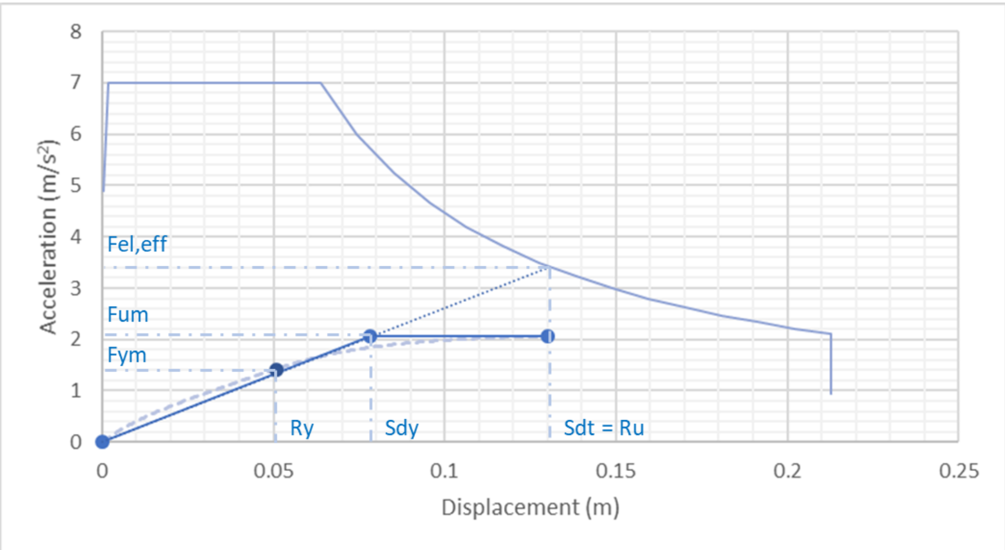

Figure 5.2 Example of application of N2 method to one of the POF solutions of case-study 3-1.

For every case-study, for every solution, the behaviour factor (q), its plastic overstrength-dependent component (q_s) and its ductility-dependent component (q_μ) are calculated:

- Behaviour factor (q) – Can be defined as $q = F_{el,eff}/F_{yd} = 1.5 \cdot q_s \cdot q_\mu$, where the value of 1.5 relates to F_{ym}/F_{yd} (mean yield/design yield), used in EC8, which also accounts for actual amount of reinforcement used among other factors (Fardis, et al. 2005). Overall, it accounts for overstrength in the elastic range.
- Plastic overstrength-dependent component (q_s) – Is defined as the ratio F_{um}/F_{ym}, which are both identified in Figure 5.2.
- Ductility-dependent component (q_μ) – Is the ratio $F_{el,eff}/F_{um}$, which are both identified in Figure 5.2.

The obtained behaviour factor values are presented for comparison with the behaviour factor values prescribed in EC8. The logic in calculating the behaviour factors of the POS solutions is answering the question: “How much would the behaviour factor need to be, in order to obtain a solution with similar seismic resistance to the one obtained from the optimization algorithm?” Furthermore, the solutions generated and analysed during the optimization runs each provide a behaviour factor value. The set of behaviour factor values of all solutions, not only optimised ones, yields an idea of the range of values for the behaviour factor, associated to different pier irregularities, among other variables.
In Table 5.4, Table 5.5 and Table 5.6, the results of the POS obtained from the optimization runs of three case-studies (CS 3-1, CS 4-1 and CS 8-1) are presented. Here the variables of the optimal solutions are presented with the results of the behaviour factor, the partial components related to overstrength and ductility, the reduced axial force, among other characteristics. R_y, Sd_y and Sd_t are all defined in Figure 5.2. The behaviour factor prescribed in EC8 - part 2 for ductile bridges is q_{EC8}=3.5.

Table 5.4 Optimization variables and results of the POS solutions for case-study CS 3-1.

SteelP1	SteelP2	SteelP3	PierD(m)	Sd_t(m)	R_y(m)	Sd_y(m)	v_k	1.5q_s	q_μ	q	q/q_{EC8}	$q_{dy}=S_{dt}/R_y$
3.50%	3.40%	1.65%	1.575	0.137	0.056	0.098	13.1%	2.44	1.38	3.37	0.96	2.46
3.30%	3.40%	0.65%	1.6	0.136	0.054	0.094	12.7%	2.42	1.43	3.45	0.99	2.51
3.30%	2.75%	0.65%	1.625	0.135	0.053	0.091	12.3%	2.37	1.47	3.48	0.99	2.53
3.45%	1.90%	0.60%	1.65	0.132	0.053	0.086	11.9%	2.29	1.53	3.49	1.00	2.51
3.50%	1.05%	0.80%	1.675	0.131	0.052	0.082	11.6%	2.23	1.59	3.53	1.01	2.54
3.40%	0.75%	0.60%	1.7	0.130	0.051	0.078	11.2%	2.19	1.64	3.59	1.03	2.57
3.05%	0.70%	0.60%	1.725	0.130	0.049	0.076	10.9%	2.20	1.68	3.70	1.06	2.65
2.55%	0.80%	0.60%	1.75	0.132	0.048	0.076	10.6%	2.22	1.72	3.83	1.09	2.77
2.35%	0.70%	0.60%	1.775	0.132	0.046	0.074	10.3%	2.23	1.75	3.92	1.12	2.86
2.00%	0.65%	0.60%	1.8	0.134	0.045	0.073	10.0%	2.24	1.81	4.06	1.16	3.00
1.65%	0.65%	0.60%	1.825	0.136	0.043	0.071	9.8%	2.27	1.88	4.26	1.22	3.18
1.40%	0.60%	0.60%	1.85	0.138	0.041	0.070	9.5%	2.27	1.93	4.39	1.26	3.35
1.15%	0.60%	0.60%	1.875	0.139	0.039	0.069	9.2%	2.31	1.99	4.58	1.31	3.56
0.80%	0.75%	0.65%	1.9	0.142	0.036	0.070	9.0%	2.42	2.01	4.87	1.39	3.94
0.65%	0.75%	0.65%	1.925	0.143	0.034	0.069	8.8%	2.47	2.05	5.05	1.44	4.19

Table 5.5 Optimization variables and results of the POS solutions for case-study CS 4-1

SteelP1	SteelP2	SteelP3	PierD(m)	Sd_t(m)	R_y(m)	Sd_y(m)	v_k	$1.5q_s$	q_μ	q	q/q_{EC8}	$q_{dy}=Sd_t/R_y$
3.50%	0.60%	0.60%	1.8	0.124	0.048	0.075	10.02%	2.21	1.61	3.56	1.02	2.59
3.25%	0.60%	0.60%	1.825	0.123	0.047	0.074	9.75%	2.22	1.63	3.61	1.03	2.64
3.00%	0.60%	0.60%	1.85	0.123	0.046	0.074	9.49%	2.23	1.64	3.66	1.05	2.70
2.75%	0.60%	0.60%	1.875	0.123	0.044	0.072	9.24%	2.25	1.67	3.77	1.08	2.79
2.45%	0.60%	0.60%	1.9	0.125	0.043	0.072	9.00%	2.26	1.70	3.86	1.10	2.88
2.15%	0.60%	0.65%	1.925	0.127	0.042	0.072	8.76%	2.30	1.73	3.98	1.14	3.04
1.95%	0.60%	0.60%	1.95	0.127	0.041	0.071	8.54%	2.31	1.76	4.06	1.16	3.12
1.75%	0.60%	0.60%	1.975	0.128	0.040	0.070	8.33%	2.32	1.79	4.16	1.19	3.22
1.45%	0.60%	0.60%	2	0.131	0.038	0.070	8.12%	2.37	1.84	4.37	1.25	3.48
1.35%	0.60%	0.60%	2.025	0.131	0.037	0.070	7.92%	2.39	1.84	4.41	1.26	3.58
1.20%	0.60%	0.60%	2.05	0.132	0.036	0.069	7.73%	2.41	1.87	4.51	1.29	3.69
0.90%	0.60%	0.60%	2.075	0.138	0.034	0.069	7.54%	2.46	1.95	4.79	1.37	4.09
0.65%	0.60%	0.60%	2.15	0.139	0.030	0.069	7.03%	2.56	1.97	5.05	1.44	4.60

Table 5.6 Optimization variables and results of the POS solutions for case-study CS 8-1

SteelP1	SteelP2	SteelP3	PierD(m)	Sd_t(m)	R_y(m)	Sd_y(m)	v_k	$1.5q_s$	q_μ	q	q/q_{EC8}	$q_{dy}=Sd_t/R_y$
3.50%	3.20%	3.20%	1.375	0.159	0.066	0.110	17.2%	2.37	1.43	3.38	0.97	2.42
3.50%	2.85%	2.20%	1.425	0.152	0.063	0.102	16.0%	2.31	1.48	3.42	0.98	2.43
3.50%	2.80%	1.60%	1.45	0.149	0.062	0.098	15.4%	2.27	1.51	3.42	0.98	2.41
3.50%	3.00%	0.75%	1.475	0.146	0.060	0.094	14.9%	2.23	1.54	3.44	0.98	2.42
2.90%	3.10%	0.80%	1.5	0.145	0.058	0.093	14.4%	2.28	1.55	3.55	1.01	2.52
1.95%	3.20%	0.90%	1.525	0.148	0.054	0.092	14.0%	2.39	1.60	3.83	1.09	2.76
1.30%	3.45%	0.60%	1.55	0.150	0.050	0.090	13.5%	2.49	1.66	4.12	1.18	3.03
1.20%	2.95%	0.80%	1.575	0.149	0.048	0.088	13.1%	2.49	1.69	4.20	1.20	3.10
1.50%	2.30%	0.60%	1.6	0.147	0.049	0.083	12.7%	2.34	1.75	4.10	1.17	2.99
1.30%	1.90%	0.75%	1.625	0.147	0.047	0.080	12.3%	2.35	1.82	4.27	1.22	3.12
1.55%	1.15%	0.80%	1.65	0.145	0.048	0.076	11.9%	2.23	1.90	4.23	1.21	3.05
1.40%	1.00%	0.60%	1.675	0.145	0.046	0.072	11.6%	2.19	2.00	4.38	1.25	3.14
1.35%	0.60%	0.70%	1.7	0.144	0.045	0.068	11.2%	2.16	2.09	4.53	1.29	3.24
0.90%	0.65%	0.60%	1.725	0.147	0.041	0.064	10.9%	2.18	2.26	4.93	1.41	3.57
0.65%	0.65%	0.60%	1.75	0.147	0.038	0.062	10.6%	2.21	2.36	5.22	1.49	3.86
0.60%	0.60%	0.60%	1.775	0.145	0.037	0.060	10.3%	2.22	2.38	5.30	1.51	3.96

The previous tables show that the minimum values of the behaviour factors obtained are very similar to the EC8 – part 2 values prescribed for RC bridges, albeit being slightly lower in a few cases. As for the maximum value, it is significantly higher, reaching in some cases values 1.5x the prescribed EC8 – part 2 value. This indicates that EC8 - part 2 q-factor of 3.5 for ductile bridges is suitable for bridges of different configurations, levels of irregularity and axial force.

One of the main particularities to retain from the tables is the range of values of reduced axial force between case studies. These values are closely related to the irregularity of each bridge. The more irregular the bridge the lower the maximum reduced axial force. This will be made more apparent in later figures and tables.

Another interesting detail is the evolution of the behaviour factors as we increase the pier cross-section diameter of the solutions. In fact, the behaviour factor increases, even though the target displacement is kept more or less constant. This happens because the yield displacement decreases with the increase in cross-section. Subsequently, the ratio between target displacement and yield displacement increases, leading to an increase of the ductility-dependent component (q_{μ}). It is also interesting to note that the overstrength-dependent component ($1.5q_S$) remains more or less constant among case-studies.

In Figure 5.3, results of the POS solutions of each of the three previously presented case-studies are presented, namely the values of reduced axial force (v_k) and behaviour factor (q). It is visible that there is a correlation between q and v_k, and that in the case of the v_k, it varies between different values for each case-study, typically the larger the pier irregularity the smaller the admissible reduced axial force since axial force has a negative effect on ductility. From right to left, the case-study bridges increase in pier irregularity, showing the aforementioned negative effect of the irregularities on the ductility.

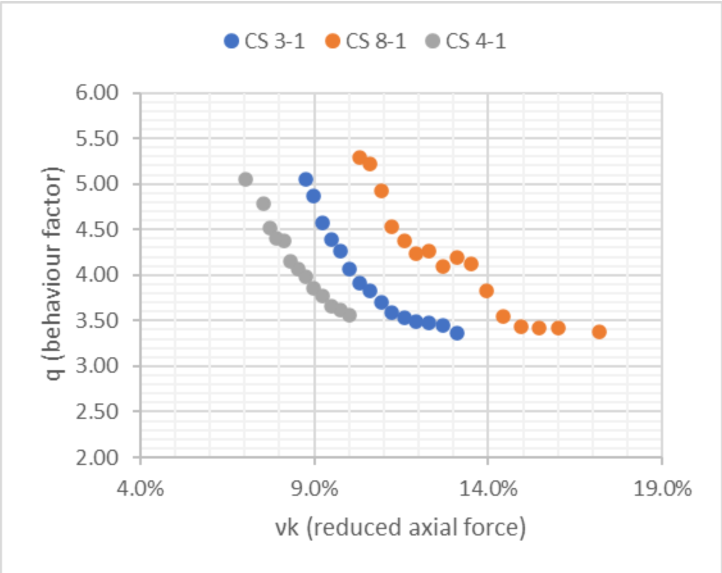

Figure 5.3 Results for q and v_k of POS solutions from CS 3-1, CS 4-1 and CS 8-1

In Figure 5.4, the same POS solutions for the three case-studies are now presented by q and q_{dy}, which is the ratio between the target displacement (Sd_t) and the real yield-displacement (R_y). There is a linear relation between both variables, and the physical meaning is by how much q varies with the increase in the ratio between target displacement and yield displacement of the stiffest pier. It will be shown that the rate of that variation is closely related to pier irregularity as well.

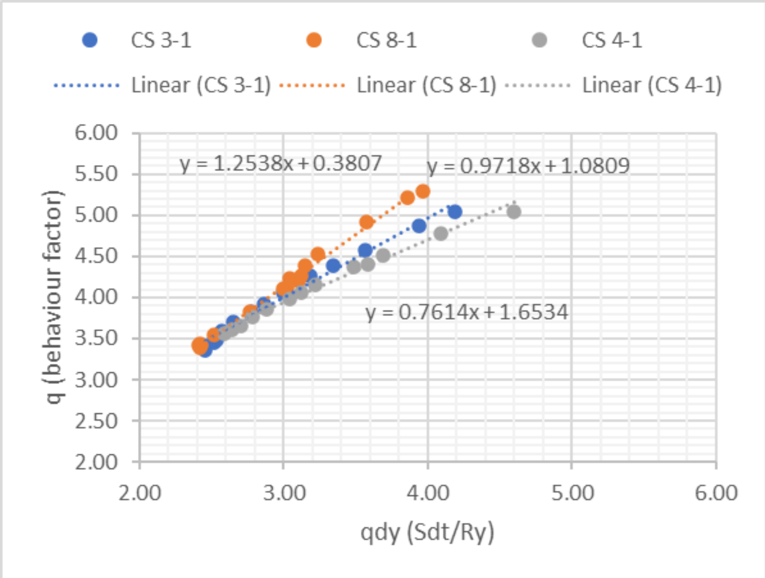

Figure 5.4 Results for q and q_{dy} of POS solutions from CS 3-1, CS 4-1 and CS 8-1. Linear regression of each graph.

5.5.3 Analysis and discussion

The results from the entire set of case-studies are presented and discussed in this section, along with the presentation of a pier irregularity measure and the definition of an alternative expression for the behaviour factor. The presented results relate to two sets of solutions:

1. The solutions associated to the POS obtained from the optimization run for each case-study
2. An extended set of solutions which include all the solutions analysed during each optimization run (All Pop) that respect a condition of proximity between Sd_t and R_u. This set includes the optimal solutions (POS) and all the sub-optimal solutions that fall in the condition that relates to "use of ductility". That condition was defined by the following expression:

$$-0.05 \leq \frac{(R_u - Sd_t)}{R_u} \leq 0.05 \tag{5.2}$$

In Table 5.7, the minimum and maximum values for the behaviour factor and reduced axial force (**v**) are presented for all "Ductile" case-studies and for both sets of solutions, POS and All Pop.

Table 5.7 Minimum and maximum values, per “Ductile” case-study, for q and v_k.

	POS				All Pop			
Case-study	Min q	Max q	Min v	Max v	Min q	Max q	Min v	Max v
1_1	3.66	5.65	10.9%	17.2%	3.40	5.87	10.6%	19.2%
1_3	3.44	5.18	12.0%	18.5%	3.26	5.54	11.5%	21.2%
2_1	3.28	4.77	11.2%	20.8%	3.30	5.04	13.5%	32.5%
2_3	3.47	5.01	12.3%	22.6%	3.58	5.20	16.6%	32.5%
2_4	3.44	4.96	8.9%	15.6%	3.44	5.27	12.9%	24.4%
2_5	3.49	5.08	13.4%	23.2%	3.32	5.20	13.1%	27.0%
3_1	3.37	5.05	8.8%	13.1%	3.34	5.05	8.5%	13.1%
4_1	3.56	5.05	7.0%	10.0%	3.31	5.16	6.7%	11.2%
4_3	3.83	5.32	9.8%	12.3%	3.51	5.52	9.0%	13.5%
5_1	3.49	5.50	6.4%	9.0%	3.36	5.59	6.1%	10.0%
6_1	3.45	5.35	5.2%	8.1%	3.30	5.38	5.2%	8.3%
7_1	3.49	4.52	5.2%	7.4%	3.28	5.02	5.2%	7.7%
8_1	3.38	5.30	10.3%	17.2%	3.23	5.30	10.0%	18.5%
9_1	3.63	5.62	7.9%	11.6%	3.43	5.67	7.5%	12.7%
10_1	3.65	5.62	9.2%	13.5%	3.39	5.69	8.8%	14.9%
11_1	3.50	5.42	7.0%	10.6%	3.36	5.52	6.9%	11.2%
12_1	3.55	4.88	6.4%	9.0%	3.40	5.19	5.6%	9.8%

In Figure 5.5, the results relative to the POS for all case studies are presented. In a) the results refer to the “Ductile” case-studies, and in b) the “Limited Ductile” case-studies. The different colours in both a) and b) refer to different case-studies, i.e., irregularity levels.

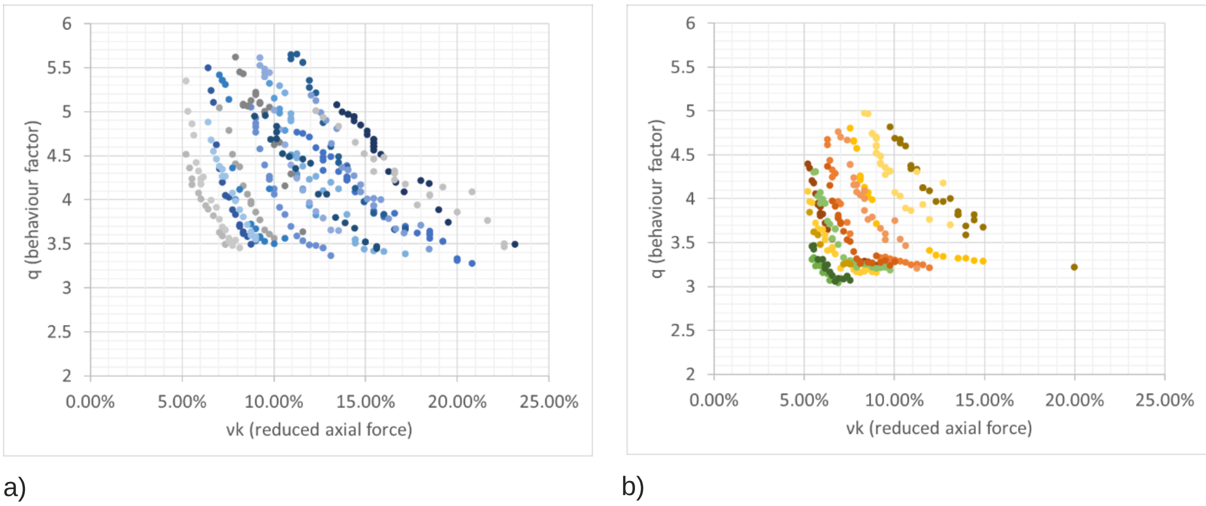

Figure 5.5 Results from all case-studies POS solutions q and v_k values. In a) “Ductile” case-studies and b) “Limited Ductile” case-studies.

From a) it is apparent that the range of the behaviour factor values does not change much between case-studies. It seems that the minimum for all case-studies is around 3.3-3.5 while the maximum is usually around 5-5.7. On the other hand, the reduced axial force changes a lot between case-studies.

The results for the “Limited Ductile” (LD) case-studies in b) show very large behaviour factors, considering the 1.5 values prescribed by EC8 – part 2. However, as the collapse mechanism assumed was also associated to excessive compressive strain in the concrete plastic hinge, this entails that capacity design is assumed. And since capacity design provisions are not mandatory for LD solutions, the values obtained may be, in fact, excessive. However, the results are still interesting to show, as the values regarding minimum confinement for LD prescribed in EC8 – part 2 are capable of originating solutions with much higher behaviour factor values than the prescribed value of 1.5.

Figure 5.6 shows the results of the “Ductile” case-studies for the All Pop set of solutions. Figure 5.6 a) is analogous to Figure 5.5 a), but for the All Pop set instead of POS. The range of values for the behaviour factor is very similar between POS and All Pop. This shows that the behaviour factor is not lower for sub-optimal solutions obtained in the course of the optimization procedure. Furthermore, there is little difference between the range of behaviour factors obtained from the non-optimal set of solutions and the optimal set of solutions. The only difference between optimal and non-optimal solutions is that the optimal solution uses less material to achieve the same behaviour factor. And so, the obtained behaviour factors are not exclusively for optimized solutions.

Figure 5.6 b) is analogous to Figure 5.4, but for the All Pop set and for all the “Ductile” case-studies. As was already perceived in Figure 5.4, the graphs all show a linear relationship between q and q_{dy}. The difference between them are different rates for different case-studies. These different rates are associated to pier irregularity. Therefore, a measure of irregularity must be defined.

Figure 5.7, shows both sets of solutions, POS and All Pop, superimposed for a case-study example.

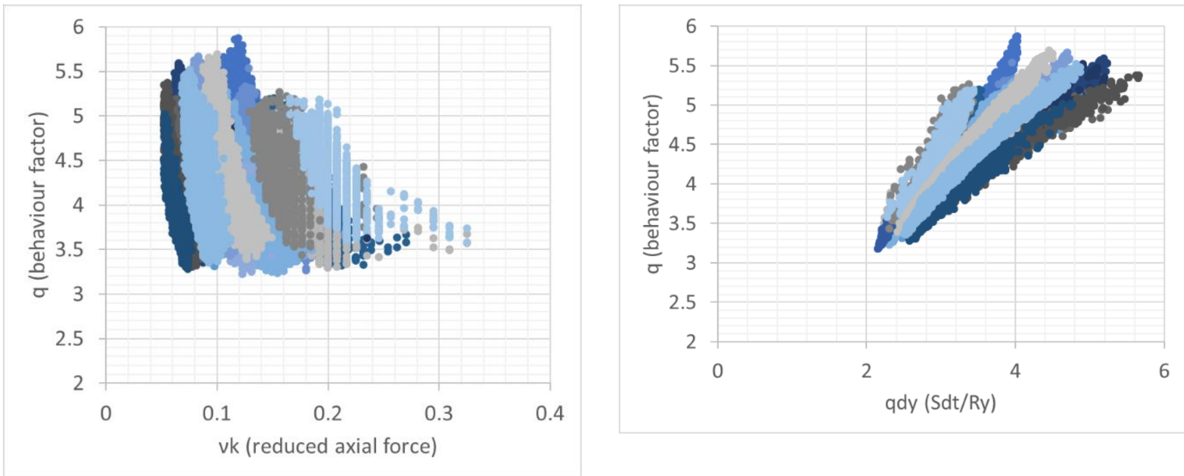

Figure 5.6 Results for All Pop set of solutions from “Ductile” case-studies. a) Results of q and v_k. b) Results of q and q_{dy}.

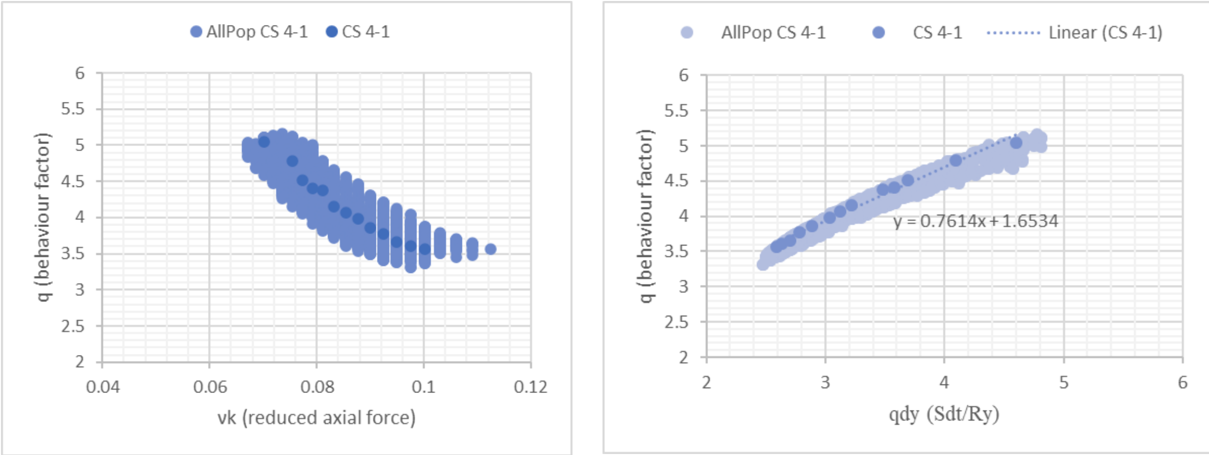

Figure 5.7 Presentation of results for All Pop and POS sets regarding CS 4-1. a) Results of q and v_k. b) Results of q and q_{dy}.

By defining a measure for pier irregularity similar to the coefficient of variation (CoV) of the yield displacements of the piers one can obtain a clear relationship between pier irregularity and energy dissipation, as will become apparent. The measure of pier irregularity (PIrr) is equal to the square-root of the variance of the yield displacements of the piers in relation to the minimum yield, instead of the average yield value, divided by the square of the minimum of the yield displacements of the piers.

The rationale of this measure of irregularity is that it can be characterized by measuring for how many piers and by how much is their yield displacement larger than the yield displacement of the stiffest pier. This can be obtained by a measure of the sum of the variation between the minimum yield value and the yield value of each pier. Equation (5.3) shows the expression for the pier irregularity (PIrr):

$$PIrr = \sqrt{\frac{\sum_{i=1}^{n}\left(d_{yi} - R_y\right)^2}{n \cdot R_y^2}} \tag{5.3}$$

Where d_{yi} is the yield displacement of pier i, R_y is the minimum value of the piers' yield displacements and n is the number of piers.

The linear regression of each case-study's All Pop q vs q_{dy} graph as from Figure 5.6 b) gives the gradient/slope between q and q_{dy}. The physical meaning of this gradient/slope is associated to energy dissipation and it relates the dissipation with the ratio between the target displacement and the displacement at first yield ($q_{dy} = Sd_t/R_y$). That dissipation value is thus a function of q_{dy} and irregularity, since the larger the bridge irregularity the less dissipation is generated for the same q_{dy}. By plotting the value of the slope of each case-study with the corresponding PIrr value, Figure 5.8 is obtained.

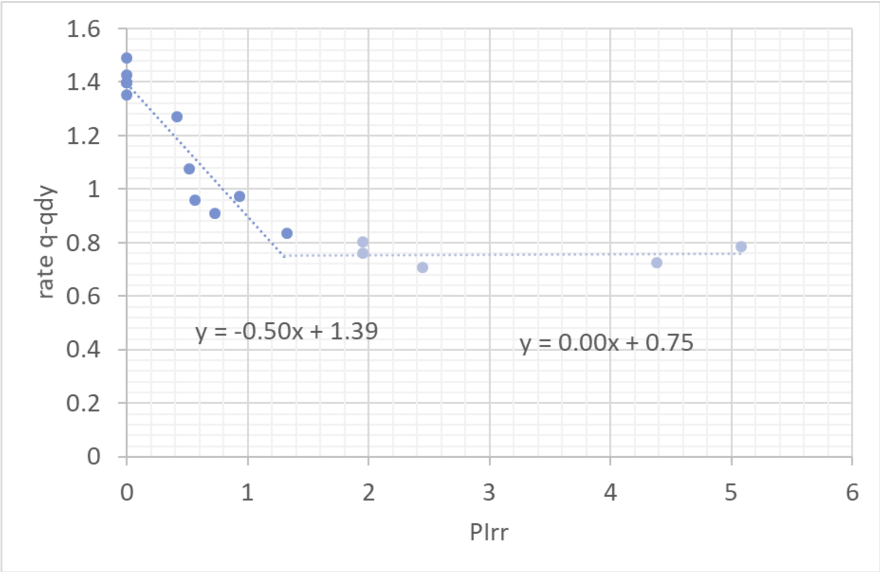

Figure 5.8 Relationship between the q vs q_{dy} slope and the irregularity measure, PIrr. The q vs q_{dy} slope was obtained from the linear regression of all graphs from Figure 5.6 b).

There is a clear relationship between the q vs q_{dy} slope value and the PIrr irregularity measure. The larger the irregularity, the smaller the behaviour factor for the same amount of ductility of the stiffest pier. By clear association of the q vs q_{dy} slope with PIrr, and since q_{dy} depends on characteristics of the stiffest pier, namely its yield displacement, it becomes possible to derive an expression for the behaviour factor value, which has as input the target displacement of the structure. That target displacement could be defined arbitrarily by the designer, considering the ultimate displacement of the stiffest pier or a percentage of it. The value of this expression would be to provide an estimate for the behaviour factor without being bound to EC8's conservative value of 3.5. The expression does not intend to be a replacement of the EC8 values, but rather a non-conservative approximation of the actual behaviour factor. Let's refer to the q vs q_{dy} slope as m_q. The value for m_q is, as seen in Figure 5.8, given by:

$$\begin{cases} m_q = -0.50 \cdot PIrr + 1.39, if\ PIrr \leq 1.28 \\ m_q = 0.75, if\ PIrr > 1.28 \end{cases} \tag{5.4}$$

The expression for the behaviour factor is then:

$$q = m_q(PIrr) \cdot \frac{Sd_t}{R_y} + c \tag{5.5}$$

Where Sd_t/R_y is q_{dy}, and Sd_t is the target displacement of the structure and R_y the yield displacement of the stiffest pier. The value for *c* is calibrated with the entire population of solutions generated during the optimization runs, in order to minimize error. The obtained value for c and final expression for q is:

$$c = 3.26 - 2.21 \cdot m_q \tag{5.6}$$

$$q = m_q(PIrr) \cdot \left(\frac{Sd_t}{R_y} - 2.21 \right) + 3.26 \tag{5.7}$$

The expression was applied to the POS solutions of all case-studies, and the results are presented in Figure 5.9 compared with the real q-factor value.

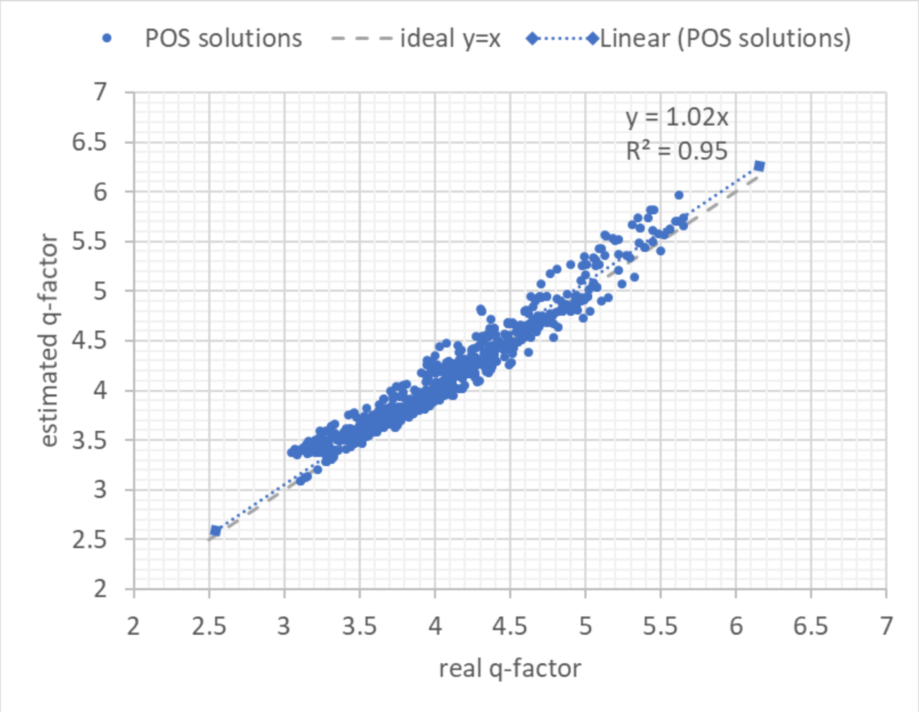

Figure 5.9 The estimated q-factor and the real q-factor for all POS solutions.

Figure 5.9 shows that the expression provides a good estimate of the q-factor, albeit some small variation from the ideal diagonal, which happens for relatively small number of solutions. The value of the expression, besides providing an approximation for the q-factor, not bound by the EC8 – part 2 value of 3.5, also provides an expression that is independent of ductility class and other factors such as axial force, since those factors are implicit in the Sd_t and R_y input values.

5.6 Conclusions

In this study, a methodology is presented, with the use of evolutionary algorithm techniques, to optimize the seismic design of RC viaducts with four 30-meter spans in the longitudinal direction, with the goal of obtaining the maximum behaviour factors that can be applied to bridges, according to ductility class and pier irregularity. The results allow to extract the following conclusions:

- The results show that irregularity, confinement and axial force play the biggest roles in the ductility of structures, which was expected. What was not so much expected was the effect of increasing the size of cross-sections. The results show that there is an increase in the behaviour factor as cross-section size increases, associated to a decrease in the yield displacement, which increases the ratio between ultimate displacement and yield displacement.
- The minimum confinement associated to the LD ductility class is excessive considering the maximum q-factor prescribed by EC8 – part 2 for those structures (q=1.5). If, on the one hand, EC8's low q-factor considers the lack of provisions for capacity design, then the minimum confinement is excessive, unless it is considered a reserve strength. On the other hand, if the capacity design provisions were to be considered, then EC8's q-factor would be too conservative for the minimum prescribed confinement. The existence of both in simultaneous (small q-factor and relatively large minimum confinement) seems inconsistent.
- The q-factor values for all "Ductile" case-studies fall within the 3.3-5.9 range, which seem to go well with the value for maximum q-factor prescribed by EC8 – part 2 for RC bridges, which is 3.5. This shows the EC8 q-factor is well calibrated, given that this study showed its adequacy for bridges with a wide variety of irregularities and reduced axial force values.
- Furthermore, since a multi-objective optimization was performed, the result was always in the form of multiple solutions in the Pareto set, ranging from the minimum to the maximum values for each optimization variable. The result was an optimization in which a large extent of possible permutations, among design variables, was generated. This was the reason for the large variability in the behaviour factors, inside case-studies. That variability inside the same case-study typology is, on its own, valuable information, since it shows that variable selection can be important regarding the maximum behaviour factor allowed. Also, the solutions in the POS may present slightly lower overstrength values than other sub-optimal solutions, due to being obtained by an optimization procedure that minimizes the amount of material in the pier cross-sections. This, however, does not mean that the q-factor value is smaller in the POS solutions.
- It is possible to conceive the existence of some bridges in which higher behaviour factors would be acceptable due to larger overstrength. That, nonetheless, does not change the conclusions, as increasing EC8 behaviour factors would be reasonable for those bridges but unsafe for other bridges.

- The q_{dy} factor, which is the ratio between Sd_t (target displacement) and R_y (yield displacement of stiffest pier) has a linear relationship with the actual q-factor. The gradient of that linear relationship is strongly associated to pier irregularity. These notions allowed to derive an expression that approximates the real q-factor of RC bridges in the longitudinal direction. The comparison of the q-factor values obtained from the expression with the actual q-factor values, for all POS solutions show that the expression is a good q-factor estimator.
- It is proposed that the indicator of bridge irregularity is based on the columns yield displacements and not their flexural capacities at the plastic hinges, as proposed by EC8. This is due to the fact that yield curvatures vary very little with the flexural capacity.

Two possible limitations of the scope of this study could eventually be identified: i) the fact that only bridges with four spans were analysed, only in the longitudinal direction and without accounting for abutment effects, and ii) the fact that the only shape of columns cross-sections that was considered was the circular. Regarding the number of spans, its influence is reduced since in the longitudinal direction the bridges behave as SDOF systems. This means that the difference in the results between the cases with four spans, studied herein, and cases with more than four spans is small, since the increase in number of spans increase stiffness and mass in the same proportion relatively to the SDOF. Regarding the circular cross-sections used, their ductility can be more sensitive to an increase in reduced axial force, compared to rectangular cross-sections. This stems from the larger increase in neutral axis depth, when the axial force is increased, in the case of circular sections. This aspect renders the results slightly conservative when applied to other cross-sections. Therefore, as only the factor regarding the cross-section shape introduces a slight conservatism in the analysis, the main conclusions are valid for wider ranges of the length of the bridges and shape of the columns cross-section than the ones that were analysed.

6 Multivariate analysis of regular and irregular RC bridges and characterization of earthquake behaviour according to stiffness-based indexes

Seismic design of bridges in some respects is more complex than other structures especially due to, in some cases, the a priori unknown shape of the displacement profile of the structure. Bridges of irregular nature and of a certain length can have transversal horizontal displacement profiles (THDP) of the deck that are very dependent on higher frequency modes. Furthermore, the THDP might change significantly during the earthquake action, due to loss of stiffness of some elements rather than others (Kappos, Saiidi, et al. 2012). This makes most nonlinear static pushover analysis (SPA) methods inaccurate and introduces difficulties in the seismic design of these structures. In this study, several RC bridges which vary in length and irregularity, are analysed with nonlinear dynamic analysis (NDAs) and optimized via genetic algorithms with performance and cost as objectives in the longitudinal and transversal directions separately. The optimized solutions are analysed in terms of their effective stiffness and compared with each other. The results show correlation between the displacement of the stiffer piers and the overall effective stiffness of the structure. This correlation is closely linked to other parameters such as the relative stiffness index (RSI) (Priestley, Seible and Calvi 1996). The results and the parameters allow to identify cases in which the bridges develop “long bridge behaviour” in the THDP of the bridge, and also in which situations the longitudinal and transversal peak displacement of critical piers are similar, which is useful knowledge to optimize seismic design in terms of cost and performance. Practical recommendations for the optimization of the seismic design of irregular bridges are offered.

6.1 Introduction

The dynamic behaviour of bridges under earthquake excitation has been the focus of studies for many years, and the difficulties in analysis and design have been well established. The work (Kappos, Saiidi, et al. 2012) discusses several issues regarding the modelling and analysis of bridges to earthquake action among which is a presentation of the methods of analysis that are viable for different types of bridges, for instance, long irregular bridges with short piers at the centre can only be analysed either by nonlinear dynamic analysis (NDA) or by adaptive pushover techniques such as the ACSM (Antoniou and Pinho 2004) (Casarotti and Pinho 2007). The reason is that the dynamic behaviour of certain bridges, particularly long irregular ones, can be complex, and suffer qualitative changes as the penetration in the nonlinear range increases. The dynamic behaviour of bridges and the subsequent transversal horizontal displacement profile (THDP) can depend strongly on higher frequency modes and also change during the seismic action. The shape of a bridge’s THDP can also be different between seismic actions of different intensities. Because of this complexity, the study of bridge irregularity has been done to a large extent with many published works such as the aforementioned work (Kappos, Saiidi, et al. 2012), which contains a collection of works that focus on the issue of seismic analysis of irregular bridges, among others. In (Kohrangi, Bento and Lopes 2015), a comparison of many SPAs (nonlinear static pushover analysis methods) on the analysis of irregular bridges with the results from NDAs, to ascertain the validity of the employment of said SPAs in the analysis of bridges of varying irregularity measured by the RSI, Relative Stiffness Index, (Priestley, Seible and Calvi 1996) and RP, Regularity Parameter, (Calvi, Pavese and Pinto 1993) parameters. The RSI parameter, which is of easy calculation, is employed in this study. A recent work (Akbari and Maalek 2018) does a state-of-the-art review on seismic behaviour of irregular bridges. The various regularity parameters that have been proposed by various authors are presented, in which RSI and RP are included. The work gives relevance to the displacement-based design methodology and its advantages regarding bridge design and also to the advancements in the understanding of higher mode effects and the subsequent inadmissibility of certain analysis methods for bridges with certain characteristics and irregularity layouts. At the end of the review, a series of recommendations are made. Two of the recommendations from (Akbari and Maalek 2018) are highlighted here and are somewhat approached by this study: "It would be helpful to define an acceptable level of bridge irregularity – by way of a simple and common regularity index – for each of the simplified or more complex analysis methods"; "In order to obtain more uniform distribution of ductility demand or to reduce the torsional effects in irregular bridges, to the best knowledge of the author, no research works have been reported on the effects of the use of piers of different and/or variable cross-sectional dimensions, together with different reinforcement arrays, on the seismic behaviour of such bridges." This list of works is by no means exhaustive since many other works have approached the issue of irregular bridges. In addition to the study of irregularity, in the last decades, many works have focused on the definition of different analysis and design strategies that move away from the more traditional force-based paradigm. One very well-known example and the focus of many current research works is the displacement-based design method (Priestley, Calvi, et al., Displacement-Based Seismic Design of Structures 2008) which was also modified for bridges (Calvi, Priestley and Kowalsky, Displacement-Based Seismic Design of Bridges 2013). This method approximates the peak response of the bridge by means of estimation of the equivalent damping and effective period. There have been several works which present ways to approximate or reduce to a single-degree-of-freedom (SDOF) (Gkatzogias and Kappos 2019) the peak displacement of damped structures under seismic excitation. The formulations typically are associated to parameters such as effective stiffness and effective damping. There are some works that are somewhat contradictory in their findings, and others that show that the formulations to assess effective damping of structures are not very consistent with actual damping values (Dicleli and Buddaram 2007). One of the issues is, regarding the transversal direction of bridges, defining the percentage of inertia force that is resisted by the piers and by the abutments, where much less energy is dissipated, at peak response, since this percentage may present very significant variation during the seismic action.

This study intends to address the effect of irregularity and length on the dynamic behaviour and earthquake resistance of a common type of RC bridges, characterized by relatively small spans (20 to 45-meter) repeated many times. These bridges can reach long lengths (> 900-meters) without having intermediate expansion joints and often have significant pier-length irregularity. In this study, the bridge case studies are subjected to NDAs by a set of strong motions that have been carefully chosen and which are presented in Section 6.5. There are essentially three objectives in this study:

- The first objective is to define, based on the bridges' dynamic behaviour, the difference between short and long bridges, resorting to the RSI parameter (Relative Stiffness Index), which is an easy to calculate index that compares the stiffness of the superstructure (deck) with that of the piers. This separation into short and long bridges allows the definition of different design approaches/principles, which is associated to objective 2 and 3.
- The second objective is to show how local and global stiffness affect the bridge's behaviour according to length and irregularity profile. Here the interest is to see how the pier design, that is, pier cross-section size and the distribution of flexural steel reinforcement (fsr), affect local and global displacement demand along different bridges. To this end, a genetic algorithm (GA) is employed to perform the search inside each bridge typology. The reasons for choosing a GA for this task are as follows:
    - The GA is not biased in the way it designs the bridges; thus, it performs the search without assuming a prior design technique which would be biased by a prior understanding of bridge dynamic behaviour and earthquake resistance.
    - The goal can be seen as an optimization search because the idea is to ascertain how fsr distribution affects bridge behaviour, while focusing the search on feasible solutions and solutions that have different levels of performance.
    - The output of the second task/objective is thus a set of several solutions with varying pier diameters and varying fsr amount and distribution. These two variables (diameter and fsr) affect the stiffness of the piers and their ductility. Thus, with the variety of solutions given by the GA it is possible to observe how local and global fsr amounts affect the critical pier displacement demand and seismic performance. Finally, it is shown that total effective stiffness of the piers is very well correlated with average pier displacement demand and can be useful to estimate displacement demand
- The third objective of the study is to offer guidelines for the optimization of seismic design of long irregular bridges based on the results of the aforementioned procedures. This is attained with the information obtained from both procedures. The first procedure varies bridge solutions across length and irregularity layouts, while maintaining constant pier design variables, while the second procedure varies the pier design variables inside a given bridge layout (constant length and irregularity layout). The two analysis complement each other and allow to reach the warranted objectives.

In the next section, the objectives described are linked with the applied methodology, and further details on each objective are explained.

6.2 Methodology

In this section, a few more details are given regarding objectives 1 and 2 and their link to the adopted methodology.

Concerning objective 1, the shape of the THDP of the bridge is correlated with pier irregularity, bridge length and RSI, as will be shown. The definition of a threshold value to separate short bridge behaviour from long bridge behaviour is sought, since conception rules for design are different whether a bridge is short or long, as will be shown later on. To that end, a first procedure concerns a multivariate sampling of bridges in which the relative stiffness between superstructure and piers is varied as well as irregularity layout and total bridge length. From the analysis of the generated solutions it is verified whether the THDP of the bridge reflected the existence of an irregularity or not, which is then correlated with the RSI indicator, as well as other aspects. The expression for the RSI is the following:

$$RSI = \frac{K_{SS}}{K_{IS}} = \frac{\frac{384 \cdot E_{c,SS} \cdot I_{SS}}{5 \cdot L_{SS}^3}}{\sum_p Keff_p} \tag{6.1}$$

Where K_{SS} and K_{IS} are the superstructure (deck) stiffness and infrastructure (columns) stiffness, respectively. $E_{c,SS}$, I_{SS} and L_{SS} represent the Young modulus, moment of inertia of the deck cross-section around a vertical axis and length of the bridge, respectively. And $Keff_p$ is the effective stiffness of pier p, calculated via the method presented in EC8 - part 2 (CEN 2005), concerning a horizontal displacement at the top of the pier in the transversal direction.

Concerning objective 2 of the study, the goal is to associate the amount and distribution of material, and subsequent pier stiffness, to global resistance to earthquake action. Through multi-objective optimization one can direct a search towards simultaneously attempting to minimize materials and maximize resistance. These two are objectives that cannot be optimized concurrently, and so the output is a set of solutions that go from having less material and eventually less resistance, to more material and ultimately more resistance. The subsequent Pareto front translates the relation between pier stiffness and global resistance to earthquake action, by showing the trade-off between cost (amount of material) and performance. The advantages of using multi-objective optimization are two-fold: 1) it allows to obtain a trade-off between solutions regarding two of the main criteria for design which are amount of material and seismic performance and 2) the procedure is a powerful sampling tool which samples solutions close to good values for these objectives yet maintaining a uniform distribution of the sampling in relation to the objective space, that is, without sacrificing variety in terms of decision variables. Furthermore, the entire set of sampled solutions can then be used to study the influence of pier stiffness in the seismic performance.

Thus, essentially two procedures compose this methodology, which are presented in Figure 6.1. Procedure 1 refers to Objective 1 and Procedure 2 refers to Objective 2.

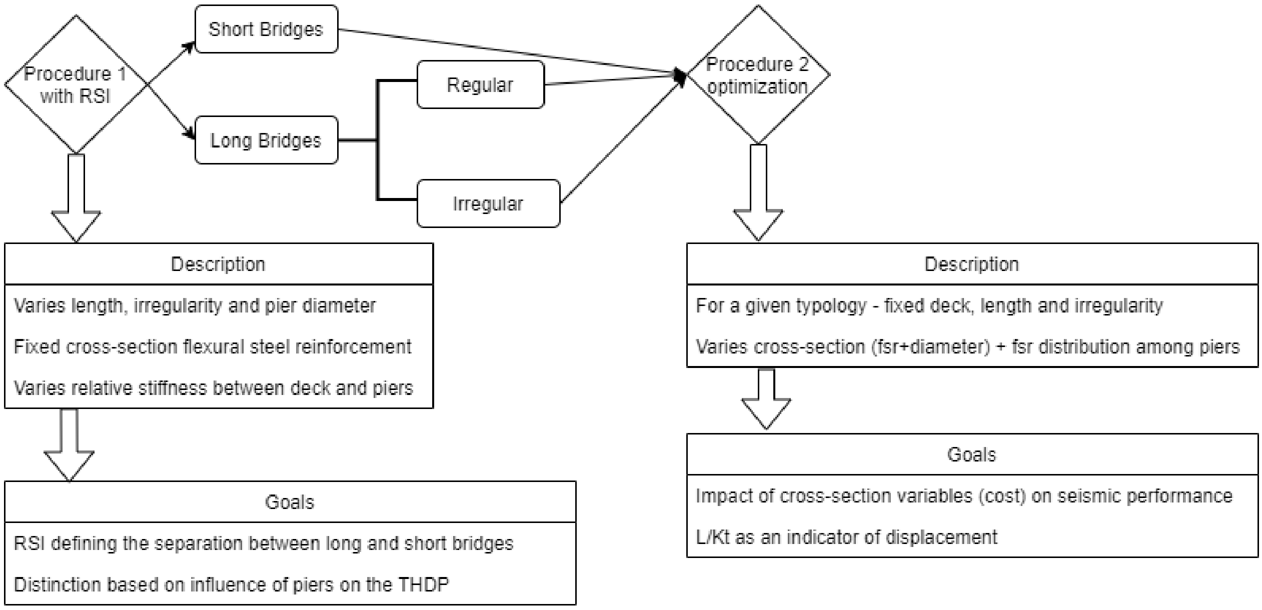

Figure 6.1 Flowchart for analysis procedures 1 and 2.

In the analyses, the transversal direction will receive the main attention, due to its importance to the objectives of the study. Nonetheless, the longitudinal direction will be analysed as well, to ascertain the relative importance of the effects of the earthquake action in both directions.

To undertake both procedures/objectives, very significant computational effort was needed. Thousands of bridges were simulated, each analysed with NDAs using multiple strong motions. To perform this task, there was a necessity to employ computers with the ability to parallelize the needed computational tasks, between several threads. This was achieved with the AMD Threadripper 1950X processor, which has 16 cores/32 threads. The computations were parallelized between 32 threads, which lead to a very significant speed-up of around 20x compared to a non-parallelized implementation. A second computer, performing 8-thread parallelization, was also employed to assist with the load task.

In the following, a detailed explanation of each procedure is given.

6.2.1 Procedure1: Sensitivity analysis

As stated, in this procedure, bridges are generated in a systematic way by combination of variables. The objective is to ascertain the impact of certain variables in the dynamic behaviour of bridges, particularly irregularity and length. The procedure can be summarized as follows:

- Definition of bridge variables for the analysis:
  - Choice of irregularity layout and pier lengths and pier flexural reinforcements (these variables are fixed for each analysis.
  - Definition of minimum and maximum pier diameter, and variable step-size.
  - Definition of minimum and maximum bridge length, and variable step-size.

- Definition of minimum and maximum superstructure transversal moment of inertia (about the vertical axis that includes the cross-section centre of mass), and variable step-size.

- Generation of cases for analysis corresponding to all permutations with the defined variables and corresponding range – full factorial analysis.
- Analysis of the bridges with 9 accelerograms.
- Analysis of results capturing maximum displacement envelope, RSI, among other indicators.

The irregularity layouts of the bridges essentially follow the irregularity layouts presented in Table 6.1. The case-studies were generated with three groups of piers with or without different lengths (according to the irregularity layout in question).

Table 6.1 Irregularity layout type concepts used to generate the case-studies, and irregularity designation codes.

Category	***Explanatory figure***
Regular	
Irregularity 1 ex.: 123321	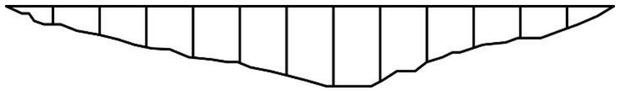
Irregularity 2 ex.:112233	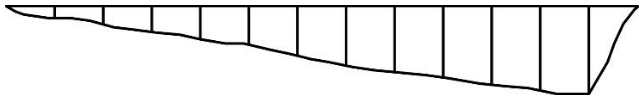
Irregularity 3 ex.: 321123	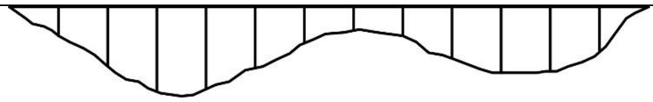

6.2.2 Procedure 2: Optimization with GA

In this procedure, the objective is to observe the influence of differential variation of fsr in the piers, which affects the local and global stiffness of the piers, in the shape of the THDP. This is done by searching for optimized solutions according to objectives of performance and cost which push the search towards having a high variability of combinations of pier diameter and fsr. Unlike in the previous procedure, in this case there is also variation of fsr among different piers from the same bridge solution. The optimized solutions will show the influence of this factor in the dynamic behaviour of the bridges.

For each case-study in this procedure, the optimization procedure, presented in Section 6.4, is applied. The defined case-studies are presented in Table 6.2. As with procedure 1, they follow the irregularities in Table 6.1 conceptually, but without gradual height variation. In all case-studies the height variation is more abrupt than in the figures present in Table 6.1, and the irregularities are created with five different pier heights (5 m, 7 m, 9 m, 11 m, 14 m), as shown in Table 6.2. For irregular bridges, the irregularities are constituted by three different groups of piers. This will be presented along the manuscript as 1-2-3, where 1 is the shortest pier and 3 is the longest, or as 9-7-5 (for example), where the numbers represent the piers' lengths in meters.

It is important to clarify that, in this work, there was not any analysis of the effects of different foundation soils, or different pier-deck connections along the bridge. The reason is that the effect that both have on the stiffness of the piers is equivalent to changing the actual length of the piers. Therefore, in the framework of this thesis, irregularity is only derived from the actual pier length and, in Procedure 2, by the differential flexural steel reinforcement between pier groups.

Table 6.2 Case-studies for optimization: LBridge – bridge length; Dir – Direction (Longitudinal-L, Transversal-T); Irreg- Irregularity profile; ADeck – area of the deck cross-section; EQsf – earthquake scale factor; Pier Length – Length of each pier along the bridge (associated to irregularity profile)

Case-study	LBridge(m)	Dir	Irreg	ADeck(m^2)	EQsf	Pier Length
480_I3_L5_A12_EQ1_T	480	T	Irreg 3	12	1	9-9-9-7-7-7-5-5-5-7-7-7-9-9-9
480_I3_L7_A12_EQ1_T	480	T	Irreg 3	12	1	11-11-14-14-11-11-7-7-7-11-11-14-14-11-11
480_I3_L5_A12_EQ1_T	480	T	Irreg 3	12	1	9-9-9-7-7-7-7-5-7-7-7-7-9-9-9
480_I3_L5_A12_EQ1_T	480	T	Irreg 3	12	1	9-9-9-7-7-5-5-5-5-5-7-7-9-9-9
480_R_L5_A12_EQ1_T	480	T	Reg	12	1	5-5-5-5-5-5-5-5-5-5-5-5-5-5-5
480_R_L7_A12_EQ1_T	480	T	Reg	12	1	7-7-7-7-7-7-7-7-7-7-7-7-7-7-7
270_I3_L7_A12_EQ1_T	270	T	Irreg 3	12	1	14-14-11-7-7-11-14-14
270_R_L5_A12_EQ1_T	270	T	Reg	12	1	5-5-5-5-5-5-5-5
270_R_L9_A12_EQ1_T	270	T	Reg	12	1	9-9-9-9-9-9-9-9
270_R_L5_A12_EQ0.5_T	270	T	Reg	12	0.5	5-5-5-5-5-5-5-5
270_R_L5_A12_EQ0.75_T	270	T	Reg	12	0.75	5-5-5-5-5-5-5-5
270_R_L7_A12_EQ1_T	270	T	Reg	12	1	7-7-7-7-7-7-7-7
270_R_L5_A9_EQ1_T	270	T	Reg	9	1	5-5-5-5-5-5-5-5
210_R_L7_A12_EQ1_T	210	T	Reg	12	1	7-7-7-7-7-7
540_R_L5_A12_EQ1_T	540	T	Reg	12	1	5-5-5-5-5-5-5-5-5-5-5-5-5-5-5-5-5
540_R_L7_A12_EQ1_T	540	T	Reg	12	1	7-7-7-7-7-7-7-7-7-7-7-7-7-7-7-7-7
540_I3_L7_A12_EQ1_T	540	T	Irreg 3	12	1	11-11-14-14-11-11-11-7-7-7-11-11-11-14-14-11-11
660_R_L5_A12_EQ1_T	660	T	Reg	12	1	5-5-5-5-5-5-5-5-5-5-5-5-5-5-5-5-5-5-5-5-5
480_R_L7_A12_EQ1_L	480	L	Reg	12	1	7-7-7-7-7-7-7-7-7-7-7-7-7-7-7
480_I3_L7_A12_EQ1_L	480	L	Irreg 3	12	1	11-11-14-14-11-11-7-7-7-11-11-14-14-11-11
270_I3_L7_A12_EQ1_L	270	L	Irreg 3	12	1	14-14-11-7-7-11-14-14
210_R_L7_A12_EQ1_L	210	L	Reg	12	1	7-7-7-7-7-7-7-7
480_I1_L5_A12_EQ1_T	480	T	Irreg 1	12	1	5-5-5-5-5-7-9-9-9-7-5-5-5-5-5
480_I2_L5_A12_EQ1_T	480	T	Irreg 2	12	1	5-5-5-5-5-5-7-7-7-9-9-9-9-9-9
180_R_L5_A12_EQ1_T	180	T	Reg	12	1	5-5-5-5-5
270_R_L5_A15_EQ1_T	270	T	Reg	15	1	5-5-5-5-5-5-5-5
360_R_L5_A12_EQ1_T	360	T	Reg	12	1	5-5-5-5-5-5-5-5-5-5-5
480_R_L5_A12_EQ1_L	480	L	Reg	12	1	5-5-5-5-5-5-5-5-5-5-5-5-5-5-5
480_I3_L5_A12_EQ1_L	480	L	Irreg 3	12	1	9-9-9-7-7-7-5-5-5-7-7-7-9-9-9
270_R_L5_A12_EQ1_L	270	L	Reg	12	1	5-5-5-5-5-5-5-5

6.3 RC Bridge Typology and Modelling

6.3.1 Superstructure

This study's focus is on a particular typology of bridges characterized by relatively short spans (around 30-meter long) and the most common types of deck cross-sections, such as the ones shown in Figure 6.2.

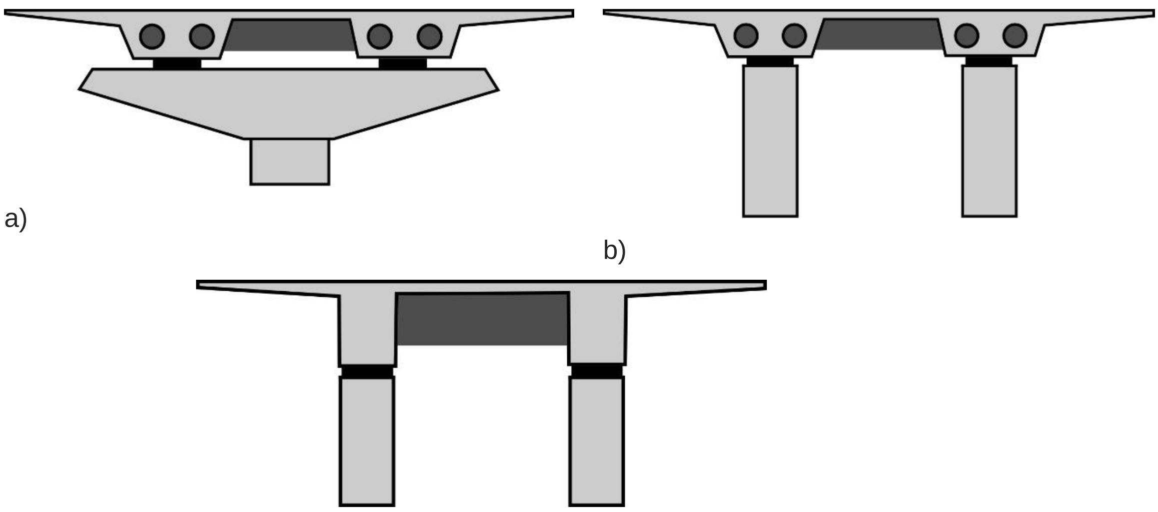

a) b) c)

Figure 6.2 Superstructure typology employed in the case-studies.

The presented superstructure typology is typically associated with two types of infrastructure, one illustrated by Figure 6.2a) and the other by Figure 6.2b) and c). The latter is used throughout the study, but both are referred since they have relevant differences of dynamic behaviour under horizontal actions, that stem from two factors, which are torsion and rotational compatibility between pier(s) and deck.

The dynamic behaviour of the superstructure represented by Figure 6.2a) can be characterized by a total compatibility of rotations along a longitudinal axis, between superstructure and infrastructure. Furthermore, there can be rotation of the deck and the pier, and so there is torsion in the deck.

The superstructure represented by Figure 6.2b) and c) has different behaviour, without rotation of the superstructure around a longitudinal axis due to the torque formed by both piers. Also unlike the superstructure of Figure 6.2a), in Figure 6.2b) and c) there is no compatibility in rotation between the deck and the piers, where the piers can rotate independently of the deck, depending on the type of connection (rigid/monolithic, fixed, etc.)

The superstructure is not modelled explicitly as either one of the deck types presented above. Instead, the area, density and the inertia are used in creating a linear elastic element. In Table 6.3, the deck inertia values are given. The area of the deck was usually 12m^2 and Table 6.2 has more details on that, on a case-to-case basis. For procedure 1, the three inertia cases were used, but for procedure 2 the value of 150m^4 was used for all case-studies.

Table 6.3 Area and inertia used in the deck sections of the case studies.

Area (m^2)	9 – 12
I_{yy} (m^4)	75 – 150 – 400
J (m^4)	5

6.3.2 Infrastructure

Circular pier cross-sections were chosen for this study, since they have some advantages in terms of analysis, design and interpretation of results. With circular piers, it is easy to analyse a cross-section when subjected to a bi-directional action, since there is no main reference axis in a circular section. Even if the analyses in both directions are being done separately, there is an advantage in having circular sections since the effects between both directions are comparable, also the steel reinforcement, both flexural and confinement, is easy to define.

In Figure 6.3, an example of the modelled cross-section is shown.

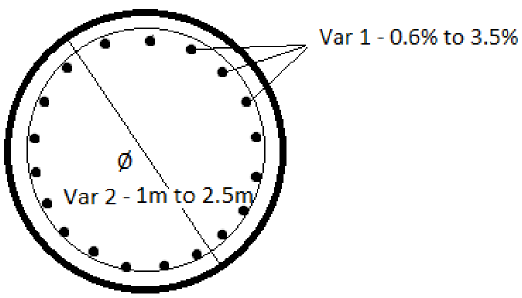

Figure 6.3 Circular cross-section optimization variables: flexural reinforcement and diameter, identified with corresponding variable intervals.

6.3.3 Finite element model definition

The structural models used for the simulation of the earthquake response were defined and analysed with OpenSEES software (McKenna and Fenves 1999), particularly the variant OpenSEESMP which facilitates to run several models in parallel. The OpenSEES/OpenSEESMP software is a library extension of the Tcl/Tk language interpreter. This facilitates the integration of structural analysis with several pre- and post-processing programming procedures, which is fundamental for integrating structural design and analysis with optimization algorithms.

For the modelling of the bridges in OpenSEES, fibre elements were used for the piers, specifically force-based fibre elements. Each pier was divided into three elements, where the elements containing the expected plastic hinges had a larger density of integration points, with 5 points, to capture the curvature variations more accurately. The reason for this subdivision into sub-elements is that the sections closer to the extremities are the expected locations for plastic hinge formation, thus in the two end elements there are more integration points per unit length to better capture the nonlinear behaviour, than in the

central element. As for the deck, it was modelled as a linear elastic element, as it is usually a prestressed element in which yielding of the reinforcement does not occur.
In the case of shear, constraints on slenderness of columns were used to avoid solutions where shear effects might be relevant. Therefore, shear effects and anchorage-slip effects were not modelled.

6.3.3.1 Material properties

The mean values of the materials' mechanical properties were used. For the steel, the material used was A500NR, and C30/37 for the concrete. The properties of both are in the following table.

Table 6.4 Mean properties for C30/37 concrete and A500NR steel.

Concrete (C30/37)	
f_{cm} (MPa)	38
E_{cm} (GPa)	33
ε_{cu} (unconfined) (‰)	3.5
Steel (A500NR)	
f_{ym} (MPa)	585
E_{ym} (GPa)	200
ε_{su} (‰)	94

6.3.3.2 Materials' constitutive relationships

The model used for the concrete fibres was a Kent-Scott-Park concrete material object with degraded linear unloading/reloading stiffness and no tensile strength (Scott, Park and Priestley 1982). The constitutive relationship for the confined concrete follows the expressions in EC8 - part 2. Confined concrete was used in the concrete core while the cover concrete was modelled with unconfined constitutive relationship.
For the steel reinforcement fibres, a uniaxial Giuffré-Menegotto-Pinto (Giuffrè and Pinto 1970) (Menegotto and Pinto 1973) model with isotropic strain hardening was used.

6.4 Genetic Algorithms

As mentioned, the present work employs meta-heuristic search algorithms, more precisely, an algorithm from the genetic/evolutionary algorithm family (Deb 2001) (Goldberg 1989) which is a modification of the well-known NSGA-II (Deb, et al. 2002).
The NSGA-II (non-dominated sorting genetic algorithm) is a proven algorithm, capable of tackling problems which present inherent complexities such as truly disconnected multi-objective optimization

problems (TYD-MOPs) (Chow and Yuen 2012), which are among the most complex multi-objective optimization problems to solve since besides being non-convex, their Pareto-fronts/sets are disconnected both in the objective and decision space. This makes the algorithm suitable to be applied in this type of problems guaranteeing, in principle, conversion towards the real Pareto-set/front.
The modifications that were incorporated in the NSGA-II algorithm, and that were presented in previous chapters, were aimed at making it almost parameterless regarding the main genetic operators, crossover and mutation. To achieve that goal, the operators from the MODdeA algorithm (Chow and Yuen 2012) were inserted in the NSGA-II. The resulting algorithm is thus almost entirely parameterless, with the exception of the population size. The resulting algorithm and application to RC bridges subjected to seismic action has already been presented in previous works (Camacho, Horta, et al. 2020) (Camacho, Lopes and Oliveira 2020).

6.4.1 Optimization and Case-Study Variables

The solutions are defined by the optimization variables and case-study variables. The latter are associated with fixed parameters within each case-study. Parameters such as bridge length (number of piers), pier irregularity layout (pier length and location), material properties, pier confinement and earthquake action. These variables are constant for all solutions within a case-study. The material properties used in all optimization case-studies are the ones in Table 6.4.

The optimization variables, on the other hand, are varied within the optimization procedure undertaken for each case-study. These variables are visible in Figure 6.3 and are the main pier design variables. Variable 1 is flexural reinforcement of the pier, and variable 2 is the pier diameter. These variables are varied within the interval of values presented in Figure 6.3. Variable 2 is related to all piers in a given solution, that is, it translates into only one variable for each bridge, i.e., all piers have the same diameter. As for flexural reinforcement, this can be different between piers. In order to keep the number of variables from becoming too large, the piers are divided into groups inside which all piers have the same flexural reinforcement. The piers are divided among said groups according to the height and location along the bridge. During the course of the optimization search, the algorithm tries different combinations of flexural reinforcement quantities between pier groups, which translates into different stiffness between pier groups.

6.4.2 Optimization Objectives

The defined optimization problem, solved by the NSGA-II algorithm, is a two-objective MOP (multi-objective optimization problem). The two objectives are performance and cost:

- The cost objective is very straightforward and refers to the cost of materials obtained from the volume calculation of the materials in the piers (concrete and steel), obtained from the optimization variables and pier length. This objective is a minimization objective.

- The performance objective is obtained after the seismic analysis which is performed via the OpenSEESMP software. At each pier, the maximum compressive concrete strain is monitored at each step, and the maximum registered concrete compressive strain during the entire analysis is registered and compared to the ultimate compressive strain value which is defined as 16‰. This value is relatively large and is very similar to the value obtained with the minimum prescriptions by EC8 - part 2 (CEN 2005) for Ductile structures. The difference between ultimate compressive strain and maximum compressive strain registered is the performance, ε_{cu}-ε_{c}. This objective is a maximization objective.

Both objectives form a clear trade-off since they are both competing objectives, which cannot be optimized simultaneously.

6.5 Earthquake Action

As in the previous case where NDAs are employed in the search procedure, the 4-pair set in Figure 2.49 was chosen for the analysis.

6.6 Results

In this section, the results of the application of both procedures are presented.

6.6.1 Results from Procedure 1

The first step of Procedure 1 is the choice of irregularity layout and corresponding pier lengths. To obtain comprehensive results and capture the dynamic behaviour of bridges for many possible cases, many irregularity layouts were analysed:

1) Regular bridge – all piers with equal length. Variables: total bridge length (L_{SS}) (120m to 900m; step-size of 60m); pier diameter (D) (1.0 m to 1.5 m; step-size 0.25 m) and deck moment of inertia around the vertical axis (I_{SS}) (75 m^4; 150 m^4; 400 m^4).

This irregularity layout allows to perceive the effect of length on the THDP of a bridge. As the length increases the importance of the deck's stiffness decreases and the piers gain larger influence. The RSI is a measure that relates to that effect.

Figure 6.4 shows the progression of the THDP shape of bridges of increasing length with irregularity layout "Regular", and a fixed value for the deck's moment of inertia. The THDPs presented are the maximum envelopes and it is clear that there is a modification in dynamic behaviour with the increase in length, where other (higher) mode shapes tend to increase their influence in the overall pier displacement. In the figure, each graph corresponds to a bridge of a different length.

In Figure 6.5 the correlation between the inertia of the deck and the diameter of the piers with the average value of pier displacement (d_T) is presented. It becomes clear that the influence of the deck stiffness in the average d_T falls very fast with the increase in bridge length, and that for bridges over 200-meter long, the piers are essentially in control.

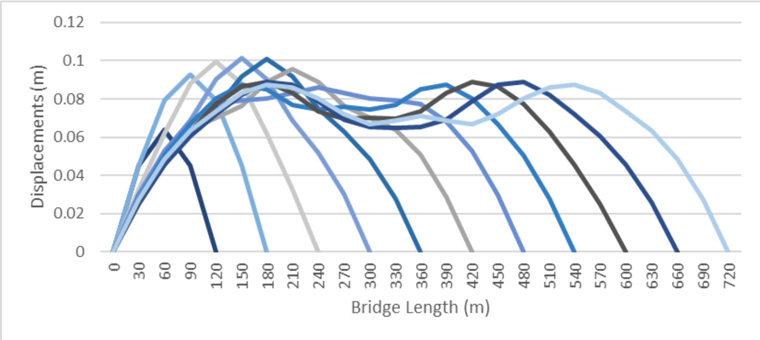

Figure 6.4 THDP of Regular bridges for varying bridge lengths.

While Figure 6.5 relates to a superstructure with a Figure 6.2 b) or c) cross-section and pier-deck interface, Figure 6.6 relates to a superstructure of the type Figure 6.2 a). The fundamental difference between both, as mentioned earlier, is the way in which torsion and pier-deck rotation is handled. In Figure 6.2 a), due to the nature of the pier-deck interface, there is absolute compatibility between pier and superstructure rotation about a horizontal axis in the longitudinal direction of the bridge, therefore associated to displacements in the transversal direction. Also, deck torsion is a factor and thus torsional stiffness affects the THDP, as it is visible in Figure 6.6. Here, the deck moment of inertia and the pier diameter are no longer the sole responsible for the THDP. It is also clear that torsional stiffness is more relevant to the THDP than the transversal horizontal deck stiffness, which is low for bridges over 200-meter long.

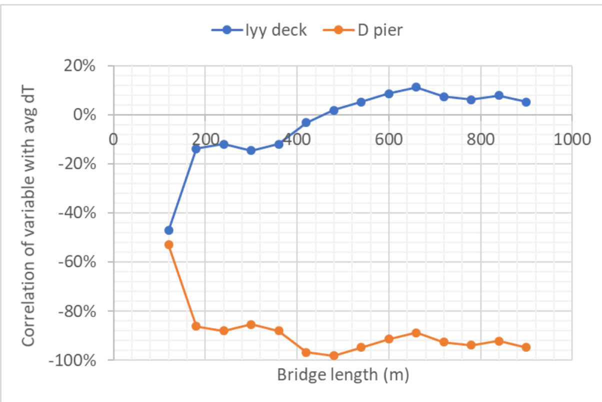

Figure 6.5 Correlation between deck inertia and pier diameter with the average deck displacement value. Values relate to Figure 6.2 b) type superstructures.

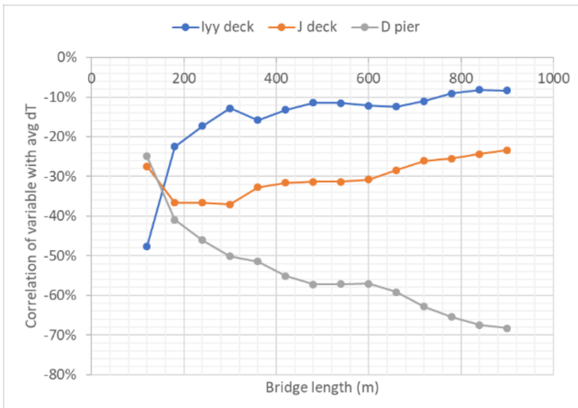

Figure 6.6 Correlation between deck inertia, pier diameter and deck torsion constant with the average deck displacement value. Values relate to Figure 6.2 a) type superstructures.

2) Irregularity 3 – 3321233 (Table 6.1). Variables: total bridge length (300 m to 900 m; step-size of 120m); pier diameter (1.0 m to 1.5 m; step-size 0.25 m) and deck moment of inertia (75 m^4; 150 m^4), number of short piers (1) (from 3 to 9, depending on total bridge length).

This type of irregularity typically has a very large impact on bridge THDP. The corresponding bridge dynamic behaviour is complex, and these types of bridges typically cannot be analysed by SPA methods (Kappos, Saiidi, et al. 2012).

The results of the analysis provide some interesting insights on the behaviour and on the value of indicators such as RSI.

In Figure 6.7 and Figure 6.8 the normalizing effect of the superstructure in the case of short lengths, which is the effect of the deck in equalizing the displacements (d_T) of short and long piers, is shown, and the correlation with the RSI value is made clear. In bridges where the piers are more flexible and the THDP is controlled mainly by the stiffness of the superstructure, the piers do not have influence on the THDP and so the superstructure controls the pier displacements. That is visible for bridges with ln(RSI) values over -4, where the maximum displacement of the piers is the same regardless of the difference in stiffness among them. From here onwards we designate ln(RSI) as lnRSI. As the superstructure becomes less rigid, the maximum displacement of the shorter piers becomes different from that of the longer piers. This effect is important for structural safety, since a stiff superstructure can lead a stiff pier to collapse, if the piers do not have sufficient capacity to influence the THDP of the bridge.

The effect is global and can be seen to occur for the same lnRSI values independently of the irregularity layout. In Figure 6.8 this effect is visible since the figure compares the ratio between maximum displacements of short piers with long piers. The value of -4 for the *lnRSI* indicator is a very clear frontier for the THDP behaviour, and the shape of the scatter plot can be seen very close to a sigmoid function, which is commonly referred to as an activation function. A sigmoid function is characterized by having a quasi-binary output, where it takes on a value for an $x \geq c$, and another value for an $x < c$, where c is some threshold value for x, in this case around -4. This result is very interesting for bridge design, since it is relevant to assess the safety and resistance of piers to know what their influence in the bridge THDP is.

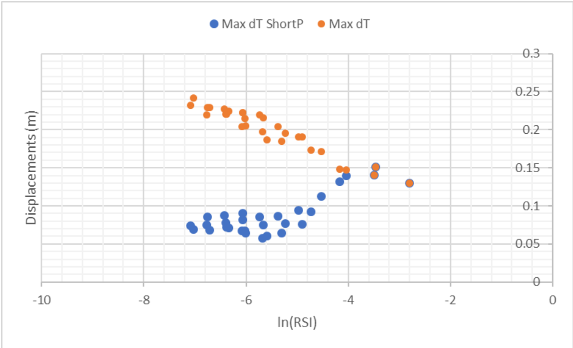

Figure 6.7 Maximum displacement of long piers and maximum displacement of short pier as a function of lnRSI For stiff superstructure (ss) /flexible pier, the superstructre normalizes pier displacement, while stiff pier/flexible ss, the piers have larger influence on their individual displacement.

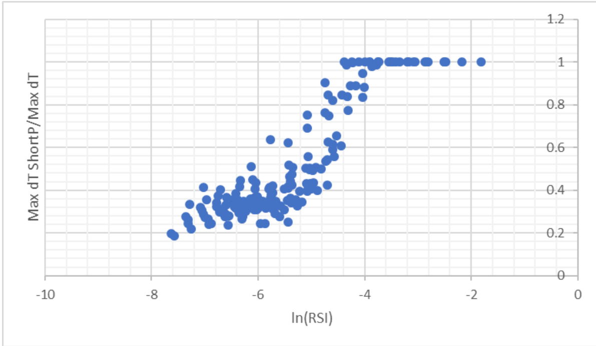

Figure 6.8 Ratio between maximum displacements of short and long piers, as a function of lnRSI. Shows a definite threshold value for RSI regarding the influence on the THDP shape.

In Figure 6.9, the THDP of some bridges related to irregularity layout 3 is presented. It becomes more apparent the change in THDP. One can see that as the length of the bridge increases, the THDP progressively becomes more sensitive to the pier irregularity profile. In the figure, each graph corresponds to a different bridge length but with the same irregularity layout type 3.

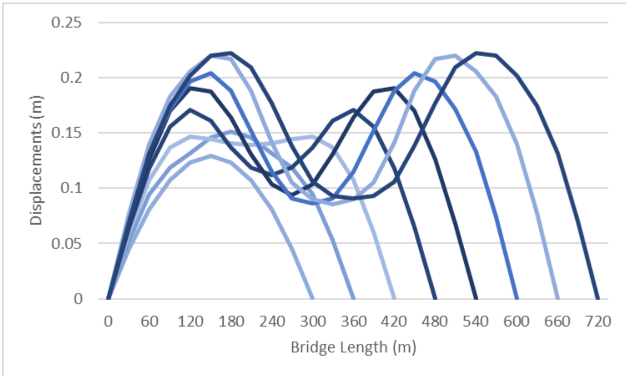

Figure 6.9 THDP of bridges with irregularity layout type 3, for increasing bridge length.

3) <u>Irregularity layout 21212</u>

For the present irregularity layout, characterized by a periodic repetition of long and short piers, with variation in bridge length and "wavelength" of the irregularity. The "wavelength" is defined by a number from 1 to 5 that represents the number of consecutive piers with the same length. So, a "wavelength" of 1 is equal to a pier length sequence like 21212, and a wavelength of 3 is like 222111222111222. The amount of repetitions then depends on the total length of the bridge.

The objective of this irregularity layout is to ascertain the importance of the "wavelength" on the shape of the THDP. In addition, it allows to show, for another irregularity layout, the eligibility of the lnRSI indicator as a predictor for THDP alterations. Regarding this aspect, Figure 6.10 shows that, for values of *lnRSI* larger than -4, the influence of the irregularities on the THDP is negligible, while for values smaller than -4 it isn't. However, the discussion of this particular point is somewhat conceptual, as some of the examples are academic, such as irregularity format 212121.

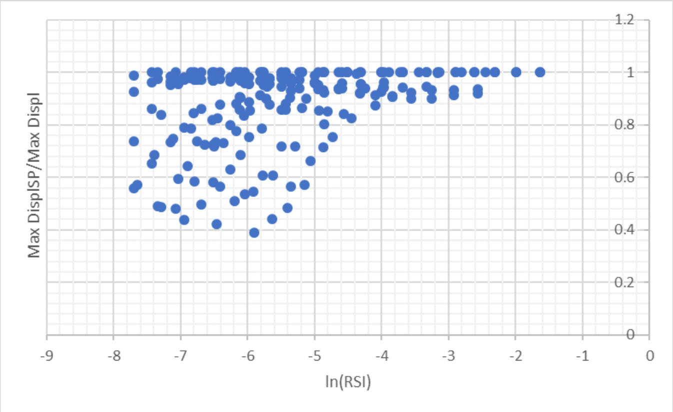

Figure 6.10 Ratio between maximum displacements of short and long piers, compared to lnRSI values, associated to irregularity layout 21212.

Figure 6.11 shows the impact of the irregularity "wavelength" on the modification of the THDP, characterized by the ratio between maximum displacement of short and long piers. For very short wavelengths (1 and 2), the superstructure cannot accommodate higher modes that fit the wavelength of the irregularity, and so the displacements are similar for short and long piers. This happens because the stiffness of the deck is enough to prevent any relevant variation in the THDP due to variations in stiffness of the piers, for instances due to higher modes with configurations that fit the wavelength of the irregularity. For wavelengths of 4 and 5 piers (120 to 150-meter) the superstructure is flexible enough to adapt itself to the irregularities and the THDP is different, showing that for longer wavelengths the effect of the deck is not enough to uniformize horizontal transversal displacements at the top of the piers. In Figure 6.12, the displacements for short and long piers are presented for a set of bridges with the same pier diameter (1.5m) and different irregularity wavelengths.

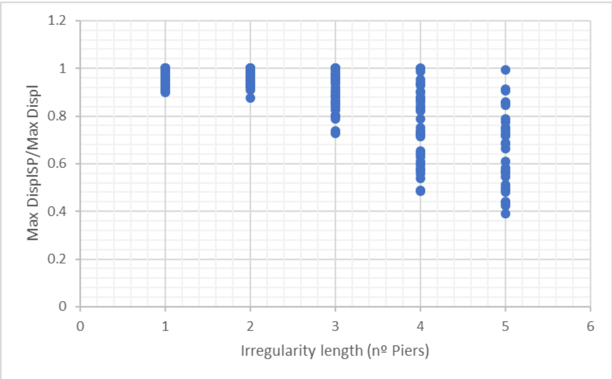

Figure 6.11 Ratio between max. displacements of short and long piers and irregularity "wavelength", for all cases in irregularity layout 21212.

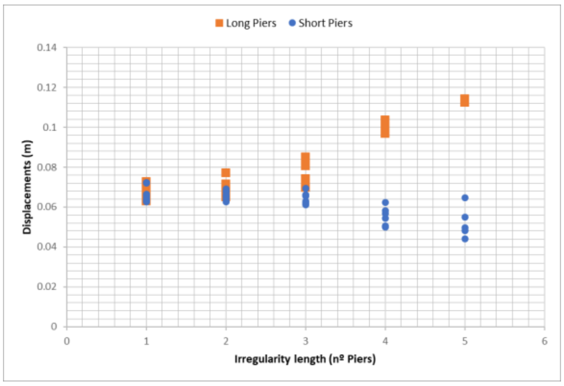

Figure 6.12 Maximum displacements of short and long piers and irregularity "wavelength" for cases with 1.5-meter pier diameter.

4) <u>Joint Results from all Irregularity layouts</u>

The joint results from all irregularity layouts provided an interesting notion. Previously, it had already been shown that the lnRSI is a good indicator of influence of the piers in the THDP of the bridge, showing that there seems to be a threshold value of lnRSI, above which the deck controls the transversal horizontal displacements and below which the piers gain influence over the THDP of the bridge.

For short bridges (high RSI values), the shape of the THDP is close to the parabolic shape of the fundamental vibration mode of the bridge, associated essentially to the deck vibrating in the horizontal plan as a simply supported beam on both extremities. The horizontal seismic displacements in the transversal direction are therefore controlled essentially by the stiffness of the superstructure (deck). For long bridges (low lnRSI values), the shape of the THDP depends on the irregularity layout, however the average seismic displacement in the piers is associated to the total infrastructure stiffness, as will be shown.

In Figure 6.13, Figure 6.14 and Figure 6.15, the relation of the infrastructure stiffness, characterized by L/K_{total}, where L is bridge length and K_{total} is the total stiffness of the piers, and the average peak displacement (average of the peak horizontal displacement on top of all piers) is presented. Each of the figures presents a set of the solutions. Figure 6.13 represents all solutions and shows a large variation in the results of average peak displacement. In the following scatter plots, different markers and colours correspond to different case studies concerning irregularity layout. Points with the same marker correspond to the same bridge irregularity layout but different pier diameter and length. The fsr in the piers is equal to 2.5% in every pier of every bridge. The average peak displacement is calculated for each case and compared to L/K_{total}.

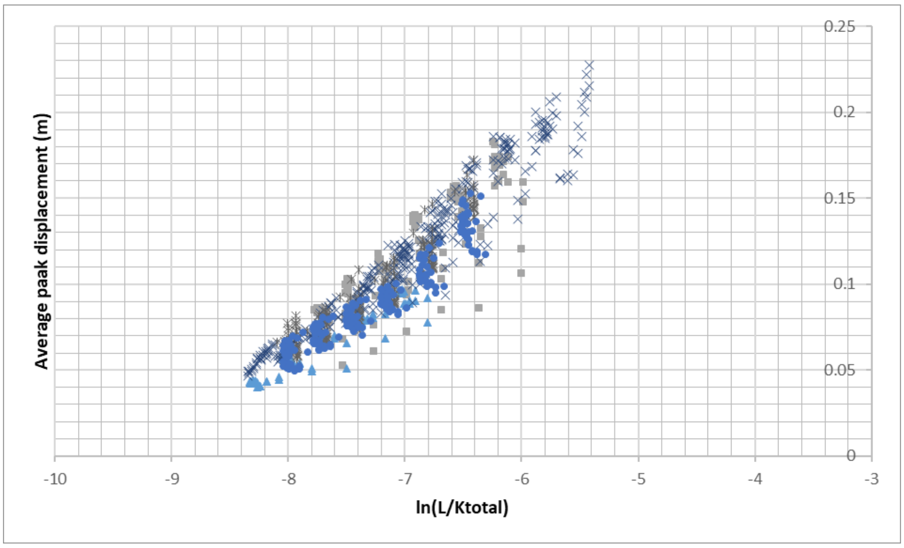

Figure 6.13 Average peak displacement plotted against infrastructure stiffness ($\ln(L/K_{total})$). All cases from all irregularity layouts. Different markers refer to different cases of irregularity layout.

By dividing the set in Figure 6.13 into two subsets (Figure 6.14 and Figure 6.15) one obtains much tighter scatter plots which give evidence of a good correlation between infrastructure stiffness and average peak displacement. This subdivision into two sets was performed on the basis of their lnRSI value, and so bridges with lnRSI value smaller than -4 (long bridges) are presented in Figure 6.14 and bridges with lnRSI value larger than -4 (short bridges) are presented in Figure 6.15.

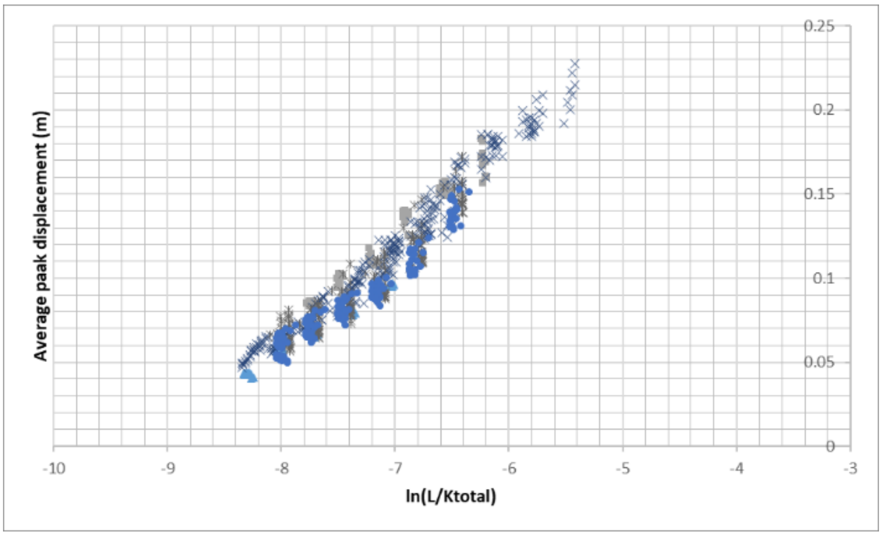

Figure 6.14 Average peak displacement plotted against infrastructure stiffness ($\ln(L/K_{total})$). Cases with lnRSI smaller than -4 (long bridges), from all irregularity layouts.

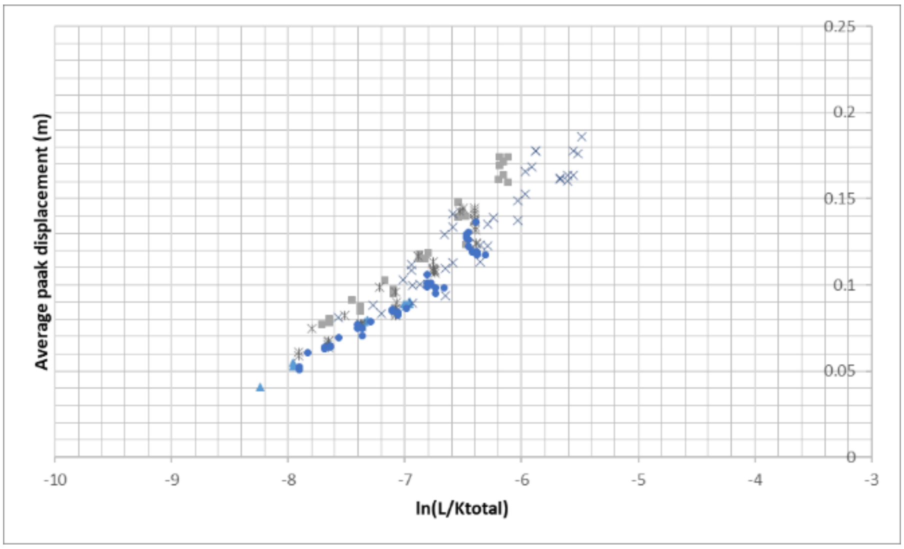

Figure 6.15 Average peak displacement plotted against infrastructure stiffness ($\ln(L/K_{total})$). Cases with lnRSI larger than -4 (short bridges), from all irregularity layouts.

It is important to mention that the cases studied do not vary in terms of earthquake action nor superstructure cross-section (mass). The results are comparable because these values are kept constant. Nonetheless, the results show that even though very significant irregularities are introduced, and significant modifications imposed on the THDP, the RSI and the total stiffness are good indicators of the dynamic behaviour of the bridge and can be used to perform estimates on the response.

6.6.2 Results from Procedure 2

In procedure 2, there is simultaneous variation of pier diameter and fsr in the piers. Regarding the fsr there is also variation between piers, that is, different fsr distributions among piers, unlike in procedure 1 where not only fsr did not change but the fsr was also the same for all piers. The application of procedure 2 renders, for each case-study, a set of solutions which vary in their use of material and in the difference between the maximum strain demand and the strain associated to the collapse criterion. More material employed generally implies more safety (larger gap between maximum and collapse strains) provided that ductility is preserved. The optimization search is done by varying the diameter of the piers and the flexural steel reinforcement for different pier groupings. An interesting solution for presentation of results is by transforming the cost function into the aforementioned $ln(L/K_{total})$ measure, which is also dependent on the pier diameter and flexural steel reinforcement variables, as is the cost function. The results with this ratio, $ln(L/K_{total})$, will be compared among case-studies.

An example of the output obtained from the optimization procedure is presented in Figure 6.16. Here the different colours differentiate the Pareto front solutions from the rest of the solutions generated in the optimization search.

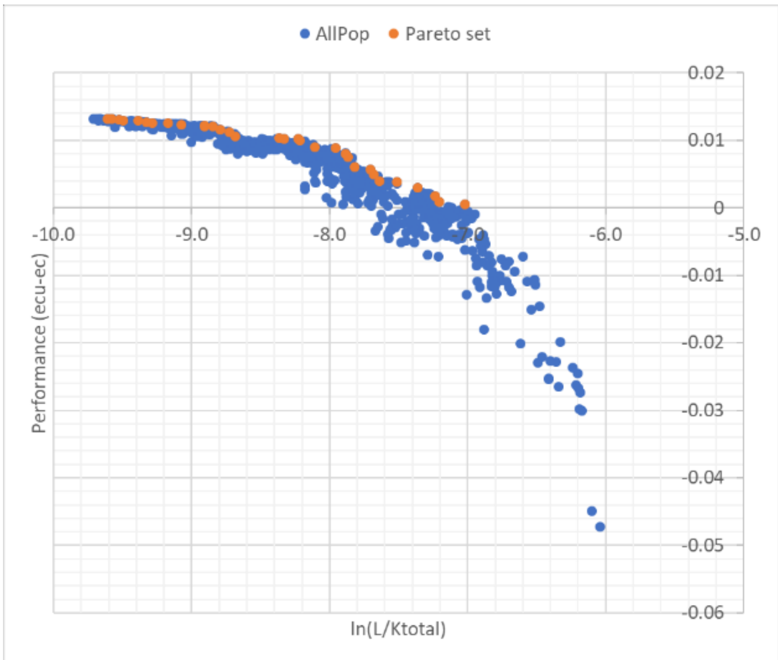

Figure 6.16 Result for case-study 480_R_L5_A12_EQ1_T presented by Performance vs Bridge Length/Total Stiffness.

It is clear that the solutions which belong to the Pareto set of optimized solutions are the ones which maximize performance for a given level of stiffness. This is visible in Figure 6.16. Nonetheless, it can be said that there is a very clear relationship between total stiffness and the performance level albeit some variation. This variation is associated essentially with the distribution of flexural steel reinforcement among the piers. This variation is larger for long bridges than for short bridges. This is due to the larger influence that the distribution of stiffness among piers has in the THDP for long bridges. This effect is shown in Figure 6.18.

In Table 6.5, the corresponding information about the solutions belonging to the Pareto set in Figure 6.16 regarding optimization variables, performance, total stiffness, *ln(L/K_{total})* and *lnRSI* is presented.

Table 6.5 Results for case-study 480_R_L5_A12_EQ1_T relative to the Pareto set solutions

Steel1	Steel2	Steel3	Diam	ε_{cu}-ε_c	K_{Total}	$ln(L/K_{total})$	ln(RSI)
1.95%	2.30%	3.05%	1.05	0.00053	537404.7	-7.02	-5.0
2.40%	3.35%	3.30%	1.05	0.00084	645624.0	-7.20	-5.2
2.25%	3.45%	3.05%	1.1	0.00295	755573.1	-7.36	-5.4
1.95%	3.15%	2.50%	1.175	0.00379	877796.6	-7.51	-5.5
0.90%	2.30%	1.35%	1.2	0.00178	666064.3	-7.24	-5.3
2.00%	3.00%	2.25%	1.225	0.00399	998868.7	-7.64	-5.7
2.40%	3.25%	2.60%	1.35	0.00901	1590788.7	-8.11	-6.1
1.15%	2.20%	1.20%	1.35	0.00494	1038782.0	-7.68	-5.7
0.95%	2.30%	1.50%	1.4	0.00603	1197779.4	-7.82	-5.9
2.30%	3.10%	2.60%	1.4	0.00995	1773405.9	-8.21	-6.2
0.75%	2.30%	0.70%	1.4	0.00567	1068412.0	-7.71	-5.7
1.20%	2.30%	1.50%	1.4	0.00753	1251647.7	-7.87	-5.9
1.30%	2.30%	1.50%	1.4	0.00796	1273153.3	-7.88	-5.9
2.40%	3.10%	2.60%	1.4	0.01015	1794649.1	-8.23	-6.3
1.35%	2.30%	1.50%	1.425	0.00886	1370989.0	-7.96	-6.0
2.55%	3.25%	2.60%	1.425	0.01016	1987397.4	-8.33	-6.4
2.50%	3.15%	2.45%	1.45	0.01038	2068648.9	-8.37	-6.4
2.20%	3.05%	2.30%	1.6	0.01053	2837587.6	-8.68	-6.7
2.40%	3.10%	2.50%	1.6	0.01119	2964426.3	-8.73	-6.8
2.60%	2.85%	2.65%	1.65	0.01203	3344558.3	-8.85	-6.9
2.60%	3.35%	2.65%	1.65	0.01206	3547711.1	-8.91	-6.9
2.35%	2.30%	2.50%	1.675	0.01156	3161936.6	-8.79	-6.8
2.25%	2.65%	2.05%	1.725	0.01222	3547842.1	-8.91	-6.9
2.45%	3.10%	2.50%	1.75	0.01236	4200318.2	-9.08	-7.1
2.60%	2.85%	2.65%	1.85	0.01252	5181764.6	-9.29	-7.3
2.60%	2.75%	2.70%	1.875	0.01269	5404619.3	-9.33	-7.4
2.00%	2.20%	2.00%	1.9	0.01250	4604811.1	-9.17	-7.2
2.50%	2.65%	2.40%	1.925	0.01288	5713918.5	-9.38	-7.4
2.55%	3.00%	2.60%	1.95	0.01293	6401304.5	-9.50	-7.5
2.60%	2.75%	2.70%	1.975	0.01299	6597704.2	-9.53	-7.6
2.55%	3.05%	2.75%	2	0.01321	7165604.4	-9.61	-7.6
2.65%	2.75%	2.60%	2	0.01316	6924513.4	-9.58	-7.6

From the results, it is apparent that there is a tendency to place more flexural steel in the second group of piers (Steel2) than the other two groups. The groupings in this case are as follows: 1-1-1-2-2-2-3-3-

3-2-2-2-1-1-1, where the numbers 1, 2 and 3 represent the pier groups and Steel1, Steel2 and Steel3 represent the respective flexural steel reinforcement percentages of each pier group. In Figure 6.17, the results from the THDP of the bridges in the aforementioned Pareto set are presented. The various THDP profiles vary in terms of maximum peak displacement, which can be presented as a function of $ln(L/K_{total})$.

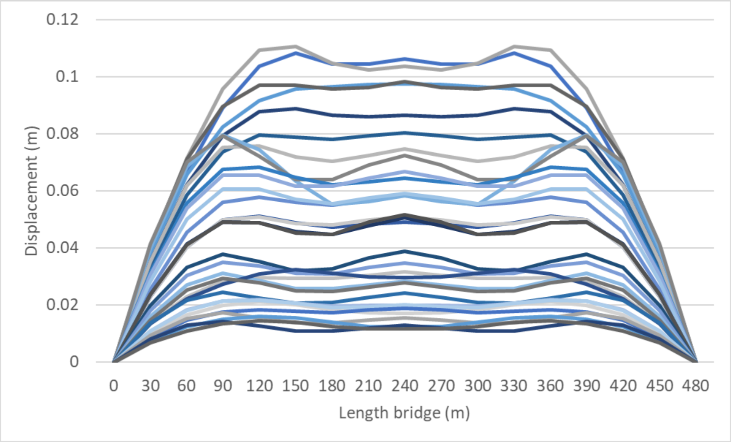

Figure 6.17 THDP of Pareto set solutions. The graphs represent the max envelope of the horizontal deck displacements.

The issue of flexural steel distribution is of large importance, especially when bridges become longer, and the piers' stiffness affects the THDP of bridge and not only the maximum displacement. From Figure 6.18 and Table 6.6, this influence is visible. Two similar cases which only vary in terms of steel distribution have a visible difference in terms of THDP. It is interesting to realize that in both cases the average displacement along all piers is exactly the same, and only the THDP shape changes. This shows that, for longer bridges, an optimized flexural steel distribution is important.

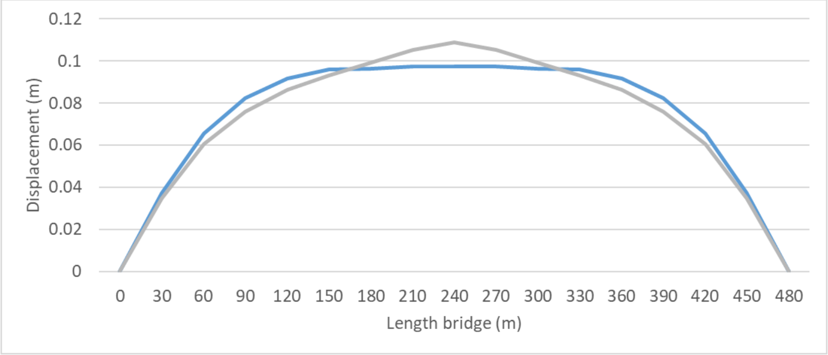

Figure 6.18 Comparison of solutions with same overall infrastructure stiffness but different stiffness distribution.

Table 6.6 Average peak displacement and maximum peak displacement for each solution from Figure 6.18.

Flex. Steel P1-P2-P3	Avg d_T(m)	Max d_T(m)
2.25%-3.45%-3.05%	0.072	0.098
3%-3%-3%	0.072	0.109

The results for the various case-studies are presented as performance vs. $ln(L/K_{total})$ in Figure 6.19. The performance, as mentioned earlier is taken as the difference between the ultimate concrete strain associated to the confinement and the minimum concrete strain (maximum absolute value) registered at any pier at any cross-section. This performance was shown previously to be very dependent on the overall stiffness of the infrastructure in Figure 6.16. In Figure 6.19, many of the transversal case-studies are shown and they clearly become divided into two groups. As it happens, these groups are related to the irregularity layout. The case-studies represented by circles are from case-studies where the irregularities do not have much influence on the THDP, which happens for short bridges, or long bridges with regular pier height. The case-studies represented by *xs*, refer to case-studies whose irregularity layout influences the THDP. As a result, the stiffness associated to optimal design is lower than in the set of case-studies associated with regularity. This result is related to Figure 6.7 and Figure 6.8. In those figures it is shown that for long irregular bridges the displacements of long piers and short piers become “separated” lowering the demand on short critical piers. That becomes once again apparent in Figure 6.19, where to maintain the same values of performance for critical piers, the global stiffness of the piers can be reduced, which is the same as saying that for the same value of total pier stiffness there is less demand on critical piers. In this case, in the following scatter plots, different markers and colours correspond to different case studies concerning both length and irregularity layout. Points with the same marker correspond to the same bridge in terms of length and irregularity layout but different pier design variables.

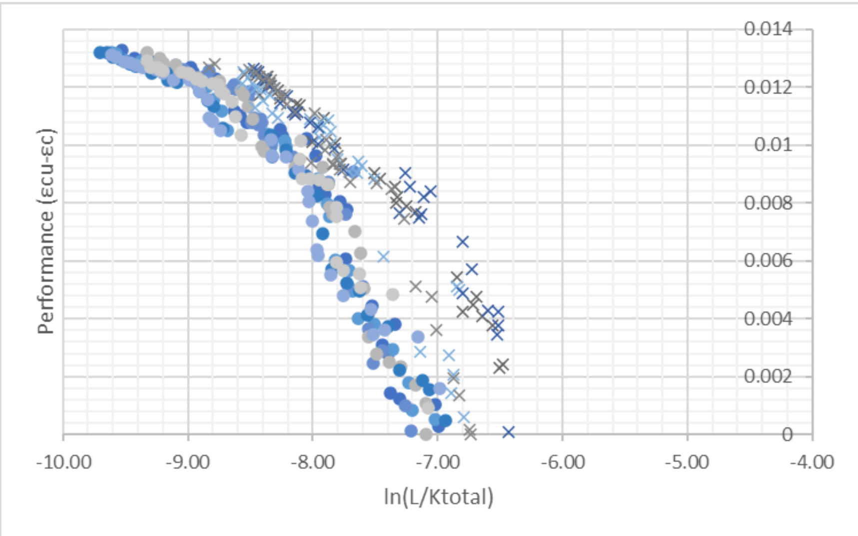

Figure 6.19 Graph comparing performance measure of differential between ultimate concrete strain and measured concrete strain with $\ln(L/K_{total})$ indicator. Crosses represent long irregular case-studies with irregularity layouts 2 and 3, while circles represent regular case-studies and also case-studies with irregularity layout 1.

For each POS (Pareto-optimal set) solution of each case-study, the displacement of the critical pier was plotted against the usual $ln(L/K_{total})$ indicator in Figure 6.20 and Figure 6.21, giving a better understanding of the effects mentioned previously. In Figure 6.20, the peak displacement of the critical pier is plotted against $ln(L/K_{total})$. In this figure, only regular case-studies and case-studies where the superstructure controls the THDP, were considered. In Figure 6.21, regular case-studies both in the longitudinal and transversal direction are presented. This shows a similarity between the peak displacements for both directions, for bridge lengths high enough for the effect of the abutments to be negligible.

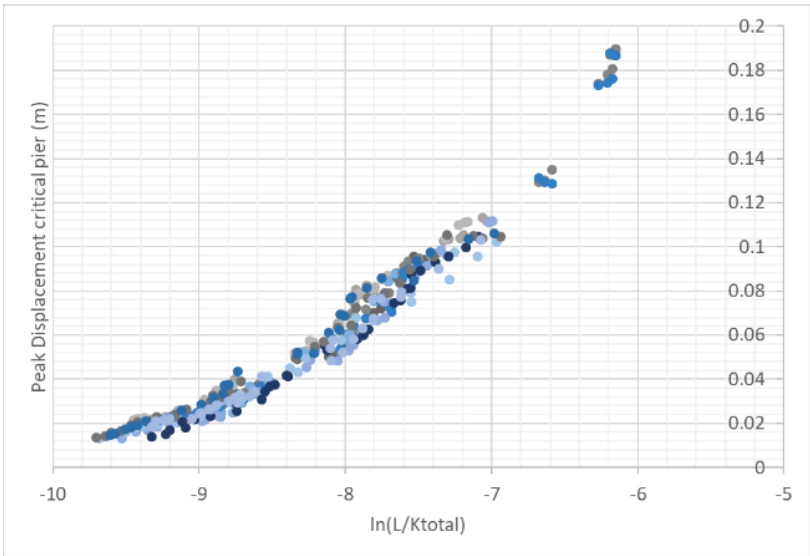

Figure 6.20 Peak displacement of critical pier against ln(L/K_{total}). Regular bridges and short irregular bridges.

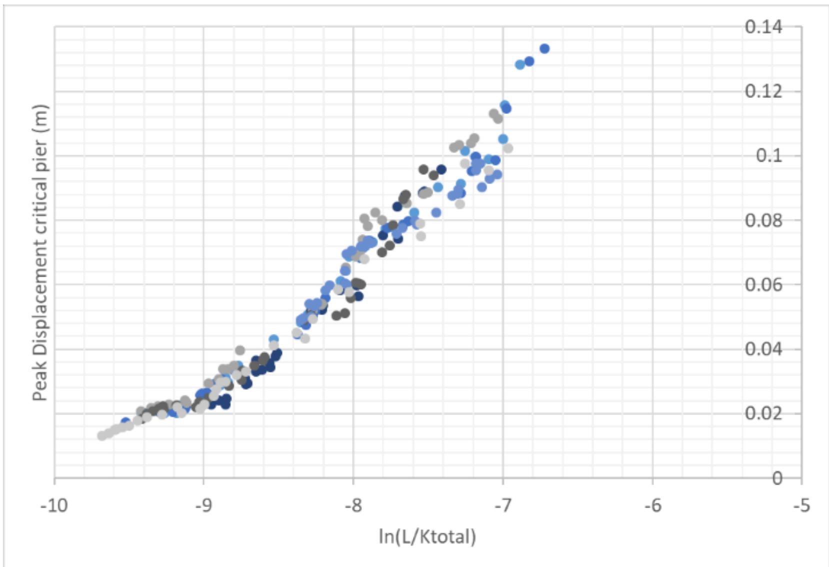

Figure 6.21 Peak displacement of critical pier against ln(L/K_{total}). Regular bridges – longitudinal and transversal direction.

In Figure 6.22, case-studies with all irregularity layouts are presented and there is a difference between two types of case-studies, as seen before in Figure 6.19. The solutions from long irregular bridges need less overall pier stiffness for the same peak displacement of critical piers. This is associated to the modification of the THDP due to the irregularities and the subsequent larger influence of higher modes. This THDP modification redistributes displacements to longer piers thus reducing the displacements on critical piers.

In Figure 6.23 and Figure 6.24 the THDP from two case-studies, one associated to a short bridge and another to a long irregular bridge with irregularity layout 3, are shown.

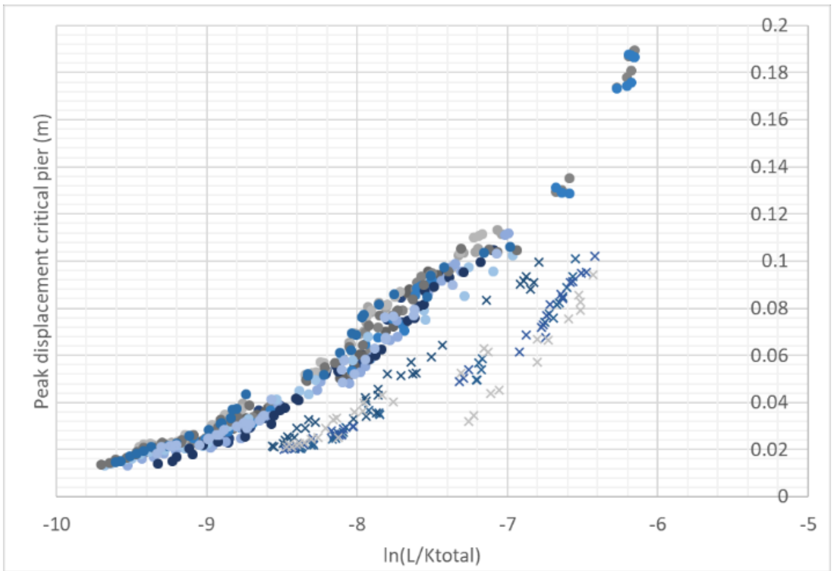

Figure 6.22 Peak displacement of critical pier against ln(L/K_{total}). transversal direction all types of irregularity layout and length.

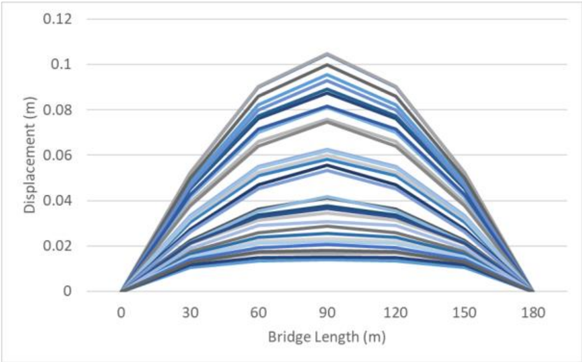

Figure 6.23 THDP of solutions from POS of short bridges case-study.

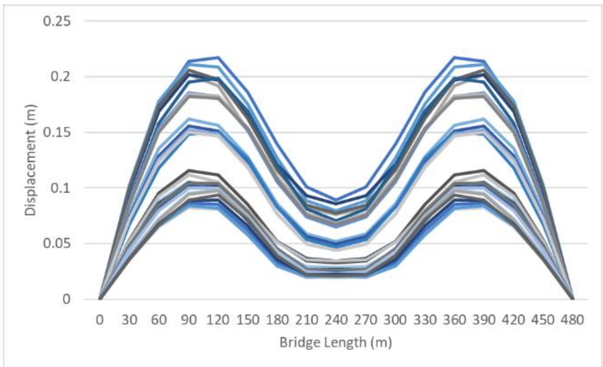

Figure 6.24 THDP of solutions from POS of long bridge case-study with irregularity layout 3.

6.7 Discussion

In this section, the results obtained in the previous section concerning the two employed procedures are thoroughly discussed. It is also important to reinforce that all results are strictly associated to bridges in which the torsion of the deck is suppressed at the supports due to the torque formed by axial forces in the piers. For other types of superstructure, the dynamic behaviour can be significantly different and some of the following considerations and conclusions may not apply. The information gained from this is associated to information obtained from Procedure 1 and can be summarized in the following:

- In short bridges, varying the relative stiffness between piers has little influence in the THDP and in the displacement of critical piers. In these cases, the superstructure controls the THDP and depending on the length of the bridge, the piers' total stiffness can have more (if the bridge is longer) or less (if the bridge is shorter) influence on the average pier displacement.

- Short bridges and long bridges can be defined through the RSI or lnRSI indicator. For various irregularity layouts, the dynamic behaviour of the bridge changes noticeably at around *lnRSI* = -4. For *lnRSI* values inferior to -4 there is a separation of displacements of piers with different stiffness, which are indicative of modification of the THDP, and larger pier influence in the bridge's dynamic behaviour. This "long bridge" behaviour has some positive effects for earthquake resistance since it allows displacements at critical piers to be redistributed to non-critical piers.
- Thus, in long bridges the distribution of flexural steel reinforcement between piers, while maintaining the total pier stiffness constant, has significant impact in terms of earthquake resistance because the stiffness variation influences the bridge THDP. This can lead to differences in the displacement demand at critical piers, even though the average pier displacement remains equal. In short bridges, this does not happen, and the deck defines the THDP while the total pier stiffness (K_{total}) may influence the average pier displacement. In the case of very short bridges, which in Figure 6.5 are the cases below 180 meters in length (for a deck transversal moment of inertia of 150 m^4), the influence of the deck becomes very pronounced and controls the THDP and the amplitude of displacements regardless of the stiffness and irregularity of the piers, due to the effect of abutments. In these cases, the abutments absorb a large percentage of total transversal inertia force. Even though the columns shape may have some influence, in general, bridges in which the length of the deck is not more than 6 to 8 times the respective width, exhibit very short bridge behaviour.
- For very short bridges, with shorter total lengths or much higher deck transversal stiffness (short and very wide decks) the piers may have no influence whatsoever in the THDP. In such cases, which are not covered in this work, most of the inertia force is transmitted directly to the abutments and the piers essentially have to sustain imposed displacements by the abutments, at least in the transversal direction of movement.
- It is interesting to see that for long regular bridges the peak displacements in the longitudinal and transversal directions are similar (for circular sections). This observation is important in terms of pier design, as it may facilitate the analysis in the transversal direction applying simplified models applicable in the longitudinal direction.
- For long irregular bridges, the effects of the irregularities in modifying the THDP are beneficial for critical piers, as previously discussed. The results also show that the displacements at the critical piers are lower for the same total stiffness, in these cases, than for regular bridges. This suggests that the results for the displacement demand of piers in regular bridges in terms of total stiffness can work as a conservative first iteration approach for the displacement demand of piers in irregular bridges.
- Besides the ratio between superstructure (deck) stiffness and infrastructure (piers and foundations) stiffness, defined by the *lnRSI* indicator, the wavelength of the irregularity is important in defining how the irregularity influences the THDP of the bridge. If the wavelength

of the irregularity is short, the superstructure is not able to deform accordingly since a small bending length implies larger relative deck stiffness in the transversal direction and so the THDP does not change much within the zone of the wavelength. Therefore, this part of the bridge has some features of behaviour similar to short bridges, as for instances, the THDP being influenced by the overall stiffness of the piers regardless of the distribution of stiffness between them (within certain limits for those stiffness variations).

- Reiterating, the *lnRSI* seems to be a very good indicator for the definition of long bridges and short bridges, and definition of subsequent behaviour patterns. The $ln(L/K_{total})$ indicator is strongly associated to average and peak pier displacements. These results have to be parameterized in order to account for deck mass and earthquake intensity. This indicator is conservative when the bridge is long and irregular, since, as previously explained, the displacement at critical piers is redistributed to long piers.
- The wavelengths of the irregularities are important in defining whether the bridge will behave irregularly or not. For small wavelengths, the deck cannot adapt to the imposed irregularity and the bridge will have an almost regular displacement profile. For long wavelengths, the bridge can develop an irregular dynamic behaviour and affect the THDP. The discussion of this particular point is somewhat conceptual and some of the examples are academic, such as irregularity format 212121. Nonetheless they are useful in showing the influence of such irregularity patterns in the THDP.
- The question of the wavelength depends on whether the irregularity is due to long piers together with a majority of short piers, or vice-versa. This is explained qualitatively in Figure 6.25. From there it follows that even for an isolated irregularity, there is a difference if it is due to a short pier or a long pier. A short pier will usually affect the THDP while a long pier might not. Figure 6.25 also illustrates, for periodic irregularities, the importance of the irregularity wavelength, captured previously in Figure 6.11 and Figure 6.12.

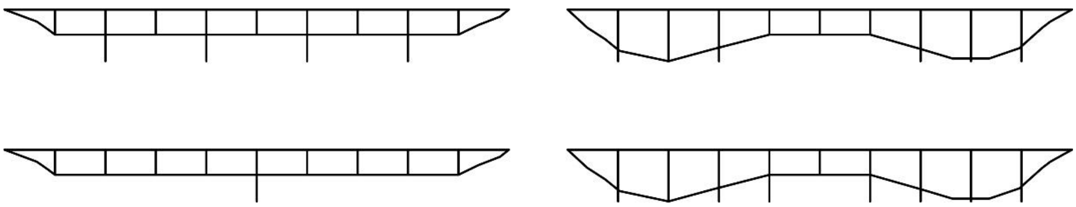

Figure 6.25 Effect of pier irregularity on the THDP, according to wavelength and pier length associated to the irregularity layout.

- Future works should be done with other types of superstructure, especially in terms of the deck torsion and rotation with the pier/s. In addition, performing optimization searches by also varying the pier diameter between pier groups (different diameters along the bridge) could be interesting to show even more pronounced effects of pier stiffness variations in long bridges. However, the analysis performed is the most relevant, as standardization of dimensions of structural elements is relevant for the economy of construction.

- As for the approach to bridges whose deck is susceptible to torsion, that is, bridges that have rotation of the piers and deck, the RSI should be altered, or another parameter should be devised to account for the torsional stiffness.

6.8 Conclusions and Recommendations

In this work, short and long, regular and irregular bridges are analysed resorting to two procedures. The first procedure varies progressively the length and other factors in a full factorial design, and for different irregularity layouts, and then analyses the results and variations. The second procedure attempts a multi-objective optimization of a bridge with a fixed length and fixed irregularity layout by alteration of the pier design variables (flexural steel and pier diameter) and according to cost and performance objectives. Both procedures have complementary objectives. The first procedure attempts to highlight the influence of bridge length according to irregularity and utilizes the RSI indicator, based on the stiffness ratio between deck on one side and columns plus foundations on the other. This procedure allows to perceive where a "short bridge" ends and "long bridge" initiates and how irregularities modify the THDP (Transversal Horizontal Displacement Profile) of a bridge. The second procedure varies the distribution of flexural steel to obtain the distribution that optimizes the dynamic behaviour of the bridge, which is to say that better distributes the deck displacements and ductility demand in long irregular bridges, according to the critical piers' available ductility. As has been mentioned in previous works (Akbari and Maalek 2018), there are no studies in the literature in which the dynamic behaviour of irregular bridges is analysed by differential changing of the piers' cross-sections (increasing/reducing pier stiffness in some parts of the bridge in relation to other parts). In this study, this last point is analysed under Objective/Procedure 2. Another added value from Objective/Procedure 2 is that the results can be described in terms of displacement of critical pier versus total pier stiffness and be compared among various case studies.

6.8.1 Conclusions

The conclusions from this chapter can be summarized in the following points:

- For short bridges, the THDP is controlled by the superstructure and the total stiffness of the infrastructure is correlated to the maximum pier displacement. In these cases, the distribution of the stiffness of the piers is not very important, only the total stiffness. This means the flexural steel can be redistributed arbitrarily, as long as the total stiffness is kept constant.
- For long bridges, the localized stiffness variations (stiff piers, wavelengths of irregularities, etc.) influence the critical pier displacement. The average displacement of the deck, however, can be associated to the total stiffness of the infrastructure (piers and foundations). For long bridges, the distribution of the stiffness along the infrastructure is important for the safety of the piers, as it influences both the average displacement of the deck and the THDP.

- In irregular bridges, the RSI indicator (ratio between deck and columns stiffness) can yield a good estimate of whether the bridge can be considered long or short in terms of THDP (lnRSI = -4). This is important for pier safety since, with long bridge behaviour the displacement (which is a measure of the ductility demand) of critical (short) piers can be redistributed to long piers, and the superstructure (deck) accommodates these displacement variations. As for short bridge behaviour (excludes very short bridges, where the deck controls both the THDP and the average transversal displacement), the critical piers are not able to affect the THDP and might undergo excessive displacements.

6.8.2 Recommendations

Finally, regarding design recommendations, the following can be said:

1) Short bridges can essentially be designed in the transversal direction in similar fashion as to the longitudinal direction, that is reduced to a SDOF, in the sense that the total pier stiffness, and not individual pier stiffness, is what defines maximum displacement demand, since the shape of the THDP is essentially controlled by the superstructure.
2) In long bridges, the total pier stiffness is of great importance, but so is the stiffness distribution since the piers are able to influence the bridge THDP. For that reason, the critical piers and the piers adjacent to critical piers have to be designed carefully in order to simultaneously increase the available ductility and control the ductility demand of critical piers. First, this means increasing the ductility of critical piers through increase in confinement reinforcement. It may also be worth studying the possibility of increasing the stiffness of piers adjacent to the critical piers by increasing their flexural steel reinforcement, in order to control the displacement demand on the latter. However, this may have negative effects, such as reducing the available ductility on those piers, and induce changes on the overall seismic behaviour of the bridge that may be either positive or negative for different piers. So, this recommendation should only be implemented after careful balance of its positive and negative effects.
3) Irregularities in long bridges should be approached, from a design standpoint, with the goal of smoothening the differences between long and short piers, since a very abrupt stiffness variation generally means that the short pier adjacent to the transition will suffer excessive displacement demands. This transition may be achieved by means of assigning less stiffness to the shorter piers through providing less flexural reinforcement, which strongly influences the stiffness after cracking and yielding. At the same time, providing more flexural reinforcement to the longer piers increases their stiffness, thus smoothening the stiffness transition.
4) In short irregular bridges, the irregularity has little effect on the THDP, and so to overcome this either the critical piers’ stiffness is lowered to increase its ductility while maintaining the overall stiffness of the infrastructure, or the total stiffness is increased to decrease the ductility demand on critical piers. Either way, the THDP in short bridges, is usually unaffected by localized stiffness variations.

5) Regarding long regular bridges, they can be designed similarly in both the longitudinal and transversal directions.
6) Some of the concepts applicable to short bridges, namely increasing the available ductility of the shortest piers by means of reducing their flexural reinforcement, may also apply in parts of long irregular bridges if the stiffness of the deck in those parts is high enough to uniformize transverse displacements in that part of the bridge, in a way similar to what happens in short bridges.

6.9 Use of machine learning algorithms to train surrogate models for structural seismic performance. – Case study application

The machine learning algorithms employed herein are from well-known Python libraries, and there are many works that introduce these methods of machine learning and data analysis, in a Python framework, which the reader should check for in-depth information on the methods (Géron 2019) (McKinney 2017) (Raschka and Mirjalili 2017) (Rokach and Maimon 2014).

In this section, the modified NSGA-II algorithm, employed in (Camacho, Horta, et al. 2020) is used for the optimization of a long irregular bridge with short central piers. The seismic action is applied both in the longitudinal and transversal direction. The results for different solutions are compared in terms of performance, stiffness distribution, total cost, etc. Afterwards, classification trees, neural networks and random forests are employed to define critical variables and to create surrogate models. These techniques are applied to the entire set of solutions that were generated and analysed during the GA runs.

6.9.1 Objectives and MOP definition

6.9.1.1 Objectives

The design of RC bridges for earthquake resistance essentially focuses on the RC bridge's infrastructure, piers and abutments. The design of RC piers compounds several variables from 1) pier-deck connections, to the piers' design variables, which are 2) flexural steel reinforcement (longitudinal reinforcement) 3) cross-section shape and dimensions, and 4) transverse steel reinforcement, including confinement. These variables all have complex interdependences and strongly influence bridge dynamic behaviour. For instance, the variation of 1), 2) and 3) modify, simultaneously, the piers' stiffness, ductility and strength.

The objective, in this section, is to apply the optimization algorithm, presented in previous chapters, to the optimization of the seismic design of a long irregular bridge, that belongs to the group of irregular bridges with short central piers, considering most variables associated to pier design (1, 2 and 3).

The results obtained from the application of the MOEA show trade-off solutions for cost and performance objectives, showing how the design variables vary between solutions inside the optimal Pareto set. Furthermore, the subsequent application of different machine learning algorithms trained over the entire population of classified solutions, returns a ranking on the relative importance of each variable, regression of the performance, and classification concerning feasibility with generation of the shortest path towards classification. The gain is a framework that allows to define: a) a surrogate model that can be used in other applications (neural network); b) a variable rank according to importance for design (random forest); c) a decision tree for design that summarizes design rules (classification tree).

6.9.1.2 MOP definition

The objective functions, for this case-study, concern cost and performance., which regarding the work in Chapter 4, concern objective-set 2.

Regarding the decision variables there are three: 1) pier-deck connections, 2) flexural steel reinforcement and 3) cross-section size (only circular piers were considered). The fourth variable mentioned in the introduction as 4) (pier confinement), here is taken as a constant approximately equal to the minimum confinement for ductile bridges in EC8 - 2 (CEN 2005). As for the three variables, the following are their limit values between which they were sampled:

- Pier-deck connections: [1-monolithic, 2-fixed]-connection
- Flexural reinforcement steel: [0.6, 3.5]- %
- Pier Diameter: [1.0, 2.5]-m

All the piers, in each bridge solution, are modelled with the same pier diameter. Regarding the other two variables, their value in each pier depends on the adopted standardization criteria (pier groups).

6.9.2 Case-study definition

6.9.2.1 FEM analysis

The seismic analyses were performed resorting to OpenSEES software (McKenna and Fenves 1999), more specifically OpenSEESMP for the conduction of the seismic analysis in parallel processes. Since the population evaluation in a MOEA is a fully parallelizable process, this allowed a significant reduction of the total run-time by a factor of around 20, due to the utilization of 32 parallel processors. The population size of the MOP, in each generation, is 64.

6.9.2.2 Case-study definition

The case-study selected for analysis is an irregular bridge with relatively short central piers, and with a total length of 480 meters. An illustration of the type of irregularity is given in Figure 6.26.

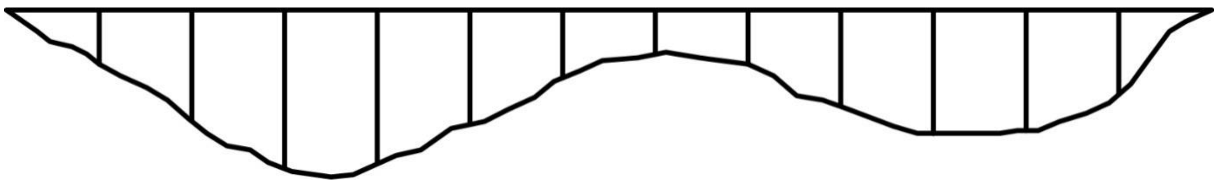

Figure 6.26 Irregularity layout of case-study bridge.

In addition, the length of each pier and the pier groups defined for the analysis are presented in Table 6.7. The bridge has a total of 15 piers and the chosen standardization criteria assembles the piers into four groups. In Table 6.7, on the left-hand side the pier lengths along the bridge and on the right-hand side the pier groups, where the numbers (1 to 15) correspond to the position of the pier regarding the left abutment. For example, group 1 is represented by (1, 2, 14, 15), which means the two piers closest to the left abutment (1 and 2) and the two piers closest to the right abutment (14 and 15).

Table 6.7 Case-study pier lengths and pier variable groupings used in the optimization procedure. The bridge has 15 piers in total, numbered 1 through 15.

Pier lengths (m)	Pier groups (pier position)
11 11 14 14 11 11 7 7 7 11 11 14 14 11 11	(1 2 14 15) (3 4 12 13) (5 6 10 11) (7 8 9)

The cross-sections of both the piers and the deck are presented in Figure 6.27. In the case of the piers, the corresponding design variables associated to the pier's cross-section are highlighted.

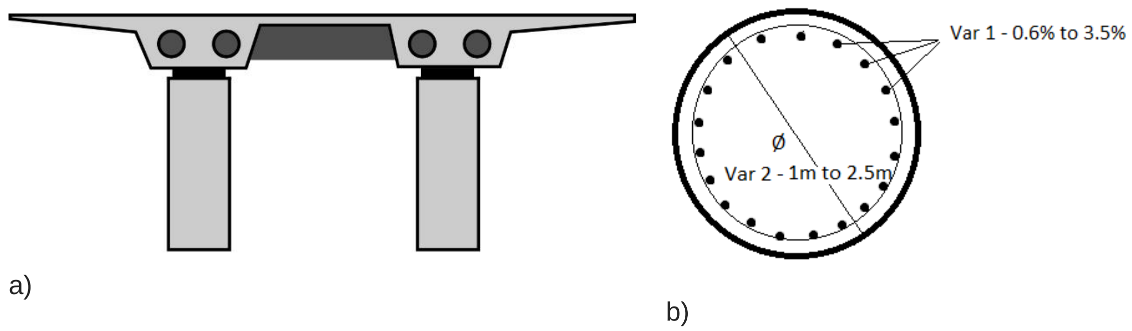

Figure 6.27 Cross-sections of a) the deck and b) the piers.

6.9.3 Methodology

In this study, the methodology consists of running the MOEA on the bridge case-studies, thus obtaining the Pareto-optimal front (POF) and also keeping the entire search procedure results, i.e., all solutions from all generations. With those results, machine learning algorithms are trained and tested, for feature selection and to attain surrogate models. The methodology's sequence is presented in the following:

1. Definition of case-studies.

2. Running MOEA on case-studies, in the transversal and longitudinal direction.

3. Analysis of MOEA results particularly via the solutions in the POF, and extraction of entire search history (data set) to use in the next procedures.

4. Data set treatment, data set standardization and feature engineering (creation of new features).

5. Definition of feature importance and feature selection via Random Forest algorithm.

6. Training and testing of ANN regression models.

7. Training and testing of Classification tree models.

8. Testing the different models (regression and classification) on data sets obtained from other case-studies (different bridges in terms of irregularity profile).

6.9.4 Optimization results: analysis and discussion

In this section results are presented pertaining to the optimization procedure with the MOEA.
In the optimization procedure, the case-study was optimized separately in the transversal and longitudinal directions. These two optimizations are of interest because in the longitudinal direction the bridge can be reduced to a single degree-of-freedom (SDOF), while in the transversal direction it is a long bridge with short central piers and expected very nonlinear behaviour with significant influence of higher modes in its dynamic behaviour and resulting transverse horizontal displacement profile (THDP) of the deck. In the following section, the MOEA results are presented for the different directions of analysis. The author only presents the result of one run and is aware that the stochastic nature of the algorithm usually demands more runs, however in a previous work by the author (Camacho, Horta, et al. 2020) it had already been shown that there is not much variability in the results between POFs, for these problems. The huge computational cost of GA with structural nonlinear dynamic analyses (NDAs) is the main reason for only using the results of one run. This increases the relevance of this work in the search of surrogate models with ANNs and design rules and guidelines with decision trees.

6.9.4.1 Transversal direction

The optimization results are presented in the objective space in Figure 6.28. There, the solutions are divided into three groups: feasible solutions, which are solutions that were able to resist the seismic action; infeasible solutions, so defined by failing any constraint, particularly the seismic action; and Pareto-optimal solutions, which are defined by being non-dominated solutions, simultaneously for both objectives, by any other solution in the entire population set.
The Pareto-optimal front (POF) is the set of all Pareto-optimal solutions, represented by the blue dots, in the objective space. It is clear from the POF that there exists a knee-region located between x-axis values of 30 000 and 60 000. The knee-region in terms of multi-objective optimization is a region before and after which a small gain in one objective implies a large loss in the other. It is therefore an ideal region for choosing a smaller set of solutions from the POF (Parreiras and Vasconcelos 2009). It is also clear, from the figure, that solutions with costs in the knee-region range vary significantly in terms of performance, that is, the solutions costing close to 30000 have performance values ranging from 0.010 to -0.020. It is, therefore, crucial to be able to understand the factors that influence that variance in performance for solutions with equal costs.

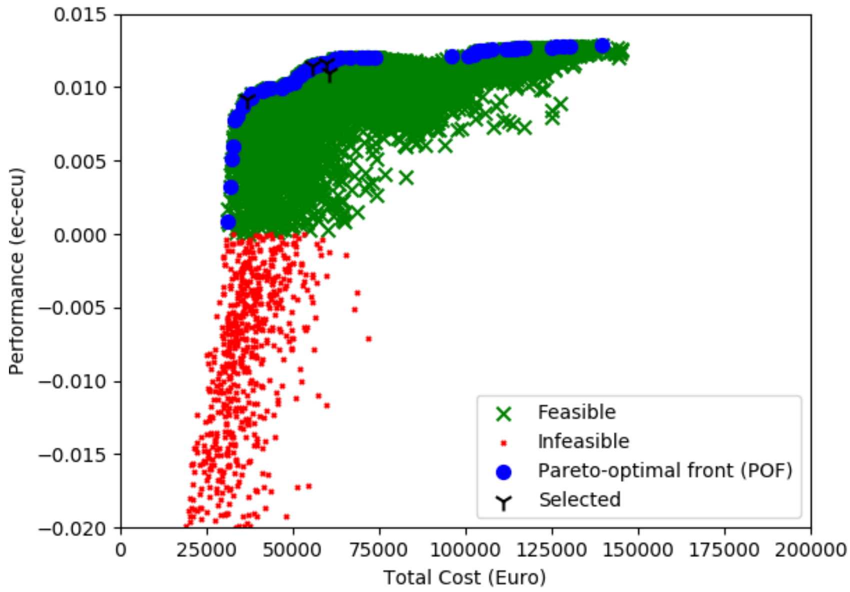

Figure 6.28 Cost vs. Performance objectives. All analysed solutions in the objective-space identified as feasible or infeasible, with POF solutions highlighted.

From the knee region, three solutions are chosen to illustrate the results in the decision-space, i.e., in the space of the design variables. A fourth solution, which is sub-optimal, i.e. does not belong to the POF, is also presented. This fourth solution has similar performance to the three optimal solutions and is presented because it takes different variable values and significantly different dynamic behaviour. The four solutions are presented in Table 6.8 and Figure 6.29.

Table 6.8 Variables from four solutions, where solutions A to C are from the knee-region of the POF, and solution D is a sub-optimal solution with good performance.

	Pier-deck connections				Flex. Steel (%)						
Id	Gr.1	Gr.2	Gr.3	Gr.4	Gr.1	Gr.2	Gr.3	Gr.4	Diam. (m)	Cost (euros)	Perform. (ε_{cu}-ε_c)
A	2	1	1	1	0.60	1.15	1.55	2.90	1.525	55844	0.0114
B	2	1	1	1	0.60	1.80	2.50	2.45	1.475	59761	0.0117
C	2	1	1	1	0.65	0.85	1.10	2.30	1.3	36588	0.0092
D	1	1	1	2	0.65	1.30	3.20	0.75	1.525	60292	0.0110

The POF solutions (A, B and C) have fixed connections for piers in Group 1 and monolithic connections for the other pier groups. Furthermore, the pier groups closer to the centre of the bridge (Groups 3 and 4) have substantially more flexural steel than Groups 1 and 3. The design of solutions A, B and C is done with stiffer piers closer to the centre of the bridge and more flexible piers closer to the abutments. This is the opposite of solution D, which has monolithic connections for Groups 1, 2 and 3 and fixed connections for Group 4. Additionally, in the case of solution D, Group 4 piers (central piers) have very low flexural steel, which together with the fixed connections make more flexible piers. Conversely, Group

3 piers are very stiff, with 3.2% of flexural steel. The reason for both design schemes is that both promote different bridge behaviour. Solutions A to C, increase stiffness of central piers (Groups 3 and 4) and the result is a THDP closer to a third vibration mode, with little displacement at the centre of the bridge and large displacement at the ¼ and ¾ positions. Therefore, the stiffer short piers have less displacement demand even though they also have smaller ultimate displacements. For solution D, on the other hand, the design increases the stiffness of long piers and decreases the stiffness of short piers. The resulting THDP is close to a first mode and the short central piers, due to the low flexural steel and fixed connections have large ultimate displacement. At the same time, the large stiffness of Group 3 piers controls the amplitude of the THDP, thus limiting the displacement demand to the flexible central piers (Group 4).

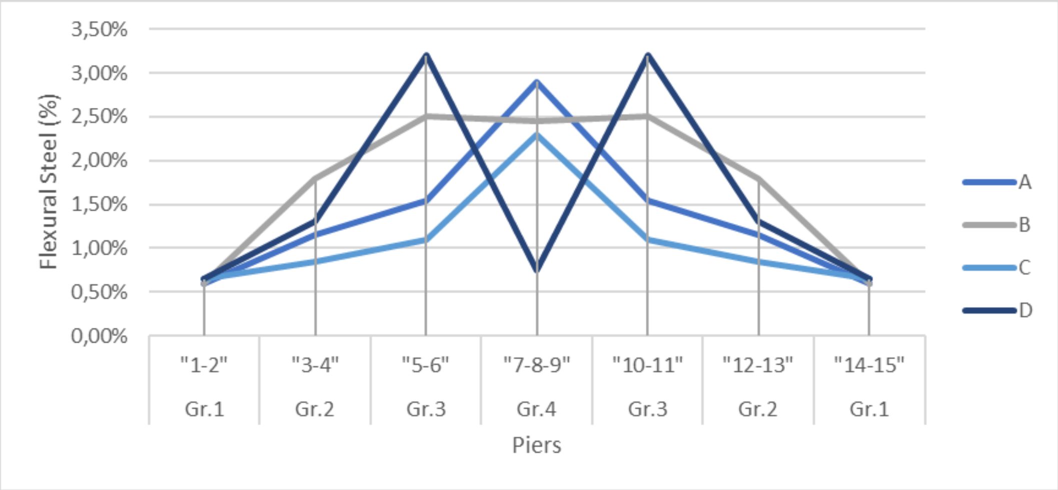

Figure 6.29 Flexural steel distribution along the bridge for each pier group and regarding the four chosen solutions.

6.9.4.2 Longitudinal direction

The optimization procedure was also performed for the longitudinal direction. In Figure 6.30, the comparison between the POFs of both directions is presented. Both POFs seem to have some similarities, which is somewhat expected, even considering that it is an irregular bridge. The reason is that for long bridges with circular piers the frequency in both directions tend to be similar, because the circular piers have the same stiffness regardless of the direction and, in the transversal direction, the effect of the abutments is small due to the length of the bridge. As a result the total inertia forces at the piers are similar in both cases (longitudinal and transversal) even if the ideal distribution of strength is different in both cases. The difference is more noticeable for smaller values of total cost, which makes sense because the performance for larger values of total cost tends to an asymptotical maximum value which is the same for both directions, and so it makes sense to have coinciding POFs for larger values of total cost. Of course, regarding the difference between graphs for lower values of total cost, it is difficult to say how much is due to the stochastic nature of the GA and how much is the actual difference between the POFs from both directions, but the issue of more runs has already been commented on and the reason for having only two runs (one per direction) is associated to the time complexity of the optimization using NDAs.

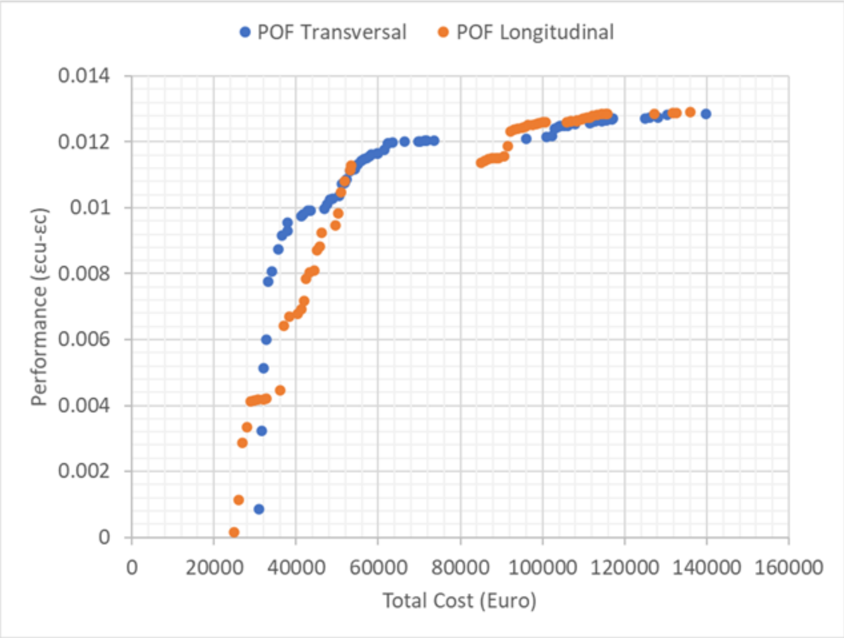

Figure 6.30 POF of each optimization run, longitudinal and transversal.

In Table 6.9, two solutions from the POF were selected, located close to the knee region. It is interesting to compare with the solutions in Table 6.8, where there seems to be less flexural steel reinforcement in the solutions in the longitudinal direction. In addition, the pier deck connections in the longitudinal direction clearly follow the schema of "D". This is expected since in the longitudinal direction the displacement demand is the same for all piers, due to the SDOF, which means that the shorter piers are better off having fixed connections to increase the maximum displacement capacity.

Table 6.9 Variables from two POF solutions, both located close to the knee region and with similar cost and performance values from the solutions in Table 6.8.

	Pier-deck connections				Flex. Steel (%)						
Id	Gr.1	Gr.2	Gr.3	Gr.4	Gr.1	Gr.2	Gr.3	Gr.4	Diam. (m)	Cost (euros)	Perform. (ε_{cu}-ε_c)
E	1	1	1	2	0.7	0.6	0.85	1.00	1.525	44493	0.0081
F	1	1	1	2	0.7	0.6	0.65	1.30	1.675	53324	0.0113

6.9.5 Surrogate Models: application of Machine Learning for regression and classification

In this section, the entire population of solutions generated and analysed during the GA runs are used to train both classification and regression machine learning algorithms. The logic is that the GA, besides performing a multi-objective optimization search, can be thought of as performing a sort of importance sampling in the boundary of the feasibility region of the hypervolume in the direction of the ideal objective vector. In the case of earthquake engineering, that means that the optimization search concentrates its search close to the boundary that separates the solutions that resist and do not resist the earthquake action, in the direction that minimizes the objective functions in the objective space. That means that the observed search space has the potential of having the information to effectively train both classification and regression algorithms for performance and feasibility prediction. Furthermore, the employment of the GA search gives additional use to the big amount of data generated and the computational cost of performing the search with the GA.

In the following sections, the steps and output of training different algorithms with different objectives is shown. The potential of their use to extract more information from the data and to make sense of the results is shown.

Before training any algorithm for supervised learning, as the ones that are presented in this section, the data has to be prepared so that the algorithms perform how they are supposed to. To that end, the following procedures are essential:

- removing or correcting wrong/incomplete instances
- defining new features from intuition/knowledge
- performing dimensionality reduction or feature selection
- standardizing or normalizing the data

This list is by no means exhaustive, and different problems and different data might need different preparation, but in the case of this work, these were the procedures performed on the data obtained from the optimization runs.

6.9.5.1 New added features and feature standardization

The first procedure on the list was to remove a few instances, from the optimization runs, that had not converged and that had been flagged as non-convergent. These instances did not have a value for performance and so their removal is important prior to the training of the learners. The second step was then to improve the feature space by including features that had physical significance, thus potentially increasing the predictive ability of the algorithms. To that end, 6 features were added corresponding to normalized stiffness and normalized axial force in the piers. Since all piers have the same diameter, the normalized axial force is essentially the same for all the piers (ignoring length, proximity to the abutments and amount of flexural steel reinforcement) and is a function of pier diameter since the cross-section of the superstructure is not an optimization variable. The piers were divided into pier groups in which piers have the same flexural steel reinforcement. The sum of the effective stiffness of the piers in each group was computed and a feature was created with the length of the respective bridge section. The last feature added was the total length of the bridge divided by the effective stiffness of the piers. The six added features are then:

- Normalized axial force: v
- Normalized pier-group effective stiffness: $\ln(L_1/K_1)$, $\ln(L_2/K_2)$, $\ln(L_3/K_3)$, $\ln(L_4/K_4)$
- Normalized total effective stiffness: $\ln(L/K_t)$

Following the addition of the new features, the feature set is standardized to get all the features in the same scale. This is to avoid that features that have variance values orders of magnitude higher than others dominate the objective function and hinder the ability of the learner from learning with other features. To all features, the following expression is applied:

$$z = (x - \mu)/s \tag{6.2}$$

Where x is an instance of the original feature, μ is the mean value of that feature, and s the standard deviation of that feature.

6.9.5.2 Random forests for feature selection

The feature selection, which was performed on the original features that were the design variables from the GA plus additional features that were added from experience, was performed by resorting to an ensemble of classifiers called random forests. Going into depth regarding random forests is beyond the scope of this work, but if the reader is interested, he can start by checking (Rokach and Maimon 2014). In summary, an ensemble learner is a collection of weak learners whose powerful performance comes from the joint prediction by all of its components. Typically, each individual component is worse (or simpler) than a more complex individual classifier, however, the joint performance of the ensemble usually supersedes that of the complex single classifier. This idea of wisdom of crowds is based on the Condorcet Jury theorem proposed by the Marquis of Condorcet in the 18th century. In the theorem, it was proposed that the probability of a collection of voters being correct, whose individual probability of being correct is only slightly higher than a coin toss (0.5), approaches 1.0 as the number of voters tends to infinity.

In the case of a random forest, the individual voters are weak individual trees built on a random subset of the data and the features. One of the properties of random forests is their capability in defining feature importance, based on the information gain by different trees that used different features to classify the instances. To generate the random forests the RandomForestClassifier from the scikit-learn (Pedregosa, et al. 2011) Python library was used.

6.9.5.3 Neural networks for regression

The learner that was trained for prediction was an artificial neural network (ANN), using TensorFlow (Abadi 2016) and Keras (Chollet 2015), and for classification was a classification tree using the CART algorithm, available in the scikit-learn library (Pedregosa, et al. 2011). Concerning the ANN, a traditional "vanilla" multilayer perceptron (MLP) architecture was used with two hidden layers, with 6 neurons each, and ReLU activation functions at the hidden layer, as well as L2 regularization after the first hidden layer to aid in preventing overfitting of the models on the training data. The Adam optimizer was chosen for the network optimization, and the mean square error was taken as the loss function. The network was trained over 100 epochs with 80% of the data set used for training and 20% for validation. In Figure 6.31, the ANN architecture is shown. The 3 nodes in the input layer are the three best input features obtained from the feature selection with the random forest algorithm. The output (y) is the performance (ε_{cu}-ε_c) shown in Table 6.8 and Table 6.9.

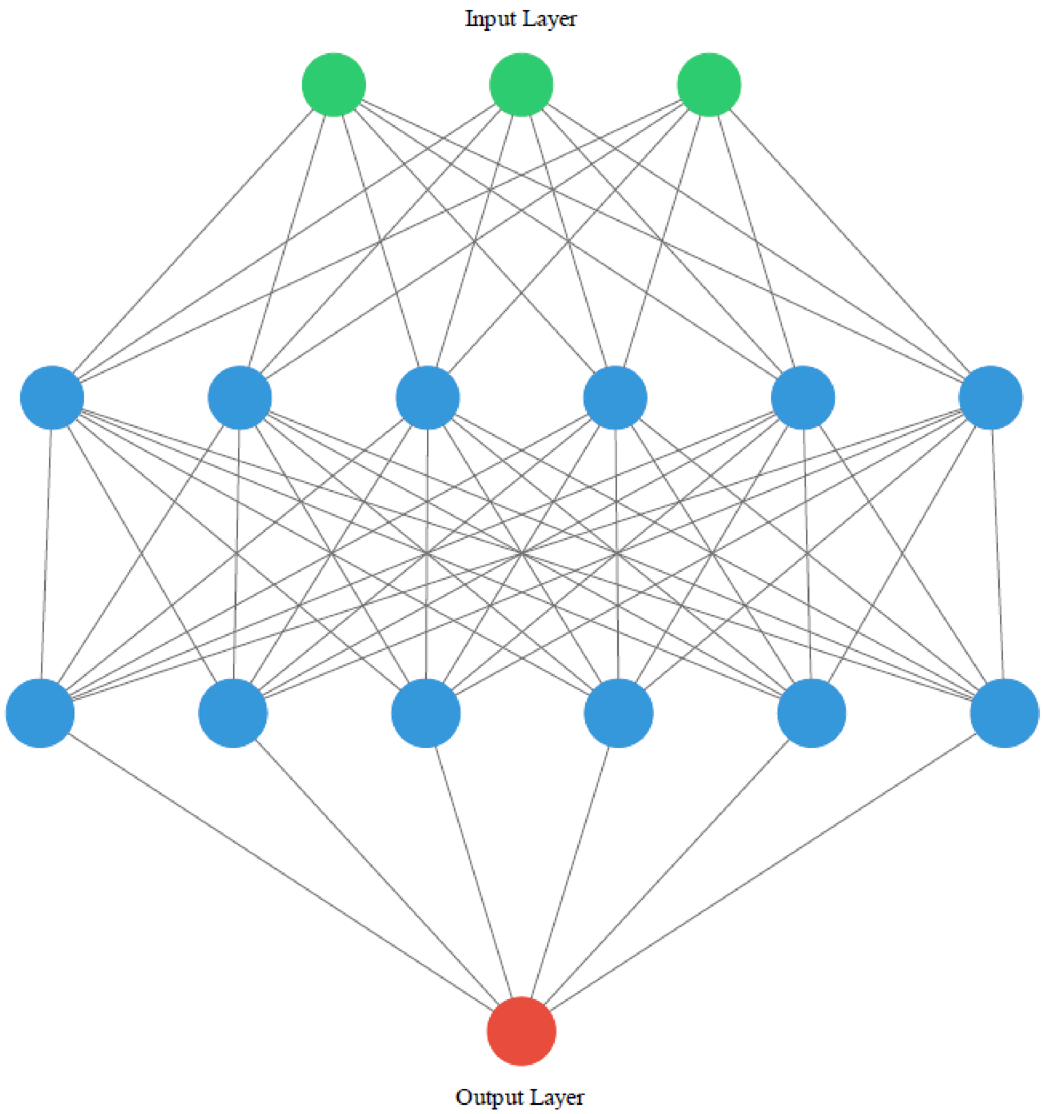

Figure 6.31 A visualization of the trained ANN architecture

6.9.5.4 Decision trees for classification and extraction of design rules

The classification tree algorithm employed is the CART learner available in the scikit-learn library (Pedregosa, et al. 2011). The CART stands for Classification and Regression Tree, which as the name entails, is an algorithm that can be used for both classification and regression problems. In this instance, it will be applied for classification.

The behaviour of the bridge is distinctively nonlinear, with the design of each pier not only influencing its own displacement demand, but also the displacement demand of other piers and the global dynamic behaviour of the bridge. This nonlinear behaviour makes the design of the bridge somewhat difficult. The optimization procedure in the previous section not only provides a series of possible solutions, but is also an efficient sampling tool, obtaining solutions with a high likelihood of being feasible, as the algorithm's search progresses. The entire population of analysed solutions obtained during the optimization can be used afterwards to define which features are more important to obtain solutions with good seismic behaviour. To that end, the use of classification trees, coupled with feature selection, can be used to define design rules.

A classification tree groups all the instances in a data set according to pre-determined classes. In this case, two classes were defined as “FAIL” and “OK”, characterizing instances that failed to resist the earthquake action and instances that resisted the earthquake action, respectively. The classification tree chooses the features to perform each split according to information gain, i.e., at each branch the feature that best separates the data set is chosen, until reaching the leaf node, which classifies the instance according to the prevalent predefined class. As with the regression models, the classification tree algorithm was trained on both the longitudinal and transversal direction data.

Additionally, due to the imbalanced nature of the data set, which has much more OK labelled data instances than FAIL labelled data instances, sub-sampling was employed with the use of a combined sampling technique (over-sampling and under-sampling) defined as SMOTE-Tomek technique. The SMOTE (Synthetic Minority Oversampling Technique) and Tomek Links techniques are available from the Python library imbalanced-learn (Lemaître, Nogueira and Aridas 2017). The use of these techniques allowed to generate a balanced dataset with the same number of OK and FAIL instances. This allows the algorithm to not emphasize one class over the other when the model is being created.

6.9.6 Results from the application of the Machine Learning techniques

6.9.6.1 Feature importance and feature selection

The random forest was generated with 1000 estimators (trees) and was trained on the data of each optimization run (transversal and longitudinal). The instances were divided into four classes to be used for the classification by the random forest. The classes were a discretization of the performance objective where instances with negative values are classified as “FAIL”, and positive values are classified as “Level1”, “Level2” and “Level3” according to two arbitrarily defined split values for the performance objective. The result of the feature importance by each random forest trained on each data set (transversal and longitudinal) are presented in Figure 6.32 and Figure 6.33, respectively.

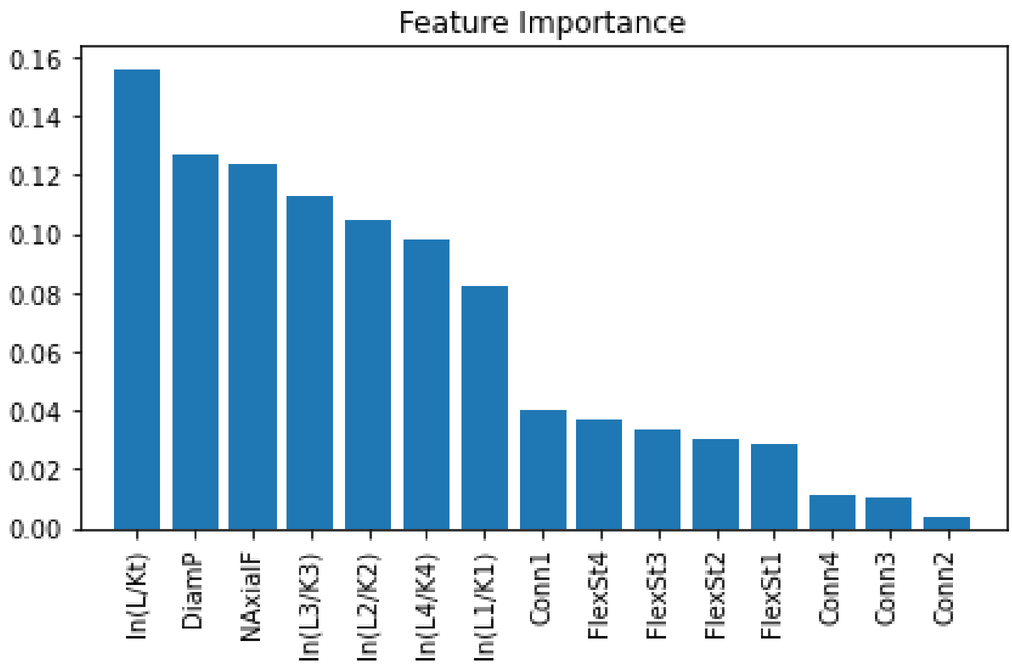

Figure 6.32 Feature importance rank for the transversal direction data

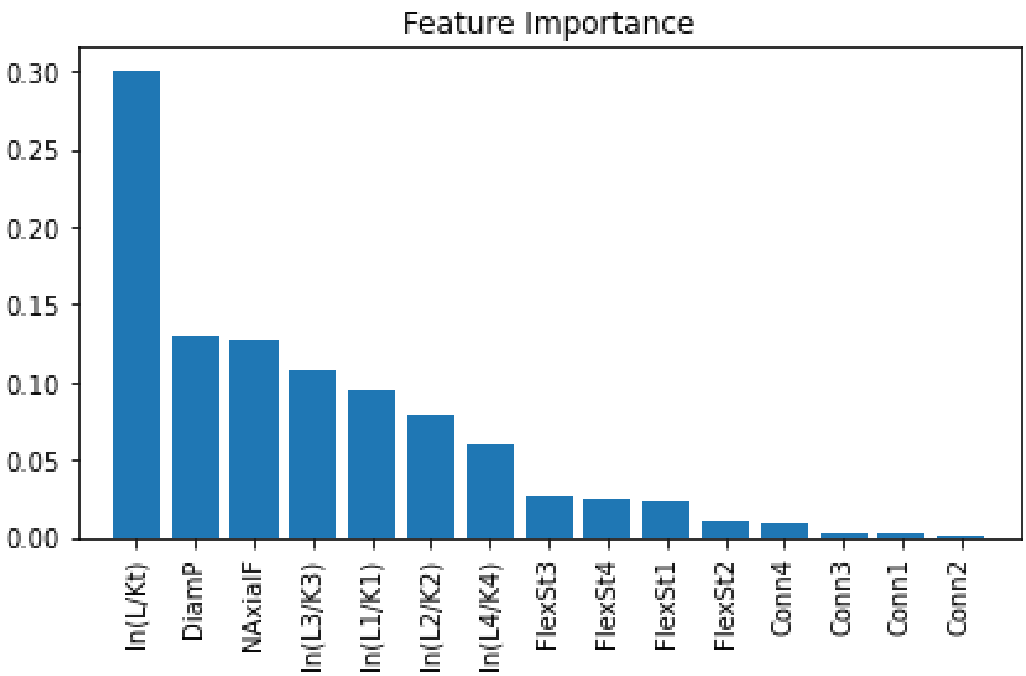

Figure 6.33 Feature importance rank for the longitudinal direction data

In both figures:

- $\ln(L/K_t)$ represents the normalized total effective stiffness.
- $\ln(L_1/K_1)$, $\ln(L_2/K_2)$, $\ln(L_3/K_3)$ and $\ln(L_4/K_4)$ represent the normalized pier group effective stiffness.
- NAxialF is the normalized axial force in the piers.

- $FlexSt_1$, $FlexSt_2$, $FlexSt_3$ and $FlexSt_4$ represent the flexural steel in the piers from each pier group.
- $Conn_1$, $Conn_2$, $Conn_3$ and $Conn_4$ represent the pier-deck connections used in each pier group.

From both figures it is clear that the inserted features do a better job in splitting the data for the classification according to performance compared to the decision variables from the optimization problem, which means that the new features were very good inclusions in the feature set, particularly L/K_t which is ranked 1st for both data sets. It is also interesting to see that L/K_t has more importance in the longitudinal direction than in the transversal direction, which is expected since in the longitudinal direction the structural behaviour can be reduced to a single DOF, and so total effective stiffness is closely related to the displacement demand.

From these results of feature importance, the decision has been to select two of the five stiffness-related features that were added through feature engineering plus the normalized axial force (v – NAxialF) to be used in the regression models. The diameter, even though it is shown to be the second ranked feature, is essentially equivalent to v (NAxialF) and the latter is more non-specific because it is adaptable to other shaped piers and also implies the weight/mass of the superstructure. Therefore, to train the ANN in the next section, the following features are used: v, $\ln(L_3/K_3)$, and $\ln(L/K_t)$.

6.9.6.2 Neural networks for regression

6.9.6.2.1 Transversal direction

The predicted y and the actual y are shown in Figure 6.34, where it is shown that the algorithm was able to learn well with the given features. The mean squared error (MSE) is 3.255e-06. In Figure 6.35 the mean absolute error (MAE) for both the training and validation sets are presented over the 100 training epochs. It is clear that both error graphs are very close and follow the same trend, which indicates that overfitting is unlikely to have occurred. Furthermore, in Figure 6.36 the prediction results for the test set reinforce this idea.

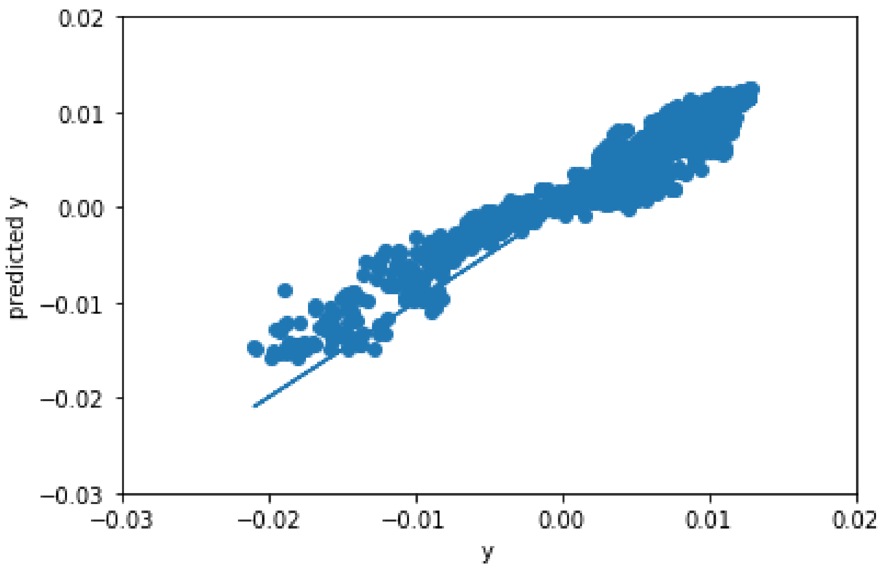

Figure 6.34 Predicted y vs. real y for all instances in the transversal direction.

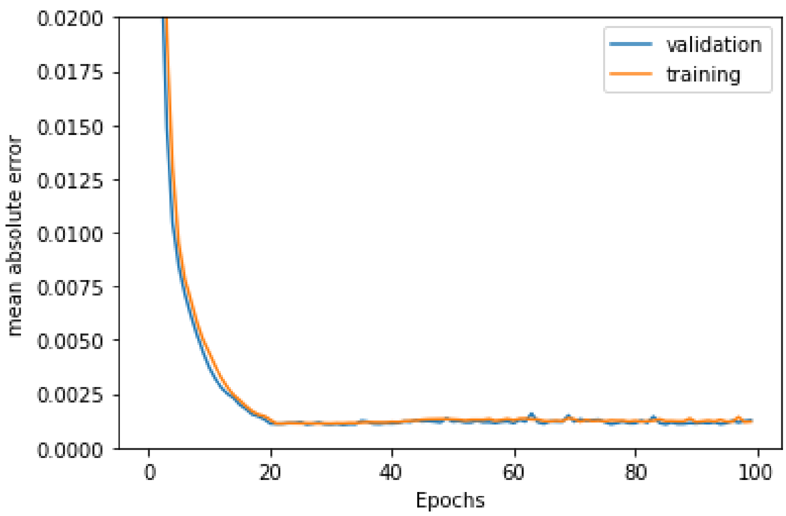

Figure 6.35 MAE for training and validation during the ANN training, for the transversal direction.

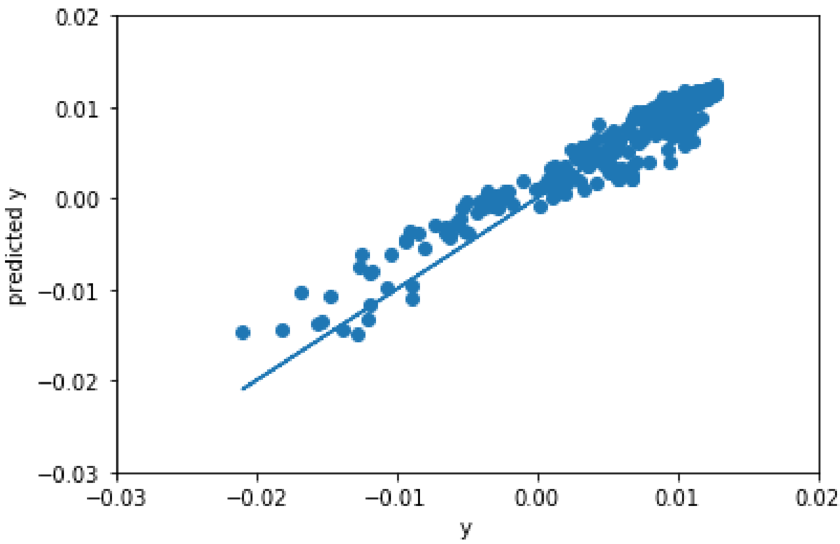

Figure 6.36 Predicted y vs. real y for the test set of the transversal direction.

From the results it seems that an ANN trained on the added features, concerning stiffness and reduced axial force, is able to generalize well for unseen solutions and provides a good approximation for the earthquake performance of irregular bridges. This suggests that this ANN could be employed as a surrogate model for an optimization run, with a similar bridge, at the very least on an initial phase to approximate the feasible region.

In the following, the same approach is applied to the data in the longitudinal direction.

6.9.6.2.2 Longitudinal direction

The ANN in Figure 6.31 is trained on the data that corresponds to the optimization run in the longitudinal direction, over 30 epochs. In Figure 6.37 and Figure 6.38, the results of the ANN trained on the longitudinal data are shown. The results suggest good generalization ability of the neural network based on the patterns of predicted output against the actual output in both the test and training data. The value of the MSE is equal to 4.77e-06 which is slightly higher than for the transverse direction model.

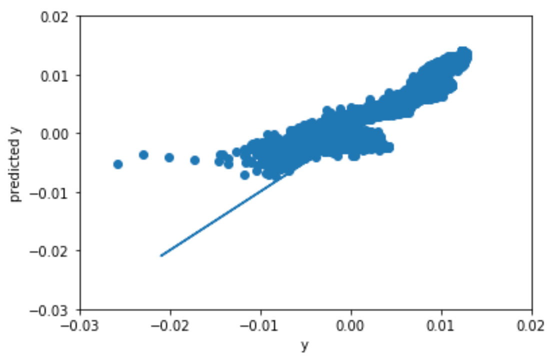

a)

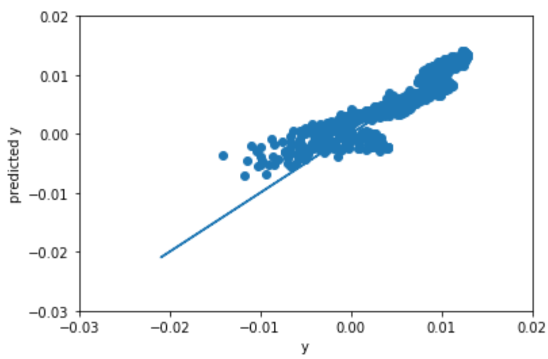

b)

Figure 6.37 Prediction of y, for the longitudinal direction, a) over the entire set and b) only for the test set.

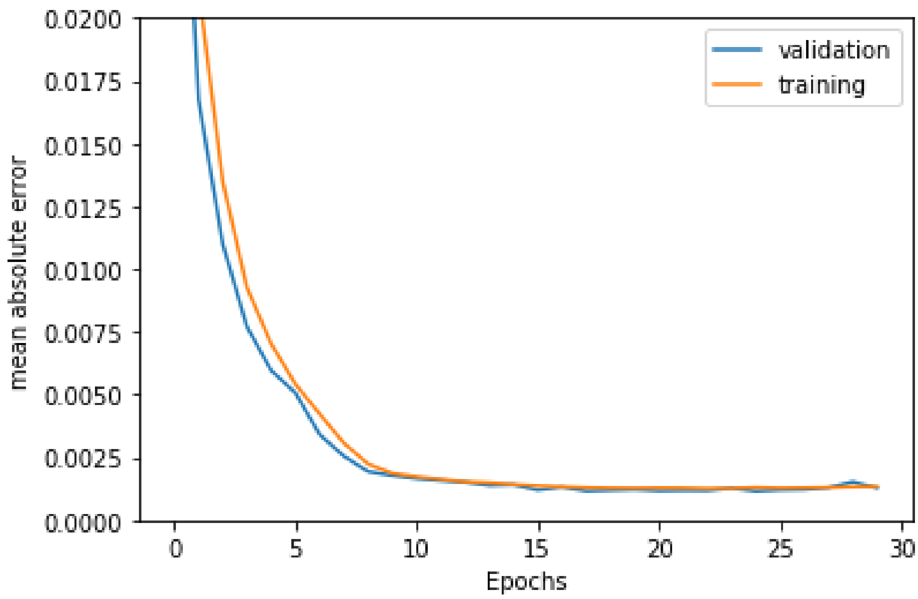

Figure 6.38 MAE for the training and validation set per epoch during training.

6.9.6.3 Classification trees

6.9.6.3.1 Transversal direction

The obtained classification tree is shown in Figure 6.39. The features that best divide the instances are, above all others, ln(L/K_t) and ln(L_3/K_3). The tree is concise, with only 4 levels and 15 nodes, and has high accuracy, with 95% correctly classified instances, as seen in Table 6.10. In Figure 6.40 the tree's normalized confusion matrix is given, where the correctly and incorrectly classified instances per class are displayed.

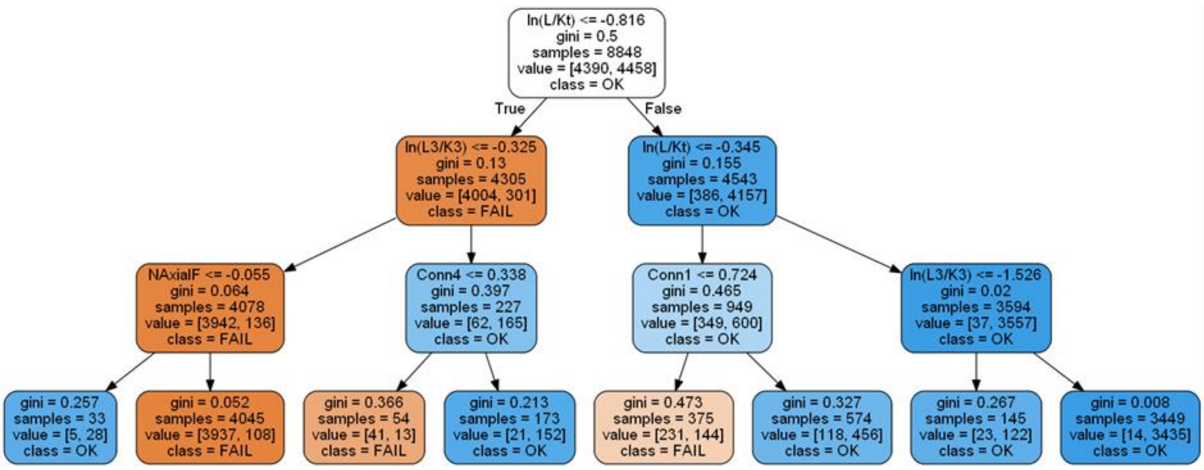

Figure 6.39 Classification tree – transversal direction. ln(L/K_t)-total bridge length divided by the total pier effective stiffness; NAxialF – Normalized axial force; ln(L_3/K_3) – Length of the bridge section corresponding to Group 3 piers divided by the effective stiffness of Group 3 piers, $Conn_4$ and $Conn_1$ – type of connection in pier groups 4 and 1 respectively (negative values correspond to monolithic connections and positive values correspond to fixed connections).

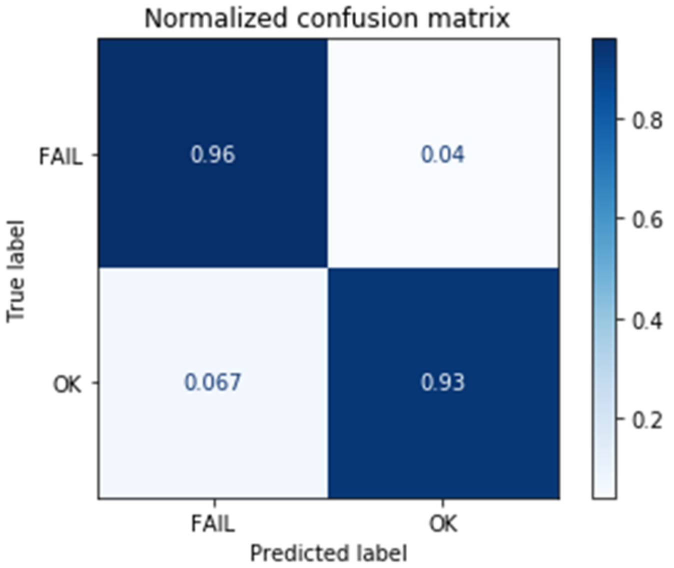

Figure 6.40 Classification tree's normalized confusion matrix – transversal direction.

Table 6.10 Classification metrics – transversal direction

	precision	recall	f1-score
FAIL	0.94	0.96	0.95
OK	0.96	0.93	0.94
accuracy			0.95
macro avg	0.95	0.95	0.95
weighted avg	0.95	0.95	0.95

The results show very good classification accuracy, with high recall and precision for both classes. Particularly the FAIL class has high recall and only 4% of false positives (FAIL predicted as OK). The model has a good performance considering the need of only four levels and 15 nodes and 95% accuracy. The structural meaning of the features used in each node are very important since the decision tree translates a structural meaning, which makes sense for design engineers. The small tree also implies very little chance of overfitting and a useable model for design rule definition.

6.9.6.3.2 Longitudinal direction

The data pertaining to the longitudinal direction was used to train the classification tree learner. The resulting tree is in Figure 6.41, the normalized confusion matrix in Figure 6.42, and the classification metrics in Table 6.11.

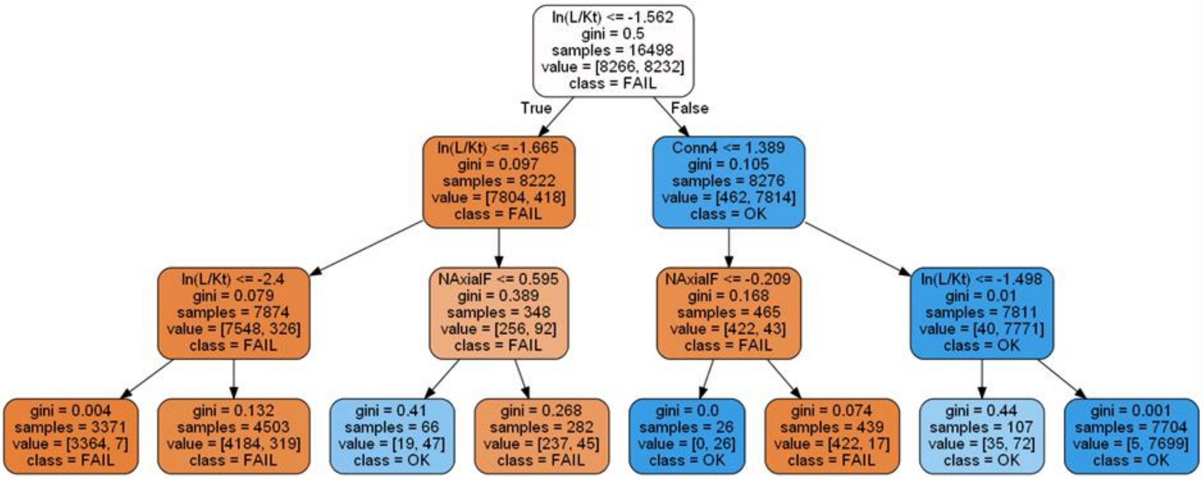

Figure 6.41 Classification tree – longitudinal direction. ln(L/K_t)-total bridge length divided by the total pier effective stiffness; NAxialF – Normalized axial force; $Conn_4$ – type of connection in pier group 4 (negative values correspond to monolithic connections and positive values correspond to fixed connections).

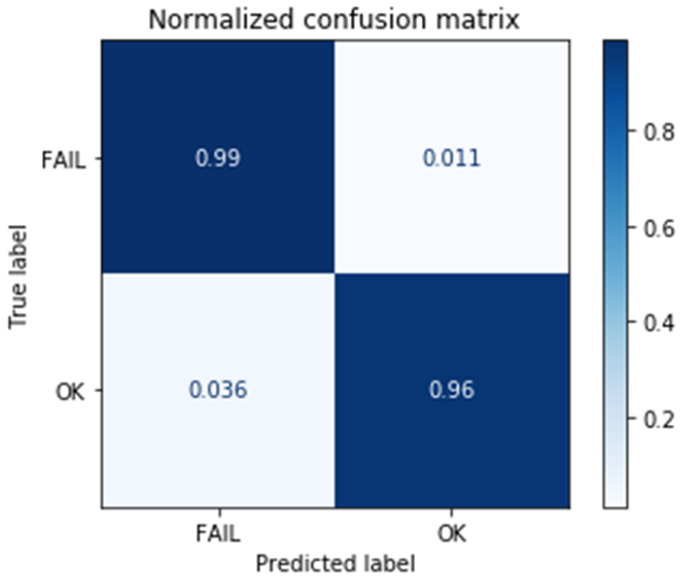

Figure 6.42 Classification tree's normalized confusion matrix – longitudinal direction.

Table 6.11 Classification metrics – longitudinal direction.

	precision	recall	f1-score
FAIL	0.96	0.99	0.98
OK	0.99	0.96	0.98
accuracy			0.98
macro avg	0.98	0.98	0.98
weighted avg	0.98	0.98	0.98

The tree has high accuracy with 98% and has very high recall for the FAIL class which means it is very strong in identifying FAIL instances, with only 1.1% of false positives. Similarly to the transversal direction, the features used to split the data in the nodes are $\ln(L/K_t)$, NAxialF and $Conn_4$.

6.9.6.4 Generalization ability of the models with data from other bridges

In this section, the models are used on previously unseen data from other bridges with different lengths and irregularities. Additionally, the models are used on the data in the other direction, i.e., the longitudinal model with the transversal data and vice-versa.

6.9.6.4.1 Transversal direction analyses data belonging to two bridge typologies

Two bridge typologies are introduced and were subjected to NDAs in the transversal direction. The generation of bridge solutions was done by running the GA for 30 generations. The two bridge typologies are presented in the following table, one with a length of 540 meters and a different pier irregularity. Bridge 2 is 480 meters long and has a very different irregularity layout, having all piers equal in length. The idea is to use the generated solutions from both typologies to test the generalization ability of the models for unseen data and different bridges.

Table 6.12 The two introduced bridge typologies.

Bridge	Pier lengths (m)	Pier groups (pier position)
1	11 11 14 14 11 11 7 7 7 7 7 11 11 14 14 11 11	(1 2 16 17) (3 4 14 15) (5 6 12 13) (7 8 9 10 11)
2	7 7 7 7 7 7 7 7 7 7 7 7 7 7 7	(1 2 14 15) (3 4 12 13) (5 6 10 11) (7 8 9)

6.9.6.4.1.1 Regression models

In Figure 6.43 and Figure 6.44, the scatter plots concerning the predicted y and actual y values are given for both bridges. 1 and 2 respectively.

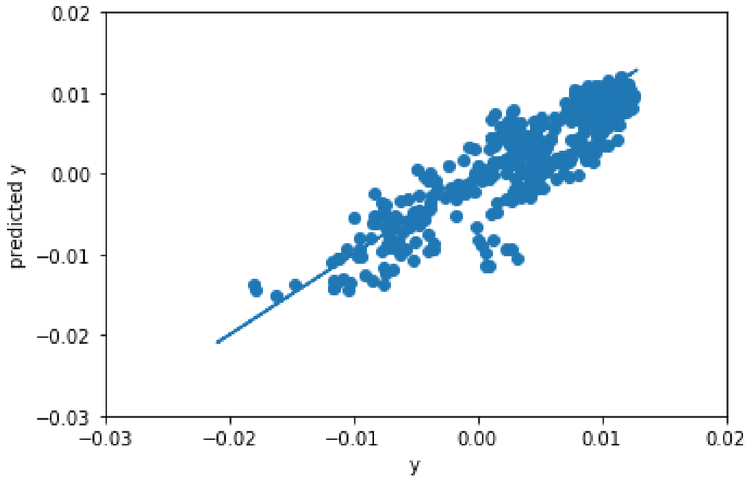

Figure 6.43 Transversal regression model predictions for Bridge 1 data.

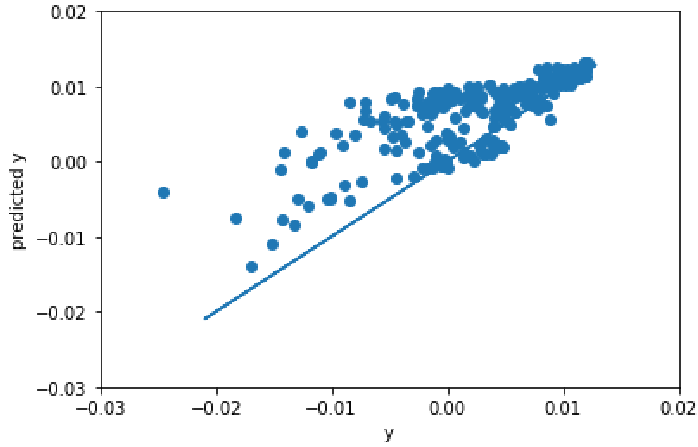

Figure 6.44 Transversal regression model predictions for Bridge 2 data.

Looking at both figures, it seems that in both cases the model is able to generalize to other bridges even though there has been loss of accuracy compared to the results with the case-study used to train the models. The loss metric MSE has value of 1.12e-05 and 5.78e-05 for Bridge 1 and Bridge 2, respectively. The MSE for Bridge 2 is an order magnitude larger than the MSE registered with the original case-study bridges.

The models are able to generalize well concerning Bridge 1, which has a similar irregularity layout to the bridge that created the model. Regarding the results for Bridge 2, there is more dispersion, and more loss of accuracy than for Bridge 1. This makes sense since Bridge 2 and the case-study bridge on which the model was trained are very different in terms of irregularity layout. It seems that the models based on ANN are able to capture the behaviour of bridges since their ability to generalize is not lost even with a somewhat significant difference in terms of irregularity layout and also bridge length. This suggests that these might be good choice for surrogate models with the presented variables. It is expected that a model that is trained on solutions from many bridge typologies might improve on these results.

6.9.6.4.1.2 Classification models

Regarding the classification models, their performance is also mixed. The model was very able to generalize for Bridge 1, with good results as seen in Figure 6.45 and Table 6.13, with an accuracy of 0.90. However, for Bridge 2, the results were poor with a low accuracy of 0.63 and a very low recall value for the FAIL class, as seen in Figure 6.46 and Table 6.14. This suggests that, in terms of classification models based on decision trees, their generalization for models with very different irregularity layouts may not return good results.

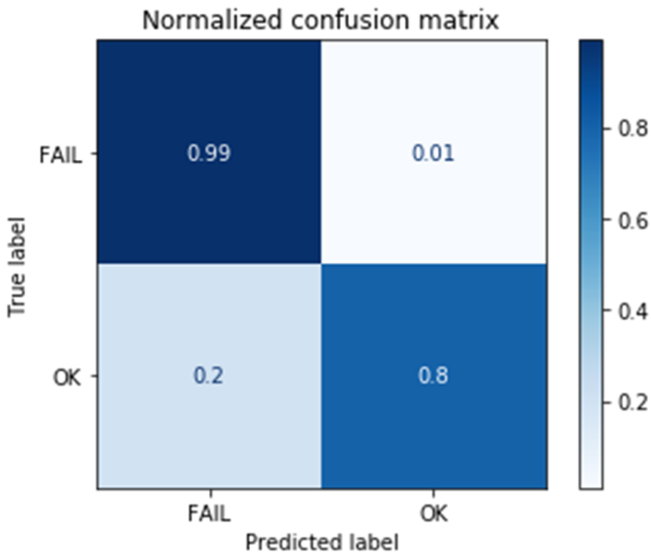

Figure 6.45 Transversal classification model's normalized confusion matrix for Bridge 1 data.

Table 6.13 Classification metrics – transversal model for Bridge 1.

	precision	recall	f1-score
FAIL	0.83	0.99	0.91
OK	0.99	0.80	0.89
accuracy			0.90
macro avg	0.91	0.90	0.90
weighted avg	0.91	0.90	0.90

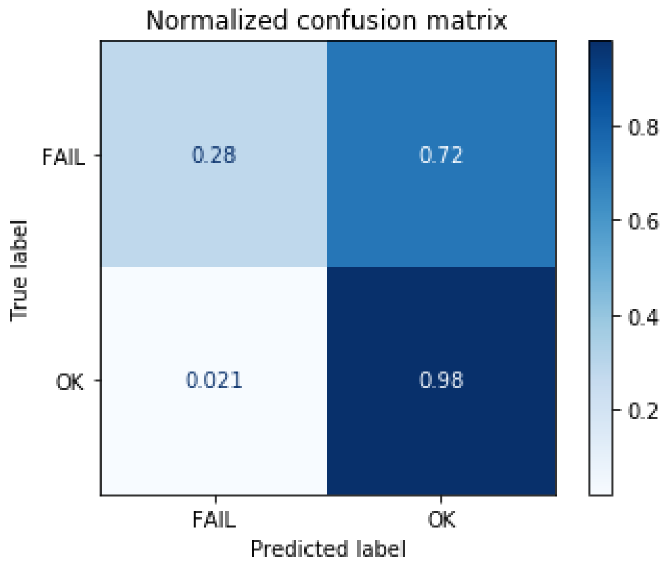

Figure 6.46 Transversal classification model's normalized confusion matrix for Bridge 2 data.

Table 6.14 Classification metrics – transversal model for Bridge 2.

	precision	recall	f1-score
FAIL	0.93	0.28	0.43
OK	0.57	0.98	0.72
accuracy			0.63
macro avg	0.75	0.63	0.57
weighted avg	0.75	0.63	0.57

6.9.6.4.2 Longitudinal model with transversal data and vice-versa

6.9.6.4.2.1 Regression models

In Figure 6.47 and Figure 6.48, the transversal model predicts the longitudinal data, and the longitudinal model predicts the transversal data, respectively. It can be seen that, even though the dynamic behaviour is different, since the longitudinal direction is essentially a SDOF problem and the transversal direction is an MDOF, both models are able to catch some of the behaviour. This shows, as did the section on prediction with the two test bridges (Bridge 1 and 2), that surrogate models based on ANN and the features defined in this work can generalize relatively well for different bridges. The MSE values for each case are 7.30e-06 and 1.14e-05 respectively, for the transversal model with longitudinal data and the longitudinal model with transversal data. The MSE results are all shown in Table 6.17 for both models on the various data sets from different case-studies.

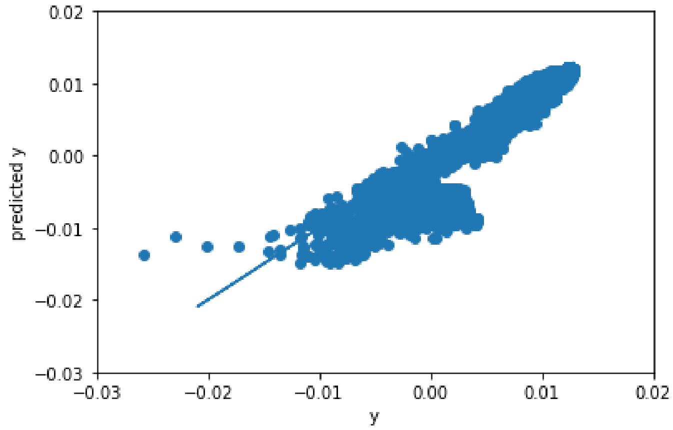

Figure 6.47 Transversal model predictions with longitudinal data.

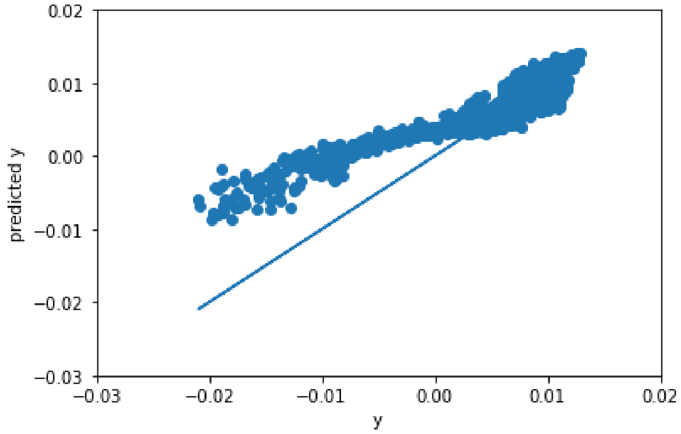

Figure 6.48 Longitudinal model predictions with transversal data.

6.9.6.4.2.2 Classification models

In Figure 6.49 and Table 6.15, the results of the transversal data predicted with the longitudinal model, and in Figure 6.50 and Table 6.16, the results of the longitudinal data predicted with the transversal model.

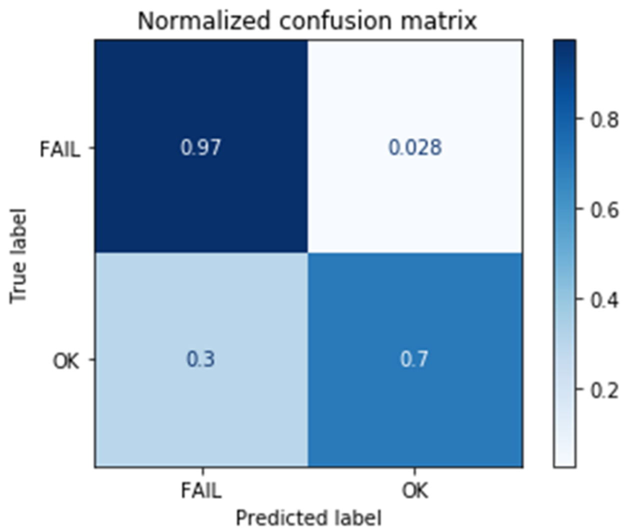

Figure 6.49 Classification tree's normalized confusion matrix – longitudinal tree with transversal data.

Table 6.15 Classification metrics – longitudinal tree with transversal data.

	precision	recall	f1-score
FAIL	0.77	0.97	0.86
OK	0.96	0.70	0.81
accuracy			0.84
macro avg	0.86	0.84	0.83
weighted avg	0.86	0.84	0.83

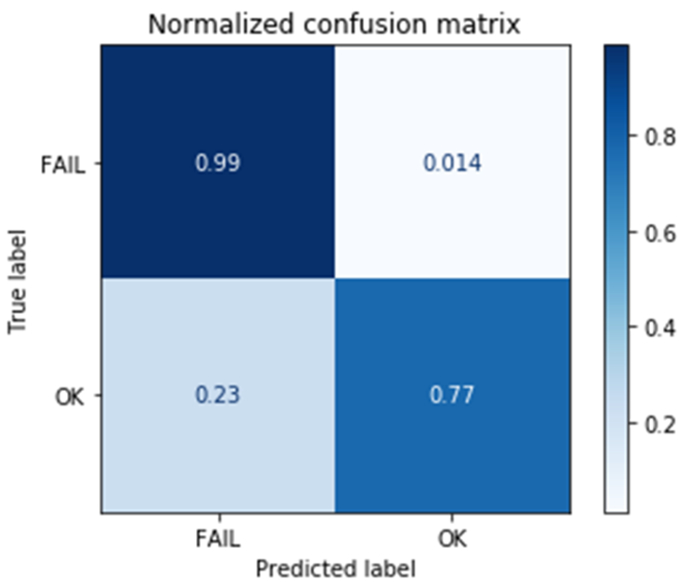

Figure 6.50 Classification tree's normalized confusion matrix – transversal tree with longitudinal data.

Table 6.16 Classification metrics - transversal tree with longitudinal data.

	precision	recall	f1-score
FAIL	0.81	0.99	0.89
OK	0.98	0.77	0.86
accuracy			0.88
macro avg	0.90	0.88	0.88
weighted avg	0.90	0.88	0.88

The results from the predictions with the models of the opposite direction have, as expected, less accuracy. However, the metrics still show relatively good results with accuracies of 0.84 and 0.88 for the longitudinal model and transversal model, respectively. Both models have high value for the recall of the FAIL class and low precision value. Conversely, the precision for the OK class is high while recall is low. That is, both models have, with the data in the opposite direction, little false negatives for the FAIL class (false positives). This means that the models are more prone to predicting an OK as a FAIL than the other way around, thus being conservative. This is in line with the no-free-lunch theorem where the improvement in classification for one class implies the loss in the other.

6.9.6.5 Summary of model results

In Table 6.17, the main metrics of both the regression and classification models are presented, concerning their application to each of the case-studies. In said table, when the model and the data match (T/T and L/L) it corresponds to the error metrics of the model on its own data set, i.e., the data set from where its training set was obtained. The other cases correspond to the error metrics of the model on data sets from other case-studies.

Table 6.17 Comparison of mean square errors of the regression models on data from different case-studies. T - transversal direction; L - longitudinal direction; B1 - Bridge 1; B2 - Bridge 2

	Model/Data	**T/T**	**L/L**	**T/B1**	**T/B2**	**T/L**	**L/T**
Algorithm	***Evaluation Metric***						
ANN - regression	*Mean squared error (MSE)*	3.25e-06	4.77e-06	1.12e-05	5.78e-05	7.30e-06	1.14e-05
CART - Classification	*Accuracy*	0.95	0.98	0.90	0.63	0.88	0.84
CART - Classification	*FAIL Recall*	0.96	0.99	0.99	0.28	0.99	0.97
CART - Classification	*OK Recall*	0.93	0.96	0.80	0.98	0.77	0.70

It is seen from the evaluation metrics that the lowest error values (or highest accuracy/recall) are found for the models on their own data set, which is expected. This is true for both the classification and regression models. What is also clear is that the models generalize well for other case-studies, with the exception of the B2 case-study, where the error values are higher. It so happens that B2 corresponds to the transversal direction data of a regular bridge (bridge with equal length piers), as seen in Table 6.12. The regularity profile of B2 in terms of pier height is significantly different from that of the other case-studies, and for that reason, there is less accuracy and larger error in the models' approximations to B2's data. That may have to do with, not only the different dynamic behaviour of B2, compared to the other case-study bridges in the transversal direction, but also to the possibility of there being many instances of B2 that have different critical piers to the other case-studies. Also interesting is the ability of the longitudinal direction model being able to generalize in the transversal direction and vice-versa. This happens for both the regression and classification models. This shows that regardless of the direction of the earthquake, and even though the dynamic behaviour is very different between the longitudinal and transversal directions, macro features such as mean reduced axial force in the piers, and total length divided by total effective stiffness can be very important in characterizing the bridge's ability to withstand an earthquake, regardless of its length, regularity profile and direction of the earthquake action.

6.9.7 Conclusions

Irregular structures are both difficult to analyse and design, especially if they are prone to having strong nonlinear behaviour. This is the case with long irregular bridges. In this section, a methodology is presented composed by several procedures which employ different machine learning algorithms: genetic algorithms (GA), classification trees, artificial neural networks (ANN) and random forests for feature selection, applied to the seismic study of a long irregular bridge, in both the longitudinal and transversal direction. The genetic algorithm, an NSGA-II, performs an optimization of the pier design variables for earthquake resistance, while the other learners make use of all analysed solutions generated during the optimization run, as input to create surrogate models and to define design rules. In the process, the search effort of the GA is given further use in the definition of important features and in classifying the solutions according to their ability to resist the earthquake. In addition, with the neural network for regression, a surrogate model is obtained capable of substituting the FEM analysis in the fitness analysis of future GA runs. The obtained results are very useful in defining strategies to design irregular bridges and allow to focus on specific characteristics of the structure to assess whether a design solution is good or not, without having to perform a full NDA analysis. The application of this methodology to many different case-studies can produce an ensemble of classifiers and regressors that can be used as surrogate models in preliminary design stages. The possibilities and applications are numerous and make sense in any situation where the nonlinear and complex nature of the problem hinders the ability to easily analyse or design a solution. Furthermore, these methodologies can be used to confirm or even find new design rules that are usually employed and are associated with engineering design experience.

6.9.7.1 Future works

In future studies, the idea is to apply these methodologies to several other types of case-studies, with different typologies and irregularities, and seeing the cross-classification accuracy of trees on bridges with different typologies than the one they were trained on. Also, analysing the same cross-accuracy of the regression models and their viability in substituting the nonlinear analysis during the optimization procedure. The constitution of an ensemble surrogate model that joins all the bridge typologies in one would be the end goal.

7 Effect of spatial variability of seismic strong motions on long regular and irregular RC bridges.

Long bridges and other lifeline systems are particularly susceptible to the spatial variability of earthquake actions. Even though it is a matter that has been substantially studied in the past decades, there are still plenty of issues with the engineering application of earthquake spatial variability. One of the difficulties is generating displacement time-histories with zero initial and small residual displacement values. This is essential to obtain results that have good quality in terms of the pseudo-static effects. Another difficulty is the uncertainty associated with the simulation of the spatial variability of the seismic ground motions in engineering applications (Zerva, Falamarz-Sheikhabadi and Poul 2018). In this study, the conditional method for simulation of spatially variable ground motions is used and the respective displacement time-histories are generated. These time-histories are then applied to perform seismic analysis of a set of long irregular RC bridges, with different irregularity layouts and different total lengths. The goal of this study is to ascertain the impact of spatial variability on the seismic behaviour of these structures, according to their length, irregularity and to the coherency model of the strong motions and comparing the results with the case without spatial variability. The relative importance between dynamic and pseudo-static effects is also ascertained for each case-study. Finally, the definition of the cases in which the effects of the spatially variable seismic ground motions (SVSGMs) are more detrimental than those of the uniform ground motions.

7.1 Introduction

The large majority of works in seismic engineering, which employ dynamic analysis, assume the seismic action affecting a structure as uniform, that is, a single (per direction) strong motion applied simultaneously to all the structure's supports. This is done essentially for two reasons: one, is that most structures have overall dimensions such that the differential motions are not influential on the seismic behaviour; and two, because it is more practical to ignore the complex characteristics of seismic actions and adopt simplified approaches proposed by design codes to define the seismic loading pattern of structures (Zerva, Falamarz-Sheikhabadi and Poul 2018). In any case, it is clear that for lifelines such as bridges (long bridges in particular) and pipelines or large footprint structures such as dams, spatial variability may have a significant impact on the earthquake response of the structure. Besides affecting the dynamic behaviour there are pseudo-static effects, which can be more detrimental to the safety of those structures than the actual dynamic effects. In chapter, the impact of spatial variability is studied in its engineering application to long irregular bridges, with different irregularity layouts and varying lengths. There are different works that define types and measures of irregularity concerning pier lengths, some focus on the layout of the irregularity (Akbari and Maalek 2018) (Kappos, Saiidi, et al. 2012), others focus on the level of irregularity based on the ratio between minimum and average pier lengths (Camacho, Lopes and Oliveira 2020) (Soleimani, et al. 2017).Two irregularity profiles, concerning pier layout, are chosen to generate the case-study bridges. One of the typologies is regular (all piers have the same length) and another one irregular with short central piers. The bridges are then generated according to both profiles and with different total lengths. The goal is to ascertain the impact on RC bridges' earthquake behaviour, according to those variables (irregularity and length) and also concerning some uncertainty associated with the spatial variability itself, namely regarding the choice of coherency model. The relative importance of dynamic and pseudo-static effects will be compared against the effects of not considering spatial variability in the analysis.

Spatial variability of earthquakes has been studied extensively in the last 40 years, initially concerning the seismological aspect and the definition of coherency models from array data. However, in the last decades plenty of works have been done in applying the coherency models in the generation of time-histories which could then be applied to earthquake engineering of structures. There have been several difficulties and there still are quite a few in the application of spatial variability, specifically concerning the generation of displacement time-histories, the uncertainty that revolves around the coherency models and other parameters associated with the earthquake action, and the computational burden associated with such analyses, to name just a few. First, it is necessary to clarify the meaning of coherency and pseudo-static effects. Coherency represents the correlation between the phases of two signals at different stations/positions (j and k) and it is obtained from the smoothed cross spectrum of the motions between the two stations j and k, normalized with respect to the corresponding power spectra (Zerva and Zervas 2002). As for the pseudo-static effects, these can be defined as the imposed displacements that originate from the difference in phase between the displacement time-histories at different positions (stations) of the structure. The intuition is that with seismic variability the difference in phase of the seismic waves at different points causes each support to have a different value of imposed displacements at any given instant.

Some of the first studies on spatial variability can be traced to the works on the SMART-1 array (Strong Motion ARray in Taiwan) all through the 1980s and 1990s. In (Abrahamson, Bolt and Darragh, et al. 1987) a review is done on the studies and applications of SMART-1 between 1980 and 1987, where the studies are divided according to the theme: spatial coherence; effects of non-vertically propagating waves for multi-support structures; source rupture; identification of wave types; computation of ground strains and rotational components of the ground motion. Regarding spatial coherence, the studies based on the SMART-1 are (Loh, Penzien and Tsai 1982), (Harada 1984), (Abrahamson 1985), (Bolt, Abrahamson and Yeh 1984), (Harichandran and Vanmarcke 1986) and (Loh and Su 1986). In (Loh, Penzien and Tsai 1982) the authors measured the absolute value of the correlation and found major differences between two events, and in (Harada 1984) the authors estimated correlation and derived an empirical expression. The authors in (Harichandran and Vanmarcke 1986) measured the absolute value of coherency for several events. They noted large variations in the frequency and distance dependence and were unable to find a single parametric form that would adequately describe the coherency for all of the studied events. In these three studies, only measurements between two stations (in the context of this chapter stations are the points at which different input motions are communicated to the structure) were used. Studies based on multi-station measurements were performed by (Abrahamson 1985) which measure the coherency over an array aperture rather than for a single station separation. In

(Abrahamson and Bolt 1987) the mathematical background for multi-station coherency is described. Studies regarding ground strains and rotational components by means of the SMART-1 array data can be found in (Harada 1984), (Oliveira and Penzien 1985) and (Oliveira, Bolt and Penzien 1985). Regarding the theme of response of linear systems to multiple support excitations, again based on the data from SMART-1 array, there are (Bolt, Loh, et al. 1982) and (Loh, Penzien and Tsai 1982). In these studies, the authors calculated the cross-correlation characteristics of the free-field ground motions as a function of separation distance and alignment with respect to the epicentre. They also developed a generalized response spectral ratio to characterize multiple support excitations. In (Abrahamson and Bolt 1985) the spatial variation of the phasing of strong ground motions was studied, and a seismic phase response spectrum was developed to complement the usual amplitude response spectrum.

Other studies also concerning the SMART-1 array are (Loh 1985), (Loh and Yeh 1988), (Hao, Oliveira and Penzien 1989) and (Oliveira, Hao and Penzien 1991), with each of these studies providing a different approach on spatial variability, be it concerning space-time correlation, stochastic modelling of differential earthquake ground motion or definition of coherency models. In (Loh 1985) the spatial correlation of seismic waves between different sites is studied, where a variance ratio is presented as an index for identification of wave types, directions and velocities. In (Loh and Yeh 1988) a stochastic model for determining differential ground movements is presented. The model considers source characteristics, attenuation of wave passages and also the spatial correlation of ground motions. In (Hao, Oliveira and Penzien 1989), multiple-station ground motion data is used to derive a coherency model. Also presented is a numerical procedure for the generation of time series compatible with the coherency model and with any given design response spectrum. Finally, in (Oliveira, Hao and Penzien 1991), further work on the generation of time-series compatible with a given coherency relationship is presented.

Other arrays have been used to conduct similar studies like the El Centro Differential array with data pertaining to the 1979 Imperial Valley, California earthquake, and Japanese dense arrays whose data was employed in several other studies.

There have been other more recent studies in the literature that have proposed different coherency models of strong motions. These coherency models assume different components associated with several factors that influence the propagation of the waves and are the causes of spatially variable seismic ground motions (SVSGMs). The main causes of SVSGMs are the wave passage, wave scattering, surface and sub-surface topography, soil properties and extended seismic source effects. In these works, some of those different causes define different components in the proposed coherency models. In (A. Kiureghian 1996), a coherency function is presented. This coherency function became one of the most used coherency functions in subsequent works and is composed by three components related to different effects that influence the coherency. Those effects are defined in the work as the incoherence effect, the wave passage effect and the site response effect. The incoherence effect is due to the scattering of waves in the heterogeneous medium of the ground as well as due to the differential superposition of waves arriving at each station from different segments of an extended source. The wave passage effect relates to the delay or the time lag in the arrival of a given wave to a station *l* after reaching station *k*, with a given incidence angle ψ. Finally, the site response effect considers the different local soil profiles between the aforementioned stations, *k* and *l*. These three components are then put together to form a composite model for the coherency function, which is presented in equation (7.1) in a simplified form:

$$\gamma_{kl}(\omega) = \gamma_{kl}^{incoherence}(\omega) \cdot \gamma_{kl}^{wave\ passage}(\omega) \cdot \gamma_{kl}^{site\ response}(\omega) \qquad (7.1)$$

In a previous work (Kiureghian and Neuenhofer 1992), the authors had proposed a response spectrum method for the seismic analysis of linear multi-degree-of-freedom, multiply supported structures subjected to SVSGMs. In this method, the same effects are considered in the spatial variability: wave passage, loss of coherency with distance and variation of local soil conditions.

In (Zerva and Zervas 2002), the authors produce an overview on the then current state-of-the-art concerning spatial variability, in particular related to studies that stemmed from data recorded at dense instrument arrays. This overview focuses on spatial coherency and the various studies that concern that theme. Comparisons are made between coherency models, and empirical and semi-empirical models are described, and the validity of different models is discussed. In the end, the study also presents and compares different simulation techniques for the generation of artificial spatially variable seismic ground motions.

Obtaining physically compliant ground motions and particularly displacement time-histories, that are compatible with coherency models, design response spectrums and “look realistic”, which entails having zero initial and small residual displacements, is complex and a necessity to be able to apply to engineering applications. Several works have been done presenting methods to simulate ground motions with these characteristics. As already mentioned, in (Oliveira, Hao and Penzien 1991) the generation of seismic ground motions compatible with a coherency model is presented. Studies by (Deoadatis 1996) and (Cacciola and Deodatis 2011) present stochastic methods for the generation of non-stationary ground motion vector processes. In both studies the methods provide ground motions that are compatible with a given response spectrum and coherency model, and in the previous three studies, only acceleration time-histories are obtained from the methods. However, the input in engineering software suites for spatial variability is in the form of displacement time-histories, and so these need to be generated from the acceleration time-histories. As mentioned previously, the main problem of this step is obtaining displacement time-histories with zero initial and small residual displacements, and at the same time compatible with the acceleration time-histories and with the response spectrum and coherency model. Two works by Boore, (Boore, Stephens and Joyner 2002) and (Boore and Bommer 2005), present methodologies for processing of accelerograms and the application of appropriate filters and step sequences to obtain good ground motions for engineering applications. It is in (Boore, Stephens and Joyner 2002) that a baseline adjustment scheme is presented that guarantees zero initial values in the velocity and displacement time-histories and negligible initial values in the acceleration time-history. In (Liao and Zerva 2006), the authors build on the work (Boore, Stephens and Joyner 2002) to obtain physically compliant, conditionally simulated spatially variable seismic ground-motions for performance based-design, and particularly displacement time-histories.

In recent years, the issue of spatial variability has been the focus of more studies with the application of the coherency models and the studies on generation of physically compliant ground-motions to obtain time-histories and apply them for structural analysis of different structures, namely bridges. However, there is still no consensus on whether the effect of SVSGMs on structures is beneficial or detrimental compared to that of uniform excitations (Zerva, Falamarz-Sheikhabadi and Poul 2018). Recently, many works on the effects of these SVSGMs applied to different structures have been produced. Many works by Hao apply spatial variability to a number of different structures: multiply supported rigid plates (H. Hao 1991), in-plane responses of incompressible circular arches (H. Hao 1993), displacement of adjacent building structures (Hao and Zhang 1999) and a parametric study on seating length for bridge decks (H. Hao 1998). References (Harichandran and Wang 1988), (Harichandran and Wang 1990) and (A. Zerva 1990) present studies on the response of simple, two-span and multi-span beams to spatially variable ground motions. Later, Price and Eberhard (Price and Eberhard 1998) present a study on the effects of SVSGMs on short bridges and the authors in (Zanardo, Hao and Modena 2002) present a study of the effects of SVSGMs on multi-span simply supported bridges. In (Kim and Feng 2003) results of fragility analyses of highway bridges under SVSGMs are presented. In this study ground motions (GMs) are artificially generated with different amplitudes, phases and frequency contents at different support locations, and Monte Carlo simulations are performed to study the dynamic response of a multi-span bridge example. The authors in (Tecchio, Grendene and Modena 2011) also assess the response of bridges, in this case long multi-span girder bridges, subjected to SVSGMs and considering nonlinear behaviours, such as hysteretic behaviour of piers, etc. An overview of the engineering applications of SVSGMs is provided by (Zerva 2009), where many themes are discussed, from presentation of most widely used coherency models, generation of conditional ground motions, to an overview of the effects of SVSGMs on the response of long structures, such as pipelines, bridges and dams.

Several recent works (Zhong, et al. 2017), (Lavorato, et al. 2018), (Li, Li and Crewe 2018) and (Papadopoulos and Sextos 2018) all present studies on the application of SVSGMs to bridges. In the case of (Zhong, et al. 2017), the study pertains to cable-stayed bridges and the employed ground motions are generated by means of the aforementioned procedure presented in (Liao and Zerva 2006). In this study, the objective is to ascertain the impact of the effect of SVSGMs on the response of long irregular RC bridges, performing a parametric study regarding the coherency model, length and irregularity layout. The study also intends to compare the results both with and without spatial variability and compare the importance of dynamic effects against pseudo-static effects. The ground motions in this work are generated by means of the conditional simulation method, and the displacement ground-motions are attained via the application of the method described in (Boore, Stephens and Joyner 2002) and (Liao and Zerva 2006). Lastly, the study intends to define in which cases the SVSGMs are detrimental to the structural response in comparison to a uniform seismic loading.

The study continues in Section 7.2 with the definition of the coherency model and methodology to obtain SVSGMs. In Section 7.3, the choice of initial ground motions and calculation of the spatially variable displacement time-histories. In Section 7.4, the presentation of the case-studies and the analysis methodology. In Section 7.5, the analysis of the results and in Section 7.6 the concluding remarks.

7.2 Methodology for the conditional simulation of spatially variable ground-motions

To attain the proposed objectives for this chapter, displacement SVSGMs must be generated. This necessity stems from the need to define strong motions by means of displacements whenever multiple input signals are used, in all FEM software programs that can address seismic analysis. In this chapter, a far-field seismic action is imposed on each case-study bridge. The simulation of far-field SVSGMs, in this study, is performed according to a methodology introduced in (Liao and Zerva 2006) which, in turn, is based on the baseline correction scheme introduced in (Boore, Stephens and Joyner 2002). Through this methodology it is possible to generate displacement SVSGMs compatible with a given coherency model and with an initial acceleration ground-motion and power spectral density. The method presented in this chapter can generate either (almost) zero or non-zero residual displacement time-histories, depending on the seismic action to be employed in the study, respectively far-field or near-field seismic action. In this thesis only far-field strong motions are generated. The difference between one method and the other is an extra filtering step for the near-field seismic action, where the low frequencies are preserved and only to the high frequencies is the coherency model applied. This is to simulate the effect of tectonic fling on the near-field GMs.

For the generation of far-field compliant displacement SVSGMs the method employed herein will generate zero initial, and small residual displacement signals. Unlike in (Liao and Zerva 2006) where the CPDF (conditional probability density function) method (Kameda and Morikawa 1992) is employed for the simulation of the ground-motions, in this study the HOP method (Hao-Oliveira-Penzien) (Hao, Oliveira and Penzien 1989) is used.

In the following, the methodology and its application are explained step-by-step. For the generation of SVSGMs, a coherency model is chosen and used to generate the ground-motions at the different input positions (stations) of the structure. The coherency model simulates the loss of correlation between the phases of two signals at different stations and is a function of frequency. It is obtained from the smoothed cross spectrum of the signals between the said stations (i and j), normalized with respect to the corresponding power spectra:

$$\gamma_{ij}(\omega) = \frac{S_{ij}(\omega)}{\sqrt{S_{ii}(\omega) \cdot S_{jj}(\omega)}} \tag{7.2}$$

There are two types of coherency models, empirical and semi-empirical. In this study, the empirical formulation of Luco and Wong is employed (Luco and Wong 1986):

$$\left|\gamma_{ij}(\omega, d)\right| = \exp\left(-\alpha^2 \cdot \omega^2 \cdot d^2\right) \tag{7.3}$$

Where ω and d are, respectively, the angular frequency and the distance between both stations, and α is the coherency-drop parameter, which accounts for how fast the seismic waves become out of phase and uncorrelated in regard to distance and wave frequency. The larger the value of α the less distance it takes to lose wave coherency. This can be measured experimentally by comparing seismic waves at different stations and calculating the cross-spectral density between both waves normalized by the power-spectral density of both waves. The value for α was varied between 2.0x10^{-4} and 3.0x10^{-4}, which corresponds to the value interval suggested by Luco and Wong.

The generation of the SVSGMs, in accordance with the prescribed coherency function, is done by affecting the power spectral density (S_0) by the coherency matrix, thus obtaining the cross-spectral density matrix,

$$S_{ij}(\omega_k) = \gamma_{ij}(\omega_k) \cdot S_0(\omega_k) \tag{7.4}$$

From the Cholesky decomposition of the coherency matrix one obtains,

$$S_{ij}(\omega_k) = L_{ij}(\omega_k) \cdot L_{ij}^T(\omega_k) \cdot S_0(\omega_k) \tag{7.5}$$

Where $L_{ij}(\omega_k)$ is the lower triangular matrix in this decomposition.

According to the HOP method, the generation of $f_i(t)$, $i=1, \ldots, M$ random processes, corresponding to M prescribed locations, are achieved according to:

$$f_i(t) = \sum_{m=1}^{i} \sum_{k=1}^{N} A_{im}(\omega_k) \cdot \cos(\omega_k \cdot t + \phi_{mk}), \qquad i = 1, \ldots, M \tag{7.6}$$

Where A_{im} and ϕ_{mk} are, respectively, the amplitudes and the random phases, which are random values uniformly distributed between [0,2π]. As for the amplitudes, these are obtained by,

$$A_{im}(\omega_k) = l_{im}(\omega_k) \cdot \sqrt{2 \cdot S_0(\omega_k) \cdot \Delta\omega} \tag{7.7}$$

Where $l_{im}(\omega_k)$ are the elements of the lower triangular matrix obtained from the Cholesky decomposition of the coherency matrix.

At this point, acceleration SVSGMs have been generated from an initial power spectral density and coherency model. This corresponds to the initial step (step 0) of the generation of displacement SVSGMs. The entire procedure, for the generation of the displacement SVSGMs, can be summarized by the following steps, also described in (Liao and Zerva 2006), albeit with some small modifications, to be applied subsequently to step 0:

1. Apply a short cosine taper function to the simulated time histories to set their initial values to zero.
2. Add time-shift due to the apparent wave propagation velocity in the bedrock, V_r.
3. Subtract the mean from the entire acceleration time-histories.
4. Integrate accelerations to velocities and apply a quadratic or a cubic function fitted to the velocity time histories in the least-squares minimization sense—zero velocity constraints are assumed at the starting time.

5. Remove the derivative of the velocity quadratic fitting function from the acceleration time histories.
6. Apply a high-pass filter to the acceleration time history.
7. Integrate the accelerations to get velocities and displacements.

Good results in many cases can be obtained without the need of applying step 6. In the case of the work developed in this chapter, step 6 was not applied. In the following section, Section 7.3, the entire procedure is applied to an initial ground motion.

7.3 Initial ground-motions and generation of displacement SVSGMs

The methodology presented in Section 7.2 is applied to generate the displacement SVSGMs that will be used as imposed displacements at the base of the case-study bridges' piers. A set of real strong motions, one of which (TH_1) is presented in Figure 7.1, were chosen to serve as initial GMs for the conditional simulation scheme.

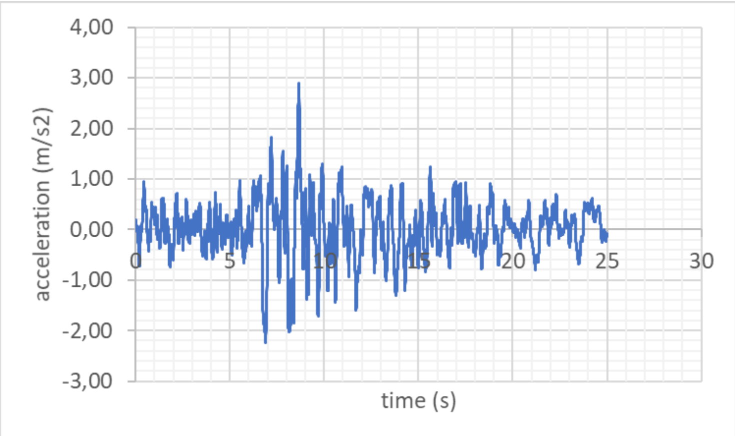

Figure 7.1 Example of TH (TH_1) used for the conditional generation of the SVSGMs.

In order to preserve the non-stationarity of the original ground-motions, an extra-step is performed prior to step 0 (Liao and Zerva 2006). In this step (Step -1) the THs are subdivided into sub-segments that are visually homogeneous, i.e., that are apparently stationary. Step 0 is then applied to each sub-segment, at the end of which, and before Step 1, the generated THs, corresponding to each sub-segment, are joined by means of a linear weighting function. Through this procedure, it is possible to preserve some of the non-stationarity of the initial GM.

The linear weighting function used to join the segments is expressed by:

$$y = a(x) \cdot (1 - x) + b(x) \cdot x \qquad (7.8)$$

Where a(x) and b(x) are the values, at point x, of the signals that are being joined, and x represents the position in the overlap region.

As an example of the application of Step -1, the TH (TH_1) in Figure 7.1 is subdivided into five 5-second sub-segments, Figure 7.2.

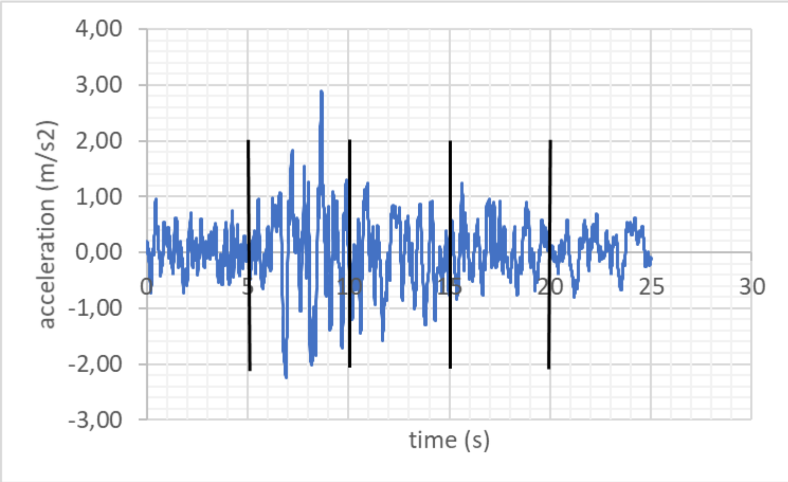

Figure 7.2 Segment subdivision for non-stationarity preservation of TH_1.

The application of Step 0 to TH_1 and its five sub-segments will generate *n* sets of five THs, where *n* is the number of stations. In Figure 7.3, an example of the THs generated for one station. Each TH corresponds to a time-interval of the original TH_1. They were generated with 10 sec duration instead of 5 sec to have an overlap region for the joining procedure prior to Step 1. In Figure 7.4, the power spectral density functions (PSD) of each of the sub-segments in TH_1 are shown.

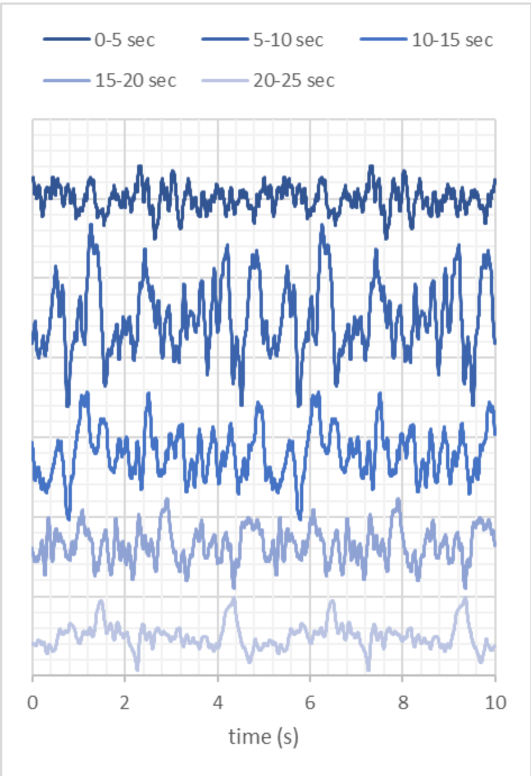

Figure 7.3 Generated THs in Step 0 for each sub-segment of TH_1, for one given station.

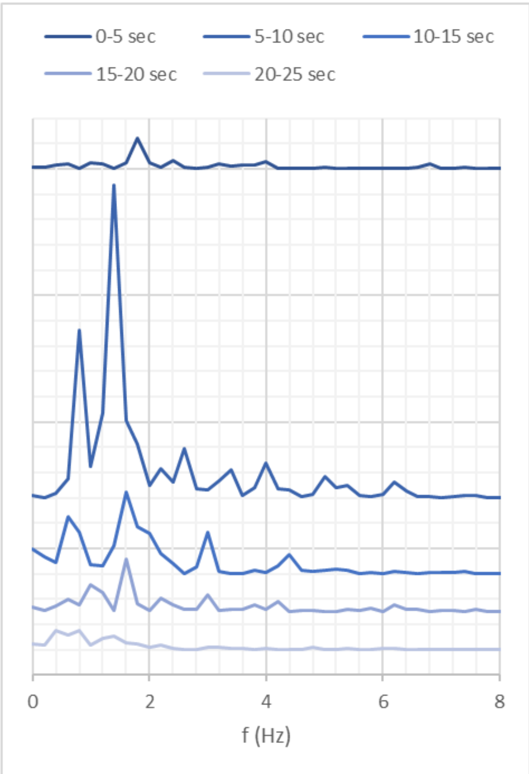

Figure 7.4 PSDs used to generate the sub-segment THs.

The case-study bridges, studied herein, have different total lengths and irregularity profiles, but all have the same deck cross-section, which will be presented in Section 7.4, and, particularly, all have the same span length of 30-meters. This span length is the station distance used to generate the SVSGMs. Additionally, the maximum bridge total length, among case-studies, is 900 meters, which corresponds to 31 stations. For that reason, for each GM in the initial set, the SVSGMs for 31 stations, spaced between each other by 30 meters, are generated.

From the application of Steps 1 through 7 on the joined THs obtained from Step 0, the SVSGMs are obtained in respect to acceleration, velocity and displacements. The output will be presented for a limited set of stations (S_1-0m, S_2-120 m, S_3-240 m, S_4-360 m and S_5-480 m) instead of the entire set of 31 stations, for reasons of presentation quality. To note that the apparent wave propagation velocity, V_r, applied to the SVSGMs to calculate the time-shift was defined at 1000m/s.

The coherency model employed is the previously mentioned Luco and Wong model (LW), which is shown for stations S_2 through S_5, relatively to station S_1, Figure 7.5.

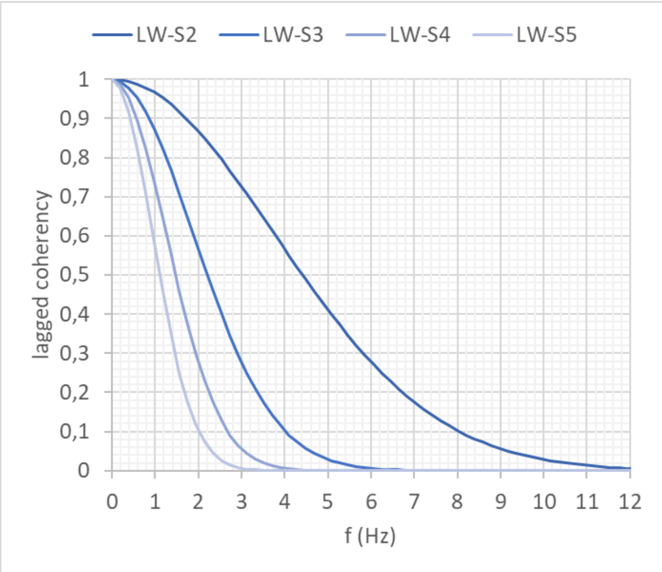

Figure 7.5 Lagged coherency according to the model of Luco and Wong (LW).

In the following figures, the generated SVSGMs are presented. Figure 7.6 shows the accelerations for stations S_1 through S5, Figure 7.7 shows the velocities and Figure 7.8 shows the displacements, where one can see the absolute value of the pseudo-static displacements between stations S_1 and S_5 ($|\Delta d(S_5-S_1)|$). The pseudo-static displacements are obtained by subtracting the obtained displacement strong motions of different stations at each time-step.

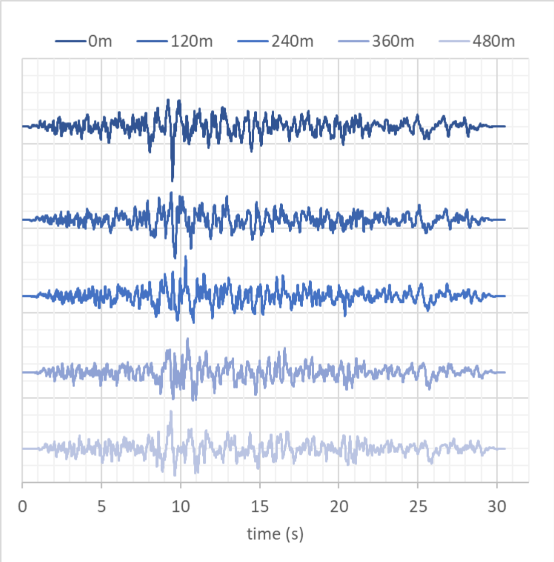

Figure 7.6 Generated acceleration SVSGMs for stations S_1 through S_5.

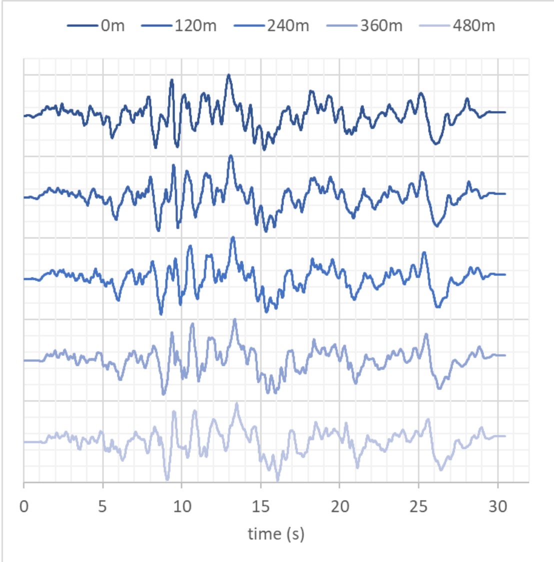

Figure 7.7 Generated velocity SVSGMs for stations S_1 through S_5.

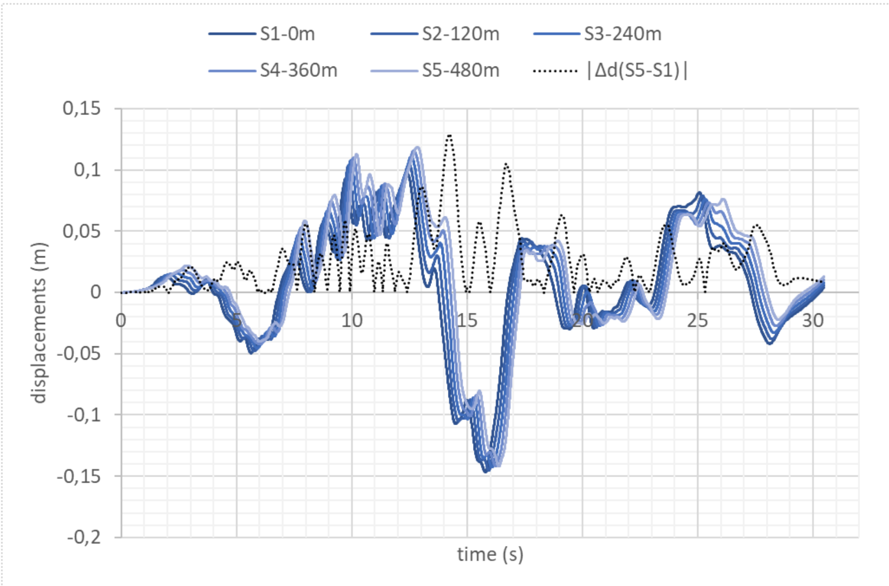

Figure 7.8 Generated displacement SVSGMs for stations S_1 through S_5 and pseudo-static displacements between S_1 and S_5.

In Figure 7.9 and Figure 7.10 the mean calculated coherency values from the generated signals of 50 simulations are presented, and the measured coherency for one of the stations is compared with the coherency model values (LW). It can be seen that there is a close match for lower frequencies and a divergence for higher frequencies, which do not tend to zero. This issue is also verified in (Liao and Zerva 2006).

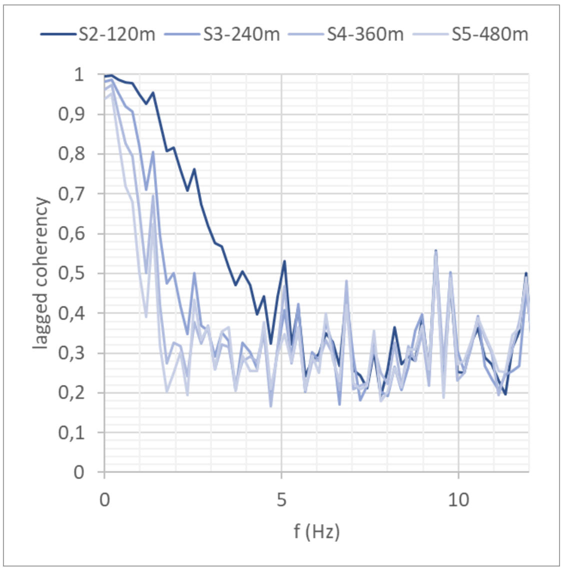

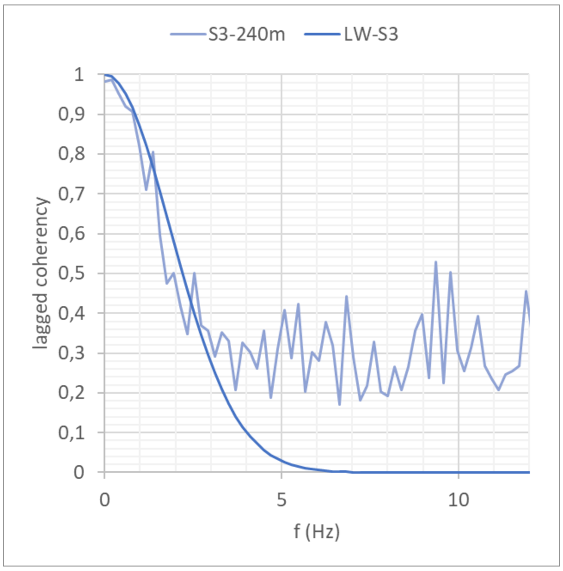

Figure 7.9 Lagged coherency calculated from generated signals.

Figure 7.10 Comparison of calculated lagged coherency and coherency model for station S_3.

In Figure 7.11, the results of the displacement SVSGMs generated for the 31 stations, based on TH_1, are shown. To note that the results with 5 and 31 stations correspond to different simulations.

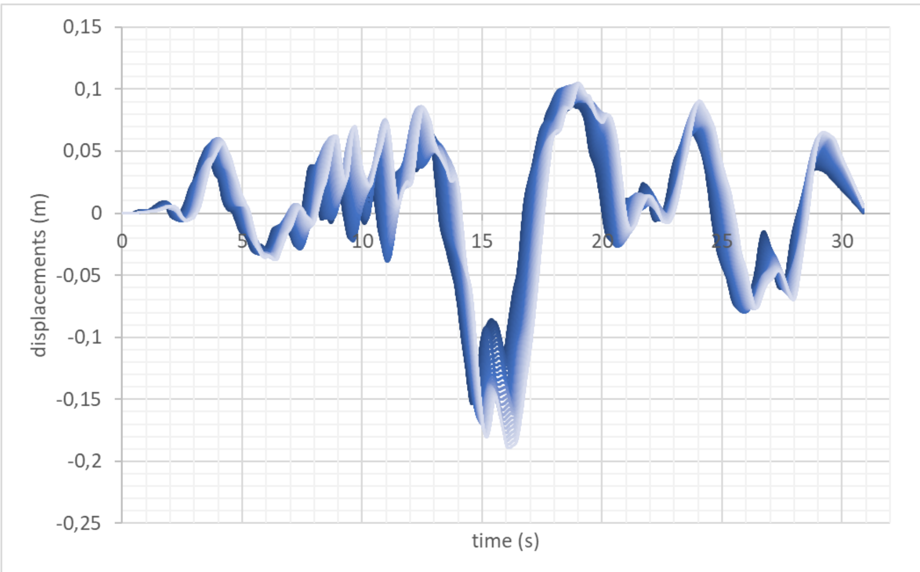

Figure 7.11 Displacement SVSGMs for all 31 stations.

7.4 Application of Spatial variability to case-study Bridges

7.4.1 Objectives

The objective of this study is to ascertain, for RC bridges of different lengths and irregularity profiles, whether spatial variability of ground-motions has favourable or detrimental effects on the seismic safety of RC bridges. To achieve such a goal, several bridges are analysed in different scenarios, related to spatial variability. The questions that the study intends to answer are whether pseudo-static effects overweigh the loss of coherency of the GMs and for which case-studies, in terms of total length and irregularity layout, that situation is verified.

In this section, the analysis methodology is presented, along with the case-study bridges and their characteristics, such as material properties and deck and pier cross-sections.

7.4.2 Methodology and analysis definitions

To attain the goals defined by the objectives, the case-studies are analysed with both SVSGMs and uniform seismic actions. This way, the impact of the spatial variability, given the coherency model, becomes clear. The uncertainty associated with the coherency model is also evaluated, with sensitivity analysis concerning the coherency-drop parameter, α, and also concerning the use of different coherency models and apparent wave propagation velocities.

The seismic analyses are performed resorting to OpenSEES (McKenna and Fenves 1999) particularly OpenSEESMP which allows for parallel processing, thus resulting in a significant speed-up of the entire process by parallelizing the individual seismic analyses between CPU threads. The OpenSEES/OpenSEESMP software is a library extension of the Tcl/Tk language interpreter. This facilitates the integration of structural analysis with several pre- and post-processing programming procedures, which is fundamental for the treatment of large amounts of data generated from the analyses of large sets of case-studies.

7.4.2.1 Seismic analysis

The seismic analysis was performed by time-step integration using Newmark's average acceleration method to compute the time history, with parameters of α and β equal to 0.5 and 0.25, respectively. The time-step of the integration was 0.01s. The solution of the nonlinear residual equation was done with Newton-Raphson algorithm with line search to increase the effectiveness of the Newton-Raphson algorithm. Non-convergence issues were only associated with non-equilibrium of P-delta effects.

7.4.3 Case-study characteristics

7.4.3.1 Superstructure

This study's focus is on a particular typology of bridges characterized by relatively short spans (30-meter long) and a common type of slab-girder deck, illustrated in Figure 7.12.

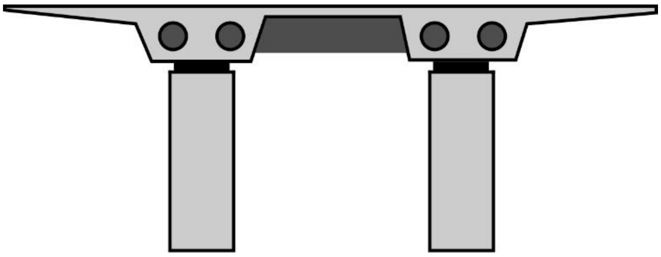

Figure 7.12 Superstructure typology employed in the case-studies.

The superstructure represented by Figure 7.12 has a particular dynamic behaviour, without rotation of the superstructure due to the torque formed by both piers. There is no compatibility in rotation (around the horizontal longitudinal axis) between the deck and the piers, where the piers can rotate independently of the deck.

7.4.3.2 Infrastructure

As in previous chapters circular pier cross-sections were chosen for this study. In Figure 7.13, the modelled cross-section is shown with the employed values for flexural steel reinforcement and pier diameter.

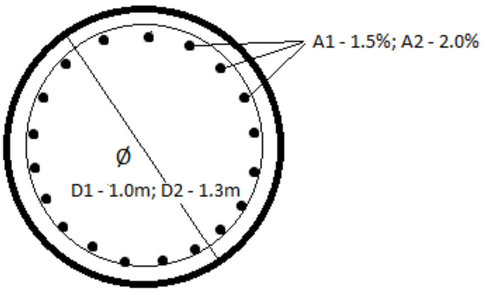

Figure 7.13 Circular cross-section used to model the piers in the case-studies.

7.4.3.3 Material properties

The mean values of the materials' mechanical properties were used. For the steel, the material used was A500NR, and B35 for the concrete. The values used to define the steel constitutive relationship were taken from (Pipa 1993) and are shown in Table 7.1. The values for the concrete are shown in Table 7.2.

Table 7.1 Mean values for the mechanical properties of the A500NR SD steel from (Pipa 1993).

Mean values	A500NR SD
f_{ym} (MPa) – yield stress	585
f_{um} (MPa) – ultimate stress	680
E_{ym} (GPa) – Young modulus	200
ε_{sy} (‰) – yield strain	2.93
ε_{sh} (‰) – strain at beginning of hardening	14
ε_{su} (‰) – ultimate strain	94

Table 7.2 Mean values for the mechanical properties of the B35 concrete.

Mean values	B35 (C30/37)
f_{cm} (MPa) – unconfined maximum stress	38
E_{cm} (GPa) – Young modulus	33
ε_{cu} (‰) – unconfined ultimate strain	3.5

7.4.3.4 Materials' constitutive relationships

The model used for the concrete fibres was a Kent-Scott-Park concrete material object with degraded linear unloading/reloading stiffness and no tensile strength (Scott, Park and Priestley 1982).

For the steel reinforcement fibres, a uniaxial Giuffré-Menegotto-Pinto (Giuffrè and Pinto 1970) (Menegotto and Pinto 1973) model with isotropic strain hardening was used.

7.4.3.5 Case-study bridges

As mentioned earlier, to obtain comprehensive results and attain meaningful conclusions, the analysis procedure or methodology must be applied to a diverse set of bridges, both in terms of length and irregularity profile. In that sense, bridges from 120 meters in length up to 900 meters, with a 60-meter step increment, are modelled (with different irregularity profiles) and analysed (with and without SVSGMs).

The case-studies are generated according to the irregularity layouts presented in Table 7.3.

Table 7.3 Irregularity profiles used to generate case-study bridges

Category	**Explanatory figure**
Regular	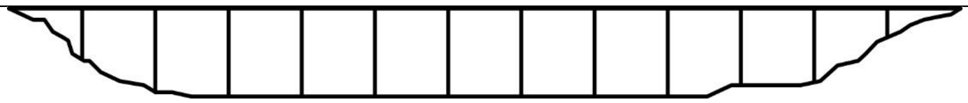
Irregular	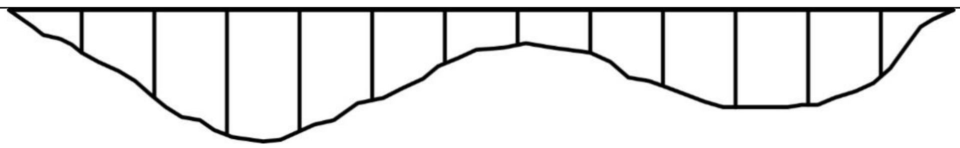

The reason for generating bridges with different irregularity profiles stems from the effect that irregularities have on the dynamic behaviour of an RC bridge and the resulting transverse horizontal displacement profile (THDP) of the deck. This means that the spatial variability might have different impact depending on the irregularity profile of the bridge, and by analysing bridges that correspond to distinct irregularity profiles, this effect may become apparent.

The chosen irregularity profiles, seen in Table 7.3, is a regular profile with all piers with the same height and an irregular profile with short central piers. The reason for choosing such an irregularity profile is that the dynamic behaviour of such a bridge is very different from the regular case, where it is probable that the irregular case's 1st vibration mode is very different from the regular case's 1st mode. In fact, the irregularity profile is defined in the literature as one where the dynamic behaviour is more complex to analyse (Kappos, Saiidi, et al. 2012). So, it was the intention to have results pertaining to very different dynamic behaviours. Regarding the irregularity classifications from the work (Soleimani, et al. 2017), the bridges generated by the irregular profile are essentially classified as extremely unbalanced due to the ratio of the pier average length with the length of the shortest pier being over 1.3, with some bridges classified as highly unbalanced with said ratio between 1.2 and 1.3.

The sensitivity analysis also concerns the characteristics of spatial variability. Both the coherency-drop parameter (α) of the Luco and Wong coherency model, and the apparent wave propagation velocity (V_r), are varied. In the case of α, it is varied between 2.0 and 3.0 ($x10^{-4}$), which are the lower and upper limit values defined in (Luco and Wong 1986). In the case of the V_r, it is varied between 0.5 km/s and 6 km/s, although 1km/s and 4km/s are usually considered to be, respectively, the lower and upper limit values for V_r (Zerva, Falamarz-Sheikhabadi and Poul 2018). Both α and V_r have been the focus of extensive discussions, particularly regarding the values that should be employed. It is reasonable to assume that they introduce significant uncertainty in the models, and since both factors have influence on dynamic and pseudo-static effects, the impact of their variation on the results should be thoroughly studied.

Table 7.4 shows the set of analyses performed on each case-study bridge concerning the type of seismic action (uniform or spatially variable), the coherency model parameters and the apparent wave propagation velocity (V_r). A full-factorial combination of the various parameters with the case-studies in Table 7.5 results in a total of 680 case-studies. The pier variables used were, primarily, A_1 and D_1, as identified in Figure 7.13. The variables labelled as A_2 and D_2 were used for additional analyses for reasons which are explained in Section 7.5.

Table 7.4 Set of analyses performed on each case-study bridge according to type of seismic action (Unif. or SVSGM), coherency model and V_r. LW – Luco and Wong, α (x 10^{-4})– coherency-drop parameter.

		SVSGMs – Coherency	
	Unif. GM	LW α=2.0	LW α=3.0
V_r (km/s)	N/A	0.5	
		0.75	
		1.0	
		1.5	
		2.0	
		3.0	
		4.0	
		6.0	

Table 7.5 shows the distribution of piers by height, for each of the case-studies, according to their respective irregularity profile. The case-studies are composed by sequences of piers with 3 possible heights: 9 m, 7.5 m and 6 m. The sequences in which the piers are arranged follow the respective irregularity profile. To illustrate, a sequence defined as (5x9-1x7.5-3x6-1x7.5-5x9) is described as having five 9-meter piers at each end, each of which are followed inward by one 7.5-meter pier, and finally, connecting both sides, three 6-meter piers at the middle of the bridge. To note that there is no variation of the pier-deck connections, since these mostly influence the effective height of piers. For that reason, and to keep the bridges' irregularity profiles only dependent on actual pier height, all piers are connected to the decks with the same (monolithic) connections. In real-world designs, different connections are used to reduce irregularity in pier heights, but in this instance, that is not the objective since the effect of irregularities are to be studied.

Table 7.5 Pier height sequence for each case-study bridge, according to irregularity profile.

		Pier sequence num x heigth(m)	
Length (m)	**Num. Piers**	**Regular**	**Irregular**
120	3	3x9	-
180	5	5x9	-
240	7	7x9	-
300	9	9x9	3x9-1x7.5-1x6-1x7.5-3x9
360	11	11x9	4x9-1x7.5-1x6-1x7.5-4x9
420	13	13x9	5x9-1x7.5-1x6-1x7.5-5x9
480	15	15x9	6x9-1x7.5-1x6-1x7.5-6x9
			5x9-1x7.5-3x6-1x7.5-5x9
540	17	17x9	7x9-1x7.5-1x6-1x7.5-7x9
			6x9-1x7.5-3x6-1x7.5-6x9
600	19	19x9	8x9-1x7.5-1x6-1x7.5-8x9
			7x9-1x7.5-3x6-1x7.5-7x9
660	21	21x9	9x9-1x7.5-1x6-1x7.5-9x9
			8x9-1x7.5-3x6-1x7.5-8x9
			7x9-2x7.5-3x6-2x7.5-7x9
720	23	23x9	10x9-1x7.5-1x6-1x7.5-10x9
			9x9-1x7.5-3x6-1x7.5-9x9
			8x9-2x7.5-3x6-2x7.5-8x9
780	25	25x9	11x9-1x7.5-1x6-1x7.5-11x9
			10x9-1x7.5-3x6-1x7.5-10x9
			9x9-2x7.5-3x6-2x7.5-9x9
840	27	27x9	12x9-1x7.5-1x6-1x7.5-12x9
			11x9-1x7.5-3x6-1x7.5-11x9
			10x9-2x7.5-3x6-2x7.5-10x9
			9x9-2x7.5-5x6-2x7.5-9x9
900	29	29x9	13x9-1x7.5-1x6-1x7.5-13x9
			12x9-1x7.5-3x6-1x7.5-12x9
			11x9-2x7.5-3x6-2x7.5-11x9
			10x9-2x7.5-5x6-2x7.5-10x9

7.5 Analysis of results

The results presented in Section 7.5, with the exception of Section 7.5.3, correspond to the average pier displacement demand (DD) envelope of the analyses with the 6 ground motions. The DD is defined as the difference between the measured displacement at the top of the pier and the ground-imposed displacement, at each recorded instant and for each pier. The envelope conveys the maximum DD to every pier during the entire strong motion set.

7.5.1 Regular bridges

The results regarding the case-studies that fall into the regular bridge category, illustrated in Table 7.3, are presented herein. This set of results include the application to regular bridges not only of varying SVSGMs, regarding spatial variation properties such as α and V_r, but also uniform (the same at all bridge foundations) strong motions to serve as point of comparison.

7.5.1.1 Coherency-drop parameter α=3.0x10^{-4} and variables A_1 and D_1 (Figure 7.13)

Figure 7.14 and Figure 7.15 show two examples of the envelope of pier displacement demand for all case-study lengths, where Figure 7.14 refers to a uniform strong motion being applied, and Figure 7.15 refers to an SVSGM set with α=3.0x10^{-4} and V_r=1km/s.

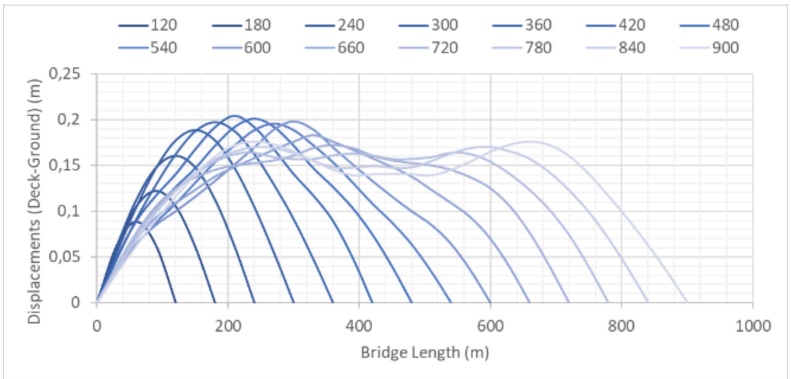

Figure 7.14 Pier DD envelope for the regular bridges subjected to uniform seismic loading.

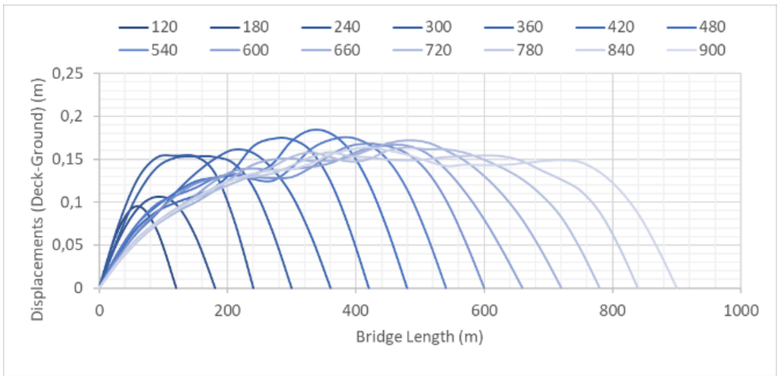

Figure 7.15 Pier DD envelope for the regular bridges subjected to SVSGMs, with α=3.0x10^{-4} and V_r=1km/s.

From these figures it is not possible to have an idea of the difference in bridge response, or rather in the DD to the piers, between each loading situation. To perform an adequate comparison, three types of figures were developed and are subsequently presented. The first type of figure simply plots the maximum DD (maximum critical pier's demand) for each bridge length, and according to each case of SVSGM, including the uniform case. The second type compares, for a given bridge length, the DD envelope of each SVSGM, including the uniform case. Finally, the third calculates the difference, at each pier position, between the DD envelope with the uniform seismic action, and each of the SVSGMs DD envelopes. This last case allows to see where SVSGM can be more detrimental to the bridge compared to the uniform seismic loading.

All results in this Section 7.5.1.1 were obtained with the application of SVSGMs obtained with a coherency drop parameter value, α=3.0x10^{-4}, to bridges modelled with pier cross-section variables A_1=1.5% and D_1=1.0m (Figure 7.13). In Figure 7.16, the aforementioned first type of figure is presented, where the maximum DD value, among all piers of each case-study bridge, is plotted against the bridge's total length.

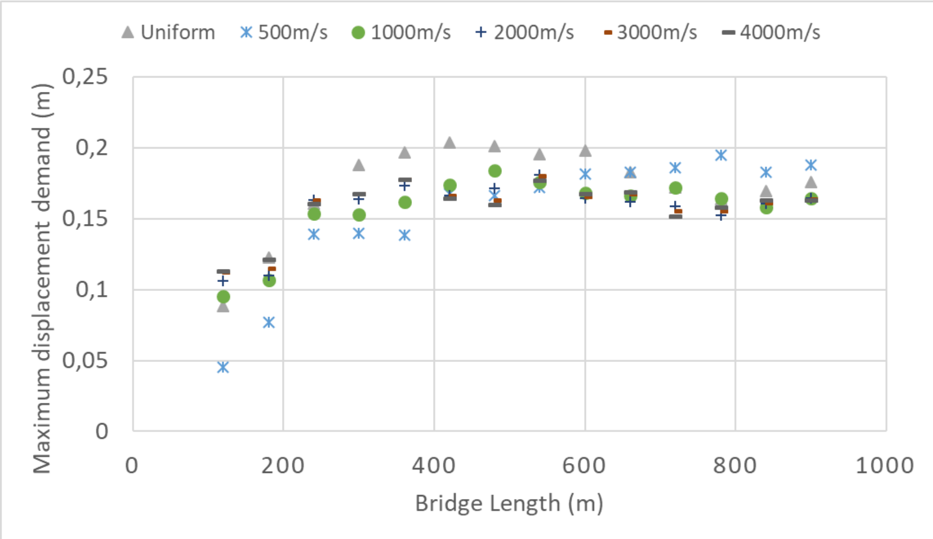

Figure 7.16 Maximum pier DD (maximum value of pier DD envelope) versus bridge total length. Each marker corresponds to a different V_r value of the SVSGM. The marker defined as Uniform corresponds to the application of a uniform seismic load.

From Figure 7.16 it is perceivable that the maximum DD is, for most cases, slightly higher for the uniform seismic action than for the SVSGMs, except in the cases of bridges under 300 meters in length and bridges over 600 meters in length with V_r = 500m/s. However, the main differences between DD envelopes do not concern the maximum value, but rather the shape/profile of the DD envelope. This is apparent in Figure 7.17, Figure 7.18, Figure 7.19 and Figure 7.20, where the DD profiles are presented for the case-studies with 300, 420, 540, 780 meters long, respectively.

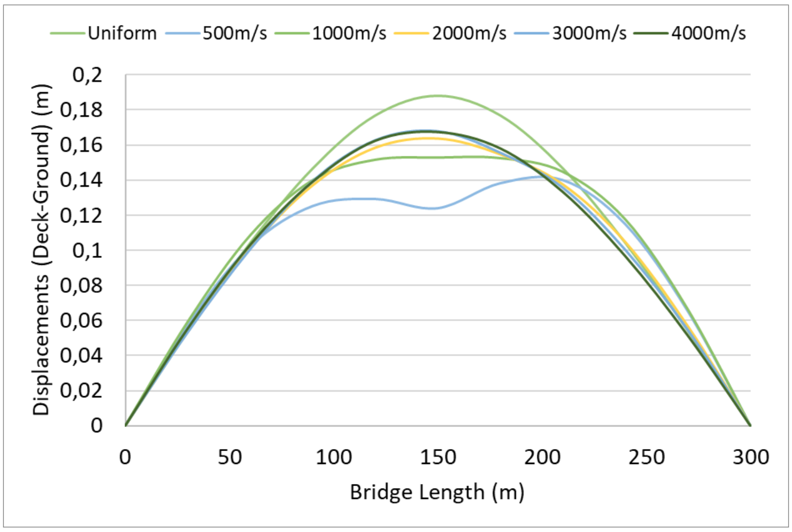

Figure 7.17 DD envelope of the regular A_1-D_1 300-meter bridge case-study, subjected to the uniform seismic load case and SVSGMs with different V_r values.

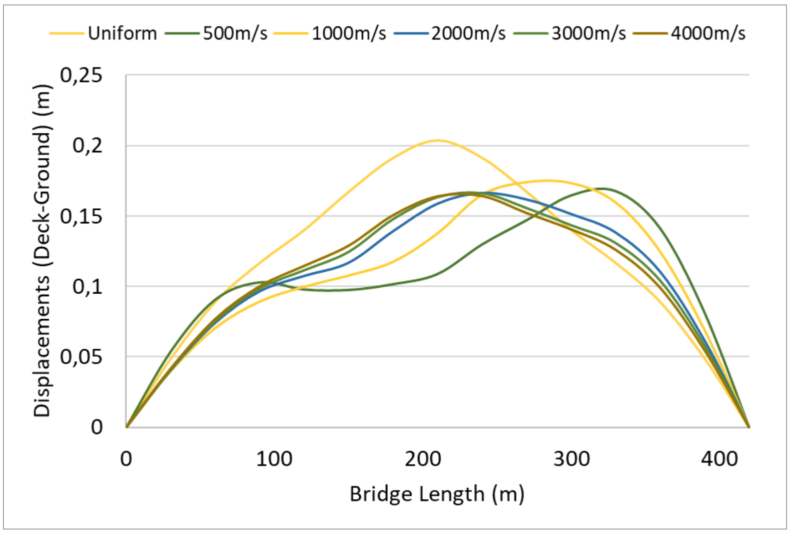

Figure 7.18 DD envelope of the regular A_1-D_1 420-meter bridge case-study, subjected to the uniform seismic load case and SVSGMs with different V_r values.

In Figure 7.17, the DD envelope profiles for SVSGM cases are not very different in shape from the case with uniform seismic loading. The main reason is that the length of the bridge is still relatively short, and the deck has “control” over the displacement profile of the bridge due to the high relative stiffness between deck and piers. Another reason is that the shorter the bridge, the less influence the loss of coherency and the apparent wave propagation velocity have on the DD envelope’s profile. In the case of Figure 7.18, there is a very clear change in the shape of the DD envelope. Albeit there being a larger maximum DD in the case of the uniform seismic loading, the change in DD envelope’s profile introduces larger DD in other piers, as well as a change of critical pier. This effect can be identified from Figure 7.18 to Figure 7.20, where there seems to be, in many of the graphs, a shift of the maximum DD to the right hand-side, which is associated with the propagation direction of the wave from the left-hand side to the right-hand side. The amount by which the SVSGM graphs shift in relation to the uniform loading case is related to the value of V_r, where lower values result in larger shifts, and higher values approximate the DD profile to the uniform loading case. This effect will be analysed more in depth in Section 7.5.3.

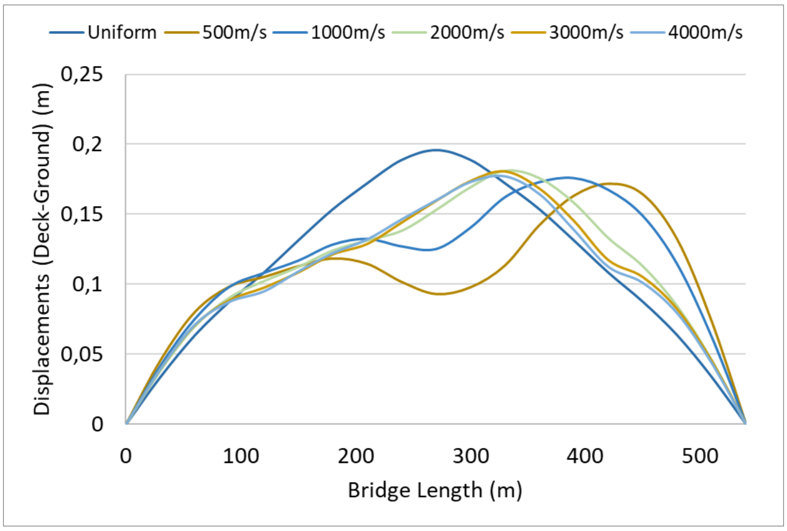

Figure 7.19 DD envelope of the regular A_1-D_1 540-meter bridge case-study, subjected to the uniform seismic load case and SVSGMs with different V_r values.

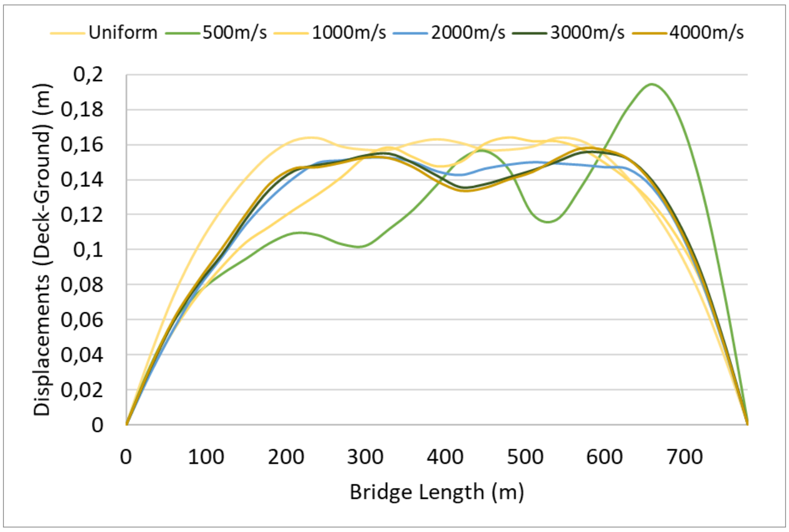

Figure 7.20 DD envelope of the regular A_1-D_1 780-meter bridge case-study, subjected to the uniform seismic load case and SVSGMs with different V_r values.

Figure 7.21 to Figure 7.24 show the difference, at each pier, between the DD of the uniform loading and each SVSGM with different V_r, normalized by the DD of the uniform loading. From these figures it seems that, even though the spatial variability mostly decreases the demand overall and particularly in the critical piers from the uniform loading, there is a very significant increase in the DD of other piers. This effect can be very detrimental if the piers were designed according to the demand from the uniform loading.

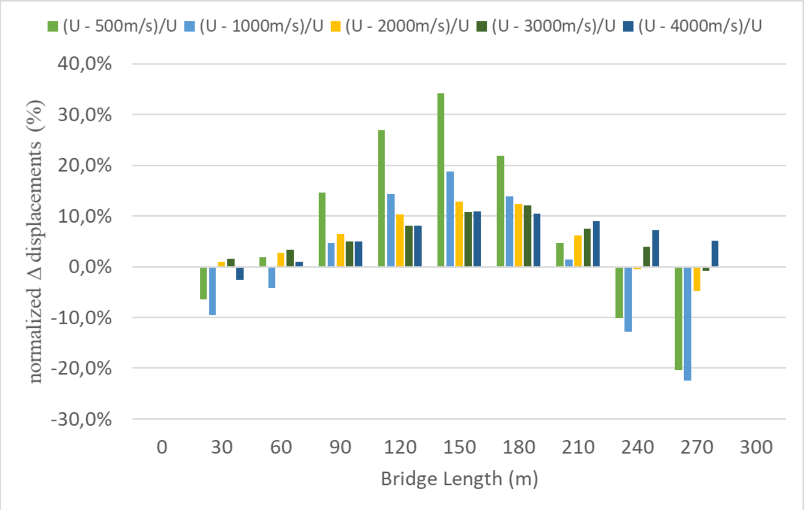

Figure 7.21 Pier DD envelope difference between the uniform load case and each of the SVSGMs for the regular A_1-D_1 300-meter bridge case-study.

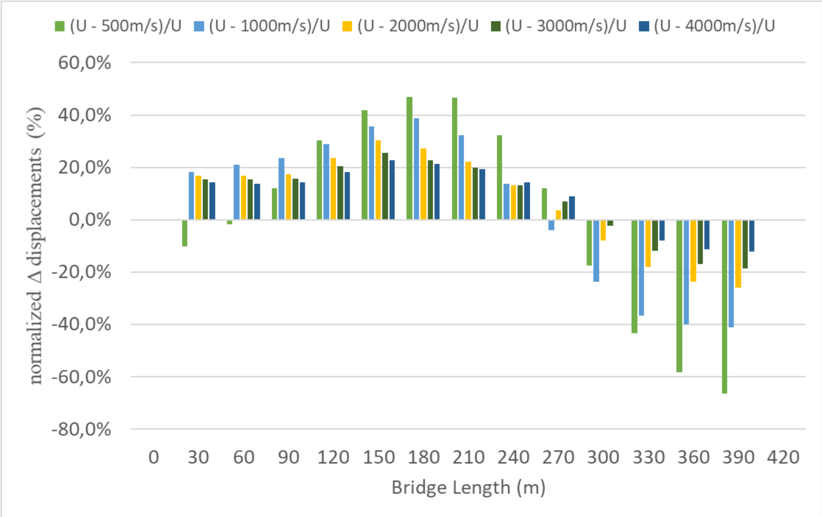

Figure 7.22 Pier DD envelope difference between the uniform load case and each of the SVSGMs for the regular A_1-D_1 420-meter bridge case-study.

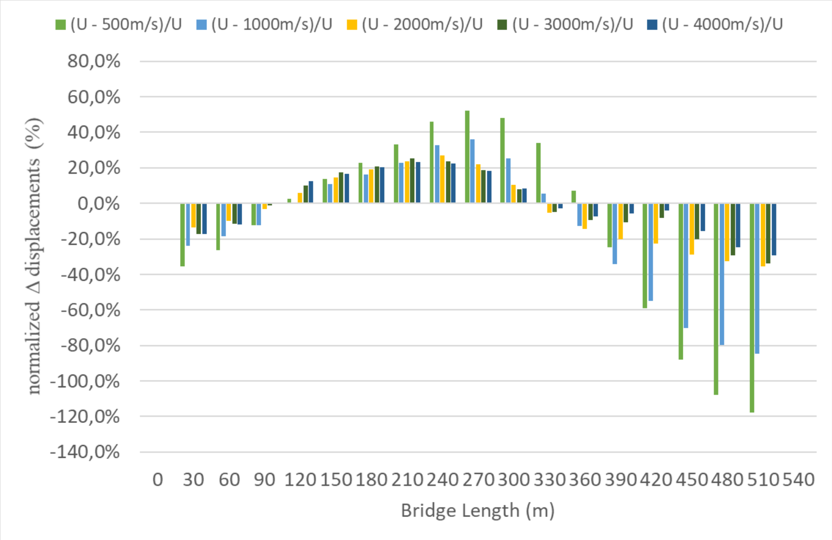

Figure 7.23 Pier DD envelope difference between the uniform load case and each of the SVSGMs for the regular A_1-D_1 540-meter bridge case-study.

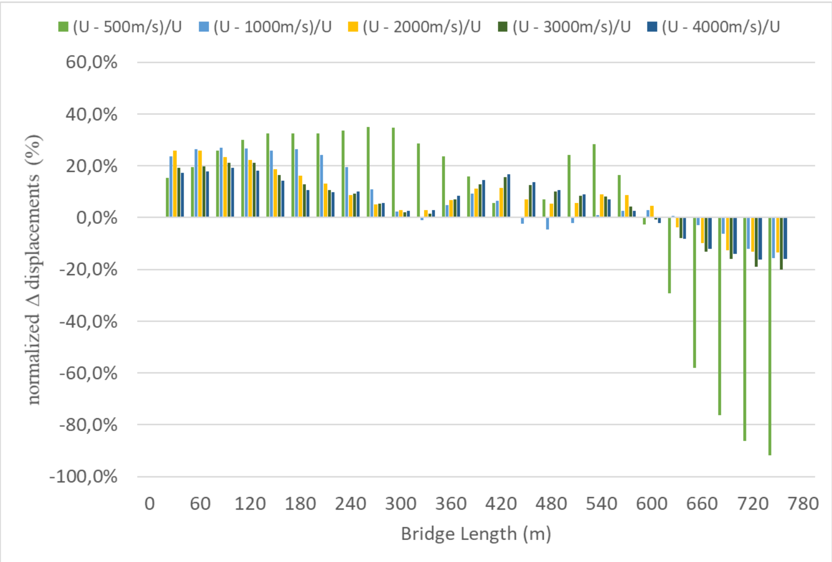

Figure 7.24 Pier DD envelope difference between the uniform load case and each of the SVSGMs for the regular A_1-D_1 780-meter bridge case-study.

From both sets of figures [Figure 7.17-Figure 7.20 and Figure 7.21-Figure 7.24] it is apparent that results from the cases with Vr equal to 500m/s and 1000m/s show the biggest difference from the uniform loading case.

7.5.1.2 Coherency-drop parameter α=2.0x10^{-4} and variables A_2 and D_2

In this section, the coherency-drop parameter takes on the value of α=2.0x10^{-4}, which is the lower limit value defined in (Luco and Wong 1986). In addition, the pier variables A_2 and D_2 are employed instead of A_1 and D_1. In Figure 7.25, the maximum pier DD for each bridge length and according to each SVSGM case (different V_r values) and uniform load case.

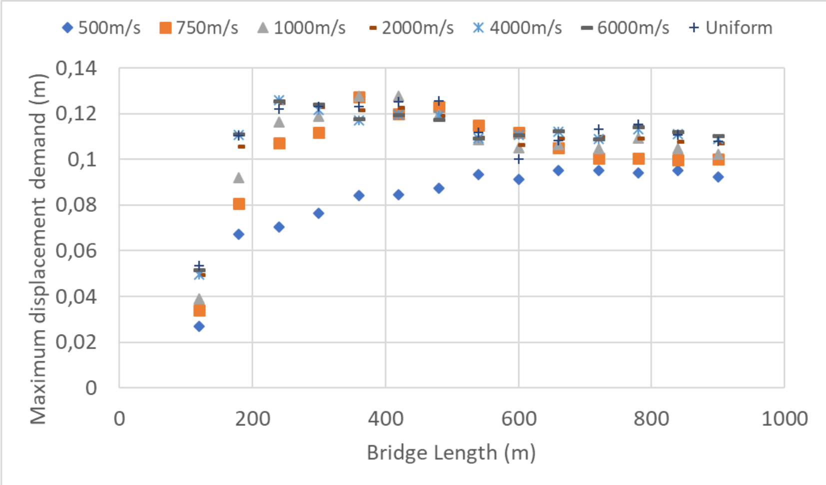

Figure 7.25 Maximum pier DD (maximum value of pier DD envelope) versus bridge total length. Each marker corresponds to a different V_r value of the SVSGM. The marker defined as Uniform corresponds to the application of a uniform seismic load.

By using A_2 and D_2, the fundamental period of the bridges after initial cracking drops approximately to half. The values of the fundamental period with A_1 and D_1 are around 1.0 sec, except for the shorter bridges (<300-meters), and with A_2 and D_2 the values of the fundamental period are around 0.55 sec, except for the shorter bridges (< 300 meters). As a result, one of the most noticeable features is that the DD for the case of SVSGM with V_r=500m/s, is much lower than the other SVSGM cases, which in comparison with the A_1-D_1 results is completely different. The drop in fundamental period results in the bridges being susceptible to larger V_r values. In this case, the lower V_r value (500m/s) that for A_1-D_1 resulted in larger DD values now results in much smaller values than the other SVSGMs. The wave passing through the bridge with a particular value of V_r may amplify or not the DD of the piers, depending on the relation between the bridge's frequency and the frequency associated with V_r. This effect is shown in a later section (7.5.3). Regarding other details of the results, the DD from the Uniform load case and the other SVSGMs are very similar, except for shorter bridges (<300 meters) where the DD for the smaller V_rs (500m/s to 1000m/s) is substantially lower.

From Figure 7.26 to Figure 7.29 the DD envelopes/profiles, for the SVSGMs with different V_r values and the uniform seismic load case, are presented for different bridge lengths.

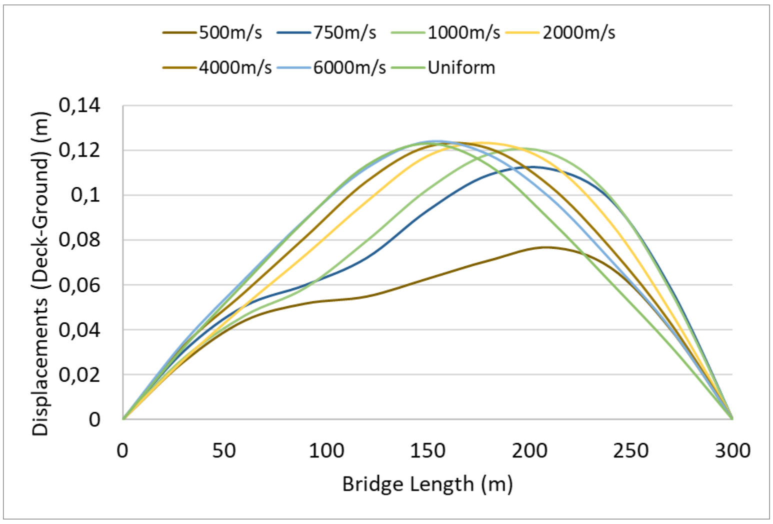

Figure 7.26 DD envelope of the regular A_2-D_2 300-meter bridge case-study, subjected to the uniform seismic load case and SVSGMs with different V_r values.

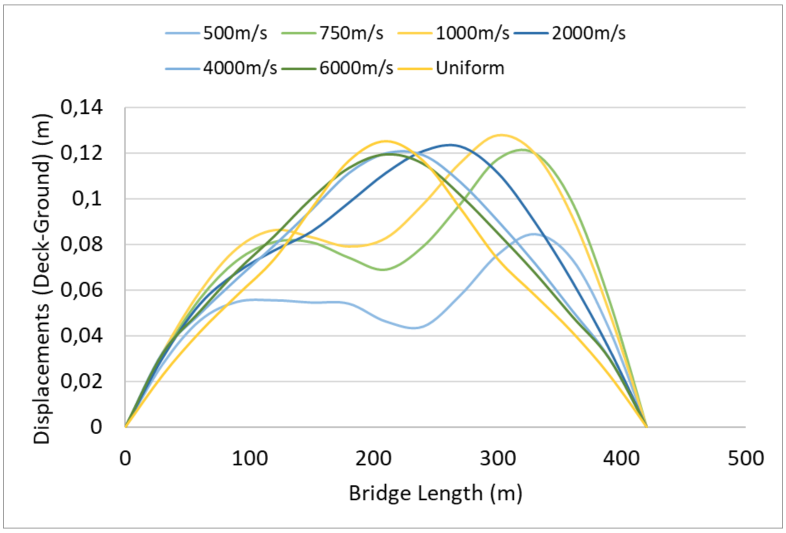

Figure 7.27 DD envelope of the regular A_2-D_2 420-meter bridge case-study, subjected to the uniform seismic load case and SVSGMs with different V_r values.

It is interesting to compare Figure 7.26 to Figure 7.17, which correspond to the same bridge length and where the only differences are the α value of the SVSGMs and especially the variables, A_2-D_2 and A_1-D_1 respectively. This change in variables from A_1-D_1 to A_2-D_2 results in a smaller relative stiffness ratio between deck and piers. As a result, the piers have larger control over the DD profile of the bridge. This is noticeable when comparing the DD profile in Figure 7.17, where all profiles are very similar regardless of the V_r value, except for V_r=500m/s, and the profile in Figure 7.26, where there is a more noticeable difference between all profiles, with a noticeable increment of DD in piers to the right-hand side of the middle of the bridge.

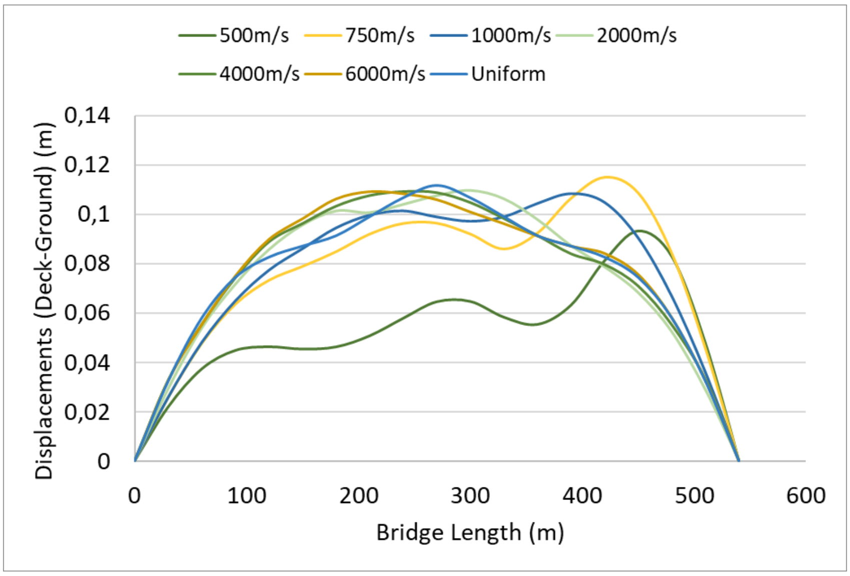

Figure 7.28 DD envelope of the regular A_2-D_2 540-meter bridge case-study, subjected to the uniform seismic load case and SVSGMs with different V_r values.

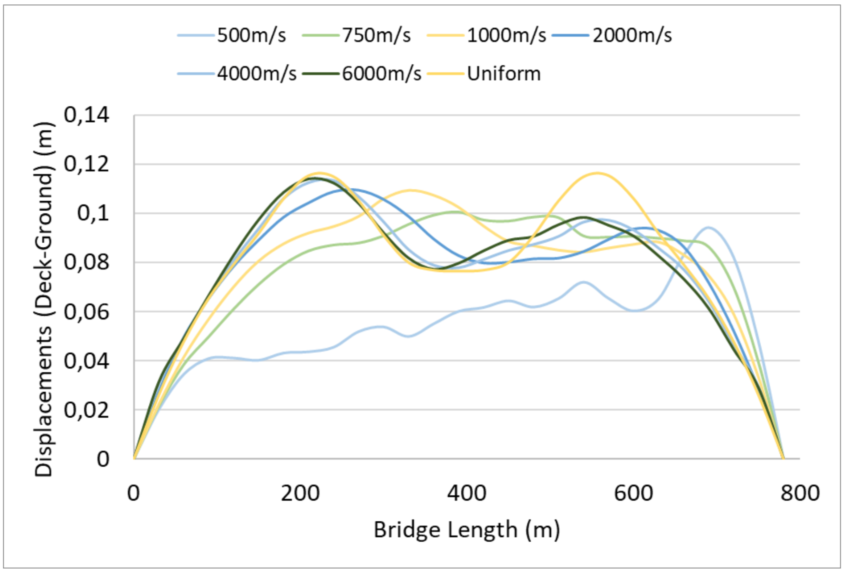

Figure 7.29 DD envelope of the regular A_2-D_2 780-meter bridge case-study, subjected to the uniform seismic load case and SVSGMs with different V_r values.

In all figures (Figure 7.26 to Figure 7.29), the information is qualitatively the same to the cases studied in the previous Section 7.5.1.1, where essentially the SVSGMs change the DD envelope's shape, causing larger DD in non-critical piers when compared to the DD envelope of the uniform load case. This difference in DD envelopes is closely related to the V_r value, resulting in larger differences for lower values of V_r and small differences for high values of V_r.

From the results it is not apparent if there is any difference in varying the value for α, nor can there be so far since the case-studies presented herein up to this point are not comparable due to having different pier variables (A_1-D_1 and A_2-D_2). In the next section, comparison will be made between case-studies whose only difference is the α value.

7.5.1.3 Comparison of α=2.0x10^{-4} with α=3.0x10^{-4}

In this section the effect of α in the results will be analysed by comparing case-studies between which only that parameter was changed. For that, SVSGMs with α values of 2.0x10-4 (SV_{20}) with and 3.0x10-4 (SV_{30}) are applied to regular bridges with various total lengths, as in previous sections, and with both A_1-D_1 and A_2-D_2 variable sets.

- With A_1-D_1 variables:

In Figure 7.30 the maximum pier DD versus bridge total length, for both α values and considering the A_1-D_1 variable set and V_r=500m/s. The graphs show that the maximum DD for both α values can be divided into three different groups, shorter bridges (<300m) which show equal maximum DD among both α cases, medium bridges (300m to 600m) which show larger values of maximum DD for SV_{20} than for SV_{30}, and longer bridges which show larger maximum DD values for SV_{30} than for SV_{20}.

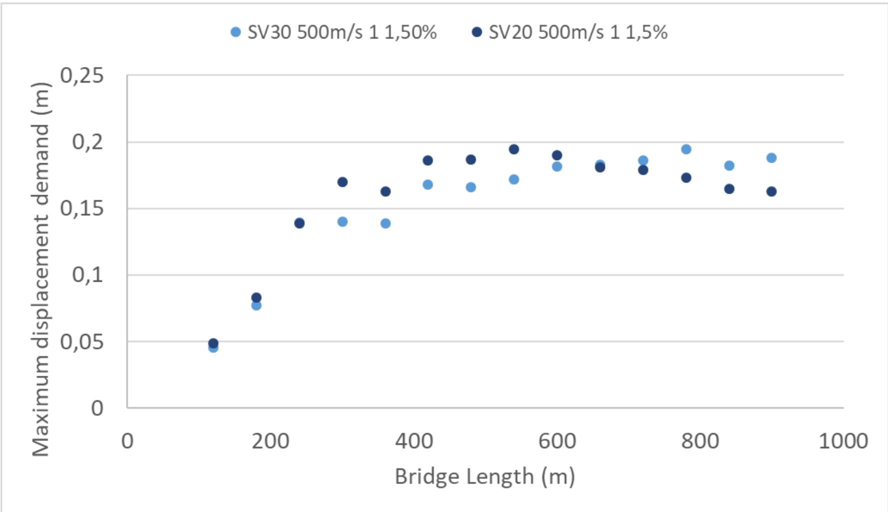

Figure 7.30 Maximum pier DD (maximum value of pier DD envelope) versus bridge total length. Each marker corresponds to a different α value of the SVSGM, where SV_{30} corresponds to 3.0x10^{-4} and SV_{20} to 2.0x10^{-4}. V_r=500m/s.

The interpretation for the results, regarding each group, is in the following:

1. For shorter bridges, spatial variability has less impact on the dynamic behaviour of the bridge, and so it follows that variation in the α value would not be apparent in the results.
2. For medium bridges, SV_{30} creates a larger disruption in the dynamic behaviour resulting in a smaller maximum DD than SV_{20}.
3. The pseudo-static effects become larger with the bridges' total length. It logically follows that for longer bridges, the pseudo-static effects are larger for a larger coherency drop value (SV_{30}) than a smaller one (SV_{20}), which, due to a bigger influence of pseudo-static effects, result in larger maximum DD for SV_{30} than SV_{20}.

In Figure 7.31 and Figure 7.32, two examples of DD envelope comparison between SV_{20} and SV_{30} (540-meter and 780-meter bridges) are shown. From both figures it is clear that the variation in α doesn't change the DD envelopes' shape very much other than maximum DD value, and overall, the impact of the α value variation is not very large, as it was varied between both limit values and did not result in significant differences between DD envelopes.

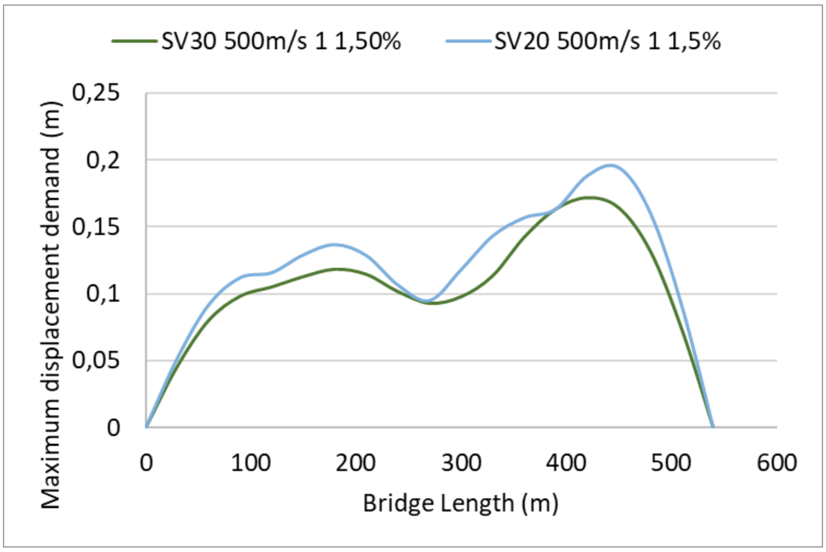

Figure 7.31 DD envelope for SV_{20} and SV_{30} (V_r=500m/s) and 540-meter bridge length.

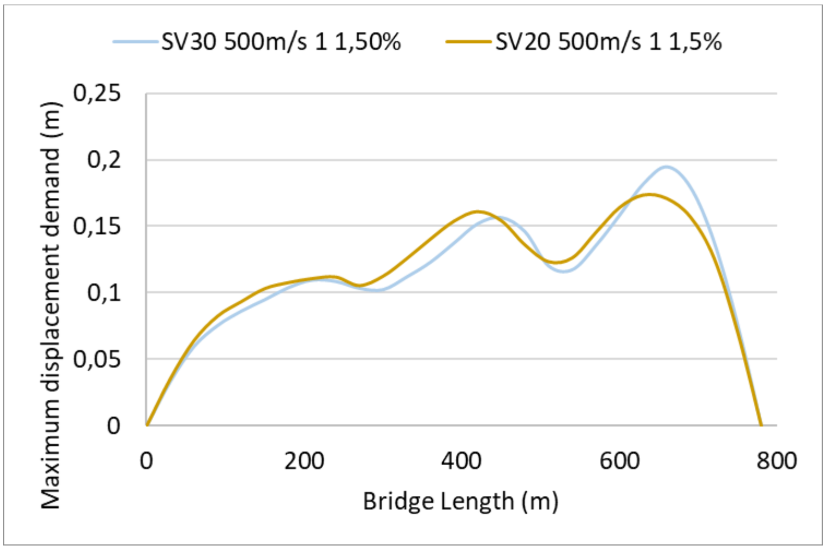

Figure 7.32 DD envelope for SV_{20} and SV_{30} (V_r=500m/s) and 780-meter bridge length.

From Figure 7.33 to Figure 7.35 another comparison is presented between SV_{20} and SV_{30}, but in this case, with V_r=1000m/s. This time the maximum DD values are almost always very similar, albeit following the same trend as in the previous example, i.e., maximum DD value for SV_{20} larger than SV_{30}'s for medium bridges, and lower than SV_{30}'s for longer bridges.

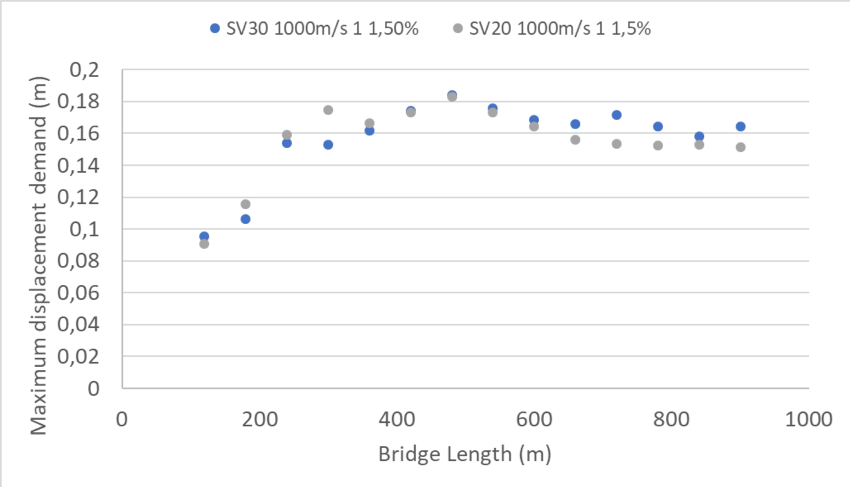

Figure 7.33 Maximum pier DD (maximum value of pier DD envelope) versus bridge total length. Each marker corresponds to a different α value of the SVSGM, where SV_{30} corresponds to 3.0x10-4 and SV_{20} to 2.0x10-4. V_r=1000m/s.

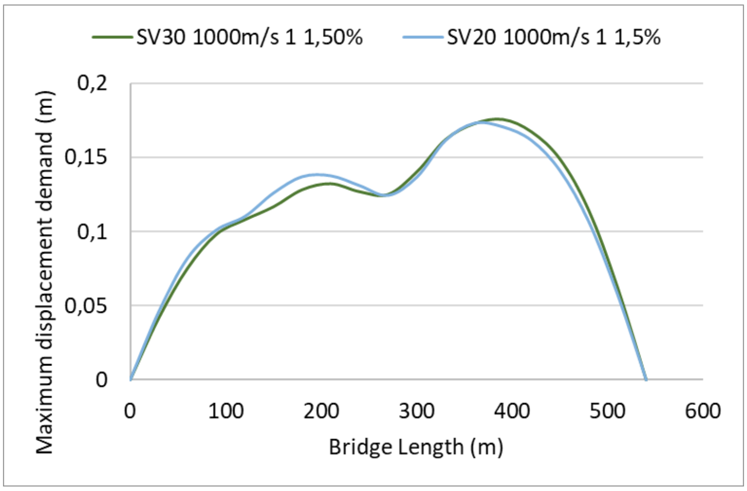

Figure 7.34 DD envelope for SV_{20} and SV_{30} (V_r=1000m/s) and 540-meter bridge length.

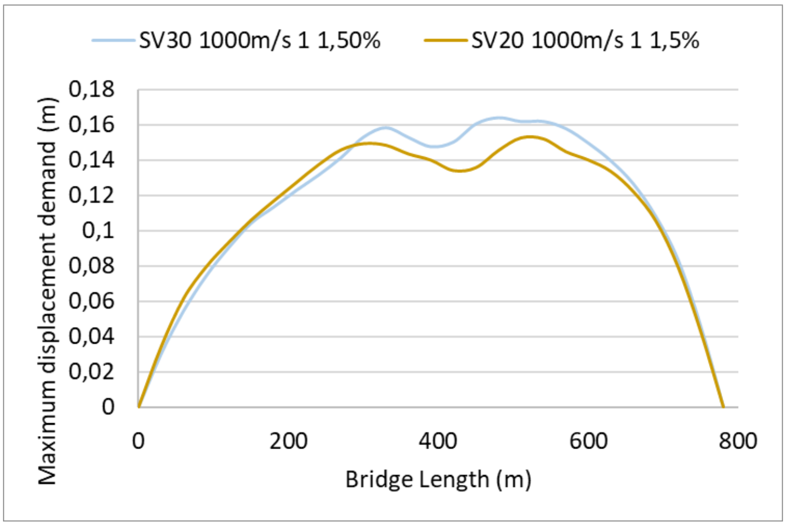

Figure 7.35 DD envelope for SV_{20} and SV_{30} (V_r=1000m/s) and 780-meter bridge length.

As in the previous case (V_r=500m/s) both SV_{20} and SV_{30} DD envelopes are qualitatively similar in shape, and the impact of α's variation is once again low.

- With A_2-D_2 variables:

With A_2-D_2 variables the results are slightly different between SV_{20} and SV_{30}. This can be, perhaps, explained by the difference in fundamental period of the case-study bridges with both variable sets. The fundamental period with A_2-D_2 variables is about half the period than with A_1-D_1. With A_2-D_2 the fundamental period is between 0.50s-0.70s (1.43Hz-2.0Hz) while with A_1-D_1 it is between 1.0s-1.4s (0.71Hz-1.0Hz). It so happens that for the said frequency ranges there is a clear larger gap between coherency functions for the A_2-D_2 frequency range, as shown in Figure 7.36.

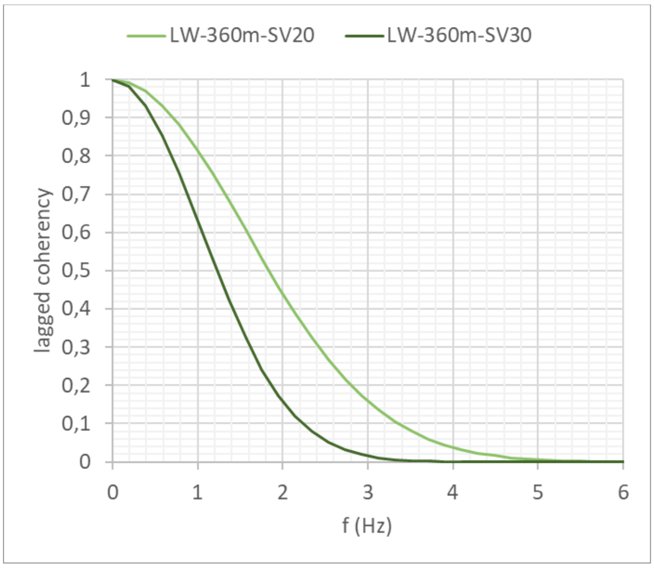

Figure 7.36 SV_{20} and SV_{30} coherency functions for 360-meter station distance.

As a result, it makes sense that there is a larger difference between SV_{20} and SV_{30} DD envelopes for the A_2-D_2 variable set than for A_1-D_1. Figure 7.37 shows the maximum DD versus bridge total length for both α values. Regardless, the same trend as before is apparent, with a larger difference for medium bridges and an approximation by SV_{30} to SV_{20} for longer bridges.

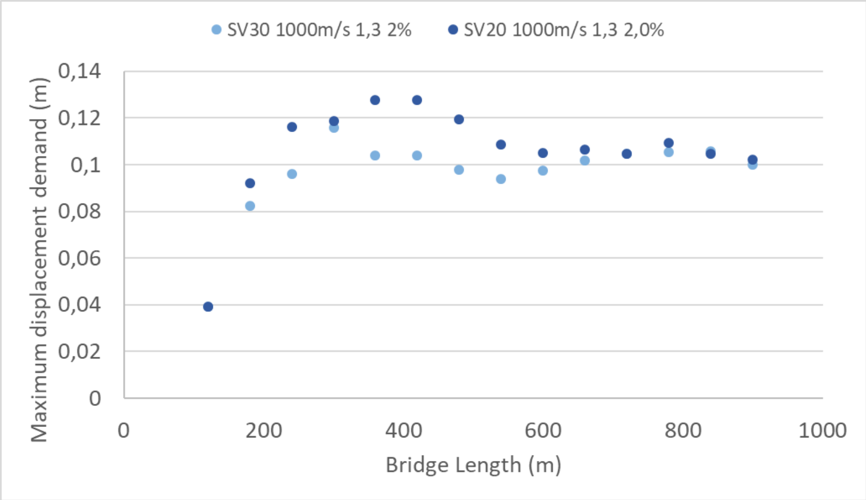

Figure 7.37 Maximum pier DD (maximum value of pier DD envelope) versus bridge total length. Each marker corresponds to a different α value of the SVSGM, where SV_{30} corresponds to 3.0x10-4 and SV_{20} to 2.0x10-4. V_r=1000m/s.

Figure 7.38 and Figure 7.39 show that there is in fact a bit of a difference between DD envelopes shape which makes sense considering the previous explanations.

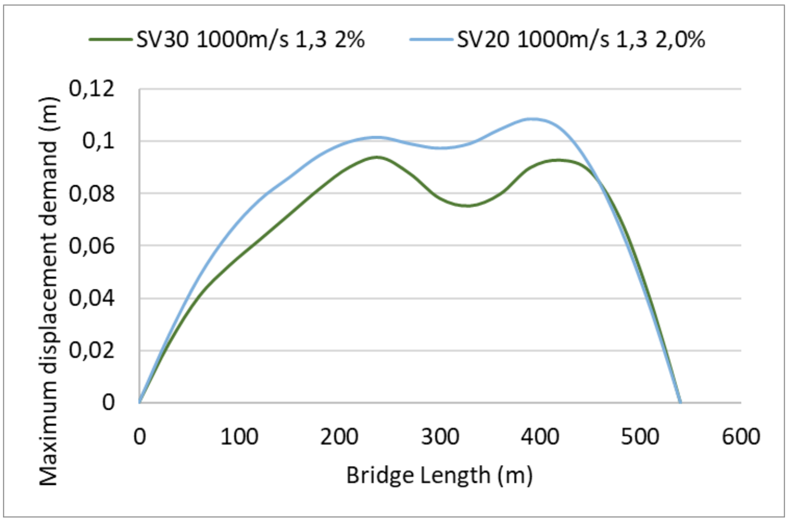

Figure 7.38 DD envelope for SV_{20} and SV_{30} (V_r=1000m/s) and 540-meter bridge length.

Figure 7.39 DD envelope for SV_{20} and SV_{30} (V_r=1000m/s) and 780-meter bridge length.

Overall, the difference between both limit values of α ends up being relatively small, considering that bridges usually have fundamental periods in the range and even higher than with the A_1-D_1 variable set. Taking that into consideration, it may be expected that SV_{20} and SV_{30} not show significant differences for most bridge cases, and so adopting the middle value of $2.5x10^{-4}$ is a good solution.

7.5.2 Irregular bridges with A_1-D_1 variables and SV_{30}

This section's focus is on the irregular case-study illustrated in Table 7.3. The same figures as in previous sections, which plot maximum DD versus bridge length, must be modified due to the existence of piers with different lengths. For that reason, only showing the maximum value does not transmit the correct idea about DD, since the maximum value may be measured at the longest pier and the shortest pier may have bigger ductility demands with smaller imposed displacements, and so the graphs shown, in this section, present the maximum DD values for both the longer piers (9m) and shorter piers (6m). In Figure 7.40 and Figure 7.41 those graphs are shown, where in the former, results for the uniform load case and SVSGMs with V_r=1000m/s and V_r=3000m/s are presented, and in the latter, only the results for the SVSGM with V_r=3000m/s is shown.

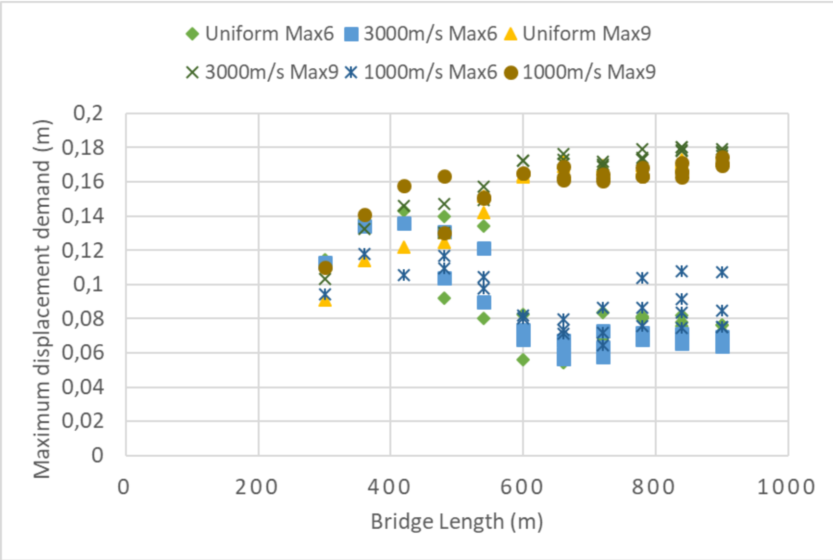

Figure 7.40 Max DD of 9 and 6-meter piers for the uniform load case and SVSGMs with V_r values of 1000m/s and 3000m/s.

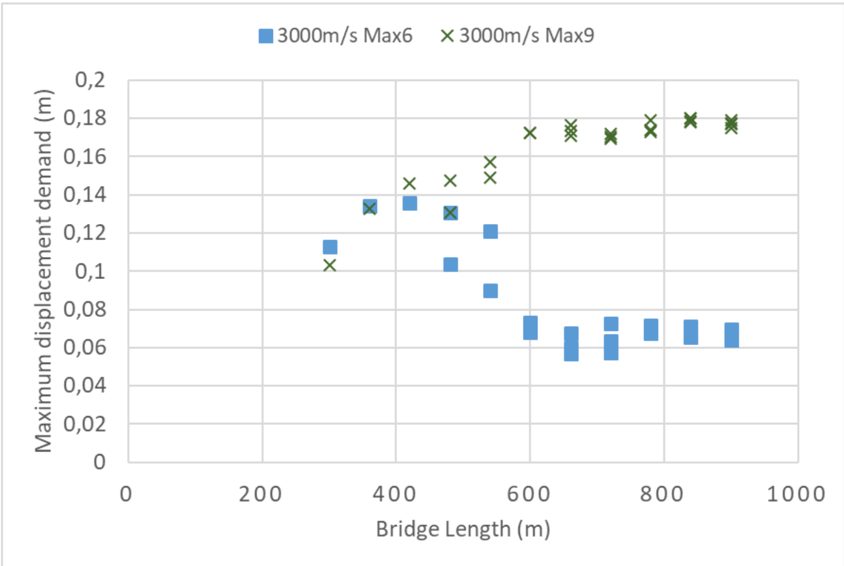

Figure 7.41 Max DD of 9 and 6-meter piers for SVSGM with V_r=3000m/s.

From Figure 7.40, it's clear there isn't a very big difference in the pier DD from all case-studies, except SVSGM with V_r=1000m/s, which shows larger DD for the short piers in bridges over 600-meters long, compared to the DD of short piers in bridges over 600-meters long for other values of V_r. As for Figure 7.41, it is of special interest because it illustrates the issue of relative stiffness between deck and piers. As shown, the DD of long and short piers are very similar up to 420-meters in length, after which the DD demand of both piers separates into two very different trends. This is the local stiffness of piers being able to change the transverse horizontal displacement profile of the bridge. This effect becomes very clear in subsequent figures.

Figure 7.42 to Figure 7.45 show the DD envelopes for each bridge length and in each one the results for SVSGMs with different V_rs as well as the uniform load case. For Figure 7.44 and Figure 7.45, the previously mentioned effect is apparent, with a clear change in the transverse horizontal displacement profile, due to influence of the short central piers. In all figures it is clear that, just like with the regular bridge case-studies, there is a modification in the DD envelope with the inclusion of spatial variability that results in an increase in the DD for certain piers, compared to the uniform load case.

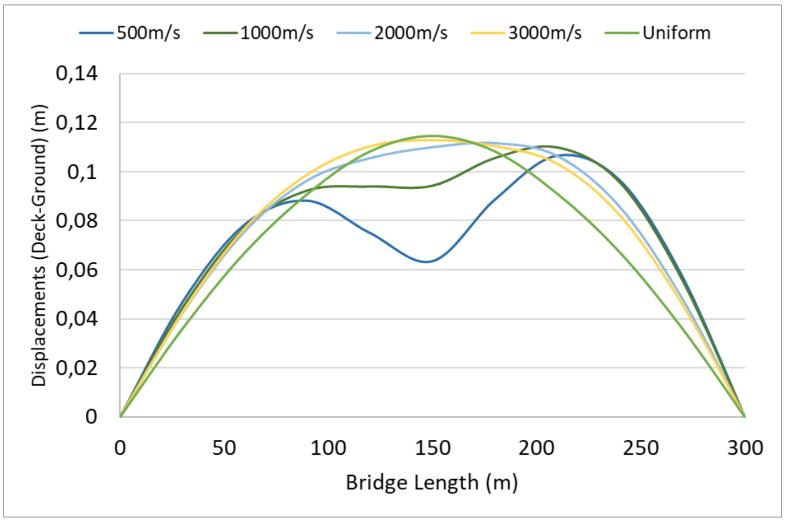

Figure 7.42 DD envelope of the irregular A_1-D_1 300-meter bridge case-study, subjected to the uniform seismic load case and SVSGMs with different V_r values.

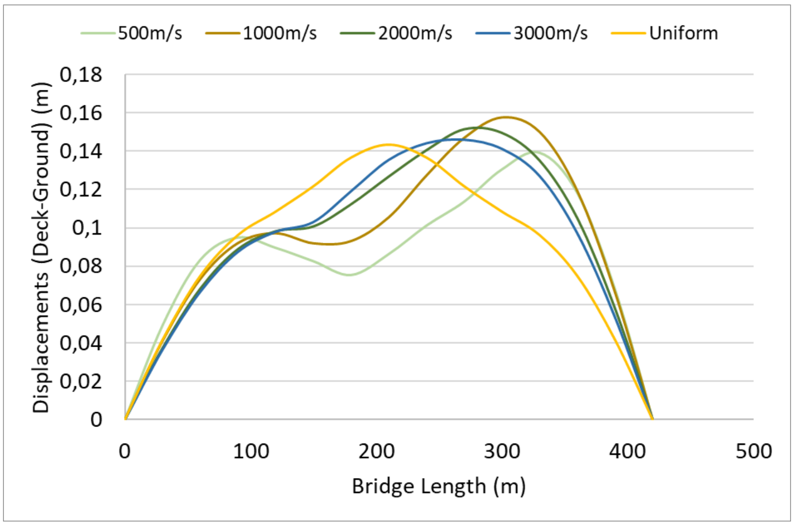

Figure 7.43 DD envelope of the irregular A_1-D_1 420-meter bridge case-study, subjected to the uniform seismic load case and SVSGMs with different V_r values.

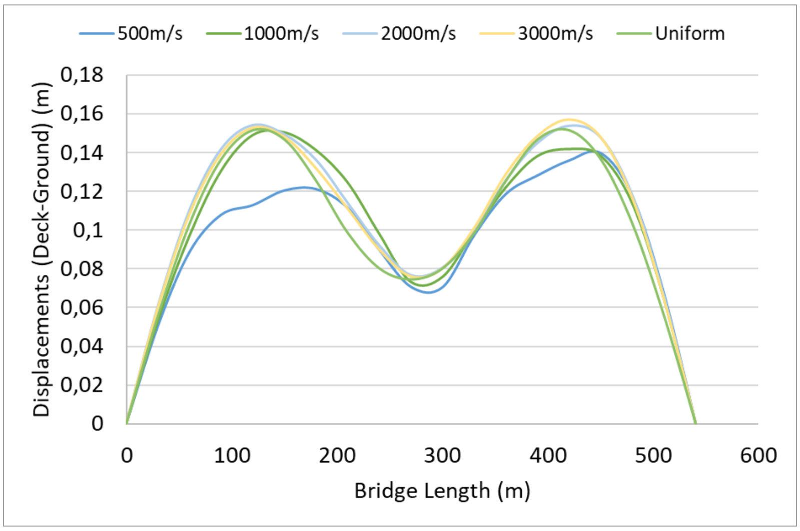

Figure 7.44 DD envelope of the irregular A_1-D_1 540-meter bridge case-study, subjected to the uniform seismic load case and SVSGMs with different V_r values.

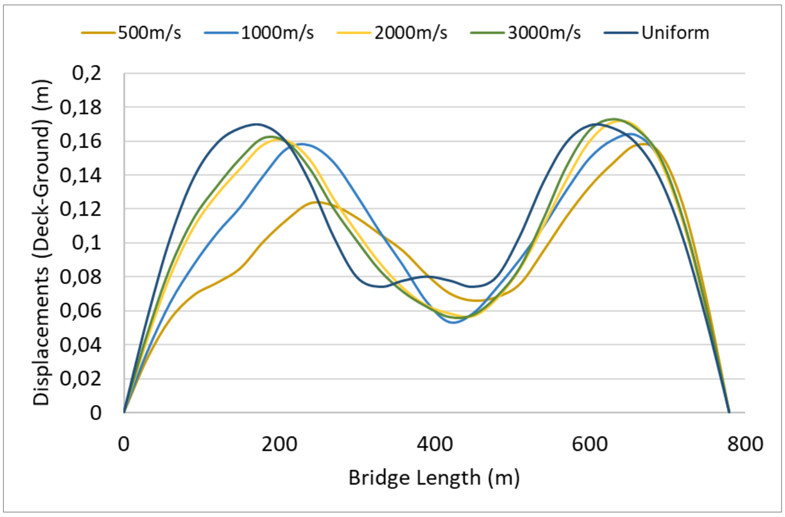

Figure 7.45 DD envelope of the irregular A_1-D_1 780-meter bridge case-study, subjected to the uniform seismic load case and SVSGMs with different V_r values.

Figure 7.46 to Figure 7.49 show, once again, the normalized difference between the uniform load case DD and each of the SVSGMs. Once again, it is apparent that there is an increment in DD for some piers due to spatial variability. For longer bridges (> 420 m) there is a significant increment in the DD of some of the short piers, which is important for the seismic resistance of the bridge. In these images, the station position and the corresponding pier height, both in meters, are displayed in the x-axis of the figures.

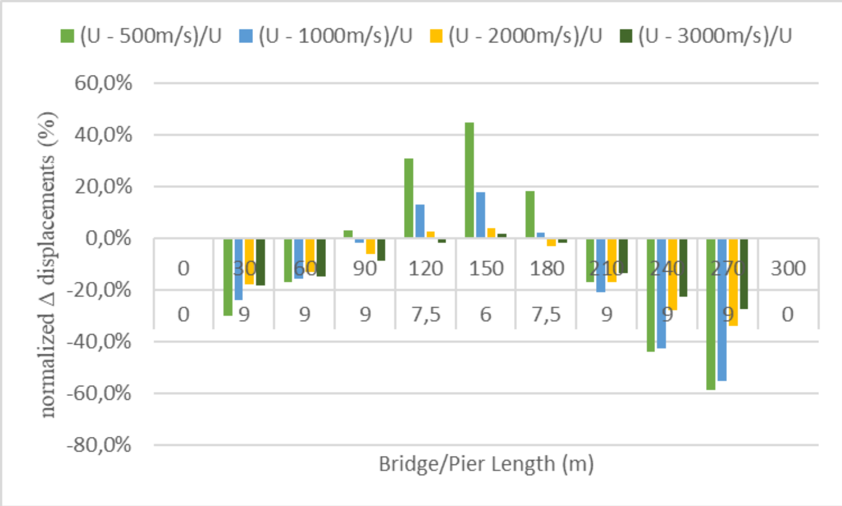

Figure 7.46 Pier DD envelope difference between the uniform load case and each of the SVSGMs for the irregular A_1-D_1 300-meter bridge case-study.

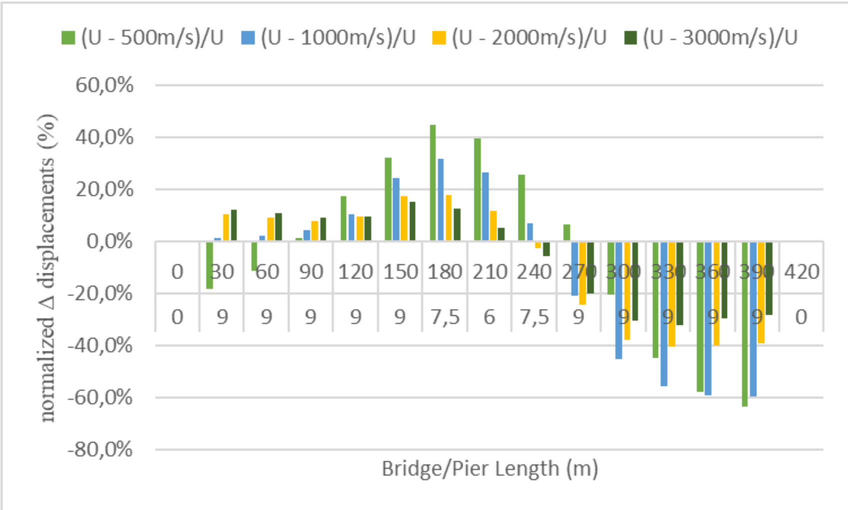

Figure 7.47 Pier DD envelope difference between the uniform load case and each of the SVSGMs for the irregular A_1-D_1 420-meter bridge case-study.

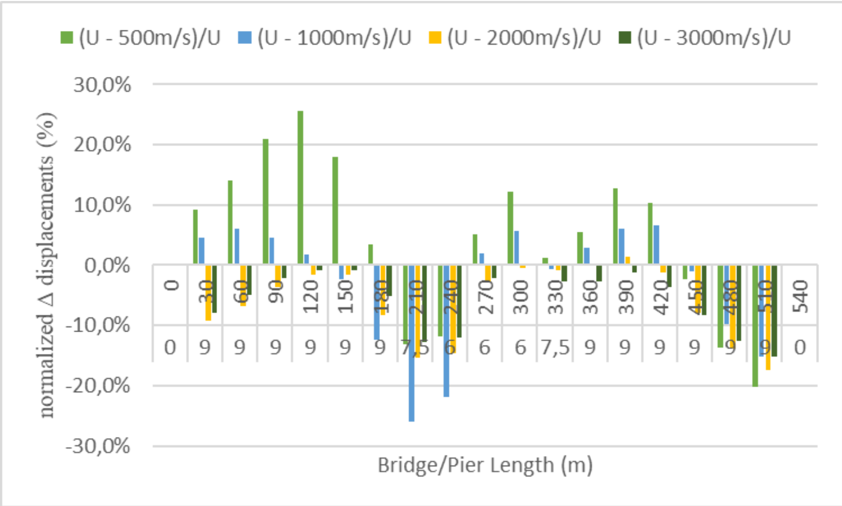

Figure 7.48 Pier DD envelope difference between the uniform load case and each of the SVSGMs for the irregular A_1-D_1 540-meter bridge case-study.

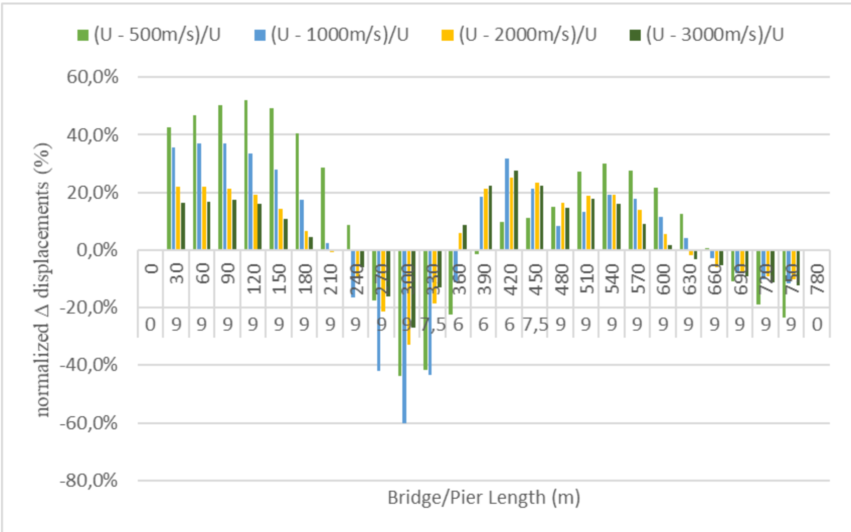

Figure 7.49 Pier DD envelope difference between the uniform load case and each of the SVSGMs for the irregular A_1-D_1 780-meter bridge case-study.

7.5.3 Effect of the apparent wave propagation velocity

In Section 7.5.1.1, it was mentioned a graph shift effect visible in the SVSGM's DD envelopes, in comparison to the DD envelope from the uniform loading case. The analysis and further interpretation of the effect was postponed to the present section. The results shown in this section correspond to only one record instead of average of maximum values as in previous sections. In Figure 7.50 and Figure 7.51, examples of regular case-studies, where the displacement profiles, at the instant in which the maximum DD is reached, are presented. From the figures, it is clear that the smaller the V_r value the more the graph is shifted to the right-hand side. Furthermore, the smaller the V_r the narrower is the wave. This effect resembles a kind of whiplash effect that is clearly correlated with the V_r (apparent wave propagation velocity) and with the bridge's fundamental period of vibration. This effect can also be composed by pseudo-static effects, and it also accounts for the increment in pier DD, which was verified for some of the piers in most SVSGM results.

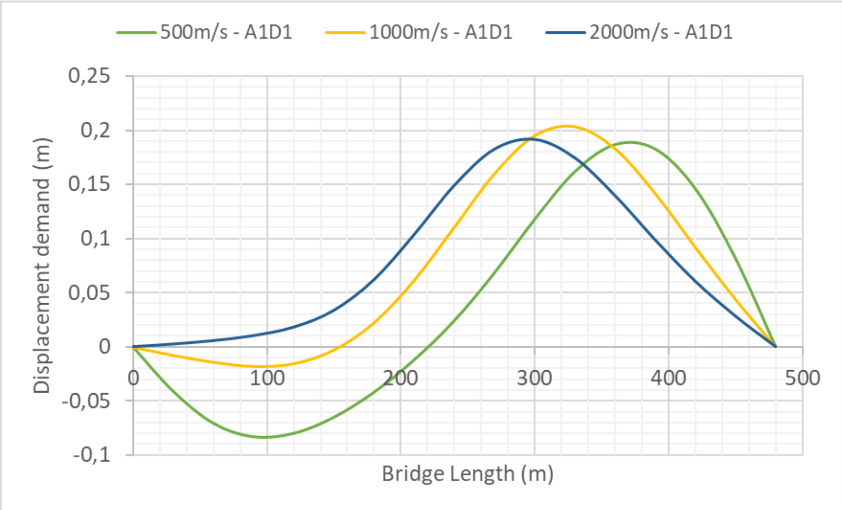

Figure 7.50 DD profile at the instant of maximum DD for three SVSGMs with A_1-D_1 variables.

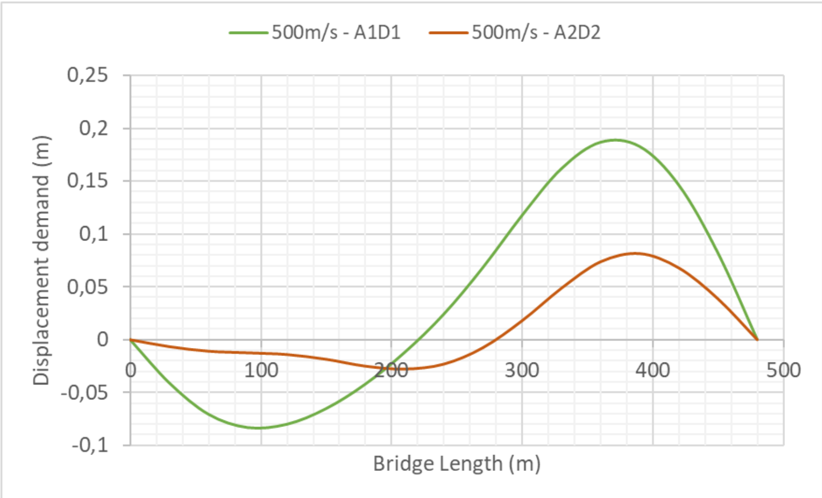

Figure 7.51 DD profile at the instant of maximum DD for one SVSGM with both A_1-D_1 and A_2-D_2 variables.

For better understanding of the effect, Figure 7.52 and Figure 7.53 show sequences of instants prior to reaching the instant of maximum DD. Figure 7.52 refers to the case-study 1000m/s A_1-D_1, from Figure 7.50 and Figure 7.53 refers to case-study 500m/s A_2-D_2 from the same figure. The figures illustrate the whiplash effect and the influence of both the V_r value and the fundamental period of the bridge on the wavelength of the whiplash.

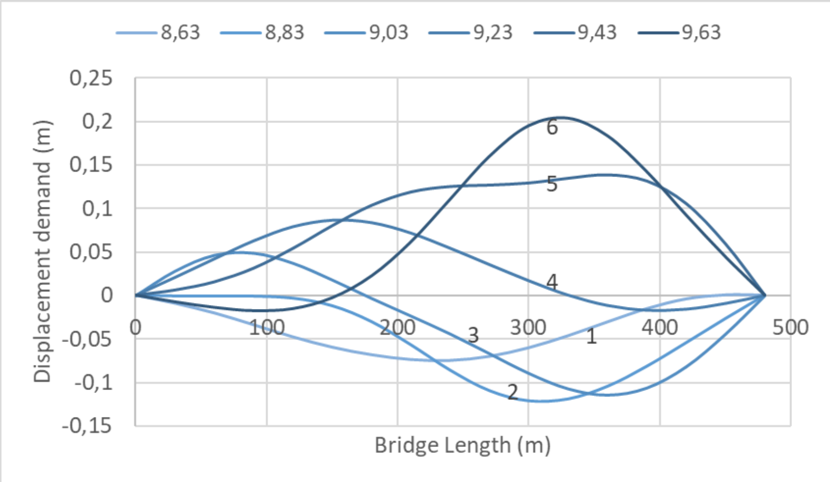

Figure 7.52 DD profile sequence prior to reaching maximum DD for 1000m/s, A_1-D_1 case-study (Figure 7.50). Values at the top of the graph represent time and values adjacent to curves represent the sequence.

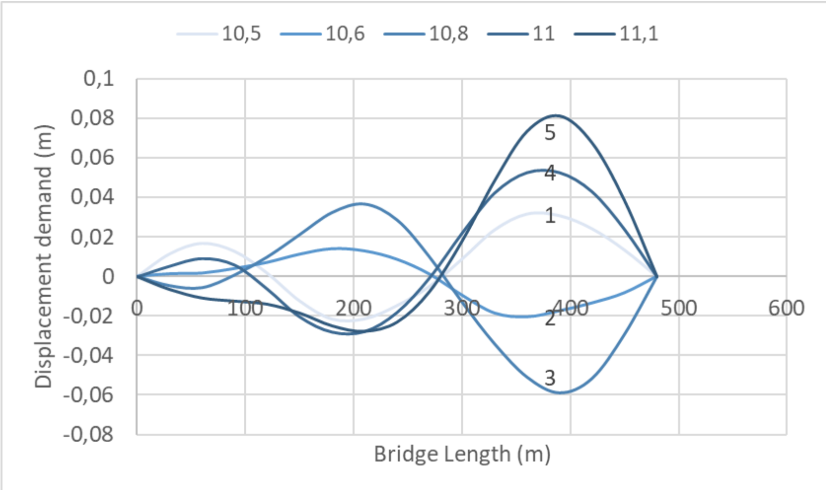

Figure 7.53 DD profile sequence prior to reaching maximum DD for 500m/s, A_2-D_2 case-study (Figure 7.50). Values at the top of the graph represent time and values adjacent to curves represent the sequence.

The whiplash effect creates a large local DD on the piers, which usually results in larger local values of DD compared to the uniform seismic load case. Furthermore, this local dynamic amplification is clearly associated with the fundamental frequency of the bridge and the V_r of the SVSGM, both of which influence the wavelength of the whiplash. Finally, Figure 7.54 shows that the whiplash effect is associated with the maximum DD, and also has a localized effect, by comparing the instant of the whiplash and the DD envelope.

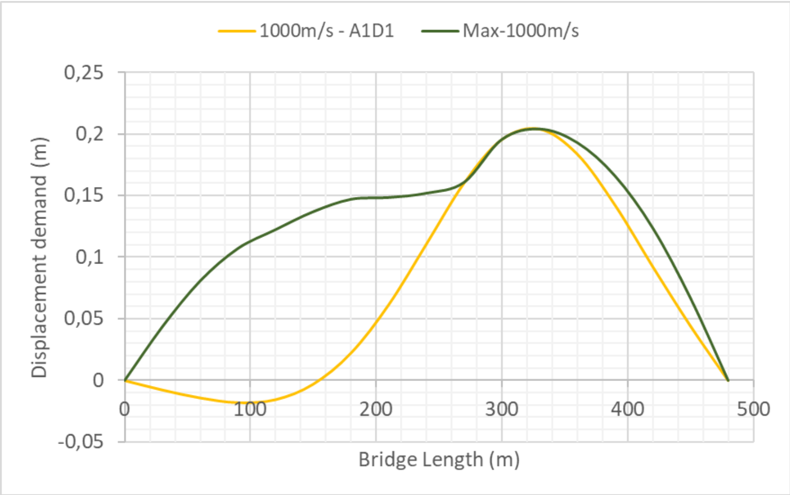

Figure 7.54 Comparison of the whiplash instant with the DD envelope for case-study 1000m/s A_1-D_1 from Figure 7.50.

7.6 Conclusions

In this study, a comprehensive analysis on the effects of spatial variability to a particular typology of RC bridges was performed. The author believes that the conclusions are, nonetheless, applicable to other bridge typologies. Overall, the main idea is that spatial variability sufficiently impacts the shape of the transverse horizontal displacement profile of the bridge, or in other words, changes the piers' displacement demand (DD) envelope's shape sufficiently that some piers along the bridge are subjected to more DD with spatially variable seismic ground motions (SVSGM) than with a uniform seismic load. It is clear, from all case-studies, that the maximum pier demand is either very similar or slightly higher for the uniform load case, but in all case-studies there are piers that have more DD with the SVSGM than with the uniform seismic load, and vice-versa. This means that design of piers according to their perceived local DD may be unsafe, and so designing all piers equal to sustain the same DD as the critical pier may be much safer when considering spatial variability.

This work applied and modified methodologies to obtain displacement SVSGMs compatible with initial ground motions and with coherency models. However, there is some uncertainty associated with the models and methodologies themselves. Some of the uncertainty was studied with the variation of the coherency drop parameter (α) and the apparent wave propagation velocity (V_r), but there is also uncertainty associated with the coherency model itself. In addition, the study does not contemplate other important factors such as local soil effects with soil changes along the bridge. Nonetheless, the results herein remain very useful and allow to perceive several mechanisms associated with spatial variability that impact long structures such as bridges.

Mechanisms such as the whiplash effect, which became evident with the variation of the V_r value and may be thought of as a mixture between dynamic amplification effects and also pseudo-static effects, contributes definitively for the increase in DD of some piers, when compared to the DD for the uniform load case. Furthermore, it was interesting to realize the seemingly correspondence between V_r, the fundamental period of the bridge, and the wavelength of the whiplash effect. Some future studies should be developed about this issue, going into a little bit more detail and trying to establish an analytical expression between the bridge and SVSGM characteristics and the whiplash's wavelength. Nonetheless, for the author it seems to be one of the main mechanisms for having increased DD in some piers.

At the same time, the variance in the α value does not seem so important, since the variation of the piers' DD seems small even when varying the α between both limit values proposed by Luco and Wong. This suggests that, even though there is some difference in the results, overall a middle value for the α may be employed, since this factor does not seem to be a very big source of uncertainty in the results. That is not the case with the value of V_r, as shown throughout the study.

Finally, the existence of pier irregularity along the bridge may result in local increments of DD as well, at those irregularities, compared to the uniform load case. The position of the piers that suffer the increase in DD is related to the direction of the wave propagation. This can be easily noted from the DD envelopes presented in this study. Also, the more abrupt the nature of the irregularity, the more these local effects are verified, and so a very sudden variation in pier length and subsequent stiffness results in important local increases in ductility demand of the piers in those positions.

In this work it also must be said that the effect of the spatial variability is only analysed in the transversal direction: it is assumed that the effects in the longitudinal direction are not as important, since the largest asynchronous effect would result from the earthquake waves propagating longitudinally relatively to the bridge which would result in larger displacements for the transversal seismic action (S-waves). Thus, for a longitudinal seismic action the asynchronous effect would be much smaller because it would mean wave propagation essentially in the transverse direction of the bridge, since S-waves which act transversally to the propagation direction are the main cause of damage. If the analysis in the longitudinal direction were to be performed, the issue can be qualitatively discussed separating dynamic from pseudo-static effects. As in this direction the bridge behaves essentially as a SDOF structure due to the axial stiffness of the deck, the dynamic effects of the asynchrony would essentially result in some reduction of the dynamic effects as compared to a uniform action in all foundations. Regarding pseudo-statics effects, even though the relative displacement demand between pier foundations is smaller than in the transversal direction, it is also necessary to bear in mind that the bridge capacity to accommodate those displacements is smaller in the longitudinal direction than in the transversal direction. This is due to the fact that in the transversal direction those displacements are absorbed by the deck's and piers' deformations, and in the longitudinal direction only by the piers' deformations due to the deck axial stiffness.

8 Final Remarks and Future Works

8.1 Final Remarks

This thesis is multidisciplinary even though its core is about earthquake engineering. It has a strong component of optimization and a significant part of the research is on the development of metaheuristic algorithms for optimization, from the family of the genetic/evolutionary algorithms. Structural optimization is a fascinating field, particularly when employing this type of search algorithms, that allow to tackle complex non-convex problems. This type of algorithms has only recently (the last 15 years) begun to be applied in earthquake engineering. Their application in this thesis was crucial, to be able to provide an automatic and systematic approach to the search for optimal bridge structures concerning their ability to withstand the earthquake action. The results were of various forms, from devising frameworks and methodologies for optimization to the application of those methodologies to large sets of case studies with the goal of extracting rules and guidelines for earthquake design of bridges. It is important to reiterate that the development of these automated design techniques is not intended as a substitution of the design engineer but rather a tool that systematizes the search for the best design and gives mathematical formalism to what design engineers already do based on experience. These techniques allow the engineer to broaden his search by allowing to analyse a much larger set of solutions than would be possible through a manual trial and error process, thus discovering design solutions that can otherwise be difficult to attain.

In these final remarks, a walkthrough of all the chapters with emphasis on the main outcomes from each one is made. In this concern the main chapters are 4, 5, 6 and 7, with some important results coming from Chapter 2.

Starting in Chapter 2, more concretely regarding Section 2.2, where the analysis on the factors that influence ductility based on a previous work by (Brito 2011) was presented. In this section, comprehensive analysis on the effects of several factors on both the yield and ultimate curvature, was done. Specifically, the modification of the EC8 – part 2 (CEN 2005) expression for the estimation of the yield curvature for circular RC cross-sections was analysed, with the introduction of a factor that accounts for the influence of axial force. The base expression is already a good estimate on the value of the yield curvature; however, the inclusion of the additional factor clearly improves the accuracy of the estimation since there can be some significant variation of the yield curvature with axial force, which is well-captured by the extra factor in the expression. The rest of Chapter 2 and the whole of Chapter 3 introduces several concepts and defines the field of application of the analyses performed in Chapters 4, 5, 6 and 7.

In Chapter 4, the development of a structural optimization framework for structures subjected to earthquake action is presented. A well-known genetic/evolutionary algorithm for optimization is modified and adapted to a methodology for structural optimization, in this instance applied to bridges subjected to earthquake actions. The presented methodology is applied to a case-study and the advantages (and also disadvantages) of the application of such algorithms in a seismic design process are explained.

Among the advantages are the systematization and automation of the optimization process for such non-convex and non-linear problems. Additionally, the application of these algorithms provides an idea of the entire set of solutions that can be used, and from that set of solutions it becomes possible to define rules and rank decision (design) variables according to their importance regarding earthquake performance. It is the performance-based design with structural optimization, which can become a powerful tool when used on different structures because the results can be used to define rules, which is precisely what is done in subsequent Chapters 5 and 6. In fact what genetic/evolutionary algorithms do, by using a population of solutions and not the typical optimization based on gradients, is what designers in fact do based on experience and considering very small populations of solutions. The mathematical formalism of genetic/evolutionary algorithms not only represents a more sophisticated framework, as it allows to widen the population of possible analysed solutions.

In Chapter 5, the application of the algorithm towards the analysis and calibration of the q-factors for the design of RC bridges in the longitudinal direction is performed. In this section it is shown that the traditional earthquake design of structures, which is done by defining the resistance of elements only as an output of seismic analysis, does not make sense, because from the optimization algorithm, it is shown that there are several distributions of flexural steel reinforcement between elements leading to similar earthquake performances, as long as their total strength/stiffness is above a given value. Of course, what influences the ability of redistribution is the irregularity of the piers and from the analyses it is shown how the irregularity affects the admissible values of q-factor. In this section a new expression for the definition of irregularity is presented which measures the variance of the yield displacements of all piers regarding the yield displacement of the shortest pier. It is then shown that this irregularity index is very much correlated with the behaviour factor of the bridge, which stems from the impact of irregularity on energy dissipation during the earthquake, since irregularity implies that piers enter nonlinear behaviour at different points in the overall force-displacement relationship. From this a function is presented that estimates the real q-factor that can be used for a given bridge, using as input the yield displacement of the shortest pier, the target displacement, and the pier irregularity index:

$$q = m_q(PIrr) \cdot \left(\frac{Sd_t}{R_y} - 2.21\right) + 3.26 \tag{5.7}$$

This function fits the nonlinear analysis very well, showing that q-factors prescribed by EC8 are well calibrated and can be safely used for the seismic design of irregular bridges. This stems from the fact that that EC8 code prescribed q-factors are conservative, a little excessively in some cases. The expression derived in this thesis allows to safely use higher values of the q.-factor by taking advantage of the reserve strengths associated with the conservatism of EC8 q-factors

In Chapter 6, the analysis and application of both the multi-objective evolutionary algorithms and the parallel computation framework capabilities are used to study the behaviour of bridges in the transverse direction. The results are then processed with the RSI index, which allows to separate short bridges from long bridges, as well as other stiffness-based indexes. The bridges studied in this section range from 120 meters to 900 meters of length and follow the different types of irregularity layouts presented in Chapter 3. The analysis of the results allowed to gain several insights on the behaviour of bridges which can be used for bridge design, particularly the correlation of the total pier stiffness with the mean displacement among piers; the impact of different irregularity, and their location, on bridge behaviour, the difference between short bridge behaviour and long bridge behaviour and how it influences pier design, the impact of the stiffness of piers adjacent to critical piers regarding structural safety, etc.; how irregularity and length influence the transverse horizontal displacement profile (THDP) of the bridge. At section 6.9, a collection of recommendations is presented regarding how the engineer can approach the design of such bridges, which issues to look out for and how the design of irregular bridges, in the transverse direction, can be approached:

At section 6.10 a particular case-study is used to illustrate the strength of the methodology and the accuracy of the previous findings. The addition of a classification technique called classification trees is used to define the path of analysis to classify the bridge as being able to resist the seismic action or not, according to global and local stiffness of the piers. The case-study corresponds to a long bridge with short central piers, which correspond to the bridges that are more susceptible of being affected by higher modes, and with critical piers located where piers usually have higher displacement demands (at the middle of the bridge). One of the most interesting conclusions extracted is that there are different ways to approach the design of the bridge, and this is objectively shown in the analysis of this case-study. It is shown that the irregularity can either be approached to reduce it, that is by means of different pier-deck connections and/or changing cross-section stiffness of the columns by means of changing the amount of flexural reinforcement of the piers, to change the transversal displacement profile of the bridge. This approach has the goal of increasing the critical pier's displacement capacity by more than the displacement demand. The other approach, which gives as good results in terms of difference between ductility demand and available ductility as the former, is to increase the irregularity by making the critical piers stiffer. This will force the bridge to deform according to higher modes (long bridge according to RSI), which reduces the displacement demand on the piers. This illustrates that, for long bridges there are many approaches that can work, which usually balance the global and local pier stiffness and shape of the THDP and the critical piers available ductility. For short bridges, the balance is essentially between global stiffness and the critical piers available ductility. The use of classification trees is very useful in that it allows to classify the variables according to their importance and defines paths of classification according to the entire set of dynamic analysis performed on the case-study bridge. The resulting tree corroborates the conclusions obtained previously in this chapter.

In Chapter 7 the work focuses on the influence of spatial variability of earthquake actions and its effect on the dynamic behaviour of bridges in the transversal direction. It is analysed what are the possible effects on bridge resistance and how this may impact seismic design. It is shown, essentially, that there are significant effects from spatial variability, especially for long bridges, and that while the maximum displacement demand does not suffer significant changes, there is often a shift according to the direction of propagation of the seismic waves, with significant increase in the displacement demand of some piers compared to the THDP obtained with uniform seismic action. The conclusions are that this should be accounted for in design by providing an extra capacity to non-critical piers and especially avoiding sudden stiffness transitions from long piers to short piers. The relevance of this chapter derives from the fact that it is one of the first studies with this type of bridges and with a large array of bridge lengths and different irregularity layouts analysed. Also of interest is the variation of factors associated with spatial variability of seismic actions, such as apparent wave propagation velocity and the coherency model's parameters. It is shown that some factors are more critical in the effect of the spatial variability and that there is significant uncertainty that stems from stochastic uncertainty of parameters such as V_r.

8.2 Future Works

This thesis covers a wide range of topics and there is a very large amount of works that could not be pursued herein due to obvious time constraints. It is clear that the thesis focuses on a particular type of bridge cross-section, and of course this should be applied to other bridge cross-sections, but also to other bridge typologies. The power of evolutionary algorithms and other meta-heuristics, such as classification trees, etc., is their ability to easily be adapted to other types of problems.

The systematic application of this methodology and of classification trees in the analysis of different case studies can be used to compose a set of rules for different bridges, according to different irregularity layouts and length classifications.

The study of other earthquake intensities and performance-based design for other levels of damage than the collapse prevention level used in this thesis would be of interest and should be studied.

Nowadays, there is ever more use of dissipation devices in bridges, such as steel hysteretic dampers and other anti-seismic devices that can be installed at the piers. The study concerning these devices is not easy due to the difficulty in obtaining prices for different devices and different resistance levels. This makes it difficult to perform cost-benefit analysis for these devices. Nonetheless they should be the subject of future studies. It seems particularly interesting to use genetic algorithms to define, for example, according to irregularity layout, where these devices should be installed for optimal performance, and how many are necessary in a given bridge with a given irregularity profile. The application of these techniques should also start being applied for other types of structures and should start to complement more the work of the design engineer. It should be said that these techniques only make sense as a complement of the engineer's work, because the engineer is always needed to filter out bad solutions or infeasible solutions that may be given by the techniques. On the other hand, the engineer can take advantage of these techniques because they allow to systematize and give consistence to knowledge that the engineer has gained from experience, but that he sometimes may not have well-structured and systematized in his mind.

Bibliography

Abadi, M. 2016. “TensorFlow: A System for Large-Scale Machine Learning.” *Proceedings of the 12th USENIX Symposium on Operating Systems Design and Implementation (OSDI ’16).* Savannah, GA, USA.

Abrahamson, N. A. 1985. *Estimation of seismic wave coherency and rupture velocity using SMART 1 strong-motion array recordings.* EERC Report No. UCB/EERC-85/02.

Abrahamson, N. A., and B. A. Bolt. 1987. “Array analysis and synthesis mapping of strong seismic motion.” In *Strong motion synthetics: Computational techniques series*, by B. A. Bolt, 55-90. New York: Academic Press.

Abrahamson, N. A., and B. A. Bolt. 1985. “The spatial variation of the phasing of seismic strong ground motion.” *Bulletin of the Seismological Society of America* 75 (5): 1247-1264.

Abrahamson, N. A., B. A. Bolt, R. B. Darragh, J. Penzien, and Y. B. Tsai. 1987. “The SMART-1 accelerograph array 1980-1987: A review.” *Earthquake Spectra* 3 (2): 263-287.

Akbari, R., and S. Maalek. 2018. “A review on the seismic behaviour of irregular bridges.” *Structures and Buildings* 171 (7): 552–580. doi:10.1680/jstbu.17.00081.

Akbari, R., and S. Maalek. 2010. “Adequacy of the seismic analysis methods for single column bent viaducts considering regularity and higher modes effects.” *Journal of Vibration and Control* 16 (6): 827-852.

Alam, M. I., B. Kanagarajan, and P. Jana. 2019. “Optimal design of thin-walled open cross-section column for maximum buckling load.” *Thin-Walled Structures* 141: 423-434.

Alvarez Botero, J. C. 2004. *Displacement-Based Design of Continuous Concrete Bridges Under Transverse Seismic Excitation.* Pavia, Italia: European School for Advanced Studies in Reduction of Seismic Risk.

Antoniou, S., and R. Pinho. 2004. “Development and Verification of a Displacement-based Adaptive Pushover Procedure.” *Journal of Earthquake Engineering* 8 (5): 643-661. doi:10.1080/13632460409350504.

Arellano, H., D. Tolentino, and R. Gómez. 2019. “Optimum Criss Crossing Cables in Multi-span Cable-stayed Bridges using Genetic Algorithms.” *KSCE Journal of Civil Engineering* 23 (2): 719-728. doi:10.1007/s12205-018-5736-2.

Azizi, M., R. G. Ejlali, S. A. M. Ghasemi, and S. Talatahari. 2019. “Upgraded Whale Optimization Algorithm for fuzzy logic based vibration control of nonlinear steel structure.” *Engineering Structures* 192: 53-70.

Beume, N., C. M. Fonseca, M. Lopez-Ibanez, L. Paquete, and J. Vahrenhold. 2009. “On the Complexity of Computing the Hypervolume Indicator.” *IEEE Transactions on Evolutionary Computation* 13 (5): 1075-1082. doi:10.1109/TEVC.2009.2015575.

Bolt, B. A., C. H. Loh, J. Penzien, Y. B. Tsai, and Y. T. Yeh. 1982. *Preliminary report on the SMART 1 strong motion array in Taiwan.* EERC Resport No. UCB/EERC-82/13.

Bolt, B. A., N. A. Abrahamson, and Y. T. Yeh. 1984. “The variation of strong ground motion over short distances.” *Proceedings of the 8th World Conference on Earthquake Engineering.* San Francisco, CA, USA. 183-189.

Boore, D. M., and J. J. Bommer. 2005. “Processing of strong-motion accelerograms: needs, options and consequences.” *Soil Dynamics and Earthquake Engineering* 25 (2): 93-115.

Boore, D. M., C. D. Stephens, and W. B. Joyner. 2002. “Comments on Baseline Correction of Digital Strong-Motion Data: Examples from the 1999 Hector Mine, California, Earthquake.” *Bulletin of the Seismological Society of America* 92 (4): 1543–1560.

Brito, A. 2011. “Design of Underground Structures Under Seismic Actions (PhD thesis).” *Instituto Superior Técnico (IST).*

Bybordiani, M., and S. Kazemzadeh Azad. 2019. “Optimum design of steel braced frames considering dynamic soil-structure interaction.” *Structural and Multidisciplinary Optimization* 60 (3): 1123-1137. doi:10.1007/s00158-019-02260-4.

Cacciola, P., and G. Deodatis. 2011. “A method for generating fully non-stationary and spectrum-compatible ground motion vector processes.” *Soil Dynamics and Earthquake Engineering* 31 (3): 351-360.

Calvi, G. M., A. Pavese, and P. E. Pinto. 1993. “Progettazione Antisismica di Ponti Non Regolari [Seismic design of irregular bridges] (in italian).” *Giornate AICAP-93.* Pisa.

Calvi, G. M., A. S. Elnashai, and A. Pavese. 1994. “Influence of regularity on the seismic response of RC bridges.” *Proceedings of 2nd International Workshop on Seismic Design and Retrofitting of RC Bridges.* Queenstown, New Zealand. 80-89.

Calvi, G. M., and A. Pavese. 1997. “Conceptual design of isolation systems for bridge structures.” *Journal of Earthquake Engineering* 1 (1): 193-218.

Calvi, G. M., C. Casarotti, and R. Pinho. 2006. “A comparative study of displacement, force and pushover approaches for design of continuous span bridges.” *Advances in Earthquake Engineering for Urban Risk Reduction* 379-394.

Calvi, G. M., M. J. N. Priestley, and M. Kowalsky. 2013. “Displacement-Based Seismic Design of Bridges.” *Structural Engineering International* 23 (2): 112-121. doi:10.2749/101686613X13439149157399.

Camacho, V. T., L. Guerreiro, C. S. Oliveira, and M. Lopes. 2021. “Effect of spatial variability of seismic strong motions on long regular and irregular slab-girder RC bridges.” *Bulletin of Earthquake Engineering* 19 (2): 767-804. doi:https://doi.org/10.1007/s10518-020-01002-y.

Camacho, V. T., M. Lopes, and C. S. Oliveira. 2020. “Revising seismic behaviour factors for reinforced concrete bridge design in the longitudinal direction using multi-objective evolutionary algorithms.” *Bulletin of Earthquake Engineering* 18 (3): 925–951. doi:https://doi.org/10.1007/s10518-019-00739-5.

Camacho, V. T., N. Horta, and M. Lopes. 2020. “Multiobjective optimization of long irregular RC bridges’ piers subjected to strong motions and definition of classification tree surrogate models.” *Proceedings of the 9th European Workshop on the Seismic Behaviour of Irregular and Complex Structures.* Lisbon, Portugal.

Camacho, V. T., N. Horta, M. Lopes, and C. S. Oliveira. 2020. “Optimizing earthquake design of reinforced concrete bridge infrastructures based on evolutionary computation techniques.” *Structural and Multidisciplinary Optimization* 61 (3): 1087–1105. doi:https://doi.org/10.1007/s00158-019-02407-3.

Casarotti, C., and R. Pinho. 2007. “An adaptive capacity spectrum method for assessment of bridges subjected to earthquake action.” *Bulletin of Earthquake Engineering* 5 (3): 377–390.

CEN. 2005. “EN 1992-1-1: Eurocode 2: Design of Concrete Structures - Part 1-1: General rules and rules for buildings.” CEN - European Committee for Standardisation.

—. 2005. “EN 1998-2: Eurocode 8: Design of Structures for Earthquake Resistance - Parte 2: Bridges.” CEN - European Committee for Standardisation.

—. 2005. “EN1998-1: Eurocode 8: Design of structures for earthquake resistance - Part 1: General rules, seismic actions and rules for buildings.” CEN - European Committee for Standardisation.

Chikahiro, Y., I. Ario, P. Pawlowski, and C. Graczykowski. 2019. “Optimization of reinforcement layout of scissor-type bridge using differential evolution algorithm.” *Computer-Aided Civil and Infrastructure Engineering* 34 (6): 523-538.

Chollet, F. 2015. *Keras.* https://keras.io.

Chow, C. K., and S. Y. Yuen. 2012. “A Multiobjective Evolutionary Algorithm That Diversifies Population by Its Density.” *IEEE Transactions on Evolutionary Computation* 16 (2): 149-172.

Christensen, P.W., and A. Klarbring. 2009. *An Introduction to Structural Optimization.* Springer Netherlands.

Curadelli, O., and M. Amani. 2014. “Integrated structure-passive control design of linear structures under seismic excitations.” *Engineering Structures* (81): 256-264.

Deb, K. 2001. *Multi-Objective Optimization Using Evolutionary Algorithms.* New York, NY: John Wiley and Sons, Inc.

Deb, K., A. Pratap, S. Agarwal, and T. Meyarivan. 2002. “A Fast and Elitist Multiobjective Genetic Algorithm: NSGA-II.” *IEEE Transactions on Evolutionary Computation* 6 (2): 182 - 197.

Deoadatis, G. 1996. “Non-stationary stochastic vector processes: seismic ground motion applications.” *Probabilistic Engineering Mechanics* 11 (3): 149-167.

Dicleli, M., and S. Buddaram. 2007. “Comprehensive evaluation of equivalent linear analysis method for seismic-isolated structures represented by sdof systems.” *Engineering Structures* 29 (8): 1653-1663. doi:10.1016/j.engstruct.2006.09.013.

Esfandiari, M. J., G. S. Urgessa, S. Sheikholarefin, and S. H. D. Manshadi. 2018. “Optimization of reinforced concrete frames subjected to historical time-history loadings using DMPSO algorithm.” *Structural and Multidisciplinary Optimization* 58 (5): 2119-2134.

Fajfar, P. 2000. “A Nonlinear Analysis Method for Performance-Based Seismic Design.” *Earthquake Spectra* 3 (16): 573-592.

Fardis, M., E. Carvalho, A. Elnashai, E. Faccioli, P. Pinto, A. Plumier, and H. Gulvanessian. 2005. *Designers' Guide to EN 1998-1 and 1998-5. Eurocode 8: Design Provisions for Earthquake Resistant Structures.* Designers' Guide to Eurocodes.

Fischinger, M. 2003. “Inelastic seismic analysis of reinforced concrete viaducts.” *Structural Engineering International* 13 (2): 111-118.

Fischinger, M., and T. Isakovic. 1999. “Seismic Analysis of Irregular Bridges, Asymmetric and Irregular Structures: Vol. 1, Irregular Structures.” 127-140. Istanbul, Turkey.

Fonseca, C. M., A. P. Guerreiro, M. López-Ibáñez, and L. Paquete. 2011. *On the Computation of the Empirical Attainment Function.* Vol. 6576, in *Evolutionary Multi-Criterion Optimization. EMO 2011. Lecture Notes in Computer Science*, by Takahashi R.H.C., Deb K., Wanner E.F. and Greco S., 106-120. Berlin: Springer, Berlin, Heidelberg. doi:10.1007/978-3-642-19893-9_8.

Fonseca, C. M., and P. J. Fleming. 1996. “On the performance assessment and comparison of stochastic multiobjective optimizers.” *Proceedings of the 4th International Conference on Parallel Problem Solving from Nature, PPSN IV.* London, UK: Springer-Verlag. 584-593.

Fragiadakis, M., and M. Papadrakakis. 2008. “Performance-based Optimum Seismic Design of Reinforced Concrete Structures.” *Earthquake Engineering and Structural Dynamics* 37 (6): 825–844. doi:10.1002/eqe.786.

Geem, Z. W., and K. S. Lee. 2004. “A New Structural Optimization Method Based on the Harmony Search Algorithm.” *Computers and Structures* 82 (9-10): 781-798.

Geem, Z. W., J. H. Kim, and G. V. Loganathan. 2001. “A New Heuristic Optimization Algorithm: Harmony Search.” *Simulation* 76 (2): 60-68. doi:10.1177/003754970107600201.

Géron, A. 2019. *Hands-On Machine Learning with Scikit-Learn, Keras, and TensorFlow, 2nd Edition.* O'Reilly Media, Inc.

Giuffrè, A., and P. E. Pinto. 1970. “Il comportamento del cemento armato per sollecitazioni cicliche di forte intensità. (in italian).” *Giornale del Genio Civile.*

Gkatzogias, K. I., and A. J. Kappos. 2019. “Direct estimation of seismic response in reduced-degree-of-freedom isolation and energy dissipation systems.” *Earthquake Engineering and Structural Dynamics* 48 (10): 1112-1133. doi:10.1002/eqe.3169.

Goldberg, D. E. 1989. *Genetic Algorithms in Search, Optimization and Machine Learning.* Boston, MA, MA: Addison-Wesley Longman Publishing Co., Inc.

Ha, M., Q. Vu, and V. Truong. 2018. “Optimum Design of Stay Cables of Steel Cable-stayed Bridges Using Nonlinear Inelastic Analysis and Genetic Algorithm.” *Structures* 16: 288-302.

Hao, H. 1998. “A parametric study of the required seating length for bridge decks during earthquake.” *Earthquake Engineering and Structural Dynamics* 27 (1): 91-103.

Hao, H. 1993. “Arch responses to correlated multiple excitations.” *Earthquake Engineering and Structural Dynamics* 22 (5): 389-404.

Hao, H. 1991. “Response of multiply supported rigid plate to spatially correlated seismic excitations.” *Earthquake Engineering and Structural Dynamics* 20 (9): 821-838.

Hao, H., and S. Zhang. 1999. “Spatial ground motion effect on relative displacement of adjacent building structures.” *Earthquake Engineering and Structural Dynamics* 28 (4): 333-349.

Hao, H., C. S. Oliveira, and J. Penzien. 1989. “Multiple-station ground motion processing and simulation based on smart-1 array data.” *Nuclear Engineering and Design* 111 (3): 293-310. doi:10.1016/0029-5493(89)90241-0.

Harada, T. 1984. “Probabilistic modeling of spatial variation of strong earthquake ground displacement.” *Proceedings of the 8th World Conference on Earthquake Engineering.* San Francisco, CA.

Harichandran, R. S., and E. H. Vanmarcke. 1986. “Stochastic variation of earthquake ground motion in space and time.” *Journal of the Engineering Mechanics Division* 112 (2): 154–174.

Harichandran, R. S., and W. Wang. 1990. “Response of indeterminate two-span beam to spatially varying seismic excitation.” *Earthquake Engineering and Structural Dynamics* 19 (2): 173-187.

Harichandran, R. S., and W. Wang. 1988. “Response of simple beam to spatially varying earthquake excitation.” *Journal of Engineering Mechanics* 114 (9): 1526-1541.

IPQ. 2010. “NP EN 1998-1. National Annex to Eurocode 8. Design of structures for earthquake resistance, Part 1: General rules, seismic actions and rules for buildings. (in Portuguese).”

Isakovic, T., and M. Fischinger. 2006. “Higher modes in simplified inelastic seismic analysis of single column bent viaducts.” *Earthquake Engineering and Structural Dynamics* 35 (1): 95-114.

—. 2005. “Pushover analysis of irregular bridges.” *Proceedings of the 4th European Workshop on the Seismic Behaviour of Irregular and Complex Structures.* Thessaloniki, Greece.

—. 2000. “Regularity indices for bridge structures.” *Proceedings of the 12th World Conference on Earthquake Engineering.* Auckland, New Zealand.

Isakovic, T., M. Fischinger, and P. Kante. 2003. “Bridges: when is single mode seismic analysis adequate?” *Proceedings of the Institution of Civil Engineers - Structures and Buildings* 156 (2): 165-173.

Isakovic, T., M. P. N. Lazaro, and M. Fischinger. 2008. “Applicability of pushover methods for the seismic analysis of single column bent viaducts.” *Earthquake Engineering and Structural Dynamics* 37 (8): 1185-1202.

Kameda, H., and H. Morikawa. 1992. “An interpolating stochastic process for simulation of conditional random fields.” *Probabilistic Engineering Mechanics* 7 (4): 243-254. doi:10.1016/0266-8920(92)90028-G.

Kappos, A. J. 1999. “Evaluation of behaviour factors on the basis of ductility and overstrength studies.” *Engineering Structures* 21: 823–835.

Kappos, A. J., M. S. Saiidi, M. N. Aydinoglu, and T. Isakovic. 2012. *Seismic Design and Assessment of Bridges, Inelastic Methods of Analysis and Case Studies.* Geotechnical, Geological and Earthquake Engineering. Vol. 21. New York: Springer. doi:10.1007/978-94-007-3943-7.

Kappos, A. J., T. S. Paraskeva, and I. F. Moschonas. 2013. “Response modification factors for concrete bridges in Europe.” *Journal of Bridge Engineering* 18 (12): 1328-1335.

Kim, S., and M. Q. Feng. 2003. “Fragility analysis of bridges under ground motion with spatial variation.” *International Journal of Non-Linear Mechanics* 38 (5): 705-721.

Kiureghian, A. 1996. “A coherency model for spatially varying ground motions.” *Earthquake Engineering and Structural Dynamics* 25 (1): 99-111.

Kiureghian, A., and A. Neuenhofer. 1992. “Response spectrum method for multi-support seismic excitations.” *Earthquake Engineering and Structural Dynamics* 21 (8): 713-740. doi:10.1002/eqe.4290210805.

Kohrangi, M., R. Bento, and M. Lopes. 2015. “Seismic Performance of Irregular Bridges – Comparison of Different Nonlinear Static Procedures.” *Structure and Infrastructure Engineering: Maintenance, Management, Life-Cycle Design and Performance* 11 (12): 1632-1650. doi:10.1080/15732479.2014.983938.

Kolias, B., M. N. Fardis, A. Pecker, and H. Gulvanessian. 2012. *Designers’ Guide to Eurocode 8: Design of Bridges for Earthquake Resistance.* Designers' Guide to Eurocodes.

Kowalsky, M. J. 2002. “A displacement-based approach for the seismic design of continuous concrete bridges.” *Earthquake Engineering and Structural Dynamics* 31 (3): 719-747.

Kowalsky, M. J., M. J. N. Priestley, and G. A. MacRae. 1995. “Displacement-based design of RC bridge columns in seismic regions.” *Earthquake Engineering and Structural Dynamics* 24 (12): 1623-1643.

Lagaros, N. D., and M. Papadrakakis. 2007. “Robust seismic design optimization of steel structures.” *Structural and Multidisciplinary Optimization* 33 (6): 457-469.

Lagaros, N. D., and Y. Tsompanakis. 2007. *Intelligent Computational Paradigms in Earthquake Engineering.* Hershey, Pensilvania: Idea Group Inc.

Lavorato, D., G. Fiorentino, A. V. Bergami, B. Briseghella, C. Nuti, S. Santini, and I. Vanzi. 2018. “Asynchronous earthquake strong motion and RC bridges response.” *Journal of Traffic and Transportation Engineering* 5 (6): 1-13.

Lee, J. 2019. “Multi-objective optimization case study with active and passive design in building engineering.” *Structural and Multidisciplinary Optimization* 59 (2): 507-519.

Lemaître, G., F. Nogueira, and C. K. Aridas. 2017. “Imbalanced-learn: a python toolbox to tackle the curse of imbalanced datasets in machine learning.” *Journal of Machine Learning Research* 18 (1): 559–563.

Li, X., Z. Li, and A. J. Crewe. 2018. “Nonlinear seismic analysis of a high-pier, long-span, continuous RC frame bridge under spatially variable ground motions.” *Soil Dynamics and Earthquake Engineering* 114: 298-312.

Liao, S., and A. Zerva. 2006. “Physically compliant, conditionally simulated spatially variable seismic ground motions for performance-based design.” *Earthquake Engineering and Structural Dynamics* 35 (7): 891-919. doi:10.1002/eqe.562.

Liu, M., S. A. Burns, and Y. K. Wen. 2003. “Optimal Seismic Design of Steel Frame Buildings based on Life Cycle Cost Considerations.” *Earthquake Engineering and Structural Dynamics* 32 (9): 1313–1332.

Loh, C. H. 1985. “Analysis of the spatial variation of seismic waves and ground movements from SMART-1 data.” *Earthquake Engineering and Structural Dynamics* 13 (5): 561–581.

Loh, C. H., and G. W. Su. 1986. “Relative ground displacement and space-time correlation of ground motions.” *Proceedings of the 7th Japan Earthquake Engineering Symposium.* Tokyo, Japan.

Loh, C. H., and Y. T. Yeh. 1988. “Spatial variation and stochastic modelling of seismic differential ground movement.” *Earthquake Engineering and Structural Dynamics* 16 (4): 583–596.

Loh, C. H., J. Penzien, and Y. B. Tsai. 1982. “Engineering Analysis of SMART-1 array accelerograms.” *Earthquake Engineering and Structural Dynamics* 10 (4): 575–591.

Luco, J. E., and H. L. Wong. 1986. "Response of a rigid foundation to a spatially random ground motion." *Earthquake Engineering and Structural Dynamics* 14 (6): 891-908. doi:10.1002/eqe.4290140606.

Maalek, S., R. Akbari, and M. R. Maheri. 2009. "The effect of higher modes on the regularity of single column-bent highway viaducts." *Bridge Structures* 5 (1): 29-43.

Mander, J. B., M. J. N. Priestley, and R. Park. 1988. "Theoretical Stress-Strain Model for Confined Concrete." *Journal of Structural Engineering* 114 (8): 1804-1826. doi:10.1061/(ASCE)0733-9445(1988)114:8(1804).

Martínez, C. A., O. Curadelli, and M. E. Compagnoni. 2014. "Optimal placement of nonlinear hysteretic dampers on planar structures under seismic excitation." *Engineering Structures* 65: 89-98.

McKenna, F., and G. Fenves. 1999. *OpenSEES - Open System for Earthquake Engineering Simulation.* Berkeley, CA: The Regents of the University of California.

McKinney, W. 2017. *Python for Data Analysis, 2nd Edition.* O'Reilly Media, Inc.

Menegotto, M., and P. E. Pinto. 1973. "Method of anaysis for cyclically loaded reinforced concrete plane frames including changes in geometry and non-elastic behavior of elements under combined normal force and bending." *IABSE Symposium of Resistance and Ultimate Deformability of Structures Acted on by Well-Defined Repeated Loads.* Lisbon: IABSE. 15-22.

Mergos, P. E. 2018. "Efficient optimum seismic design of reinforced concrete frames." *Structural and Multidisciplinary Optimization* 58 (6): 2565-2581.

Oliveira, C. S., and J. Penzien. 1985. "Spatial variation of seismic ground motions based on SMART-1 array data." *Procedings of the Earthquake Engineering Lifeline Seminar.* Taipei: National Taiwan University.

Oliveira, C. S., B. A. Bolt, and J. Penzien. 1985. "Rotational components of surface strong ground motion." *EOS (abstract)* 66: 968.

Oliveira, C. S., H. Hao, and J. Penzien. 1991. "Ground motion modeling for multiple-input structural analysis." *Structural Safety* 10 (1-3): 79-93. doi:10.1016/0167-4730(91)90007-V.

Papadopoulos, S. P., and A. G. Sextos. 2018. "Anti-symmetric mode excitation and seismic response of base-isolated bridges under asynchronous input motion." *Soil Dynamics and Earthquake Engineering* 113: 148-161.

Papadrakakis, M., and N. D. Lagaros. 2002. "Reliability-based Structural Optimization using Neural Networks and Monte Carlo Simulation." *Computer Methods in Applied Mechanics and Engineering* 191 (32): 3491-3507.

Parreiras, R. O., and J. A. Vasconcelos. 2009. "Decision making in multiobjective optimization aided by the multicriteria tournament decision method." *Nonlinear Analysis: Theory, Methods and Applications* 71 (12): 191-198.

Pedregosa, F., G. Varoquaux, A. Gramfort, V. Michel, B. Thirion, O. Grisel, M. Blondel, et al. 2011. "Scikit-learn: Machine Learning in Python." *Journal of Machine Learning Research* 12: 2825-2830.

Pedro, R. L., J. Demarche, L. F. F. Miguel, and R. H. Lopez. 2017. “An efficient approach for the optimization of simply supported steel-concrete composite I-girder bridges.” *Advances in Engineering Software* 112: 31-45.

Pipa, M. 1993. “Ductility of Reinforced Concrete Elements Under Cyclic Actions. Influence of Reinforcement Mechanical Characteristics (PhD thesis) (in portuguese).” *Instituto Superior Técnico (IST).*

Plevris, V., C. C. Mitropoulou, and N. D. Lagaros. 2012. *Structural Seismic Design Optimization and Earthquake Engineering: Formulations and Applications.* Hershey, Pensilvania: IGI Global.

Price, T. E., and M. O. Eberhard. 1998. “Effects of spatially varying ground motions on short bridges.” *Journal of Structural Engineering* 124 (8): 948-955.

Priestley, M. J. N. 2003. *Myths and Fallacies in Earthquake Engineering, Revisited.* Pavia: IUSS Press.

Priestley, M. J. N., F. Seible, and G. N. Calvi. 1996. *Seismic Design and Retrofit of Bridges.* New York, NY: Wiley-Interscience.

Priestley, M. J. N., G. M. Calvi, and M. J. Kowalsky. 2008. *Displacement-based seismic design of structures.* Pavia, Italia: IUSS Press.

Priestley, M. J. N., G. M. Calvi, M. J. Kowalsky, and G. H. Powell. 2008. “Displacement-Based Seismic Design of Structures.” *Earthquake Spectra* 24 (2): 555-557. doi:10.1193/1.2932170.

Rao, S. S., K. Sundararaju, B. G. Prakash, and C. Balakrishna. 1992. “Fuzzy Goal Programming Approach for Structural Optimization.” *American Institute of Aeronautics and Astronautics* 30 (5): 1425-1432.

Raschka, S., and V. Mirjalili. 2017. *Python Machine Learning - Second Edition.* Packt Publishing Limited.

Restrepo, J. C. O. 2006. *Displacement-Based Design of Continuous Concrete Bridges Under Transverse Seismic Excitation (Masters Dissertation).* University of Pavia, Italy: European School for Advanced Studies in Reduction of Seismic Risk (ROSE school).

Rojas, H. A., C. Foley, and S. Pezeshk. 2011. “Risk-Based Seismic Design for Optimal Structural and Nonstructural System Performance.” *Earthquake Spectra* 27 (3): 857–880.

Rokach, L., and O. Maimon. 2014. *Data mining with decision trees. Theory and applications.* World Scientific.

Sarma, K. C., and H. Adeli. 2000. “Fuzzy Genetic Algorithm for Optimization of Steel Structures.” *Journal of Structural Engineering* 126 (5): 596-604.

Scott, B. D., R. Park, and M. J. N. Priestley. 1982. “Stress-Strain Behavior of Concrete Confined by Overlapping Hoops at Low and High Strain Rates.” *The American Concrete Institute (ACI)* 79 (1): 13-27.

SeismoSoft. 2016. *SeismoSpect v2016.* http://www.seismosoft.com.

Smith, D. G. 2005. “Field assessment of unforeseen earthquake induced bridge deck movements and probable effects of geometry.” *Proceedings of the 4th European Workshop on the Seismic Behaviour of Irregular and Complex Structures.* Thessaloniki, Greece.

Soh, C. K., and J. Yang. 1996. “Fuzzy Controlled Genetic Algorithm Search for Shape Optimization.” *Journal of Computing in Civil Engineering* 10 (2): 143-150.

Soleimani, F., B. Vidakovic, R. DesRoches, and J. Padgett. 2017. "Identification of the significant uncertain parameters in the seismic response of irregular bridges." *Engineering Structures* 141: 356-372.

Tecchio, G., M. Grendene, and C. Modena. 2011. "Spatial variability of earthquake ground motion: effects on seismic response of multi-span girder bridges." *Proceedings of the 8th International Conference on Structural Dynamics, EURODYN 2011.* Leuven, Belgium. 1333-1340.

Tsompanakis, Y., and M. Papadrakakis. 2004. "Large-scale Reliability-based Structural Optimization." *Structural and Multidisciplinary Optimization* 26 (6): 429–440. doi:10.1007/s00158-003-0369-5.

Tugilimana, A., R. F. Coelho, and A. P. Thrall. 2019. "An integrated design methodology for modular trusses including dynamic grouping, module spatial orientation, and topology optimization." *Structural and Multidisciplinary Optimization* 60 (2): 613-638. doi:10.1007/s00158-019-02230-w.

Wang, J., S. Li, F. H. Dezfuli, and M. S. Alam. 2019. "Sensitivity analysis and multi-criteria optimization of SMA cable restrainers for longitudinal seismic protection of isolated simply supported highway bridges." *Engineering Structures* 189: 509-522.

Zanardo, G., H. Hao, and C. Modena. 2002. "Seismic response of multi-span simply supported bridges to a spatially varying earthquake ground motion." *Earthquake Engineering and Structural Dynamics* 31 (6): 1325-1345.

Zavala, G. R., A. J. Nebro, F. Luna, and C. A. Coello Coello. 2013. "A survey of multi-objective metaheuristics applied to structural optimization." *Structural and Multidisciplinary Optimization* 49 (4): 537-558. doi:10.1007/s00158-013-0996-4.

Zerva, A. 1990. "Response of multi-span beams to spatially incoherent seismic ground motions." *Earthquake Engineering and Structural Dynamics* 19 (6): 819-832. doi:10.1002/eqe.4290190604.

—. 2009. *Spatial Variation of Seismic Ground Motions: Modeling and Engineering Applications.* CRC Press, Taylor and Francis Group.

Zerva, A., and V. Zervas. 2002. "Spatial variation of seismic ground motions: An overview." *Applied Mechanics Reviews* 55 (3): 271-297. doi:10.1115/1.1458013.

Zerva, A., M. R. Falamarz-Sheikhabadi, and M. K. Poul. 2018. "Issues with the use of spatially variable seismic ground motions in engineering applications." *Proceedings of the 16th European Conference on Earthquake Engineering.* Thessaloniki: Springer. 225-252.

Zhang, Q., and H. Li. 2007. "MOEA/D: A Multiobjective Evolutionary Algorithm Based on Decomposition." *IEEE Transactions on Evolutionary Computation* 11 (6): 712-731. doi:10.1109/TEVC.2007.892759.

Zhang, Q., J. C. H. Chen, and P. P. Chong. 2004. "Decision consolidation: criteria weight determination using multiple preference formats." *Decision Support Systems* 38 (2): 247-258.

Zhong, J., J. Jeon, W. Yuan, and R. DesRoches. 2017. "Impact of Spatial Variability Parameters on Seismic Fragilities of a Cable-Stayed Bridge Subjected to Differential Support Motions." *Journal of Bridge Engineering* 22 (6). doi:10.1061/(ASCE)BE.1943-5592.0001046.

Zitzler, E., and L. Thiele. 1998. “Multiobjective optimization using evolutionary algorithms - a comparative case study.” *Proceedings of the 5th International Conference on Parallel Problem Solving from Nature, PPSN V.* London, UK: Springer-Verlag. 292-304.

Žižmond, J., and M. Dolšek. 2016. “Evaluation of factors influencing the earthquake-resistant design of reinforced concrete frames according to Eurocode 8.” *Structure and Infrastructure Engineering* 12 (10): 1323–1341.